Detection and Evaluation of Plant Stresses for Crop Management Decisions

RAY D. JACKSON, PAUL J. PINTER, JR., ROBERT J. REGINATO, AND SHERWOOD B. IDSO

Abstract—**The ability to quantitatively assess crop conditions using remotely sensed data would not only improve yield forecasts but would also provide information that would be useful to farm managers in making day-to-day management decisions. Experiments were conducted using ground-based radiometers to relate spectral response to crop canopy characteristics. It was found that radiometrically measured crop temperature, when compared with a reference temperature, was related to the degree of plant stress and could indicate the onset of stress. Reflectance based vegetation indices, on the other hand, were not sensitive to the onset of stress but were useful in evaluating the consequences of stress as expressed in changing quantities of green phytomass. Anatomical and physiological changes occur within plant cells when plants are stressed and increase the amount of reflected radiation. However, canopy geometrical changes may alter the amount of radiation that reaches a radiometer, complicating the interpretation of spectral response to stress. Timeliness, frequency of coverage, and resolution are three factors that must be considered when satellite-based sensors are used to evaluate crop conditions for farm management applications.**

I. Introduction

THE POTENTIAL yield of any crop can be realized only when water, nutrient, and environmental conditions are optimum, and if disease and insect problems are minimized or prevented. Whenever plant growth is retarded by less than optimum conditions, the plants are said to be stressed. The word "stress", although difficult to define from a physiological point of view, is commonly used to signify any effect on plant growth that is detrimental. The term "crop condition" implies an evaluation of the degree of stress. Visual assessment of crop stress is qualitative at best, with the terms "good" or "poor" frequently used to describe crop condition.

The quantification of plant stress using remotely sensed data was a major objective of several research projects conducted under the AgRISTARS program. Although the research goal was to quantify crop stress using satellite data, it was necessary to conduct a number of experiments using ground-based radiometers. These instruments were used over controlled plots with known stress conditions and with known plant and soil parameters to obtain the data base required to relate the remotely sensed measurement to a degree of crop stress.

During the course of the experiments it became apparent that a number of factors can complicate the assessment of stress when interpreting remotely sensed data. Obviously, some frame of reference is required if a numerical value is to be assigned to a stress condition. Furthermore, the spectral response of plant canopies is related to geometrical as well as physiological factors. In some cases, differences in spectral response of two plant canopies may be due to leaf orientation, not to different stress conditions. When plants are stressed leaves may droop and curl, causing geometrical as well as physiological changes that affect the radiation received by a remote sensor.

The results obtained using ground-based instruments should prove useful for improving stress assessment techniques using satellite data. A quantitative measure of stress from space platforms would not only improve our ability to forecast yields, but would also provide information which would aid farm managers in making day-to-day management decisions.

This report discusses some research results concerning the detection and quantification of plant stresses by remote means, examines some complicating factors in the interpretation of data, and assesses progress made in adapting remote sensing technology to provide day-by-day information on soil and crop conditions for use by farm operators in making farm management decisions.

II. Detection and Quantification of Plant Stress

Thermal-IR techniques can be used to detect and, in some cases, quantify plant stress. Although plant temperatures can indicate the occurrence of stress, they cannot identify its cause. If transpiration is restricted because of a deficit of water (water stress) [1], or by the reduction of the number of conducting vessels by disease or insects (biological stress) [2], or by high salinity in the soil water (salinity stress) [3], the net result is an increase in plant temperature.

When plants are stressed, physiological changes that take place within leaves may alter their light absorption and transmittance properties. This, along with plant geometry changes such as wilting and leaf curl, can affect the amount of reflected and emitted radiation that reaches a remote sensor. Often, by the time stress can be ascertained by measurements of reflected solar radiation, visual signs are evident, and yield reducing damage has already occurred. Thus, plant temperatures indicate the onset and degree of stress at a particular time, whereas reflected solar measurements integrate the effects of stress over time.

Manuscript received May 25, 1985; revised August 10, 1985.

The authors are with the U.S. Department of Agriculture, Agricultural Research Service, U.S. Water Conservation Laboratory, Phoenix, AZ 85040.

IEEE Log Number 8406220.

A. Water Stress

The potential of using infrared thermometers to measure canopy temperatures was demonstrated over two decades ago [1], [4]. Since then, four indices, based on infrared temperature measurements, have been proposed for the quantification of plant water stress. They are: stress-degree-day (SDD) [5], [6], which is the canopy-air temperature difference measured post-noon near the time of maximum heating; the canopy temperature variability (CTV) [7], [8], which is the variability of temperatures encountered in a field during a particular measurement period; the temperature-stress-day (TSD) [9], which is the difference in canopy temperature between a stressed crop and a nonstressed reference crop; and the crop water stress index (CWSI) [10], [11], which includes the vapor pressure deficit of the air in relating the canopy and air temperature difference to water stress. Although these indices were developed to quantify water stress, they are useful for evaluating any type of stress that causes a rise of plant temperature.

In the development of the stress-degree-day, it was assumed that effects of environmental factors (such as vapor pressure, net radiation, and wind) would be largely manifested in the canopy temperature, and that the difference between the canopy temperature (T_c) and the air temperature (T_a) would be a relatively useful indicator of plant water stress. It was later demonstrated that the SDD was insufficient to assess water stress in corn [7]. Gardner *et al.* [7] showed that stressed corn plants were below air temperature much of the time, and suggested that corn may be more sensitive to water stress than wheat. They also suggested that canopy-air temperature differences may be soil, crop, and climate specific.

The basis for the canopy temperature variability (CTV) index is that soils are inherently nonhomogeneous, causing some areas within a field to become stressed before others. Consequently, canopy temperatures would show a greater variability as water becomes limiting than they would under well watered conditions. This variability can be used to signal the onset of water deficits [7], [12]. Gardner *et al.* [7] found standard deviations of 0.3°C in fully irrigated plots of corn. In nonirrigated plots, the standard deviation was as great as 4.2°C. They concluded that plots which exhibited a standard deviation above 0.3°C were in need of irrigation.

The difference in temperature between a stressed plot and a well watered plot (called the temperature stress day (TSD) by Gardner *et al.* [8]) can also be used as a water stress indicator. Clawson and Blad [9] tested this concept as to its usefulness for scheduling irrigations. Their corn plots were irrigated when the average of all canopy temperatures measured in the stressed plot during a particular time period were 1°C warmer than the average canopy temperatures of the well watered plot. These experiments indicated that both methods, the CTV and the TSD, could be used to evaluate water stress.

The crop water stress index (CWSI) is based on the fact that the canopy-air temperature difference is linearly related to the air vapor pressure deficit (VPD). This relation, derived from energy balance considerations, can be expressed as [4], [11]

$$T_c - T_A = \frac{r_a R_n}{\rho c_p} \cdot \frac{\gamma(1 + r_c/r_a)}{\Delta + \gamma(1 + r_c/r_a)} - \frac{\mathrm{VPD}}{\Delta + \gamma(1 + r_c/r_a)} \tag{1}$$

where r_a and r_c are the aerodynamic and canopy resistances ($s \cdot m^{-1}$), R_n is the net radiation ($W \cdot m^{-2}$), ρc_p the volumetric heat capacity of air ($J \cdot m^{-3} \cdot C^{-1}$), γ is the psychrometric constant ($Pa \cdot C^{-1}$), and Δ is the slope of the temperature-saturated vapor pressure relation ($Pa \cdot C^{-1}$).

For well-watered plants the canopy resistance (r_c) is low but usually not zero [13]. Assuming that $5\ s \cdot m^{-1}$ is representative of r_c at potential evapotranspiration, $T_c - T_a$ was calculated as a function of VPD. Results of these calculations are given in Fig. 1. Also shown are lines for $r_c = 50$, 500, and ∞, which correspond to moderate, severe, and infinite stress, respectively. When $r_c = \infty$, (1) reduces to

$$T_c - T_A = \frac{r_a R_n}{\rho c_p} \tag{2}$$

which shows that the upper limit of plant temperature is dependent on the aerodynamic resistance and the net radiation.

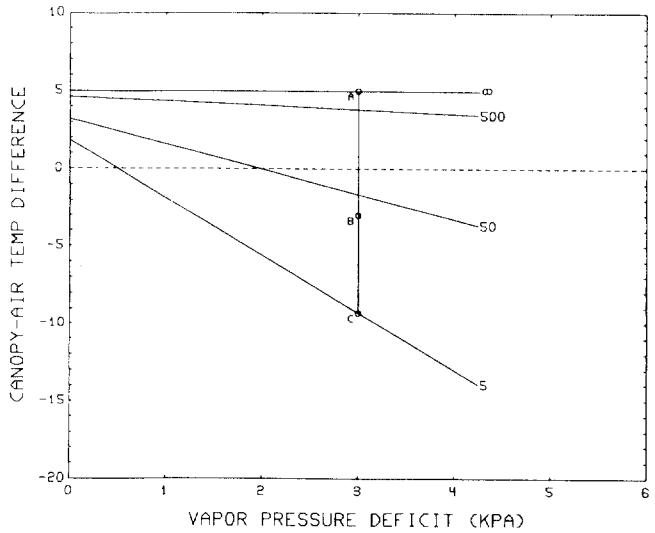

Fig. 1. Theoretical relationship between the canopy-air temperature difference and air vapor pressure deficit. Numbers at the end of the lines indicate the value of the canopy resistance (r_c) used for the calculations.

The point B in Fig. 1 represents a measured value of $T_c - T_a$. The points A and C represent the values of $T_c - T_a$ that would occur if the plants were under maximum and minimum stress, at a particular value of VPD. A crop water stress index (CWSI) was defined as the ratio of the distances BC/AC [10], [11]. The mathematical equivalent

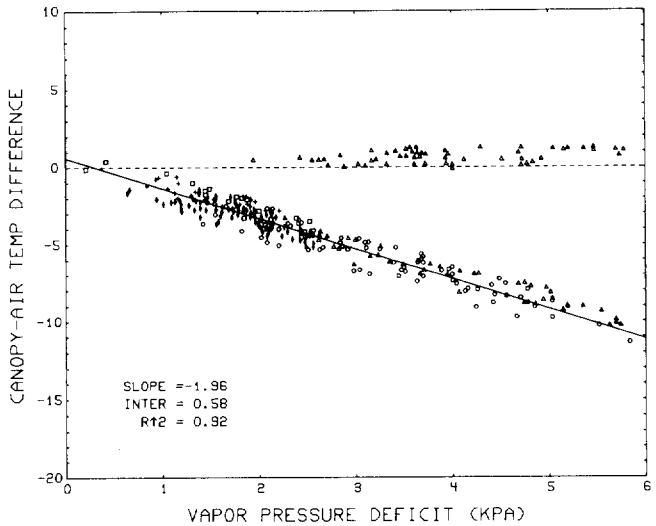

Fig. 2. Canopy-air temperature difference versus air vapor pressure deficit for well-watered plots of alfalfa assumed to be transpiring at the potential rate, and one severely water-stressed plot for which all temperature differences were positive.

$$\text{CWSI} = \frac{\gamma(1 + r_c/r_a) - \gamma^*}{\Delta + \gamma(1 + r_c/r_a)} \tag{3}$$

can also be written [11]. The term $\gamma^* = \gamma(1 + r_{cp}/r_a)$ where r_{cp} is the canopy resistance at potential evapotranspiration. Equation (3) and the graphical calculation shown in Fig. 1 have been used by a number of authors to evaluate plant water stress in the field [3], [14]–[16]. Idso *et al.* [17] obtained data for alfalfa at a number of locations in the western U.S. (Fig. 2) to demonstrate the basic validity of the concept.

B. Biological, Salinity, and Nutrient Stress

Insects and disease organisms can affect the temperature of plants by disrupting the transpiration stream. Disrupting transpiration vessels has the effect of increasing the canopy resistance, and thus increasing the canopy–air temperature difference (Fig. 1). Pinter et al. [2] used a thermal-IR radiometer to measure leaf temperatures of sugar beets infected with *Pythium aphanidermatum*. Leaf temperatures of diseased plants averaged 2.6–3.6°C warmer than leaf temperatures of healthy plants, yet the disease could not be ascertained visually without examining the roots. Temperatures of diseased plants remained higher than healthy plants even under conditions of water stress. Results with cotton infected with *Phymatotrichum omnivorum* were similar. Sunlit leaves of moderately diseased plants averaged 3.3–5.3°C hotter that those on plants with no sign of fungal infection. The temperature difference between diseased and healthy plants was evident 1 day after an irrigation. As soil moisture was depleted, the diseased plants invariably wilted first.

In arid areas, increased soil salinity is a frequent consequence of irrigation. Early detection of saline areas may permit preventative measures before the crop is significantly damaged. Myers *et al.* [18] using ground based canopy temperature measurements, determined that the canopy–air temperature difference increased about 11°C with an increase of salinity corresponding to 16 dS · m^{-1}. Recently, Howell *et al.* [3] found that canopy temperatures were as sensitive to osmotic stress as were traditional measures, but that temperatures provided a better spatial resolution.

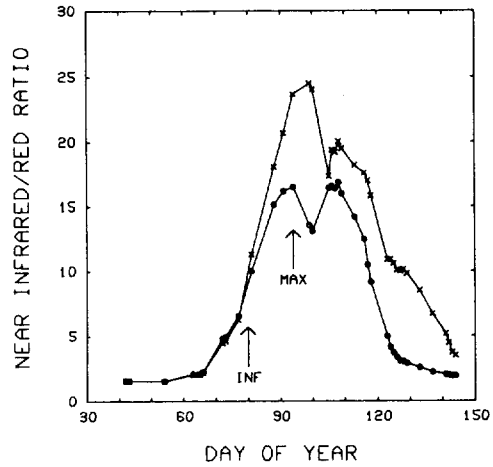

Fig. 3. The near-IR/red ratio as a function of time for a dry (circles) and a wet (x) wheat plot.

Howell *et al.* [3] determined the VPD at which cotton could maintain "unstressed" transpiration rates as related to the soil electrical conductivity in the root zone. They showed that cotton could maintain "unstressed" transpiration only if the VPD was less than 3.5 kPa. For vapor pressure deficits greater than 3.5 kPa, the plants showed symptoms of stress although soil water was not limiting.

Laboratory studies of nutrient stress showed that mineral deficiencies increased the reflectance of radiation in the visible wavelengths, whereas effects on near and middle IR reflectance varied according to the specific mineral deficiency [19]. Field measurements of corn canopies that received four nitrogen treatment levels showed that visible red reflectance increased and the near infrared reflectance decreased with decreasing nitrogen [20]. The ratio of near-IR to red radiance was related directly to the amount of nitrogen applied. Similar results have been reported for nitrogen deficient sugarcane [21].

C. Comparison of Thermal and Reflective Indices

A number of vegetation indices which are sensitive to the amount of green phytomass in the canopy can be formed from bands in the reflected portion of the solar spectrum [22]. One widely used vegetation index is the near-infrared red ratio. Fig. 3 shows this ratio as a function of time during the growing season for two plots of spring wheat, one of which was kept well watered (wet) the other given limited water (dry) [23]. Data for the dry plot are indicated by circles and for the wet plot by x. Two critical periods, the onset of stress and the maximum allowable stress, can be inferred from the vegetation index shown in Fig. 3. The well watered plot, irrigated on day 79, maintained a steady growth rate throughout the veg-

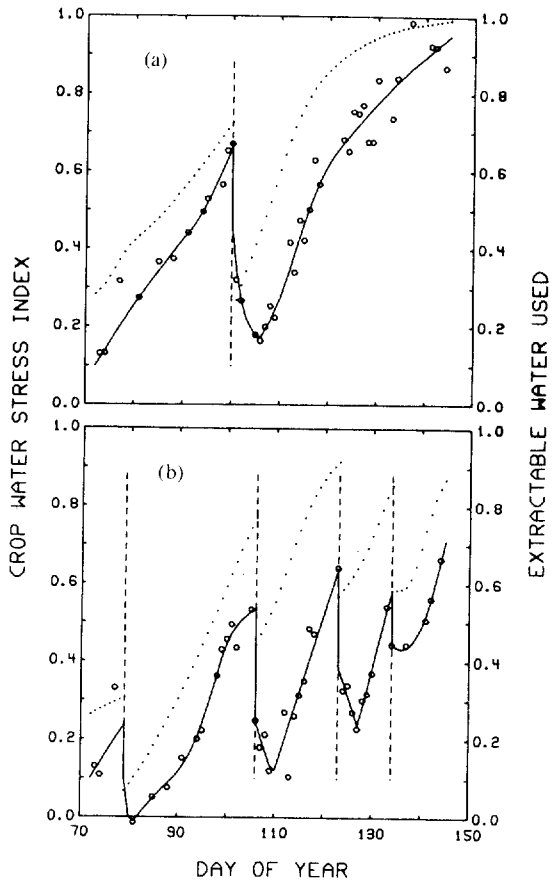

Fig. 4. The crop water stress index (circles) and the fraction of extractable water used (dots) as functions of time for (a) a dry and (b) a wet wheat plot. The dashed vertical lines indicate the dates when irrigations were given.

etative stage. Early in the season no differences were observed between the two plots, but after day 80 the growth rate of the dry plot began to decrease, as indicated by the inflection point (INF) in Fig. 3. At that time the rate of accumulation of green phytomass slowed due to lack of water in the dry plot. We interpret this as the first previsual indication of stress. Without a well watered plot for comparison, however, it would be difficult to detect the onset of stress from a time sequence of the near-IR/red ratio. Note also that the IR/red ratio for the dry plot reached a maximum on day 93 (arrow labeled MAX). At this point the net accumulation of green phytomass, as seen by the radiometer, was zero. Plant architectural changes such as wilting may have exposed more soil to the radiometer, causing a further decrease in the ratio. On day 93, visual symptoms of stress were evident, and the rate of growth was zero. After day 93, there was a net loss of green material. We interpret this point as the maximum allowable stress, because the subsequent growth rate is negative. After irrigation on day 100 the green phytomass again increased, attaining nearly the same value as the maximum reached earlier.

Fig. 4 shows the CWSI and extractable water used (EWU) [24] for the same two experimental plots. The CWSI data points are shown as circles clustering around a line drawn by eye. Smoothed values of the EWU (measured with a neutron scattering technique) are shown as dots. Irrigations are indicated by the vertical dashed lines. Both the CWSI and the EWU increased with time until an irrigation was given. At that point the EWU dropped immediately to a low value, then began to increase. The CWSI decreased, but several days were required to reach a minimum [25], after which the CWSI continuously increased signifying a stress induced reduction in transpiration [11].

To identify the values of CWSI and EWU which corresponded with a reduction in growth rate, we used the dates when the inflection and maximum points (arrows Fig. 3) were reached, and read the corresponding values of CWSI and EWU from Fig. 4. Combining the two measurements allowed the stress limits to be determined for wheat. The results indicate that, for maximum vegetative growth of wheat, the CWSI should not exceed 0.28. If the CWSI exceeds 0.52, net green phytomass can be expected to decrease. On the other hand, once the CWSI reached a minimum after irrigation, it continuously increased with time, indicating a continuous increase in stress. These results further illustrate that temperature based indices are sensitive to the onset of stress whereas the reflectance based indices can evaluate the consequences of stress as expressed in changing quantities of green phytomass.

D. Effect of Canopy Geometry on Stress Assessment

Reflectance of light from a plant canopy is a complex phenomenon which depends not only on the reflectance properties of individual leaves and stems, but also on the ways in which they are oriented and distributed. Under stress, it is likely that both of these factors will change. Laboratory measurements of leaf spectra have shown that reflectance values in the 0.4–2.5 μm region increased with decreasing leaf water content [26]. Gausman [27] demonstrated this effect using cotton leaves. He found that reflectance increased in all wavelengths as the leaves progressively dehydrated. These results can be attributed to anatomical and physiological changes within the plant cells. Crop stress also causes the geometry of the plant to change (e.g., leaf droop and curl), thus exposing different fractions of vegetation and soil (both sunlit and shaded) to the radiometer. Obviously, these changes will also affect a reflectance measurement.

The relative importance of stress induced changes in canopy architecture was studied on a cotton crop by Jackson and Ezra [28]. They measured the spectral response of a cotton canopy by repetitively traversing a radiometer over three adjacent rows of cotton. The instrument was a Barnes Multiband Modular Radiometer (MMR)[1] that has seven bands in the reflective solar and one in the thermal IR. They are: MMR1, 0.45–0.52; MMR2, 0.52–0.60; MMR3, 0.63–0.69; MMR4, 0.76–0.90; MMR5, 1.15–1.30; MMR6, 1.55–1.75; MMR7, 2.05–2.30; and MMR8, 10.5–12.5 μm. MMR bands 1–4 and 7 correspond to the The-

[1]Trade names and company names are included for the benefit of the reader and imply no preferential treatment or endorsement by the U.S. Department of Agriculture.

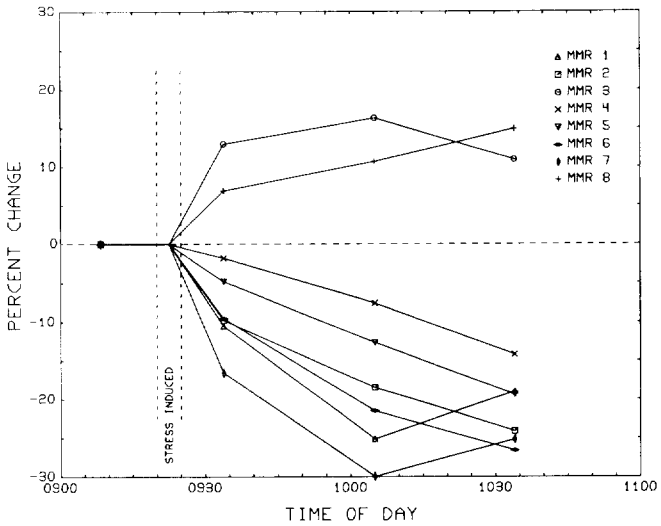

Fig. 5. Observed changes in cotton canopy reflectance and temperature as a function of time after plants were stressed by severing the main stem near the soil. Data are expressed as a percentage of energy reflected or emitted at the same time from two adjacent rows of cotton that were not stressed

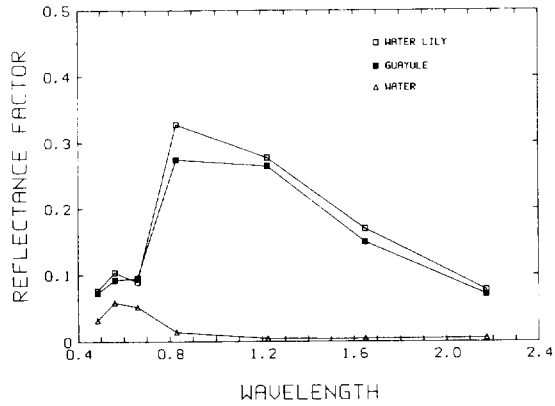

Fig. 6. Reflectance factor as a function of wavelength as measured over water lily, guayule, and water.

matic Mapper bands 1–4 and 7, MMR6 to TM5, and MMR8 to TM6.

After an initial sequence of measurements, the stems of the center row of cotton were cut at a point just above the soil. Care was taken to minimize disturbance of the canopy structure. The cut plants were supported by wooden dowels that had been inserted in the soil and to which the stems had been tied the previous day. The subsequent desiccation of plants within this row was followed by comparing its reflectance and emittance with a control row.

Visual signs of wilting were apparent almost immediately after cutting. The uppermost leaves began to curl and droop first, exposing normal appearing leaves below. Then wilting progressed slowly to the lower leaves. At the end of the experiment even the lowermost leaves showed signs of wilt. As a consequence of wilting, the geometry of the canopy rapidly changed. Prior to cutting the leaves were predominately horizontal. As wilting progressed the leaves became more vertical. The laboratory analysis of Gausman [27] had indicated that reflectance increased in all wavelengths with increasing water stress due to physiological changes of the leaves. Field results indicate that the reflectance may increase at some wavelengths and decrease at others, depending on the geometry changes that accompany stress. The data in Fig. 5 show that, for this variety of cotton, geometry changes play a major role in determining reflectance properties of canopies. The reflectance of six of the seven reflected solar bands decreased as the cotton leaves dehydrated and the leaf angles changed from horizontal to vertical. Our explanation is similar to that of Holben *et al.* [29] in that, due to leaf droop, first surface reflections were scattered into the canopy with less radiance reaching the sensor held above the canopy. For the six bands, geometric effects overshadowed the increased reflectance that occurred due to physiological changes.

Reflectance in the red (0.63–0.69 μm) showed a net increase. The same geometrical factors were active, but the physiological changes were apparently greater. Radiation in this band (known as the chlorophyll absorption band) is absorbed by green leaves and provides the energy to combine carbon dioxide and water in the complex biochemical process of photosynthesis. In a recent review, Krieg [30] concluded that the first effect of a reduction in water availability would be a reduction in this biochemical process which would subsequently trigger the closure of stomata to reduce the exchange of carbon dioxide and water with the atmosphere. Our hypothesis is that the sudden interruption of transpiration immediately affected the photosynthesis process causing some of the red radiation that was previously absorbed to be reflected back to the environment.

On a percentage basis, the visible bands reacted as rapidly to a suddenly induced stress as did the temperature (Fig. 5). A water absorption band (2.05–2.35 μm) decreased by 17 percent within 10 min of a suddenly induced stress, whereas the red band (0.63–0.67 μm) increased by about 12 percent within the same time period. The near-IR (0.76–0.90 μm) showed the least percent change. This result is contrary to the results of Holben *et al.* [29] who found that the near-IR was the most sensitive to stress. In general, our results support the statement of Knipling [26] that the visible reflectance region is as sensitive to stress as is the near infrared region. However, in the visible region the reflectance values are sufficiently small that stress caused changes may not be detectable in an operational mode.

Although the reflectance factor for water in all TM bands is low (Fig. 6), the mid-IR bands (1.55–1.75 μm and 2.05–2.35 μm) are proportedly sensitive to liquid water in plant tissues. On this basis, one could assume that these bands would be useful in detecting water stress in plants. Yet, even when liquid water is present in a scene, the geometry of the scene components can be the dominant factor and can cause confusion in interpreting the data. For example, the bidirectional reflectance factor was measured over a water surface containing water lilies (*Nuphar luteum* Sibth. & Sm.) and over a stand of the drought

adapted desert shrub, guayule (*Parthenium argentatum* Gray). The water lily leaves covered about 80 percent of the surface area, leaving about 20 percent water exposed. The guayule shrubs were about 0.5 m tall, approaching 80–90 percent cover, and in need of water. At first glance one would think that the reflectance factor for the mid-IR bands over the water lily would be small due to absorption by the water surface and the liquid water in the large green leaves. However, the reflectance factor (measured at nadir) for water lily was greater than for guayule in all bands except the red (Fig. 6). The flat water lily leaves caused radiation to be reflected upward toward the radiometer, whereas the guayule canopy caused more radiation to be scattered horizontally than vertically. This extreme case demonstrates the fact that canopy geometry must be accounted for when interpreting reflectance factor data.

III. Remote Sensing as a Farm Management Tool

Thermal infrared radiometry is extensively used by researchers for plant water stress assessment and is beginning to be used by farm operators. At present, portions of fields are surveyed with hand-held instruments that display surface temperature. The degree of stress is inferred by comparison with other fields or by combining the temperatures with ancillary data such as air temperature and vapor pressure. Surface temperatures derived from satellite data have been used for qualitative stress assessment in a research mode, but operational systems have not yet been developed. Using ground based instruments to cover an entire farm is prohibitive from the point of view of time and manpower requirements.

Reflected solar radiation has been extensively measured using hand-held and boom-mounted instruments for research purposes. Satellite data are being used for yield forecasting and qualitative crop condition assessment. Vegetation maps derived from NOAA's AVHRR data have been produced for the continent of Africa [31], and are routinely produced for the U.S. [32]. This type of information is very useful for detecting large scale vegetation changes but is not sufficient for providing crop condition assessment at the farm field level. In order to accomplish the latter, problems of timeliness, frequency of coverage, and spatial resolution of a space-based system must be addressed.

A. Timeliness

Timeliness is perhaps the most important requirement for a farm management remote sensing system. Fig. 7 is a hypothetical relation that shows how the usefulness of remotely sensed data decays with time. To obtain maximum usefulness, the data must be available within minutes. This may appear extreme, but farm operations must be carried out when crop conditions demand. A remote sensing system that required, say, 5 days after acquisition for data delivery would be essentially useless for indicating when to irrigate, because yield reducing damage would have occurred by the time water could be applied. A remote-sensing system for farm management would have an optimum data delivery time of minutes, and a maximum time of a few hours.

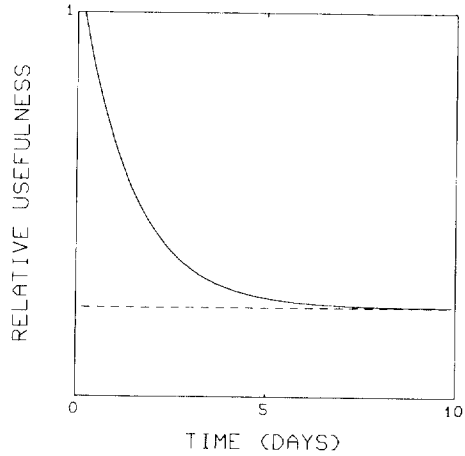

Fig. 7. Relative usefulness of remotely sensed data to farmers in relation to time from acquistion to delivery in usable form.

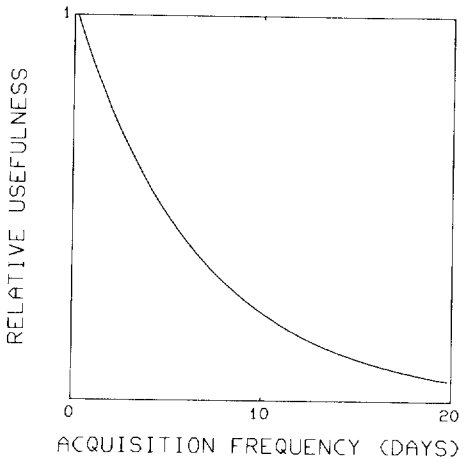

Fig. 8. Relative usefulness of remotely sensed data to farmers in relation to frequency of coverage.

B. Frequency of Coverage

Frequency of coverage is another important aspect. Fig. 8 shows a hypothetical relationship between usefulness and frequency. For farm management, the maximum usefulness would obtain if continuous coverage were available. During the growing season crop conditions continously change. In arid areas, irrigation may be required every 7 to 20 days. A system with a 16-day repeat time would provide little useful information. Also, cloud conditions may increase the time period between acquistions. Continuous coverage would be the optimum, with once a day coverage as a minimum.

C. Resolution

The resolution requirements for a farm management system are dependent upon the particular application for the data. For a farm with relatively uniform soils and a minimum field size of about 40 acres, the 30 × 30 m resolution of a sensor such as the Thematic Mapper may be

adequate. However, this is usually not the case. Many fields are considerably smaller than 40 acres, and soil heterogeneity across fields causes plant growth differences. As an example, during irrigation, areas with low water infiltration may not have the root zone replenished with water, whereas areas of high intake would. The irrigation program for that field would probably be decided on the basis of availability and cost of water and the current crop. A farmer may decide to over irrigate the high intake areas to assure good crop development over the entire field. Under limited water conditions the high intake areas may be used as the indicator of when to irrigate with the lower yields on the other areas accepted. Considering a number of factors, it appears that a resolution of 5 × 5 m would be optimum, with 20 × 20 m acceptable, if sensor design constraints will not allow a smaller figure.

IV. Concluding Remarks

Methods for detecting and quantifying crop stress using ground-based instruments are reasonably well developed. The identification of the cause of stress remains ambiguous. Water stress, being more ubiquitous, is usually the first suspect when stress is detected. However, nutrient deficiencies may cause stress symptoms that can be confused with water stress. When stress is caused by more than one factor, remotely sensed data may not provide enough information to identify the factors. For example, spectral detection of nutrient deficiencies have been demonstrated only when they were known to exist. Little, if any, work has been reported that specifically identified a nutrient deficient crop when the cause of the stress was not known beforehand. Similar statements would hold for biological and salinity stress detection. It is obvious that additional research will be required to resolve this problem.

The effect of canopy geometry on spectral response has been long known, but studied relatively little. A number of models are available that demonstrate the result of canopy architectural changes. However, the measurement of leaf angles required to characterize the canopy geometry in a field crop is difficult and tedious. The comparison of the reflectance values for water lily and guayule discussed in a previous section clearly demonstrated the importance of canopy architecture in determining the spectral response of crops. This complexity should not be ignored.

Reaching the goal of quantitatively assessing stress from space platforms will also require continued research. The problem of correcting for atmospheric effects on remotely sensed data has, and is being, addressed by several research groups. Until adequate methods for these corrections are made operational, stress assessment from space will remain largely qualitative.

Finally, the utilization of data from space platforms for aiding farm operators in day-to-day management decisions has yet to be realized. Although the benefits to agriculture of space technology have been expounded since the launch of the first Landsat satellite and have been very beneficial in some areas, they have not yet materialized for farm management. No space system is now in place that can provide data concerning crop conditions with the frequency of coverage, and resolution in time to initiate remedial procedures before yields are significantly reduced.

References

[1] C. B. Tanner, "Plant temperatures," *Agron. J.*, vol. 55, pp. 210–211, 1963.

[2] P. J. Pinter, Jr., M. E. Stanghellini, R. J. Reginato, S. B. Idso, A. D. Jenkins, and R. D. Jackson, "Remote detection of biological stresses in plants with infrared thermometry," *Science*, vol. 205, pp. 585–587, 1979.

[3] T. A. Howell, J. L. Hatfield, J. D. Rhoades, and M. Meron, "Response of the crop water stress index to salinity," *Irrig. Sci.*, vol. 5, pp. 25–36, 1984.

[4] J. L. Monteith and G. Szeicz, "Radiative temperature in the heat balance of natural surfaces," *Quart. J. Royal Meteorol. Soc.*, vol. 88, pp. 496–507, 1962.

[5] S. B. Idso, R. D. Jackson, and R. J. Reginato, "Remote sensing of crop yields," *Science*, vol. 196, pp. 19–25, 1977.

[6] R. D. Jackson, R. J. Reginato, and S. B. Idso, "Wheat canopy temperature: A practical tool for evaluating water requirements," *Water Resour. Res.*, vol. 13, pp. 651–656, 1977.

[7] B. F. Gardner, B. L. Blad, and D. G. Watts, "Plant and air temperatures in differentially irrigated corn," *Agric. Meteorol.*, vol. 25, pp. 207–217, 1981.

[8] B. F. Gardner, B. L. Blad, D. P. Garrity, and D. G. Watts, "Relationships between crop temperature, grain yield, evapotranspiration and phenological development in two hybrids of moisture stressed sorghum," *Irrig. Sci.*, vol. 2, pp. 213–224, 1981.

[9] K. L. Clawson and B. L. Blad, "Infrared thermometry for scheduling irrigation of corn," *Agron. J.*, vol. 74, pp. 311–316, 1982.

[10] S. B. Idso, R. D. Jackson, P. J. Pinter, Jr., R. J. Reginato, and J. L. Hatfield, "Normalizing the stress degree day for environmental variability," *Agric. Meterorol.*, vol. 24, pp. 45–55, 1981.

[11] R. D. Jackson, S. B. Idso, R. J. Reginato, and P. J. Pinter, Jr., "Canopy temperature as a crop water stress indicator," *Water Resour. Res.*, vol. 17, pp. 1133–1138, 1981.

[12] A. R. Aston, and C. H. M. van Bavel, "Soil surface water depletion and leaf temperature," *Agron. J.*, vol. 33, pp. 441–444, 1972.

[13] C. H. M. Van Bavel and W. L. Ehrler, "Water loss from a sorghum field and stomatal control," *Agron. J.*, vol. 60, pp. 84–86, 1968.

[14] J. L. Hatfield, "The utilization of thermal infrared radiation measurements from grain sorghum crops as a method of assessing their irrigation requirements," *Irrig. Sci.*, vol. 3, pp. 259–268, 1983.

[15] F. S. Nakayama and D. A. Bucks, "Application of a foliage temperature based crop water stress index to guayule," *J. Arid Environ.*, vol. 6, pp. 269–276, 1983.

[16] R. J. Reginato, "Field quantification of crop water stress," *Trans. Amer. Soc. Agric. Eng.*, vol. 26, pp. 772–775, 781, 1983.

[17] S. B. Idso, R. J. Reginato, D. C. Reicosky, and J. L. Hatfield, "Determining soil-induced plant water potential depressions in alfalfa by means of infrared thermometry," *Agron. J.*, vol. 73, pp. 826–830, 1981.

[18] V. I. Myers, D. L. Carter, and W. J. Rippert, "Remote sensing for estimating soil salinity," *J. Irrig. Drain. Div., Amer. Soc. Civil Eng.*, vol. 92, pp. 59–68, 1966.

[19] A. H. Al-Abbas, R. Barr, J. D. Hall, F. L. Crane, and M. F. Baumgardner, "Spectra of normal and nutrient deficient maize leaves," *Agron. J.*, vol. 66, pp. 16–20, 1974.

[20] G. Walburg, M. E. Bauer, C. S. T. Daughtry, and T. L. Housley, "Effects of nitrogen nutrition on the growth, yield, and reflectance characteristics of corn canopies," *Agron. J.*, vol. 74, pp. 677–683, 1982.

[21] R. D. Jackson, C. A. Jones, G. Uehara, and L. T. Santo, "Remote detection of nutrient and water deficiencies in sugarcane under variable cloudiness," *Remote Sensing Environ.*, vol. 11, pp. 327–331, 1981.

[22] C. J. Tucker, "Red and photographic infrared linear combinations for monitoring vegetation," *Remote Sensing Environ.*, vol. 9, pp. 169–182, 1979.

[23] R. D. Jackson and P. J. Pinter, Jr., "Detection of water stress in wheat by measurement of reflected solar and emitted thermal IR radiation,"

in *Proc. Intern. Colloquium on Spectral Signatures of Objects in Remote Sensing* (Avignon, France), pp. 399–406, 1981.
[24] L. F. Ratliff, J. T. Ritchie, and D. K. Cassel, "Field-measured limits of soil water availability as related to laboratory-measured properties," *Soil Sci. Soc. Amer. J.*, vol. 47, pp. 770–775, 1983.
[25] R. D. Jackson, "Soil moisture inferences from thermal infrared measurements of vegetation temperatures," *IEEE Trans. Geosci. Remote Sensing*, vol. GE-20, pp. 282–286, 1982.
[26] E. B. Knipling, "Physical and physiological basis for the reflectance of visible and near-infrared radiation from vegetation," *Remote Sensing Environ.*, vol. 1, pp. 155–159, 1970.
[27] H. W. Gausman, "Leaf reflectance of near-infrared," *Photogramm. Engng. Remote Sensing*, vol. 40, pp. 183–191, 1974.
[28] R. D. Jackson and C. E. Ezra, "Spectral response of cotton to suddenly induced water stress," *Int. J. Remote Sensing*, vol. 6, pp. 177–185, 1985.
[29] B. N. Holben, J. B. Schutt, and J. E. McMurtrey, III, "Leaf water stress detection utilizing thematic mapper bands 3, 4, and 5 in soybean plants," *Int. J. Remote Sensing*, vol. 4, pp. 289–297, 1983.
[30] D. R. Kreig, "Photosynthetic activity during stress," *Agric. Water Mgmt.*, vol. 7, pp. 249–263, 1983.
[31] C. J. Tucker, J. R. G. Townshend, and T. E. Goff, "African landcover classification using satellite data," *Science*, vol. 277, pp. 369–375, 1985.
[32] J. D. Tarpley, S. R. Schneider, and R. L. Money, "Global vegetation indices from the NOAA-7 Meteorological Satellite," *J. Climate Appl. Met.*, vol. 23, pp. 491–494, 1984.

*

Ray D. Jackson received the B.S. degree from Utah State University, Logan, in 1956, the M.S. degree from Iowa State University, Ames, in 1957, and the Ph.D. degree from Colorado State University, Fort Collins, in 1960, all in soil physics.

He has been at the U.S. Water Conservation Laboratory, Phoenix, AZ, since 1960. His early research was concerned with the simultaneous flow of water and heat in soils and the evaporation of water from soils and plants. He is now involved with developing remote-sensing techniques to measure evapotranspiration and to quantify water and nutrient stress in crops. His professional interests include most aspects of remote sensing applied to agriculture.

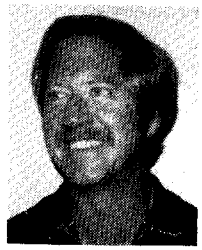

Paul Pinter received the Ph.D. degree in zoology from Arizona State University in 1976, specializing in the influence of crop canopy microclimate on the development, physiology, and survival of economically important insect pests.

He joined the Soil–Plant–Atmosphere Systems Research Unit at the U.S. Water Conservation Laboratory, USDA–ARS, in 1977 where his research has focused on identifying remote-sensing techniques for the early detection and quantification of plant stresses, water requirements, and crop yields. He is currently studying the effect of plant stress on the diurnal patterns of crop canopy reflectance factors.

*

Robert J. Reginato received the B.S. degree in soil management and conservation from the University of California, Davis, the M.S. degree in agronomy from the University of Illinois, and the Ph.D. degree in soil science from the University of California, Riverside.

He has been with the USDA–ARS Water Conservation Laboratory in Phoenix, AZ, since 1959 as a Soil Scientist. His research interests involve the physics of water movement in soils, the control of seepage from canals and ponds, the use of nuclear radiation devices to measure density and water content of soils, and, most recently, the use of emitted thermal radiation to assess crop stress and to estimate evapotranspiration.

*

Sherwood B. Idso received the Ph.D. degree in soil science from the University of Minnesota in 1967.

In that same year he joined the staff of the U.S. Water Conservation Laboratory in the USDA's Agricultural Research Service, where he is currently working as a Research Physicist. He also currently holds Adjunct Professorships in the Departments of Geology, Geography, Botany, and Microbiology at Arizona State University. He has worked for many years in the area of remote-sensing technology as applied to agriculture. He is also deeply involved in both climatic and biological research related to the effects of the rapidly rising carbon dioxide content of Earth's atmosphere.

Vegetation Assessment Using a Combination of Visible, Near-IR, and Thermal-IR AVHRR Data

VICTOR S. WHITEHEAD, WILLIAM R. JOHNSON, AND JAMES A. BOATRIGHT

Abstract—**Twelve-hour temperature difference (thermal inertia) maps generated by rectifying and registering ascending (day) passes and descending (night) passes of the NOAA-7 Advanced Very High Resolution Radiometer (AVHRR) are compared to vegetation index maps generated from the visible and near IR data from the day pass of that satellite. There appears to be significant and unique information concerning surface characteristics in the temperature difference data on the 1-km scale of the AVHRR. A scatter diagram is provided which shows the pattern of day–night temperature difference compared to vegetation index for irrigated agriculture, dry rangeland, lakes, wet areas and burned rangeland. A detailed description of the techniques employed to provide the day–night temperature maps is provided.**

I. Introduction

Over the course of AgRISTARS, research and technique development were hampered by the lack of an accurate yet easy-to-use means to rectify and register a scene viewed from one sensor or one perspective to another view of the same scene obtained through a different sensor or from a different perspective. In response to this need, a task was jointly defined by the Early Warning/Crop Condition Assessment Project and the Foreign Crop Assessment Project within AgRISTARS to provide an accurate, flexible, and easy-to-use technique to rectify and register scenes viewed from different perspectives, through different sensors, at different times, to each other and to common map projections. The results of this task [1] made possible the analysis upon which this paper is based. It has provided the opportunity to view, at a resolution of 1 km, the spatial pattern of day–night temperature difference that occurs at the surface, (sometimes referred to as thermal inertia) and to overlay this pattern on the maps of other surface characteristics. This paper describes the pattern of day–night temperature difference in two distinctly different climatic regimes, southeast Texas in spring and north Texas and Oklahoma in summer; and it compares the patterns in day–night temperature difference to that of a vegetative index.

It is the intent of this paper to demonstrate that significant information relative to vegetation is available in the day–night temperature difference on a scale of 1 km and that this could be provided now on a daily operational basis.

Manuscript received April 12, 1985.

V. S. Whitehead is with NASA Johnson Space Center, Houston, TX 77058.

W. R. Johnson and J. A. Boatright are with the Lockheed Engineering and Management Services Company, Houston, TX.

IEEE Log Number 8406234.

II. Background

Thermal inertia is the resistance of a material to temperature change, an indicator of which is the time-dependent variation in temperature over a full heating/cooling cycle. The thermal inertia within the interface of the topmost layer of soil and the air and covering vegetation is affected by both the relatively permanent characteristics of the soil, landform and geological setting, and the transients such as soil moisture, ventilation, vegetative cover and stress, albedo, and atmospheric radiation properties. Research in application of mapping thermal inertia using airborne thermal scanners performed in the late 1960's and 1970's indicated studies of geology, vegetation and crops, soil moisture and snow mapping would benefit from this additional dimension in remote sensing information [5]. During this period considerable research was also performed on the information content of thermal inertia relative to crop condition using ground based information [3]. Following these favorable results and the analysis of thermal imagery from early NOAA and NIMBUS series satellites, the Heat Capacity Mapping Mission (HCMM) was conceived (1974) and launched (1978) in a research program to address the specific objectives of:

1) producing thermal maps at optimum times for thermal inertia measurements to be used in discriminating rock types and mineral resource locations;
2) measuring plant canopy temperatures at frequent intervals to determine the transpiration of water and plant stress;
3) measuring soil moisture effects by observing the temperature cycle in soils;
4) mapping thermal effluents, both natural and man-made, and determining thermal gradients in large water bodies;
5) predicting water runoff by using frequent coverage of snowfields; and
6) monitoring the effects of urban heat islands on climatology.

The HCMM which operated from April 1978 to September 1980 was an unqualified success in providing the "proof of concept" for these objectives. The HCMM Anthology [6] provides a comprehensive summary of the

TABLE I
CHARACTERISTICS OF AVHRR AND HCMM RADIOMETER
(From [6].)

		Spectral Bands micrometers	Spatial Resolution Km	Repeat Cycle	NEAT °K	Ground Coverage Km
AVHRR	1	0.580 - 0.680				
	2	0.725 - 1.100				
	3	3.550 - 3.930	1.0	diurnal	.12	3000
	4	10.00 - 11.500				
	5	11.500 - 12.500				
HCMR	1	.55 - 1.1	0.6	diurnal, every 5-16 days	.5	716
	2	10.5 - 12.5				

value of thermal inertia data from this system for several disciplines and gives a representative sample of the some 115 sets of temperature difference and thermal inertia data that have been processed from the HCMM. The document also notes several of the shortcomings with the HCMM data. The HCMM Project Scientist summarized the prime lessons from HCMM in the following recommendation for follow on systems:

1) sampling two or more times a day is necessary;
2) more frequent revisits than those of HCMM are needed;
3) HCMM spatial resolution was marginally adequate (the text indicates that for some applications higher spatial resolution is required, but for applications involving regional analysis coarser resolution is acceptable);
4) HCMM noise equivalent $\triangle T$ was adequate;
5) HCMM calibration was not adequate;
6) scientific data should not be in an operational pipeline;
7) thermal flux for the atmosphere needs to be determined separately from surface features.

The first five of these recommendations are addressed here by compromising on spatial resolution. Through use of the NOAA Advanced Very High Resolution Radiometer (AVHRR) system, which has a spatial resolution satisfactory for some applications, temporal sampling, revisits, *NE* $\triangle T$, and calibration are all improved over HCMM. The procedure can be implemented *now* using existing real time AVHRR data to provide day/night and day/day temperature difference mapping. When used with vegetation index maps generated from the daytime data, a direct link between vegetation and thermal inertia is established. A comparison of the AVHRR and HCMM is given in Table I.

III. AVHRR DATA PROCESSING PROCEDURES

This section describes the procedures used in going from the standard NOAA AVHRR Local Area Coverage tape to the maps of thermal inertia and vegetative index discussed later. Channels 1, 2, and 4 are used.

The NOAA Polar Orbiter Data User Guide [4] details the record and file structure of the Local Area Coverage/High Resolution Picture Transmision (LAC/HRPT) digitized data from the AVHRR on the NOAA series satellites. These data are processed initially to provide percent albedo values for channels one and two (no sun angle correction) and radiance values (mW/(m^2 · sr · cm^{-1})) for channel 4. Albedo and radiance values are calculated using the calibration coefficients provided in each logical record. The radiance values of channel 4 are converted to brightness temperature by using the inverse of Planck's radiation equation

$$T(E) = \frac{C_2 V}{\ln (1 + C_1 V^3/E)}$$

where

T is the temperature (K),
E is the energy value (irradiance at instrument aperture),
V is the central wave number of channel filter (cm^{-4}),
$C_1 = 1.1910659 \times 10^{-5}$ mW/(m^2 · sr · cm^{-4}), and
$C_2 = 1.438833$ (cm · K).

The channel 4 central wave numbers for NOAA -6, -7, and -8 are 912.14, 927.22, and 914.305, respectively.

For the data discussed here no atmospheric absorption or path radiance corrections have been applied. Also, radiation tempertature is equivalent black-body radiation temperature at the aperture, i.e., emissivity is assumed unity, which could result in a temperature several degrees Celsius different than would be observed *in situ*. This error is minimized by taking the day–night difference, however.

A. Imagery Products

All processed imagery has pixel values which range from zero to 255. Channels 1 and 2 imagery consists of pixels whose values are ten times the percent albedo, i.e., 15.6 albedo has a pixel value of 156.

When delta temperature (2 P.M. to A.M. local solar time) imagery is generated, the temperature difference in centigrade is computed, multiplied by 5, and added to 50 to expand the data to fill the dynamic range of the display. When delta temperatures (day-to-day + 1, or night-to-night + 1) are computed, the temperature difference in centigrade is multiplied by 20, and added to 100.

Vegetative Index Number (VIN) imagery is generated by subtracting the channel 1 albedo from the channel 2 albedo, multiplying by 10, and adding to 100.

B. ICARUS—Image Correction and Registration Utility System

ICARUS is a software system implemented in FORTRAN 77 (IBM VS/CMS FORTRAN) which provides the user with interactively controlled, remote sensor image data preprocessing capabilities. In this case "preprocessing" includes geometric correction of systematic distortions and rectification of an image to a base map projection.

ICARUS was initially developed to provide a NASA/

JSC capability to rectify NOAA AVHRR images to usable base maps. Data from Landsat Multispectral Scanner (MSS) and Thematic Mapper (TM) sensors can be accepted. Image data are accepted from user-specified disk files in band-sequential format, and outputs are written to another specified file in a similar band-sequential format.

Image data can be accepted in or converted to any of the following map projections: orbiting scanner (raw AVHRR data, for example), Universal Transverse Mercator map, Hotine Oblique Mercator map (as used for Landsat-2, 3 MSS), Space Oblique Mercator map (as used for Landsat-4, 5, TM or MSS), Albers Equal Area map, Lambert conformal conic map, Mercator map, polar stereographic map, cylindrical equal-spaced map, or polyconic map projection.

A centered n row by m column rectangular grid of output space coordinates are mapped, point-by-point, into input image coordinates. The input image locations corresponding to output pixels within a grid cell are determined by two-dimensional linear interpolation.

Image data resampling can be selected from an array of two-dimensional techniques: two-dimensional (four-point) resampling, nearest neighbor (NN), bilinear (BL), fraction NN/BL, cubic (with zero slopes), and cosine bell (with zero slopes).

In the analysis performed here the Icarus program is used in the following manner. Earth rotation effects are corrected based on a nominal circular NOAA satellite orbit in a plane of fixed inclination to the Equator. Earth curvature effects are corrected based on an oblate spheroid Earth model. The image space is related to the Earth spheroid by a single user-entered tie-point. The uncertainty in the tie-point is about one line and pixel; the platform attitude uncertainty yields about 1500-m uncertainty in nadir position; and the geometric correction model accuracy is about 1500 m over a 2048 × 2048 AVHRR scene. (A full scene Landsat MSS or TM image and an extracted AVHRR subscene near nadir will overlay within about 1500 m when both are corrected to a common map base utilizing ICARUS.)

Once the initial extraction has been performed on the image, the second phase of Icarus processing begins. This step involves the point-by-point mapping of a rectangular grid of output locations into input image coordinates to register the extracted image to the desired map. The aforementioned tie-point and scene parameters can be used to define the orientation and positional displacement of the imagery relative to the map. At this juncture of the processing, the user employs one of the resampling methods to register the image to the map. During resampling the precise input image location corresponding to a particular output pixel location is determined by two-dimensional linear interpolation among the four mapping grid vertices surrounding that pixel.

The Albers Equal Area Projection was selected as being ideally suited for gridding data in a network fashion. By definition, scenes with the same number of pixels and scanlines represent equal areas over the surface of the Earth providing both scenes are rectified to the Albers projection and have the same resolution.

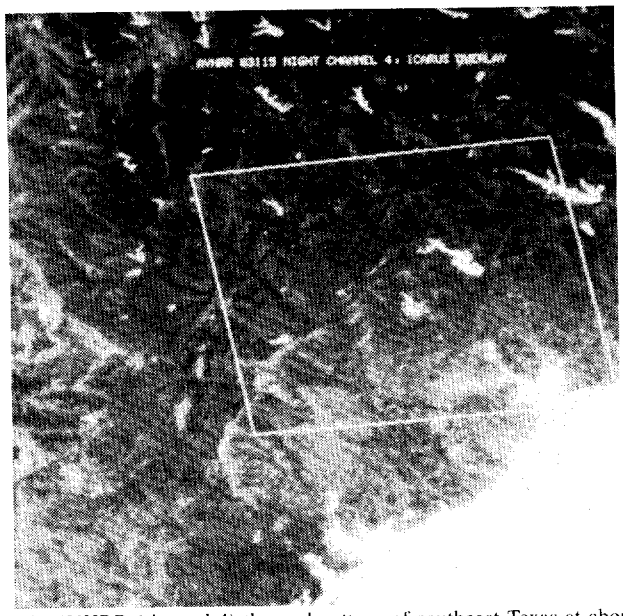

Fig. 1. AVHRR (channel 4) thermal pattern of southeast Texas at about 2 A.M., April 25, 1983. Brightness proportional to relative equivalent blackbody radiation temperature.

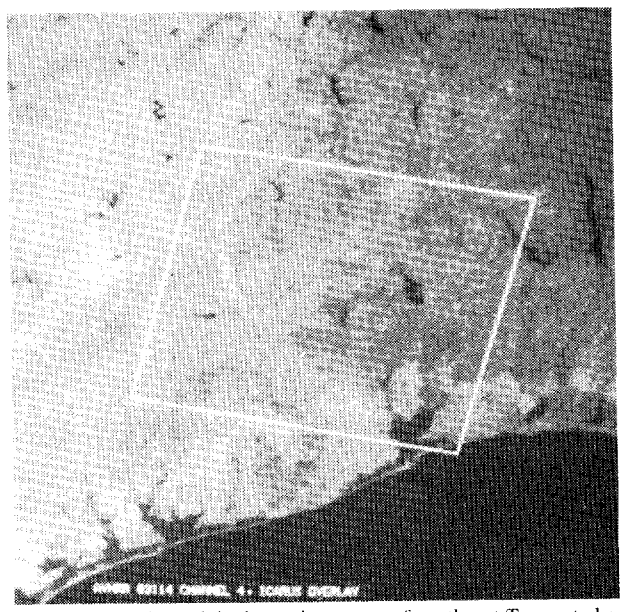

Fig. 2. AVHRR (channel 4) thermal patterns of southeast Texas at about 2 P.M., April 24, 1983. Brightness proportional to relative equivalent blackbody radiation temperature.

C. Analysis

The analysis was performed for two very different climatic regimes, spring in a relative humid area, summer in an arid area. In the first case April 24, 1983, a 2 A.M. descending pass and the following 2 P.M. ascending pass are paired. The scene is the upper Texas coast and much of east and central Texas. The thermal channel (channel 4) displays a map of the relative temperature pattern at about 2 A.M. (Fig. 1). In this figure water bodies, lakes and the gulf, appear brighter (warmer) than the surrounding terrain. In Fig. 2, taken the previous afternoon

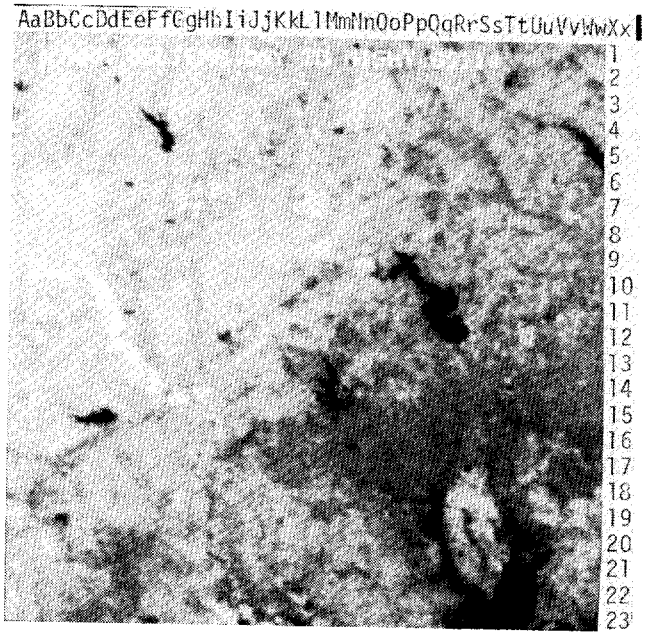

Fig. 3. AVHRR (channel 4) day–night thermal difference pattern. Brightness proportional to relative difference.

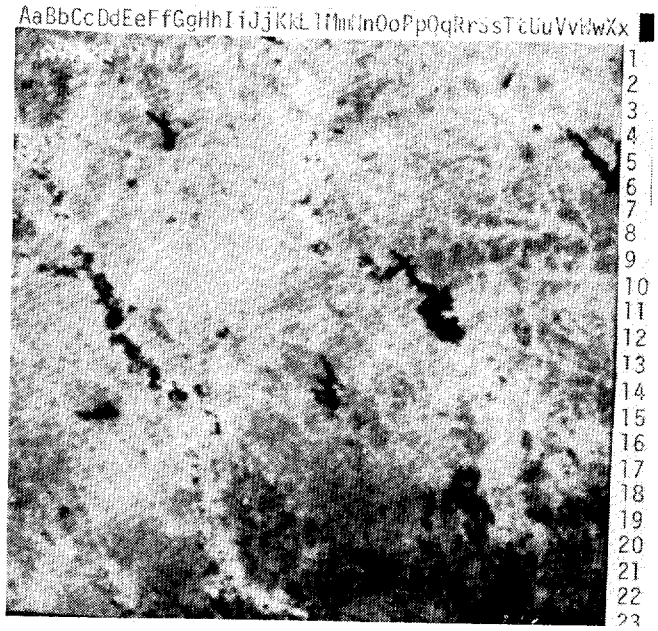

Fig. 4. Gray–McCrary vegetation index (AVHRR Channel 2–Channel 1) at about 2 P.M., April 24, 1983. Brightness proportional to relative vegetation contribution.

(2 P.M.), a reversal of that pattern is shown. A subset of the pixels of each view was selected for processing Icarus by defining four corner points as shown by the boxes in these figures. Note that the corners of the boxes are near to but not necessarily at the same geographic position in the two views. Using the satellite ephermeris data provided in the header, Icarus was then used to register the two views to a geographic map base (in this example an Albers Equal Area Projection was employed). Resampling was performed by using the nearest neighbor technique. A single tie-point was selected and the two views registered and differenced.

The map of day–night temperature difference is shown in Fig. 3. Temperature differences in the lakes (R-12) and bays (T-23) are very small, of the order of 1°C. The forest to the north of Galveston Bay (Q-15) consisting of mixed pine and hardwood shows a modest 14°–17°C difference. The prairie to the upper left side of the figure (D-7) shows a difference of 20°–23°C and the bare soil prepared for planting in the Brazos bottoms (D-10 to G-15) (ropelike bright area to left of figure) and the rice land lower right (W-19) show the greatest differences, 25°–28°C.

Paralleling the temperature difference pattern a measure of vegetation was derived from the daylight pass by differencing (channel 2–channel 1) [2]. This difference is shown in Fig. 4. (The brighter the pixel the more vegetated it is.) Here, the bare soil in the Brazos Bottoms and the rice land appear very dark. Some major transportation arteries with their development appear in the vicinity of Houston, bottom center right. Note that the registration obtained between ascending and descending passes through ICARUS (Fig. 3) is degraded little if any from that obtained from the simultaneous view (Fig. 4). Comparison of values of individual pixels in these figures suggests that for land surfaces higher values of vegetation index are associated with lower values of temperature difference and vice versa as would be expected with the evapotranspiration of actively growing vegetation.

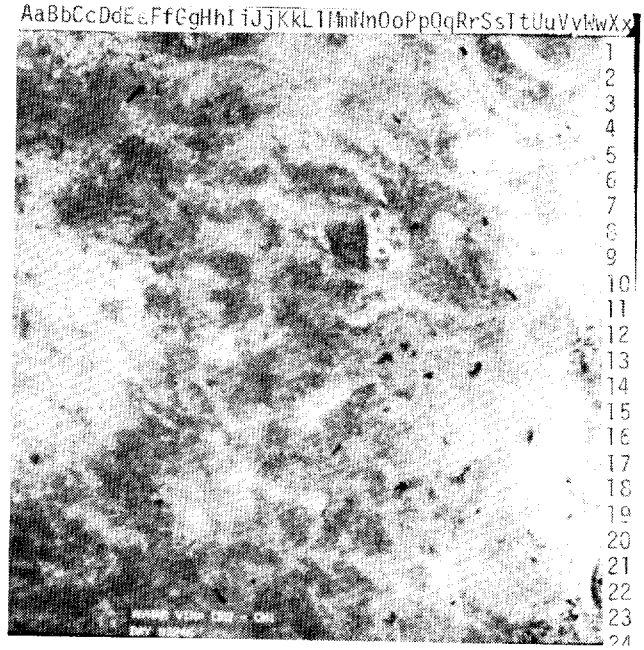

Fig. 5. Vegetation index, north Texas and southwest Oklahoma, as observed at 2 P.M., September 3, 1983. White is highly vegetated, black little vegetation. Clouds, mid-right and lower right, and lakes appear in black.

The second scene, depicted in Figs. 5–7, is north Texas and southwest Oklahoma during the late summer of 1983. For reference Oklahoma City is at X-6, Fort Worth at X-18, Lubbock at C-13 and Amarillo at C-5. The vegetation index shows high values along the eastern edge of the frame in Fig. 5, and also in the high plains between Lubbock and Amarillo along the western edge. Patches of high

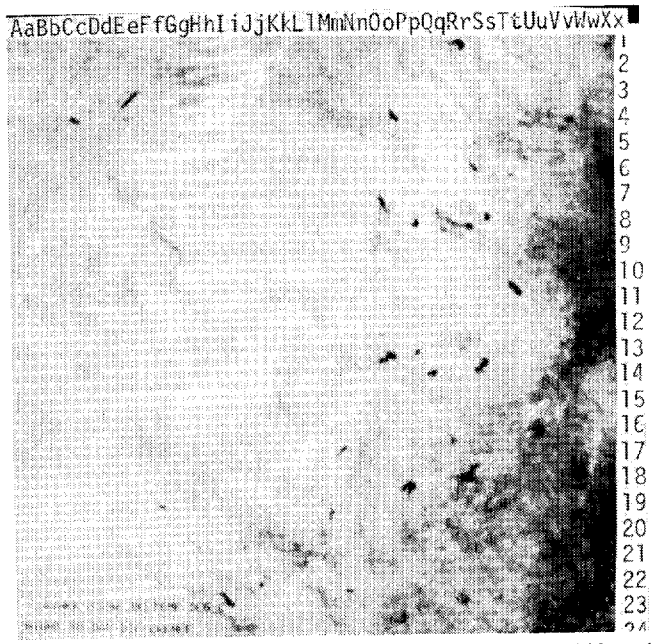

Fig. 6. Temperature difference between 2 P.M., September 3, 1983, and 2 A.M., September 4, 1983, generated by differencing the ICARUS products for those times. Scattered nighttime cloud appears in the upper left in white. Daytime clouds mid-right and lower right in black. White indicates large day/night difference, black small day/night difference.

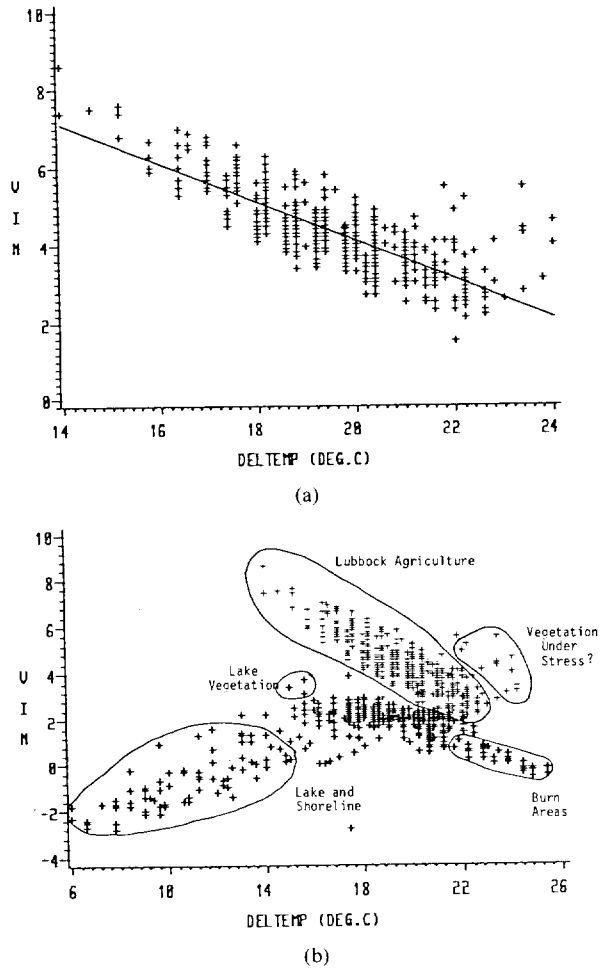

Fig. 7. (a) Pattern of 12-h temperature change versus vegetative index on September 3, 1983, for an agricultural area near Lubbock, TX. (b) For the Lubbock area and an area near Witchita Falls, TX.

values appear over the remainder of the scene but in general values are low indicating the poor state of vegetation in the unirrigated rangeland. Note for later discussion, the pattern of "lakes" in the vicinity of Wichita Falls P-13.

Fig. 6 shows the 12-h temperature difference for the same region. To the east, where the vegetative index is greatest, relative low values of temperature difference are observed. In the Lubbock–Amarillo area inspection shows the same pattern in fine detail indicative of the irrigation patterns. Referring again to the "lakes" in the Wichita Falls area, note that while most lakes have both low values of temperature difference and vegetation index, two of the "lakes" here show high values of temperature difference, higher even than the surrounding terrain. It has been determined that these are instead artifacts of range fires that occurred earlier in the summer (telecommunication with land owner). A color composite of the two parameters (not presented) appears to provide more detail than Figs. 5 and 6, taken separately.

A scatter diagram (temperature difference versus vegetation index) is provided in which pixel values are plotted for a highly vegetated, irrigated area near Lubbock (Fig. 7(a)). The orderly pattern of these data demonstrate the effect of vegetation on the diurnal temperature range, i.e., the more vegetated a pixel the more evapotranspiration suppresses the maximum temperature and the smaller the day–night temperature difference. The outliers to the far right above the regression line are in a position where stressed vegetation would be expected to appear, but verification of the status of this vegetation is not possible without additional information.

The scatter diagram provided in Fig. 7(b) combines the pixels from Fig. 7(a) with those from an area near Witchita Falls. Several clusters are apparent. There is a gradual transition from the pure "deep" water pixels in the lower left to the shallower and more vegetated shore-included pixels with a vegetation index of about 2 and a temperature difference of about 14. The burn area shows the largest temperature difference, however, that cluster slopes up to the left similarly to the Lubbock agricultural area indicating that where vegetation is returning the temperature difference is suppressed somewhat. The native range (not circled) does not appear to have any appreciable pattern in vegetation but does show a significant variation in temperature difference. The significance of this is not understood but is under study.

IV. Conclusions and Recommendation

There appears to be significant and unique information concerning vegetation in thermal inertia data on this scale. The technology to study thermal inertia and its relation to vegetation cover on a coarse scale (1 plus km pixels) now exists. The satellites to acquire the data are in place and are now providing data daily. The software and procedures are formulated and can be made available to interested scientists. In performing this early study and in the detailed follow-up now in progress we have found complications in attempts to track the patterns described here in

time. This is due in part to changes in atmospheric characteristics that affect the evapotranspiration rate and in part to the difference in viewing geometry that affects the vegetation index. These problems are solvable and need to be addressed before the full potential of this approach to vegetation condition assessment can be realized. The application of this technique to problems such as monitoring drought and rangeland productivity changes should be attempted once these improvements are made.

References

[1] J. A. Boatright and W. M. Bradley, "Image correction and registration utility system," ICARUS Design Document, Lockheed Engrg. and Management Services Co., 1985.

[2] T. I. Gray and D. G. McCrary, "AVHRR radiometer data estimation for use in monitoring vegetation," in *Extended Abstracts 15th Conf. Agriculture and Meteorol.*, Amer. Meteorology Soc., 1981.

[3] R. D. Jackson, S. B. Idso, R. J. Reginato, and P. J. Pinter, Jr., "Canopy temperature as a water stress indicator," *Water Resour. Res.*, vol. 17, 1981.

[4] K. B. Kidwell, *NOAA Polar Orbiter Data User's Guide*, NOAA, NESDIS, NCDC, SDSD, Washington, DC, 1983.

[5] J. C. Price, "Estimation of regional scale evapotranspiration through analysis of satellite thermal infrared data," *IEEE Trans. Geosci. Remote Sensing*, vol. GE-20, 1982.

[6] N. M. Short and L. M. Stuart, "The heat capacity mapping mission anthology," NASA SP-46.

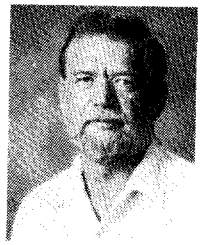

Victor S. Whitehead received the B.A. degree in physics and math from Baylor University, the M.S. degree in meteorology from Texas A & M University, College Station, and the Ph.D. degree in engineering sciences from the University of Oklahoma.

Since 1968, he has been employed at the NASA Johnson Space Center, Houston, TX, in a variety of Earth Observations Program and Remote Sensing Program Assignments, including LACIE and AgRISTARS.

*

William R. Johnson received the B.S. degree in meteorology from the University of Chicago and the M.S. degree in meteorology from Florida State University.

He is a Principal Scientist at Lockheed Engineering and Management Services Company, Houston, TX. His current assignment involves determination of information content for land-inventory tasks. Formerly, he served as a Meteorology Consultant during Skylab missions.

*

James A. Boatwright received the B.S. degree in physics from Texas A&M University, College Station, in 1965.

He is currently a Systems Engineer with Lockheed Engineering and Management Services Company, Houston, TX. He has contributed to the development of several Earth Resources image-processing systems for the NASA Johnson Space Center since 1965. The ICARUS system is the latest of these, and incorporates his "orbiting scanner" map projection to rectify NOAA AVHRR (or similar) images to the Earth's surface.

Analysis of Forest Structure Using Thematic Mapper Simulator Data

DAVID L. PETERSON, WALTER E. WESTMAN, NATE J. STEPHENSON, VINCENT G. AMBROSIA, JAMES A. BRASS, AND MICHAEL A. SPANNER

Abstract—**Remotely sensed data from forested landscapes contain information on both cover type and structure. Structural properties include crown closure, basal area, leaf area index, and tree size. Cover type and structure together are useful variables for designing forest volume inventories. The potential of Thematic Mapper Simulator (TMS) data for sensing forest structure has been explored by principal components and feature selection techniques. Improved discrimination over multispectral scanner (MSS) data proved possible in a mixed conifer forest in Idaho for estimating crown closure and tree size (saplings/seedlings, pole, sawtimber). Classification accuracy increased monotonically with the addition of new channels up to seven; the four optimum channels were 4, 7, 5, and 3.**

The analysis of TMS data for 123 field sites in Sequoia National Park indicated that canopy closure could be well estimated by a variety of bands or band ratios (r = 0.62–0.69) without reference to forest type. Estimation of basal area was less successful (r = 0.51 or less) on average, but improved for certain forest types when data were stratified by floristic composition. To achieve such a stratification, sites were ordinated by a detrended correspondence analysis (DECORANA) based on the canopy of dominant species. Within forest types, canopy closure continued to be the best predictor of spectral variation. Total basal area could be predicted in certain forest types with improved or moderate reliability using various linear ratios of TMS bands (e.g., red fir, 5/4, r = 0.76; lodgepole pine, 4/3, r = 0.82). Spectral reflectance can be expected to be a better predictor of sapwood basal area than total basal area, as evidenced by poor prediction of total basal area in older stands with large numbers of long-lived individuals such as giant sequoia. An analysis of forest structure in the Sequoia data suggests that total basal area will be most successfully predicted in stands of lower density, and in younger even-aged managed stands.

I. Introduction

THE USDA FOREST SERVICE has used aerial photography effectively in forest inventory for many years. The photographs are used to stratify the forest landscape by cover type and structural characteristics (stocking density, tree height, canopy closure) in order to optimize allocation of expensive ground surveys. Derivation of structural information from Landsat data offers the potential for saving costs in large-area surveys. The objective of the Renewable Resources Inventory (RRI) project of AgRISTARS was to develop, test, and evaluate methods and techniques for applying remote-sensing technology to the inventory, monitoring, and management of forest and rangeland renewable resources. The capacity to estimate forest cover type and structural information was also a goal of other NASA programs that funded the work reported here: the Domestic Crops/Land Cover project of AgRISTARS, the Landsat Applications Program, the Global Biology Research Program, and the Terrestrial Ecosystems Research Program.

The inventory procedure of the USDA/Forest Service Region 5 of California exemplifies the level of structural detail typically sought [1]. Aerial photography is used to map forestlands into stands identified by their height, stocking density, and vegetation type (usually by dominant species). Stand height is estimated in turn from crown diameter and stocking density. In Region 5, crown diameter is divided into five classes: seedlings and saplings, poles, diameter up to 12 ft (4 m), small timber (12–23 ft (4–7 m)), medium timber (24–39 ft (8–13 m)), and, large timber (over 40 ft (13 m)). Stocking density is usually related to percent crown closure of commerical conifers in pure stands and those mixed with hardwoods. The distinctions are: nonstocked (less than 10-percent crown closure), sparse (10–19 percent), poor (20–39 percent), not adequate (40–69 percent), and good (over 70 percent). This high level of stratification has been shown to reduce variance and improve efficiency in sampling for volume and productivity estimates as well as having utility for multiresource analyses. For example, the California Wildlife Habitat Relationships Task Force has developed rankings of these strata against the needs of wildlife species for nest sites, feed, and shelter [2]. For the purposes of timber inventory, however, fewer strata can still yield good predictions and efficient designs. Within a regional type, crown diameters can often be reduced to two classes (large trees or commercial, and small trees or precommercial) while stocking density can be reduced to two strata (good (over 40 percent) and poor (under 40 percent)), or three (good, not adequate, poor).

While crown closure and crown size (or height) are the most common measures of forest structure, other structural variables can also be used effectively to predict specific functional properties of forest ecosystems. Leaf area index, the total leaf area or projected one-sided leaf area per unit of ground area (LAI), has been shown by Gholz

Manuscript received January 30, 1985.

D. L. Peterson and J. A. Brass are with the NASA Ames Research Center, Moffett Field, CA 94035.

W. E. Westman is a National Research Council Associate at the NASA Ames Research Center, Moffett Field, CA 94035.

V. G. Ambrosia, and M. A. Spanner are with Technicolor Government Services, Inc., NASA Ames Research Center, Moffett Field, CA 94035.

N. L. Stephenson is with the Section of Ecology and Systematics, Cornell University, Ithaca, NY 14853.

IEEE Log Number 8406235.

[4] to be an effective predictor of aboveground net primary productivity (NPP). The prediction of NPP was obtained for temperature coniferous forests of the Pacific Northwest having a one-sided LAI range from one to twenty. Leaf area index is not being used to predict growth by the Forest Service as yet, probably due to the difficulty in measuring LAI over large regions. Instead, the strata already described are used with yield tables to derive growth estimates. Our own efforts to estimate leaf area index by remote sensing are cited below.

Earlier experience with Landsat MSS data [5]–[12] led us to develop the hypothesis that the variance in a remote-sensing image of a forested area will be due as much to variation in structural properties of communities (crown closure, tree size, tree spacing, leaf area) as to variations in species abundance and cover type. Indeed, the "noise" of forest structure can contribute to the loss of classification accuracy [13]. As the spatial resolution of sensors is increased from 60 to 30 m, there should be an increase in variance as the resolution size approaches the natural frequency of canopy structural characteristics, such as crown diameter. Therefore, Thematic Mapper data might be expected to contain increased structural information at the loss of cover type classification accuracy. For timber volume estimation, this is an acceptable, perhaps preferred, tradeoff as structural properties are more closely associated with functional variables like net primary productivity and state variables like volume.

II. Simulated Thematic Mapper Analyses

A. Forest Structure in Clearwater National Forest, Idaho

A region from the Clearwater National Forest in northern Idaho was chosen for analysis in the Renewable Resources Inventory program of AgRISTARS to evaluate the capabilities of the Thematic Mapper. Simulated TM (TMS) data were acquired for this mixed-conifer intensely-managed forest. A complete range of regrowth conditions exists here. Similar results arose from both a principal components analysis and a Monte Carlo simulation selecting features (channels) that optimize for accuracy of classification of a training data set. A classification scheme and appropriate training sites were selected purposely to highlight structural features (good/poor stocking; seedlings/saplings, poles, sawtimber) as well as the harvesting patterns and other cover conditions in the area. Channel 4 (760–900 nm), channel 7 (thermal: 10 400–12 500 nm), channel 5 (1530–1730 nm), and channel 3 (630–690 nm) were the optimal bands, in that order, to explain scene variance. Training site statistics were used to classify the scene by maximum likelihood techniques. Classification accuracy for seven-channel 30-m TMS data were found to be superior to a four optimum channel (3, 4, 5, 7) 30-m data set. These in turn consistently outperformed a simulated three-channel MSS data set. The Monte Carlo technique showed that the classification accuracy increased monotonically as each new channel up to the full seven was added to the analysis. Virtually no stand dimensional data were available for this site. Thus further analyses to establish the particular structural or other variable contributing most strongly to these results were not possible [14]. This study laid the groundwork for further research at two new locations for which carefully measured structural properties were obtained. Results of a study in Oregon have been reported elsewhere [15]; we discuss below our most recent efforts in the montane forests of California.

B. Forest Structure in Sequoia National Park, California

Sequoia National Park, in the southern Sierra Nevada, represents a particularly complex vegetation mosaic, ranging from chaparral shrubland and broad-leaved forest to montane and subalpine coniferous forest stands. Most of the vegetation has not been logged in the past 95 years, resulting in mixed-age mixed-species stands characteristic of natural, rather than heavily managed, forest landscapes. Airborne Thematic Mapper (ATM) data were obtained over 120 0.1-ha and 3 0.02-ha sites for which ground data were available in the Park. The ground data were collected by N. L. Stephenson during 1982–1983. The data included information on species composition in the canopy, canopy closure, and basal area by species. We sought to determine the extent to which the forest structural variables influenced, and in turn could be predicted by, the spectral data.

C. Collection and Refinement of Spectral Data

ATM data (flight 83-164) were collected on September 2, 1983, between 11 : 40 A.M. and 12 : 16 P.M. (solar noon). The Daedalus Airborne Thematic Mapper (ATM) was flown aboard a NASA U-2C aircraft at 19 800 m, along four N–S trending flight lines of 16.6-km swath width. The scan angle of the sensor was 43° with 716 pixels per scan line. Ground resolution with an IFOV of 1.3 mrad at the mean Park elevation of 2300 m was 23.2 m. The ATM acquires twelve channels of information of which the seven simulated TM bands were used: channel 1 (450–520 nm), 2 (520–600 nm), 3 (630–690 nm), 4 (760–900 nm), 5 (1530–1730 nm), 6 (2100–2300 nm), and 7 (10.4–12.5 μm).

Because the sun angle was not in the plane of the flight line, the proportion of reflected radiation coming from the ground and from atmospheric backscattering changed with scan angle. These limb brightening conditions were corrected by a column-averaging program in which values away from the scanner nadir were corrected for average deviation from scene nadir values [16].

D. Collection and Refinement of Ground Data

The following information was available for each of the 123 sites for which spectral data were collected: elevation, slope, aspect, total canopy closure (percent), percent of canopy dominated by each species, abundance of dominant tree species in each of 12 diameter at breast height (DBH) classes, and date of most recent fire within the past

78 years (from Park records). To convert aspect (in degrees) to a scalar which varied from +1 for most mesic aspects (NE) to −1 for most xeric aspects (SW), aspect in degrees was transformed to sin (aspect +45). The data on tree diameters was used to construct basal area totals in each of five size classes: less than 10-cm DBH, 10–20 cm, 20–40 cm, 40–80 cm, 80–140 cm, more than 140 cm. In the major conifer forests of the park (white and red fir (*Abies concolor, A. magnifica*), giant sequoia (*Sequoiadendron gigantea*)), the first two basal area classes would generally constitute understory saplings.

Several sources of variation in spectral reflectance are not directly accounted for by such a data set. The leaf area index is not known, but from studies in Oregon [15] we know that the TM 4/3 band ratio increases linearly with coniferous leaf area index up to a LAI of 7–8. For higher LAI values (up to 12), the TM 4/3 band ratio gradually becomes asymptotic with LAI [17]. The Oregon studies also indicated a linear relationship between LAI and basal area [15] so that basal area may be considered a crude surrogate for LAI in our data set for sites with lower basal area (and presumably lower LAI). The percent of exposed rock and rock reflectance is not known, but most sites occurred on a single rock type (granite); the other rock type in the data set is metamorphic rock. Terrain (slope, aspect) and solar zenith and azimuth angles together affect solar irradiance reaching the canopy surface. To the extent that aspect influences reflected solar irradiance, a high correlation between reflectance data and site aspect should appear. Correlations between the sin of aspect +45° and TM bands were $r = 0.01$–0.08 for all bands except band 4 ($r = 0.15$). Aspect was not selected as a significant variable in any stepwise multiple linear regressions involving TM bands or band ratios, suggesting that sun angle differences are not of major significance in this data set.

Additional sources of variation include variability in number of pixels included in each sample site delineated (mean of 48; range of 16–146), in the range of forest types included within a delineated site, and potential errors in location of image sample sites in relation to ground sample sites. Changes in atmospheric effect (transmittance, path radiance) with elevation are also uncorrected.

III. Data Analysis

A. Broad Correlations Between Spectral Reflectance and Forest Structure

We began our analysis by examining correlations within the spectral data, and between spectral reflectance and site variables. All bands except 4 and 7 were highly intercorrelated across the 125 sample sites ($r = >0.92$). Bands 1, 2, 3, 5, and 6 were also correlated with band 4 to a similar extent ($r = 0.75$–0.79). For this reason, an index of the sum of bands 1, 2, 3, 5, and 6 was tested (TMN4) for correlation with site variables. Band 7 showed lowest correlation with other bands ($r = 0.46$–0.48), and was most highly correlated with bands 5 and 6 ($r = 0.59$). This general pattern of band intercorrelation was also observed across the Oregon transect although the intercorrelation to band 4 was much lower ($r < 0.2$) [15]. We also examined the behavior of the ratios of bands 4/3, and 5/4, and 2/3, the normalized difference TMND43 : (4 − 3/4 + 3), TMND54 : (5 − 4/5 + 4), and the three TM tasseled cap axes [18], which use principal component transformations of the seven-band data, based on interpretations of these bands with crop scenes.

Our initial correlation analysis between spectral and ground data indicated highest correlations between all individual bands or band ratios and total canopy closure ($r = 0.62$–0.69), with band 4 showing a lower level of correlation ($r = -0.44$). Elevation of the site was the next most strongly correlated site variable for all bands or band ratios ($r = 0.62$–0.69), with band 4 again showing a lower level of correlation ($r = 0.34$). Of the various band ratios and tasseled cap transformations, no single ratio or index behaved significantly and consistently better than the others.

We next tested the relationship between spectral and ground data using stepwise multiple linear regression with forward selection and backward deletion (minimum F-to-enter 4.0; maximum F-to-enter 3.9), to examine the relative contributions of the structural variables to overall spectral reflectance. Table I shows that, with the exception of bands 4 and 7, individual bands and band ratios performed similarly in being predicted by canopy closure and elevation alone with R-square of 0.58–0.65, with only 0.01–0.05 additional R-square contributions made by various basal area classes to particular bands or band ratios. Bands 4 and 7 alone were poorly predicted by any variable combination (R-square = 0.20, 0.50).

B. The Role of Species Composition

We also examined the extent to which species composition of sites affected spectral reflectance. In addition, we wished to examine whether basal area became a more important predictor of reflectance once variation due to species composition was extracted. A floristic classification of sites would not satisfy these aims, since we would be unable to trace how changes in abundance within a floristic class affected spectral response. In order to obtain a numerical index which varied continuously with floristic change, we ordinated the sample sites using detrended correspondence analysis (DECORANA) [19], [20]. DECORANA positions stands along successive independent axes which maximize floristic variation in sample space. Units along each ordination axis represent equal increments of floristic change. DECORANA is a revised form of reciprocal averaging [21] in which higher order axes are made independent of the first, and samples are spaced to achieve an even rate of turnover of species along the axes. Reciprocal averaging derives, in turn, from principal components analysis.

We used percent canopy cover contributed by each species as measures of species importance for the ordination. We deleted chaparral and subalpine stands which had no tree canopy. The first run of the remaining 107 stands was

TABLE I
COEFFICIENTS OF DETERMINATION (r) FOR TM SPECTRAL BANDS AND BAND RATIOS WITH CANOPY CLOSURE, TOTAL BASAL AREA, AND BASAL AREA OF TREES >40-cm DBH
(Significance of difference between vegetation classes, $P < 0.01$ for basal area, $P < 0.04$ for canopy closure.)

	White fir	Wh/red fir	Red fir	Lodgepole	Absolute average of four forest types	All forest types
A. Correlation with total basal area in vegetation classes.						
n =	27	13	17	11	68	103
TMTC1	-.28	-.01	-.51	-.82	.41	-.32
TMTC2	-.03	.21	.60	.82	.42	.19
TMTC3	.21	.14	57	.31	.31	.31
TMN4	-.21	.07	-.53	-.82	.42	-.30
TM 4/3	-.07	.05	.44	.82	.35	.13
ND43	.00	.13	.52	.84	.37	.18
TM 2/3	-.01	.02	.39	.73	.29	.20
ND54	-.18	-.09	-.50	-.47	.31	-.29
TM54	-.23	-.12	-.54	-.44	.33	-.31
TM1	-.25	-.03	-.53	-.83	.41	-.27
TM2	-.25	-.01	-.52	-.83	.40	-.27
TM3	-.19	-.07	-.53	-.82	.40	-.27
TM4	-.29	.24	-.37	-.82	.43	-.31
TM5	-.27	-.05	-.53	-.77	.41	-.33
TM6	-.23	-.15	-.56	-.80	.44	-.30
TM7	-.15	-.14	.17	.54	.25	-.31
x r-value for column	.18	.09	.48	.73	.37	.27
x BATOT, m^2/ha ± std. error	121±32	73±15	74±9.5	17±6.8		
B. Correlation with basal area of large trees (DBH>40) in veg. classes						
TMTC1	-.29	.02	-.45	-.72	.37	-.29
TMTC2	-.04	.17	.54	.69	.36	.15
TMTC3	.21	.11	.50	.42	.31	.28
TMN4	-.24	-.03	-.47	-.72	.31	-.27
TM 4/3	-.07	.01	.41	.71	.30	.09
ND43	.00	.08	.48	.72	.32	.17
TM 2/3	.00	-.01	.36	.63	.25	.15
ND54	-.18	-.06	-.46	-.54	.31	-.26
TM54	-.22	-.09	-.50	-.53	.34	-.27
TM1	.25	.00	.46	.70	.35	.24
TM2	.25	.01	.46	.71	.36	.25
TM3	-.19	-.03	-.46	-.70	.35	-.24
TM4	-.30	.23	-.31	-.71	.39	-.31
TM5	-.27	-.02	-.47	-.72	.37	-.30
TM6	-.22	-.12	-.49	-.71	.39	-.27
TM7	-.22	-.04	-.46	-.48	.30	-.28
x/r/ x BA40P± s.e., m^2/ha	.18 108±33	.06 66±15	.45 67±9	.56 12±6.2	.34	.24
C. Correlation with canopy closure in veg. classes						
TMTC1	-.26	-.67	-.59	-.91	.61	-.64
TMTC2	.57	.85	.58	.89	.72	.61
TMTC3	.52	.74	.61	.51	.60	.70
TMN4	-.39	-.76	-.60	-.91	.67	-.66
TM43	.42	.82	.34	.94	.63	.60
ND43	.51	.86	.47	.94	.70	.66
TM23	.32	.80	.33	.87	.58	.62
ND54	-.42	-.78	-.45	-.67	.58	.68
TM54	-.47	-.79	-.52	-.62	.60	-.68
TM1	-.31	-.78	-.58	-.89	.64	-.60
TM2	-.33	-.74	-.58	-.89	.64	-.61
TM3	-.39	-.80	-.58	-.90	.67	-.63
TM4	.23	.14	-.51	-.90	.45	-.32
TM5	-.34	-.72	-.59	.90	.64	-.67
TM6	-.50	-.72	-.63	-.92	.69	-.69
TM7	-.63	-.30	-.75	-.72	.60	-.65
x/r/for col. x canclo± s.e., %	.37 60±3.6	.70 41±4.9	.55 41±5.4	.85 12±3.3	.59	.62

Legend:
TM Thematic mapper
TC Tasseled cap transformation
TM43 Ratio of TM bands 4 and 3
ND43 Normalized difference of TM bands 4 and 3
TM23 Ratio of TM bands 2 and 3
ND54 Normalized difference of TM bands 5 and 4
TM54 Ratio of TM bands 5 and 4
TM1,2,3,4,5,6,7 TM bands 1 through 7

strongly influenced by three monospecific sites of *Pinus balfouriana* (foxtail pine). Since ordination is based on overlap of species distributions between sample sites, the fact that *P. balfouriana* did not occur mixed with other species in our sample set led the remaining stands to be condensed in axis space. The three *P. balfouriana* stands were therefore deleted. In the ordination of the remaining 104 stands, the first two axes accounted for 82 percent of the total variance extracted by the first four axes, with each of the first two axes accounting for an equal proportion of the variance. Fig. 1 shows the 104 sample sites plotted along these two axes. Visually identifiable clusters were circled, and the dominant species within each identified. Three sites were reassigned to neighboring groups in which the identity of dominants matched more closely.

The first axis was correlated with increasing elevation ($r = 0.91$) from broadleaved valley bottom sites of canyon oak (*Quercus chrysolepis*) and bay laurel (*Umbellularia californica*) through black oak (*Quercus kelloggii*) dominated and black oak-mixed conifer sites to white fir, white fir–red fir, red fir, red fir–lodgepole, and lodgepole (*Pinus contorta* ssp. *murrayana*) sites at successively higher elevations. Along the axis canopy closure decreased ($r = -0.36$) from the dense broadleaved evergreen stands to upper elevation open lodgepole sites. Higher elevation sites were also generally on shallower slopes ($r = -0.31$) with scant understories (basal area classes less than 40-cm DBH, $r = -0.33$). The second axis captured a second important elevational trend ($r = -0.33$ with elevation), from low elevation western juniper (*Juniperus occidentalis*) and Jeffrey pine (*Pinus jeffreyi*) stands to those intergrading with white fir and red fir, progressing to lodgepole with increasing elevation. These elevational changes correspond to those found generally in the Sierra Nevada [22].

Because units along the ordination axis correspond to equal increments of floristic change, one can measure the sensitivity of spectral change to particular species or species groups by examining the amount of change in a spectral ratio for a given unit of floristic change within a forest type as delineated in Fig. 1. Fig. 2 shows how spectral sensitivity to vegetation type changes with forest type. The spectral sensitivity-to-vegetation index (SSV) is defined as (maximum–minimum ratio × 100/maximum–minimum DECORANA axis 1 score per vegetation type), with higher index scores indicating greater spectral sensitivity to floristic variation in canopy cover. Fig. 2 indicates that the pine communities in particular (lodgepole ($n = 11$), Jeffrey pine alone ($n = 6$), or with red fir ($n = 4$)) exhibit a high degree of spectral change with small changes in canopy cover or composition. The canyon oak-bay laurel community also exhibits a high SSV index, though sample size is small ($n = 3$).

Among spectral ratios, the 4/3 ratio is most sensitive to vegetation change with the 5/4 and 2/3 ratios being next most sensitive, the normalized difference ratios the least. Band 4 is most able to penetrate deeply into the canopy [23]. The 4/3 ratio would accentuate this difference, the

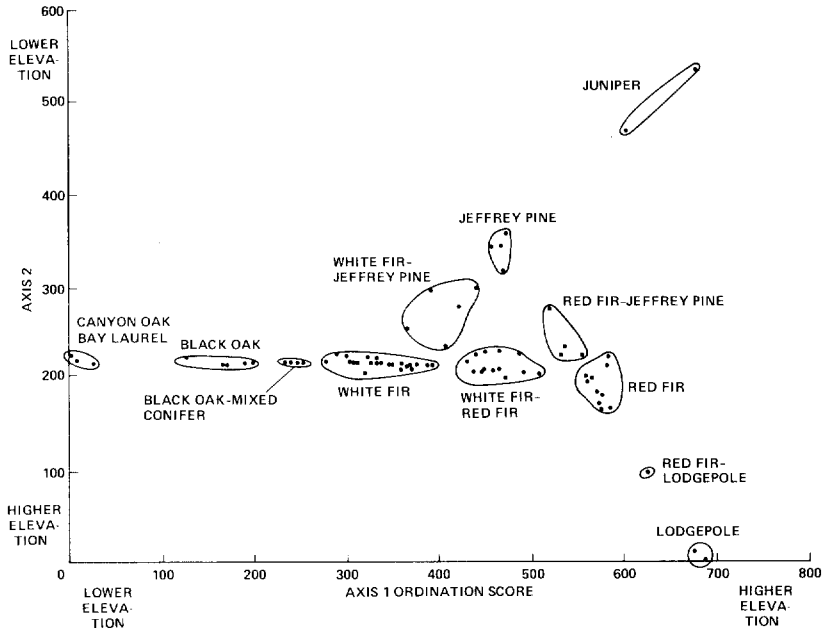

Fig. 1. DECORANA ordination of 104 sample sites at Sequoia National Park. Dominance types are outlined.

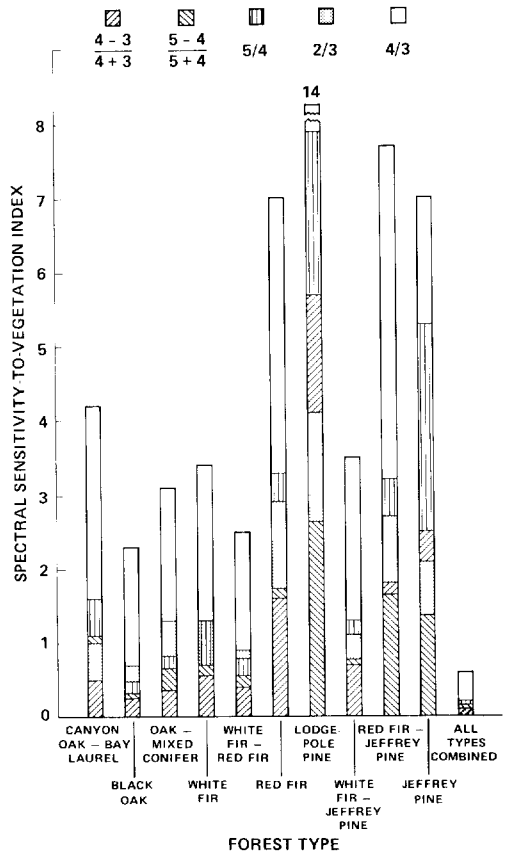

Fig. 2. Sensitivity of spectral ratios to floristic variation in canopy cover using the SSV index defined in the text (delta TM ratio × 100/delta DCA axis 1 scores). Higher index scores indicate greater spectral sensitivity to floristic variation in canopy cover.

normalized difference would lessen it arithmetically. Since band 5 is a water absorption band the observed sensitivity of the 5/4 ratio to vegetative change may reflect changes in canopy moisture content. Band 2 is sensitive to green wavelengths, which vary little along this gradient dominated by conifers of similar needle coloration.

Finally, we note that when data are combined across vegetation types, spectral sensitivity to changes in species composition and cover is lost, indicating the significance of segregating by forest type in examining spectral variation. We confirmed this finding by examining variation in bands and band ratios for all groups combined versus each forest type separately, using analysis of variance. The contribution to total variance due to forest type is highly significant (P less than 0.01, F-test) for all bands and band ratios, as well as for canopy closure and total basal area. Thus the contribution of variations in species composition to spectral reflectance is highly significant, though more so for some species or species groups than others.

C. *Analysis of Forest Structure within Forest Types*

Having identified the importance of species composition to overall variation, we proceeded to examine correlations between bands or band ratios and forest structure (canopy closure, basal area) within the four forest types of highest sample size (the number of sites is 11–27).

No one band or band ratio proved consistently most highly correlated with canopy closure or total basal area (Table I). Band 7 was the best predictor of canopy closure for red and white fir communities (r = 0.63, 0.75); the normalized difference of bands 4 and 3 (ND43) was the best predictor of canopy closure in mixed red-white fir and lodgepole stands (0.86, 0.94), and the latter and the second tasseled cap transformation (greenness) were best overall predictors for the four vegetation types (average absolute r-value of 0.70 and 0.72, respectively).

Basal area was less well predicted by any band or index (r = 0.34–0.37 versus 0.59 for canopy closure). As with canopy closure, basal area was most poorly predicted in

TABLE II
CORRELATION OF TM 4/3, 5/4, 2/3 AND NORMALIZED DIFFERENCE RATIOS OF 4 WITH 3 AND 5 WITH 4 WITH TOTAL BASAL AREA (BATOT), BASAL AREA OF LARGER (>40 cm DBH) (BA40+) OR MEDIUM-SIZED (20-40 cm DBH) (BA2040) TREES, AND CANOPY CLOSURE IN FOUR FOREST TYPES

	n	4/3	$\frac{4-3}{4+3}$	2/3	5/4	$\frac{5-4}{5+4}$	Absolute values of basal area (m^2/ha) and canopy closure (%)
White fir							
BATOT	26	.01	.06	.05	-.23	-.23	121±33[2]
BATOT[1]	24	.31	.34	.19		-.25	
BA40+	26	-.01	.05	.05	-.22	-.22	108±33[2]
BA40+[1]	24	.25		.18		-.24	
BA2040	26	.24	.23	.03	-.07	-.02	8.2±6.3
BA2040[1]	24	.22		.03		-.05	
canopy closure	27	.42	.51	.32	-.47	-.42	60±36
White fir-red fir							
BATOT	13	.05	.13	.02	-.12	-.09	73±15
BATOT[2]	11	.01		-.11		.09	
BA40+	13	.01	.08	-.01	-.09	-.06	66±15
BA40+[2]	11	-.07		-.17		.16	
BA2040	13	.31	.35	.23	-.29	-.24	5.4±4.0
BA2040[2]	11	.33		.24		-.26	
canopy closure	13	.82	.86	.80	-.79	-.78	41±4.9
Red fir							
BATOT	17	.44	.52	.39	-.54	-.50	74±9.5
BA40+	17	.41	.48	.36	-.50	-.46	67±9
BA2040	17	.33	.43	.31	-.46	-.41	5.3±5.2
canopy closure	17	.34	.47	.33	-.52	-.45	41±5.4
Lodgepole pine							
BATOT	11	.82	.84	.73	-.44	-.47	17±6.8
BA40+	11	.71	.72	.63	-.53	-.54	12±6.2
BA2040	11	.65	.68	.54	.12	.04	3.8±5.0
canopy closure	11	.94	.94	.87	-.62	-.67	12±3.3

[1]Deletes two stands with ≥45% canopy closure contribution by giant sequoia.
[2]Deletes two stands with ≥5% canopy closure contribution by giant sequoia.

those vegetation types with the highest absolute values of closure or basal area. When absolute values were comparable, the vegetation type with the highest standard error was predicted more poorly. For total basal area, bands 4 and 6 alone performed best overall (r = 0.43, 0.44) as did the sum of all bands but 4, and the greenness transformation (r = 0.42). When smaller trees (<40-cm DBH) were excluded, similar results occurred, though overall predictive power decreased (r = 0.37–0.34), confirming earlier results on the contribution of smaller trees in gaps to total reflectance.

The separation of study sites into forest types consistently improved the relation of spectral reflectance to basal area, resulting in an average increase in r-value of 0.10. For canopy closure, however, separation into forest types did not uniformly improve predictive power (average r = 0.62 for all forest samples combined versus 0.59 for the four forest types of largest sample size). This suggests that predictions of canopy closure from reflectance data can be efficiently made in mixed conifer forests without reference to forest type.

Table II highlights the effect of canopy structure on reflectance. We note that best levels of prediction of total basal area, or of large (40 cm + DBH) or medium-sized (20–40 cm DBH) trees occurred in stands of lodgepole pine (r = 0.54–0.84 for 4/3, ND43, and 2/3 ratios). Logdepole communities were by far the least dense of the four forest types (average canopy closure 12 ± 3.3 percent versus 41–60 percent for other types), so that fewer trees were obscured and LAI was presumably lower in them.

This result is due to the good cross correlation of *Pinus*

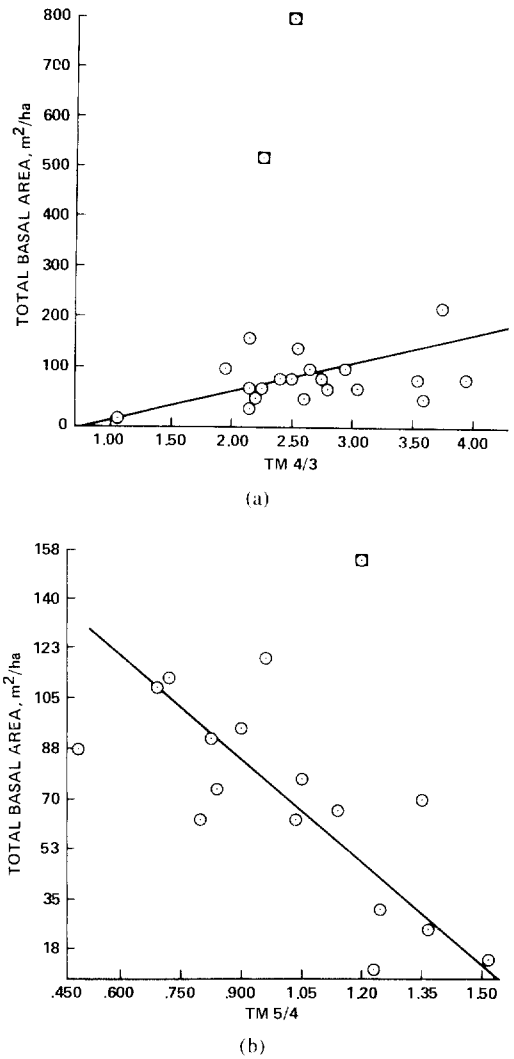

Fig. 3. Relationship of total basal area to TM Band ratios for stands in Sequoia National Park. (a) White fir versus TM 4/3. When stands with >45-percent canopy closure by giant sequoia (boxed points) are excluded, r-value improves from 0.01 to 0.31. (b) Red fir versus TM 5/4. The removal of one stand (boxed point) with >38 percent of basal area in large old trees (>140-cm DBH) improves the r-value from −0.54 to −0.76.

contorta basal area to crown closure and the strong correlation of radiance to crown closure for these open stands.

A different explanation may apply to the marked improvement in basal area estimation in white fir stands by the 4/3 or 2/3 ratio when two stands with major contributions to canopy closure (>45 percent) from giant sequoia are excluded from the data set (r improves 0.14–0.30 points for total basal area, Fig. 3(a)). It is likely that the leaf area of the sequoia is more reflective of sapwood basal area than total basal area in these very long-lived individuals.

Fig. 3(b) illustrates the nature of scatter in the relation of the $\frac{5}{4}$ ratio to total basal area in red fir stands. Removal of a single stand of high biomass concentrated in the largest trees (trees over 140-cm DBH contribute 38 percent of the total basal area in this stand) increases the correlation from r = −0.54 to r = −0.76. The reason for this is again presumably that leaf biomass is much more strongly re-

lated to sapwood basal area than total basal area, so that estimates are poor in stands with large old trees.

Our analysis of these four forest types, then, has shown that when stands dominated by large, old trees are deleted, the 5/4 ratio or the normalized difference of 4 and 3 are capable of estimating total basal area with r values of 0.84, −0.76, 0.34, and 0.13 for lodgepole, red fir, white fir, and mixed fir communities, respectively.

The prediction of basal area by size class improved in larger size classes, but the contribution of the 20–40-cm DBH was not insignificant, as noted earlier. In the case of mixed red-white fir communities, the 20–40-cm size class was predicted markedly better than larger size classes (r = 0.28 versus 0.13 for the 40-cm-plus class). Given that this improved prediction was true even for the 2/3 ratio, in which reflectance is occurring from the upper canopy surface, such results suggest that mixed fir communities in our sample have more small firs in canopy gaps. Fire ages for the three fir community types are comparable (within one standard error of each other's means) so that differences in age since fire do not effectively explain the increased exposure of smaller trees. Parker's [24] study of mixed white and red fir stands in Yosemite National Park in the central Sierra Nevada suggests that mixtures of the two firs are maintained by periodic gap creation in which red firs typically reproduce more prolifically. Our data are consistent with the notion that canopy gaps are more common in the mixed fir stands, permitting exposure of smaller trees to aerial view. Information on height/DBH distribution and historical data on storms and windthrows would help test this hypothesis.

The mixed fir forest type illustrates the difficulty of estimating basal area in stands of spatially variable LAI. Clusters of older trees, with LAI values exceeding saturation levels for spectral reflectance, and with substantial heartwood not reflected in leaf mass, will be severely underestimated, while younger trees in canopy gaps may be effectively estimated.

Of the five band ratios examined for predictive power, the normalized difference of the 4/3 ratio (ND43) performed best for both basal area and canopy closure in white fir and lodgepole community types, and was slightly better than the 4/3 ratio in this regard. The 5/4 ratio performed better than the 4/3 and ND43 ratio for red fir stands, and no ratios performed adequately for our mixed fir data. The normalized difference of 5 and 4 (ND54) generally offered no improvement over the 5/4 ratio. Hardisky *et al.* [25] recently reported that ND54 performed better than ND43 ratio in low biomass stands of *Spartina* salt marsh, and ND43 in high biomass stands. Our results, with forest species rather than grasses, indicate that the performance of the two ratios is not consistently related to biomass (as measured by basal area or canopy closure). Other factors, such as species-specific differences in canopy moisture, green coloration, and leaf area index may improve prediction or influence the choice among these ratios in particular cases. Further research with more community types and larger samples sizes are needed.

IV. Discussion

The research on forest structure using TM data is an outgrowth of earlier work with multispectral scanner data. Increased spectral noise with increased spatial resolution indicates that the "noise" is related to variations in structural properties of forest communities. Its sensitivity to forest structure makes TM data useful.

The unmanaged mixed-species mixed-age composition of the Sequoia forest landscape makes it particularly resistant to broad generalizations regarding the relationship of spectral reflectance to forest structure. As a single variable, canopy closure was most closely related to spectral response. This relationship was robust as forest type changed. Elevation proved a useful predictor as a surrogate for changes in floristic composition, as confirmed by ordination. Basal area can be predicted from the 5/4 ratio with r-values up to −0.76 for red fir and from ND43 with r = 0.84 for lodgepole pine, but only 0.34 for white fir stands. No ratio or band was highly correlated with stands identified as mixed white-red fir. These differences are not related to total basal area or stratal distribution of basal area. Other factors (leaf area index, moisture content of foliage, green coloration) will need to be tested before firm conclusions about these ratios can be made for these coniferous forests. In general, mixed-aged unmanaged stands with many older trees of high LAI and heartwood accumulation will prove more resistant to basal area estimation than younger even-aged managed stands. The 5/4 and 4/3 ratios may prove more successful in estimating sapwood basal area than total basal area in older stands.

What we have learned from our study of canopy closure and basal area will be of use when we turn in future to prediction of LAI from spectral data in the Sequoia data set. It will be important to recognize those forest types where substantial contribution to total LAI from forest understory are being obscured, since saturation effects at higher LAI values can be expected. Spectral variation between forest types may remain significant, to the extent that basal area and LAI are correlated. Red fir and lodgepole pine communities may prove particularly variable spatially in LAI based on their high spectral sensitivity index values.

While reliable prediction of total basal area or basal area classes from spectral data is unlikely to be feasible in all vegetation types for unmanaged forests such as those in Sequoia National Park, we have increased our understanding of variables contributing to spectral reflectance in these communities. We recognize canopy closure as important independent of vegetation type. The accuracy of predictions of basal area will likely vary with canopy density and closure; denser stands, and older stands with substantial heartwood, will prove more refractory to basal area estimation. Downweighting of smaller basal area classes in sites of high canopy closure is only of limited value. The value of LAI as an integrator of these subtleties in stand structure remains to be more fully tested in future research. Because spectral reflection is a direct response to

leaf mass rather than wood mass, there is reason to expect improved predictions of LAI over those for total basal area.

REFERENCES

[1] U.S. Forest Service, *Compartment Inventory Analysis: Region 5 C.I.A. Handbook, March 19, 1979*, Timber Management Staff, Region 5, USDA/Forest Service, San Francisco, CA, 1979.

[2] K. E. Mayer, "A review of selected remote sensing and computer technologies applied to wildlife habitat inventories," *California Fish and Game*, vol. 70, no. 2, pp. 102–112, 1984.

[3] J. J. Goebel and K. O. Schmude, "Planning the SCS national resources inventory," in *Proc. Arid Land Resource Inventories Workshop* (La Paz, Mexico, Dec. 1–5, 1980).

[4] H. L. Gholz, "Environmental limits on aboveground net primary production, leaf area, and biomass in vegetation zones of the Pacific northwest," *Ecology*, vol. 63, pp. 469–481, 1982.

[5] P. G. Langley, "Multistage sampling of earth resources with aerial and space photography," in *Monitoring Earth Resources from Aircraft and Spacecraft*, R. N. Colwell, Ed. NASA SP-275, 1971, pp. 129–141.

[6] D. L. Peterson, D. Noren, and G. Gnauck, "Method and results of three unequal probability multistage sampling designs for timber volume in the Pacific northwest," in *Proc. Int. Conf. Renewable Resource Inventories for Monitoring Changes and Trends* (Soc. Amer. Foresters, Corvallis, OR), pp. 326–329, Aug. 1983.

[7] J. A. Brass, W. C. Likens, and R. R. Thornhill, "Wildland inventory and resource modeling for Douglas and Carson City Counties, Nevada using Landsat data and digital terrain data," NASA Tech. Paper 2137, Mar. 1983.

[8] V. G. Ambrosia, D. L. Peterson, and J. A. Brass, "Volume estimation techniques for Pinyon pine/Utah juniper woodlands using Landsat data and ground information," in *Proc. Int. Conf. Renewable Resource Inventories for Monitoring Changes and Trends* (Soc. of Amer. Foresters, Corvallis, OR), pp. 188–192, Aug. 1983.

[9] A. R. Forbes, L. Fox, III, and K. E. Mayer, "Forest resource classification of the McCloud ranger district, McCloud, CA using Landsat data," Final Rep., USDA/Forest Service, EM-7145-2, Washington, DC, 1980.

[10] D. L. Peterson, "Remote sensing technology applied to forest assessment in California," in *Advances in Space Research*, vol. 3, no. 2. New York: Pergamon, 1983, pp. 193–197.

[11] L. Fox, III, and K. E. Mayer, "Forest resource assessment of Humboldt County, CA," Final Rep., NASA Grant NSG-2341, Humboldt State Univ., Arcata, CA, 1981.

[12] N. H. Pillsbury and J. A. Brass, "A Landsat classification of the forest resources of Tahoe National Forest and adjacent forest lands of California," Final Rep., NASA Agreement NCA2-OR678-001, Calif. Polytechnic Univ., San Luis Obispo, CA, 1982.

[13] B. L. Markham and J. R. G. Townsend, "Land cover classification accuracy as a function of sensor spatial resolution," in *Proc. 15th Int. Symp. Remote Sensing Environment* (ERIM, Ann Arbor, MI), pp. 1079–1090, 1981.

[14] M. A. Spanner, J. A. Brass, and D. L. Peterson, "Feature selection and the information content of thematic mapper simulator data for forest structural assessment," *IEEE Trans. Geosci. Remote Sensing*, vol. GE-22, no. 6, pp. 482–489, Nov. 1984.

[15] M. A. Spanner, K. Teuber, W. Acevedo, D. L. Peterson, S. W. Running, D. H. Card, and D. A. Mouat, "Remote sensing of the leaf area index of temperate coniferous forests," in *Proc. 1984 Machine Processing Remotely Sensed Data Symp.* (West Lafayette, IN, June 12–14, 1984), pp. 362–370.

[16] R. S. Latty, "Empirical models for the adjustment of scan angle-dependent variations in measured radiance," Technol. Applications Branch, Ames Research Center, Technicolor Government Services, internal memo, 1982.

[17] M. A. Spanner, D. L. Peterson, M. J. Hall, R. C. Wrigley, D. H. Card, and S. W. Running, "Atmospheric effects on the remote sensing estimation of forest leaf area index," in *Proc. 18th Int. Symp. Remote Sensing Environment* (Paris, France, Oct. 1–5, 1984).

[18] E. P. Crist and R. C. Cicone, "A physically-based transformation of thematic mapper data—The TM tasseled cap," *IEEE Trans. Geosci. Remote Sensing*, vol. GE-22, no. 3, pp. 256–263, 1984.

[19] M. O. Hill, "DECORANA. A FORTRAN program for detrended correspondence analysis and reciprocal averaging," Cornell Univ., Ithaca, 1979.

[20] M. O. Hill and H. G. Gauch, Jr., "Detrended correspondence analysis: An improved ordination technique," *Vegetatio*, vol. 42, pp. 47–58, 1980.

[21] M. O. Hill "Reciprocal averaging: An eigenvector method of ordination," *J. Ecol.*, vol. 61, pp. 237–249, 1973.

[22] P. W. Rundel, D. J. Parsons, and D. T. Gordon, "Montane and subalpine vegetation of the Sierra Nevada and Cascade Ranges," in *Terrestrial Vegetation of California*, M. G. Barbour, J. Major, Eds. New York: Wiley, 1977, pp. 559–600.

[23] J. M. Norman and P. G. Jarvis, "Photosynthesis in Sitka Spruce, III. Measurements of canopy structure and radiation environment," *J. Appl. Ecol.*, vol. 11, pp. 375–398, 1974.

[24] A. J. Parker, "Environmental and historical factors affecting red and white fir regeneration in ecotonal forests," *Forest Sci.*, 1985.

[25] M. A. Hardisky, F. C. Daiber, C. T. Roman, and V. Klemas, "Remote sensing of biomass and annual net aerial primary productivity of a salt marsh," *Remote Sensing Environ.*, vol. 16, pp. 91–106, 1984.

*

David L. Peterson received the B.S. and M.S. degrees in mechanical engineering from the University of Utah and Stanford University, respectively.

He is a Principal Investigator in biogeochemical cycling in terrestrial ecosystems through the use of modeling and remote sensing for the Ecosystems Science and Technology Branch of the NASA Ames Research Center, Moffett Field, CA. He is currently Project Manager for the Temperate Ecosystems Project for NASA. He is conducting remote-sensing research for forest inventory and mapping, forest structural information, leaf area index, and the biochemical contents of forest canopies.

*

Walter E. Westman received the Ph.D. degree in community and ecosystem ecology from Cornell University in 1971.

He taught in the Department of Botany at the University of Queensland from 1972 to 1974, the Urban Planning Program at U.C.L.A. from 1975 to 1976, and the Department of Geography at the University of California, Los Angeles, from 1976 to 1984 where he was a Full Professor of Ecosystem Analysis and Conservation. He is currently a National Research Council Resident Research Associate at the NASA Ames Research Center, Moffett Field, CA. He has written two books and numerous research articles on vegetation ecology and environmental studies. He is currently researching the remote sensing of air pollution damage to native vegetation.

*

Nate J. Stephenson is currently working toward the M.S. degree in the Section of Ecology and Systematics at Cornell University.

The field data cited in this paper were collected as part of a more extensive gradient analysis of the vegetation of Sequoia National Park that he is conducting as part of his M.S. study.

*

Vincent G. Ambrosia received the B.S. degree in geography, specializing in remote sensing, from Carroll College, WI, in 1978 and the M.S. degree in geography, specializing in remote sensing, from the University of Tennessee-Knoxville in 1980.

He is currently with Technicolor Government Services, Inc., at the NASA Ames Research Center, Moffett Field, CA, where he is a Research Scientist. At Ames, he has completed several projects involving remote-sensing research in timber modeling and inventory. His current research interests include the use of thermal sensor data for biomass conflagration and nutrient cycling, and developing multivariate techniques for quantifying land cover changes using remotely sensed data.

James A. Brass received the B.S. and M.S. degrees in forest resources, specializing in remote sensing, from the University of Minnesota.

He is currently a Research Scientist in the Ecosystem Science and Technology Branch at the NASA Ames Research Center, Moffett Field, CA. He has investigated and applied remote sensing to forest inventory, wildland mapping, and land-use monitoring in the western United States. He has developed spatial modeling studies using geographic information systems for soil conservation, fire-hazard mapping, and reforestation potential. He is currently working on the effects of biomass combustion on the biogeochemical cycling of nutrients and the radiometric characterization of fire events using remote-sensing techniques.

Michael A. Spanner received the B.A. degree in geography from Sonoma State University and the M.A. degree in geography from the University of California, Santa Barbara, specializing in remote sensing.

He is currently a Research Scientist for Technicolor Government Services, Inc. at the NASA Ames Research Center, Moffett Field, CA. He has investigated the application of geographic information systems and remote sensing to soil-loss prediction. His current research is in developing relationships between the leaf area index and biochemical contents on forest canopies to Thematic Mapper and Airborne Imaging Spectrometer data.

Mr. Spanner is a member of the American Society of Photogrammetry.

A Correlation and Regression Analysis of Percent Canopy Closure Versus TMS Spectral Response for Selected Forest Sites in the San Juan National Forest, Colorado

M. KRISTINE BUTERA

Abstract—**This investigation tested the correlation of canopy closure with the signal response of individual Thematic Mapper Simulator (TMS) bands for selected forest sites in the San Juan National Forest, Colorado. Ground truth consisted of a photointerpreted determination of percent canopy closure of 0–100 percent for 32 sites. The sites selected were situated on plateaus at an elevation of approximately 3 km with slope ≤ 10 percent. The predominant tree species were ponderosa pine and aspen. The mean TMS response per band per site was calculated from data acquired by aircraft during mid-September, 1981. A correlation analysis of TMS response versus canopy closure resulted in the following correlation coefficients for bands 1–7, respectively: −0.757, −0.663, −0.666, −0.088, −0.797, −0.597, −0.763. Two model regressions were applied to the TMS data set to create a map of predicted percent forest canopy closure for the study area. Results indicated percent predictive accuracies of 71, 74, and 57 for percent canopy closure classes of 0–25, 25–75, and 75–100, respectively.**

I. Introduction

THIS WORK was undertaken to test the capability of the Landsat Thematic Mapper (TM) sensor and to develop analytical methods for using these satellite data. This investigation uses Thematic Mapper Simulator (TMS) data acquired by aircraft to evaluate the usefulness of the data for predicting percent forest canopy closure. It is assumed that the results of this investigation will be directly applicable to TM data analysis.

Previous work in the analysis of TMS data related to forest canopy is limited. Using portable radiometers with wavelength intervals equivalent to those of the TM, some investigators have concluded that TM band 4 or the ratio of band 4/band 3 is optimum for biomass surveys [2], [7], [9]. Biomass may be considered an indicator of canopy closure. However, these studies dealt with grass rather than forest as a target, the latter being distinguished by the presence of woody tissue which has a confounding effect on the interpretation of spectral response.

Dottavio [3] examined the effect of forest canopy closure and other environmental variables on incoming solar radiation using a three-band field radiometer with wavelength intervals corresponding to TM bands 3, 4, and 5. She concluded that percent canopy closure was the most significant variable affecting incoming solar radiation, with r values of 0.84, 0.81, and 0.73 for bands 3, 4, and 5, respectively. She noted than linear models based on the above results performed less well in the midranges of canopy closure. These conclusions were limited, however, to field measurements obtained only for canopy closures ranging between 60 and 97 percent and at 0 percent. The results of this study were based on field radiometric measurements of incoming solar radiation below the canopy and therefore do not represent the same kind of reflectance measurements which would be made by an aircraft or satellite-borne sensor as it samples reflected energy *above* the canopy.

A more recent study by Dottavio and Williams [4] utilized aircraft-acquired TMS data, although the investigation did not examine forest canopy closure. Rather, the study analyzed TMS and Landsat Multispectral Scanner (MSS) data to evaluate the "future" versus the present capability to map specific forest cover types. For almost all of the TMS data-derived classes, a subset of bands 2, 4, and 5 resulted in greater classification accuracy than did the full complement of TMS bands. Anderson [1] also analyzed aircraft-acquired TMS data for forest inventory, but did not address canopy closure. In a comparison of classification accuracy for mixed forest, pine forest, and river bottom forest, he concluded that the choice of channels had a significant effect and that the same channels were not the most desirable for all three types. His analyses produced classification accuracies greater than 90 percent.

Percent forest canopy closure is an indicator of forest biomass, in general, although the quantitative relationships between percent canopy closure and forest biomass parameters are not well established. A determination of canopy closure, in addition to its significance to biomass, is also relevant to wildlife habitat assessment, watershed runoff estimation, erosion control, and other forest management activities. The objective of this investigation was to analyze the correlation between percent canopy closure

Manuscript received May 3, 1985; revised August 20, 1985.

The author was with the NASA National Space Technology Laboratories, Earth Resources Laboratory, NSTL Station, MS 39529. She is now with the Science Applications International Corporation, Washington, DC 20024.

IEEE Log Number 8406236.

and individual TMS band response for TMS data acquired over the San Juan National Forest, Colorado, in September 1981. Regression models were then developed from the correlation results to create predictive maps of percent canopy closure. The following text describes the methods used and results obtained.

II. Study Area

The study area for this investigation is an area of 26,375 ha in the San Juan National Forest in southwest Colorado. Elevation ranged from 2.4 to 4.0 km, although particular sites of interest were located on plateaus at an elevation of about 3 km. Areas of bare rock commonly occur within the study area. Annual precipitation varies with elevation and ranges from 30.5 to 127 cm per year. Predominant forest tree species include ponderosa pine (*Pinus ponderosa*, Dougl.), aspen (*Populus tremuloides*, Michx.), Engelmann spruce (*Picea engelmannii*, Parry), subalpine fir (Abies *lasiocarpa*, Hook), Douglas fir (*Pseudotsuga menziesii*, Franco), gambel oak (*Quercus gambellii*, Matt.), and Juniper (*Juniperus Scopulorum*, Sarg.). The study area is a part of the U.S. Forest Service's southern San Juan Mountains Planning Unit, the subject of a previous investigation to evaluate U.S. Forest Service lands using Landsat MSS data [6].

III. Acquisition of Remotely Sensed Data

The TMS maintained and flown on an aircraft by the NASA National Space Technology Laboratories (NSTL) has a field of view $\pm 50°$ of nadir and an aperture of 2.5 mrad, which results in a spatial resolution of 30 m × 30 m for a pixel at nadir if the data are collected from an altitude above the ground of 12 000 m. Spectral resolution for TMS and TM bands, in micrometers, is as follows:

	1	2	3	4	5	6	7
TMS	0.46–0.52	0.53–0.61	0.63–0.69	0.77–0.90	1.52–1.69	10.4–12.3	2.04–2.24
TM	0.45–0.52	0.53–0.61	0.62–0.69	0.78—0.91	1.57–1.78	10.4–11.7	2.08–2.35

The TMS data were collected by the NASA/NSTL aircraft on September 18, 1981 at 11:30 A.M. local standard time, from an altitude of 12 km above mean terrain elevation. Aircraft Mission 221 was flown along a north–south line approximately 27 km in distance. Color infrared photography was simultaneously acquired using a Zeiss RMK16/23 gyrostabilized camera. The photography collected by a U-2 aircraft, referred to later in the text, was acquired in September 1980 for an area overlapping this study area.

IV. Ground Truth Data Analysis

The TMS data at the full scan of $\pm 50°$ of nadir covered approximately 26 375 ha of ground surface. Because of spatial and spectral distortion caused by variations in illumination and pixel geometry at increasing look angles, only data $\pm 30°$ from nadir were considered in this analysis.

Study plots approximately 10.12 ha (25 acres) in size were selected for vegetation type and canopy closure of overstory, as determined by air photointerpretation. Only plots characterized by a *spatially uniform* distribution of cover were selected. The intent of the approach was to ascertain if a significant relationship existed between percent forest canopy closure, ignoring in this study the effect of varying proportions of indigenous species in the canopy, and spectral response for this environment. Future analyses will be directed at stratifying the species.

However, to reduce the effect of surface elevation, the sites used in the analysis were chosen from relatively flat mesa formations. A flat area was defined as having no greater than 10-percent slope as measured from a USGS topographic map with a scale of 1:24 000. "Flat" homogeneous plots were identified by using Mission 221 photography and topographic information. The plots were also selected to represent a full range of canopy closure (0–100 percent). Thirty-two such plots fell within the TMS coverage of the study area ($\pm 30°$ from nadir). The potential number of plots with the required characteristics located within the TMS coverage was a limiting factor in the analysis.

Enlarged prints were made from the original 3.54-cm (1:70 000 scale) Mission 221 photography. Only frames 003, 004, and 005 were used and these were printed at a final scale of approximately 1:20 000. A Bruning areagraph chart no. 4849 dot grid reduced four times was used to determine percent canopy closure with a measurement precision of about 97 percent, according to the manufacturer of the chart. The percentage of dots that overlaid tree canopies in each plot was considered to be the percent canopy closure.

Photography acquired at a scale of 1:80 000 during a U-2 mission in September 1980, a year earlier, was prepared in a similar manner. Of the 32 plots, 13 were covered by the U-2 photography. A dot count was performed on these to determine percent canopy closure for comparison with results derived from the Mission 221 photography acquired during the TMS overflight.

As a check on the photointerpretation, a field mission was conducted to collect data on each plot regarding the overstory and understory vegetation, i.e., percent canopy closure and species, April 14–18, 1982. Observations were also made on the soil surface material and general terrain.

V. TMS Data Processing

The TMS 8-bit digital data were processed through various algorithms incorporated in ELAS, a comprehensive computer software system developed by the Earth Resources Laboratory [5]. All computer processing was per-

formed at ERL on a 32-bit minicomputer configured with adequate memory, associated peripherals, and image display devices. All data processing programs cited in this report are parts of the ELAS system.

Each channel of TMS data was reviewed in black and white on an image display device to evaluate data quality. As geometric distortion in the data $\pm 30°$ from nadir was minimal, no geometric corrections were applied. Channels 1–7 exhibited several bad scan lines in the data, most probably caused by detector noise or interference from air traffic communication. Data from all channels exhibited a gradient of values across the scan caused by shadows induced by a sun angle which was oblique to the north–south flight line at the time of data acquisition. Several standard ELAS computer algorithms were employed to normalize the scan angle variations within the TMS data in each channel and to remove detector noise. Image analysis of the corrected data verified the improvement in image quality.

In the next step, the 32 plots of photointerpreted percent canopy closure were located in the TMS data. This was accomplished by referring to the photo maps and interactively outlining the boundaries of each plot on a black and white image of channel 2 of the TMS data using a cursor on an image display device. Reflectance data were extracted for the areas on the ground defined by the polygons and subjected to statistical analysis. The output data included the means, standard deviations, coefficients of variation, and covariance matrices for reflectance data in the seven channels for all the polygons.

VI. Correlation and Regression Analysis

For each polygon, a data table was created containing the reflectance statistics per channel and the percent canopy closure as determined by the photointerpretation of the TMS overflight photography. Since the canopy variable was expressed as a binomial proportion, the percent canopy closure data were transformed to better approximate the variance expected in a normal distribution by using the following formula:

$$P_t = \arcsin \sqrt{P_a} \qquad (1)$$

where P_t is the transformed percent canopy closure and P_a is the actual percent canopy closure.

The arcsin transformation of the variable supported the testing of the significance of the models. A linear correlation and regression analysis was performed on P_t as a function of TMS reflectance for each channel.

VII. Results

A. Preprocessing

As stated earlier, the analysis of the TMS data was restricted to $\pm 30°$ of nadir, equaling 418 elements per scan line. The dimension of an element at nadir for all 7 channels was approximately 30 m × 30 m. (The resolution of TM band 6 is actually 120 m.)

TABLE I
Statistical Analyses of Mission 221 TMS Data, Means, Standard Deviations, and Coefficients of Variation for the Data Set when A) Uncorrected, B) Corrected for the Sun Angle Effect, and C) Corrected for Sun Angle and Noise

A. Statistical Analysis of Mission 221 TMS Data (Uncorrected)

	CH1	CH2	CH3	CH4	CH5	CH6	CH7
MEAN	56.34	66.20	59.88	121.74	33.34	89.00	25.37
STD. DEV	8.85	13.83	18.76	27.52	11.71	26.30	10.71
COEF. OF VAR.	0.16	0.21	0.31	0.23	0.35	0.30	0.42

B. Statistical Analysis of Mission 221 TMS Data Corrected for Sun Angle

MEAN	55.84	65.66	59.32	121.15	32.79	88.39	24.83
STD. DEV	7.18	10.63	15.37	25.58	10.41	22.02	9.81
COEF. OF VAR.	0.13	0.16	0.26	0.21	0.32	0.25	0.40

C. Statistical Analysis of Mission 221 TMS Data Corrected for Sun Angle and Noise in Channels 1 and 7

MEAN	55.81	65.66	59.32	121.15	32.79	88.39	24.81
STD. DEV	7.18	10.63	15.37	25.58	10.41	22.02	9.63
COEF. OF VAR.	0.13	0.16	0.26	0.21	0.32	0.25	0.39

TABLE II
Pair-Wise Correlation Matrix for Channels 1–7 of Entire Mission 221 TMS Data Set
(Corrected for sun angle effect and noise in channels 1 and 7.)

	1	2	3	4	5	6	7
1	1.00						
2	0.93	1.00					
3	0.95	0.95	1.00				
4	0.45	0.55	0.40	1.00			
5	0.90	0.85	0.88	0.53	1.00		
6	0.68	0.68	0.70	0.38	0.75	1.00	
7	0.97	0.90	0.95	0.39	0.93	0.81	1.00

The data were corrected for scan angle variations in all channels and noise in channels 1 and 7, as mentioned. Table I presents the means, standard deviations, and coefficients of variation for the uncorrected and corrected data.

A correlation matrix, based on the corrected TMS data, shows the relationship between all band pairs (Table II). TMS band 4, the near IR band, correlates less well with all other bands than does any other individual band, indicating that it may be a unique discriminator. However, TMS band 4 did not perform well as a discriminator of biomass in this investigation, as discussed in a subsequent section of this paper.

TABLE III
SUMMARY OF GROUND TRUTH DATA FOR SAN JUAN NATIONAL FOREST, CO, STUDY SITE
(Percent canopy closure was derived from interpretation of Sept. 1981 and Sept. 1980 color IR photography and field observations. Species identification is also indicated.)

% Canopy Closure Derived From Photographic and Field Ground Truth				Species Identification		
PLOT # (25-ACRE SITE)	MX 221 (Sept. 1981)	U-2 MISSION (Sept. 1980)	FIELD OBSERVATION OF UPPER CANOPY (April 1982)	OVERSTORY	UNDERSTORY	GROUND
1	12.5			*Ponderosa pine/aspen		
2	97.1	97.2	100	Aspen (mature)	(none, no regeneration)	litter
3	5.8			*Ponderosa pine		
4	3.1		0	Englemann spruce/ Ponderosa pine/ aspen	Englemann spruce/ Ponderosa pine/ aspen	grasses/exposed soil
5	5.5	7.4	0	(None)	(None)	meadow/brush
6	4.9	7.5	0	Aspen regeneration (4-6)	(None)	grazed grasses/ exposed soil
7	0.0	0.0		*(None)	(None)	grasses
8	0.0	0.0	0	(None)	(None)	grasses/forbs
9	0.0	0.0	0	(None)	(None)	brush/grasses/ forbs
10	2.8	2.1	5	Ponderosa pine	Aspen	grazed grasses/ exposed soil
11	12.0	12.4	10	Ponderosa pine	gambel oak	grasses/forbs
12	22.1			*Ponderosa pine		
13	30.5			*Ponderosa pine		
14	88.2			*Ponderosa pine		
15	77.1			*Ponderosa pine		
16	75.5			*Aspen		
17	0.0		0	(None)	(None)	grazed grasses
18	0.0		0	(None)	(None)	grazed grasses
19	100.0	100.0	100	Englemann spruce/ sub-alpine fir	(None)	litter
20	97.4			*Englemann spruce/ sub-alpine fir		
21	23.4	12.8		*Aspen		
22	17.7			*Ponderosa pine		
23	45.0			*Ponderosa pine		
24	76.5		60	Ponderosa pine	(None)	gambel oak/ litter
25	55.2			*Ponderosa pine		
26	37.2		25	Ponderosa pine	gambel oak	grasses
27	91.9	79.6		Ponderosa pine		
28	99.5	99.6	100	Aspen	aspen (regeneration)	litter
29	95.1	99.4		*Aspen		
30	79.5			*Aspen		
31	50.8			*Aspen		
32	23.5	24.0	20	Ponderosa pine	gambel oak	grasses/ exposed soil
33	20.1		20	Ponderosa pine	(None)	grasses/ exposed soil
34	39.9		40	Ponderosa pine	(None)	grasses/ exposed soil
35	33.9	46.3		*Ponderosa pine		
36	54.9			*Ponderosa pine		

*Upper canopy species determined by photo-interpretation. No filed observations were made.

B. Ground Truth

Table III displays the results of the percent canopy closure determination from 1) photointerpretation of the TMS overflight Mission 221 photography, 2) photointerpretation of U-2 photography, and 3) field observations. Of those plots located on both photographic data sets, the mean difference between the percent canopy closure determinations was 3.1 percent. The field observations (April 1982) of a subset of the plots indicated close agreement with the photointerpreted results. Thus, the sum of these results lends confidence in the accuracy of the photointerpreted determinations of percent forest canopy closure used as the ground truth data. However, the midrange category of canopy closure (25–75 percent), was unavoidably underrepresented in the ground truth sampling.

Ponderosa pine, aspen, and gambel oak were the dominant tree species in the plots. The extent to which the fall color change might have influenced the spectral properties of the aspen and oak was considered minimal for the date of TMS data acquisition. Most of the plots did not exhibit an understory of trees, although most were covered by dry grasses or forbs, and one-third included exposed soil.

C. Correlation and Regression Analysis

The mean spectral response per band per plot was calculated and analyzed against the transformed ground truth

TABLE IV
RESULTS OF LINEAR REGRESSION ANALYSIS OF PERCENT CANOPY CLOSURE AS A FUNCTION OF TMS REFLECTANCE FROM MISSION 211 DATA
(Canopy closure data were transformed using arcsin square root function to create a normal distribution.)

TMS CHANNEL	r	r^2	m	b
1	-0.764	0.584	-3.695	239.591
2	-0.682	0.465	-2.188	175.172
3	-0.661	0.437	-1.509	124.360
4	-0.142	0.020	-0.246	66.933
5	-0.807	0.651	-2.363	114.685
6	-0.574	0.329	-0.887	116.067
7	-0.763	0.582	-2.588	99.842

r = correlation coefficient
m = slope
b = intercept

data (P_t) for the 32 plots. Table IV shows the results of the linear correlation and regression analysis. The correlations were all negative, with the strongest coefficients occurring for TMS bands, 1, 5, and 7, all bands with spectral coverage not provided by the Landsat MSS.

The linear regression model for TMS band 5:

$$\arcsin \sqrt{\text{percent canopy closure}} = 114.69 - 2.363\ (\text{TMS } 5) \qquad (2)$$

was applied pixel by pixel to the entire TMS data set, although only predictions of percent canopy closure for areas of topographic slope ≤ 10 percent were considered valid based on the ground truth data from which the model was developed. The r^2 value indicates that 65 percent of the variance in percent canopy closure is explained by the regression on TMS 5 response. The regression was found to be significant at the 99.99-percent level. Table V summarizes the predictive performance of the band 5 model for the 32 plots categorized in percent canopy closure ranges of 0–25, 25–50, 50–75, and 75–100, where the percent accuracy of prediction was 67.6, 29.2, 37.5, and 48.7, respectively. Combining the midlevel classes into one range of 25 to 75 percent resulted in a predictive accuracy of 73.9 percent for that range.

A multiple regression model was developed from covariance data and applied pixel by pixel to the TMS data. The model combines TMS bands 3, 4, 5, and 6 in the following relationship:

$$\arcsin \sqrt{\text{percent canopy closure}} = 38.359 + 1.533\ (\text{TMS } 3) + 0.427\ (\text{TMS } 4) - 4.614\ (\text{TMS } 5) + 0.15\ (\text{TMS } 6). \qquad (3)$$

In the development of this model, randomly selected combinations of the independent variables were tested.

TABLE V
SUMMARY OF PERCENT ACCURACY OF PREDICTION OF CANOPY CLOSURE USING TMS 5 MODEL

% CANOPY CLOSURE CLASS	% ACCURACY OF PREDICTION
0 - 25	67.6
25 - 50	29.2
50 - 75	37.5
75 - 100	48.7
0 - 25	67.6
25 - 75	73.9
75 - 100	48.7
0 - 50	77.5
50 - 100	88.1
0 - 100	100.0

TABLE VI
SUMMARY OF PERCENT ACCURACY OF PREDICTION OF CANOPY CLOSURE USING TMS MULTIBAND (3, 4, 5, 6) MODEL

% CANOPY CLOSURE CLASS	% ACCURACY OF PREDICTION
0 - 25	71.2
25 - 50	29.2
50 - 75	35.1
75 - 100	57.2
0 - 25	71.2
25 - 75	60.7
75 - 100	57.2
0 - 50	80.4
50 - 100	82.2

Equation (3) represents the multiple regression model with the best Wilk's Lambda statistic, indicative of significance at the 99.99-percent level, for the models tested. Table VI summarizes the predictive performance of the multiband model for the 32 plots categorized in percent canopy closure ranges of 0–25, 25–50, 50–75, and 75–100, where the percent accuracy of prediction was 71.2, 29.2, 35.1, and 57.2, respectively. The midclasses regrouped to a range of 25–75 percent canopy closure resulted in an accuracy of 60.7 percent for that range.

VIII. DISCUSSION

This study tests for a given set of conditions the relationship of plant matter to spectral response for bandwidths analogous to those of the TM. Specifically, a response in TM 3 is believed to be related to chlorophyll absorption, TM 4 to reflectance and transmittance of the internal leaf structure, and TM 5 and TM 7 to leaf water absorption [8].

In the analysis of the TMS response from each field plot in this study, it is recognized that neither species nor background is a controlled variable. Nevertheless, some statis-

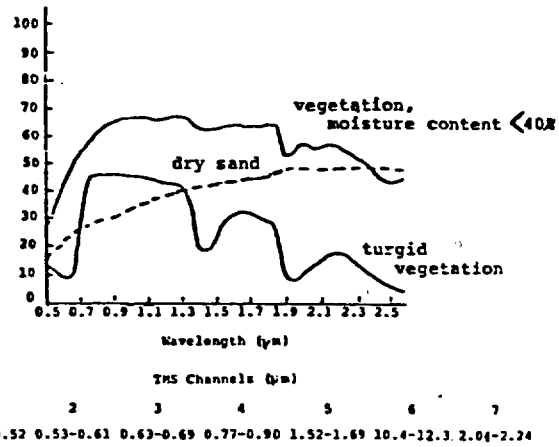

Fig. 1. Generalized spectral response curves for vegetation and soil (after [9, Figs. 5-10 and 5-13]). These curves provide an understanding conditions of high spectral contrast that can occur between background and target.

tically significant results occurred that can be supported by reasonable biophysical explanations.

An analysis of the correlation results for percent canopy closure versus TMS spectral response must address the integrated effect of target and background on reflectance. In this investigation, the correlation between canopy closure and spectral response was negative for all bands, indicating that the mean response decreased as canopy closure increased. If one considers the background of dried grasses or exposed soil, it may be hypothesized that these elements contributed relatively higher reflectance values than did the forest canopy to the overall scene. Plots with a greater percentage of canopy closure, then, also had a lesser percentage of the more highly reflective ground cover contributing to the spectral signature. Indeed, published spectral reflectance curves for vegetation and soil support this idea (Fig. 1). In the figure, reflectance curves for low-moisture-content vegetation and dry sand are both higher than for turgid vegetation.

The absolute correlation coefficient was higher for the relationship between TMS 5 and the transformed percent canopy closure than for any other band. Again referring to general reflectance curves for vegetation and soil in Fig. 1, one may infer that for the interval 1.52 to 1.69 μm corresponding to TMS band 5, it is possible that the distance between curves of turgid vegetation and a background of soil and senescing grasses might be maximized. No data were acquired representing the individual tree canopy and background spectral contributions to substantiate this hypothesis, however.

The low correlation between canopy closure and TMS band 4 was surprising in that this band is assumed to relate to internal leaf structure, which implies a relationship to biomass, at least in the case of herbaceous material. Fig. 2 displays relative signal response curves for three ground truth plots with 0-percent canopy closure and three ground truth plots with nearly 100-percent canopy closure, demonstrating the lack of discrimination in TMS band 4 with respect to the true canopy variable. It is possible that for the particular conditions of the forest target and background soil and grasses in this study, reflective responses measured for the spectral coverage represented by TMS band 4 may have been relatively equal. Fig. 2 clearly demonstrates the greater separability between curves of 0- and 100-percent canopy closure for TMS bands 1, 5, and 7.

Regression models to predict canopy closure from spectral response were developed from the results of this study and applied to each pixel to gain an understanding of the performance of the models and manipulations that could be executed on the imagery.

In development of the regression models to predict canopy closure, the influence of topographic slope as a variable was intentionally minimized. Vegetation species as a variable was minimized to some extent, but not eliminated, as the area considered for the analysis was dominated by ponderosa pine and aspen with lesser coverage by Douglas fir, Engelmann spruce, and gambel oak. Thus, it can be said that valid application of the models to predict percent canopy closure for this environment allows for associations of species and is not restricted to a monospecific condition.

A recommendation for the most accurate technique for prediction of percent canopy closure based on the results of this investigation can be derived by examination of the prediction accuracies summarized in Tables V and VI. It is apparent that these accuracies are lower for the middle classes of canopy closure, i.e., 25–50 and 50–75 percent. Dottavio [3] also noted greater difficulty in estimating canopy closure for the midranges using her incoming solar radiance technique. Regrouping the middle classes into one range class of 25–75 percent raises the accuracy, although the utility of such a broad class may be questioned.

Using only the techniques evaluated in this investigation, a combination of the results from the application of the single-band and multiband models is recommended. The optimum overlaying of the two data sets would include pixels with estimates from the band 5 model only for the 25–75 percent canopy closure class and pixels with estimates from the multiband model for the 0–25 and 75–100 percent classes. By combining results of the two models predictive accuracies for canopy closure classes of 0–25, 25–75, and 75–100 percent would then be 71.2, 73.9, 57.2 percent, respectively.

This investigation focused on correlation analysis and regression model development to predict percent canopy closure from TMS spectral response. A follow-on effort should include an evaluation of other techniques, such as feature extraction, canonical correlation, and brightness/greenness component analyses. It should also include control of obvious variables such as number of species, their distribution within a plot, and the background material. As well, the performance of the models should be evaluated on an independent data set.

IX. Conclusions

Based on the results of this study, the following conclusions were reached:

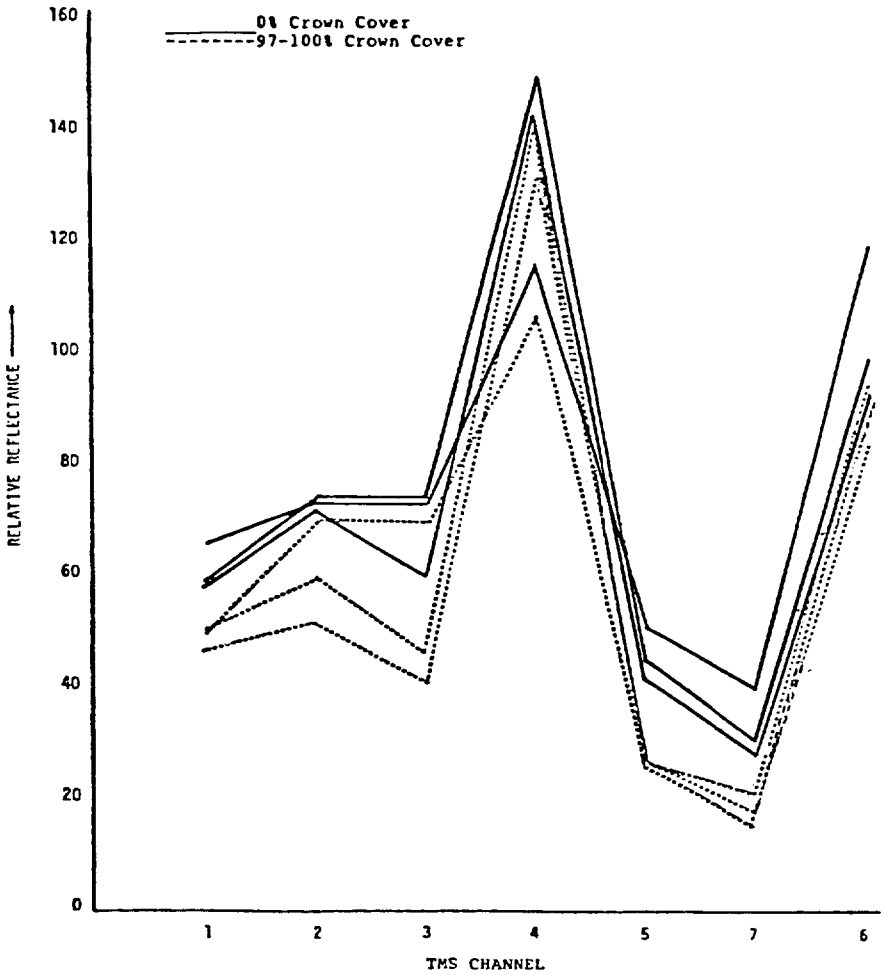

Fig. 2. Graph of relative reflectance versus TMS channels for Mission 221 data. Graphs demonstrate discrimination capability of TMS 5 for canopy closure. (CO test site, Sept. 18, 1981.)

TMS bands 1, 5, and 7, essentially wavelength intervals not covered by the Landsat MSS, proved most significant in relating percent forest canopy closure to spectral response.

The negative correlations resulting from the analysis of percent canopy closure and TMS spectral response for all bands were probably caused by a spectral contribution from the background (dry soil, senescing grasses) with higher reflectivity than that of the forest canopy.

The results of this investigation were specific to ecosystem type, time of year, and absence of slope.

For a given ecosystem, the best predictive model is developed when conditions of greatest spectral contrast between background and forest vegetation occur.

The techniques developed and conclusions reached in this TMS study are applicable to the utilization of TM data.

Acknowledgment

Special thanks are extended to M. Kalcic for her assistance in the statistical analysis in this investigation and to Dr. A. Joyce and J. Ivey for providing direction and coordination of activities related to this study.

References

[1] J. E. Anderson and M. T. Kalcic, "Analysis of thematic mapper simulator data acquired during the winter season over pearl river, MS Test Site," AgRISTARS Tech. Rep. RR-Y1-04217, NSTL/ERL-202. National Technical Information Service, Springfield, VA, 1982.

[2] L. E. Blanchard and O. Weinstein, "Design challenges of the thematic mapper," *IEEE Trans. Geosci. Remote Sensing*, vol. GE-18, no. 2, pp. 146–160, 1980.

[3] C. L. Dottavio, "Effect of forest canopy closure on incoming solar radiance," in *Proc. 1981 Machine Processing of Remotely Sensed Data Symp.* (Purdue Univ., West Lafayette, IN), pp. 375–383, 1981.

[4] C. L. Dottavio and D. L. Williams, "Mapping a southern pine plantation with satellite and aircraft scanner data: A comparison of present and future landsat sensors," *J. Appl. Photo. Eng.*, vol. 8, no. 1, pp. 58–62, 1982.

[5] B. G. Junkin, *et al.*, "ELAS-Earth resources laboratory applications software rep. 183," NASA/NSTL Resources Lab., NSTL Station, MS, 1981.

[6] P. V. Krebs, *et al.*, "Multiple resource evaluation of region 2 U.S. Forest Service lands utilizing Landsat MSS data," Type III—Final Rep. NA55-20948, National Technical Information Service, Springfield, VA, 1976.

[7] V. V. Salomonson, *et al.*, "An overview of progress in the design and implementation of Landsat-D systems," *IEEE Trans. Geosci. Remote Sensing*, vol. GE-18, no. 2, pp. 137–146, 1980.

[8] P. H. Swain and S. M. Davis, Eds. *Remote Sensing: The Quantitative Approach*. New York: McGraw-Hill, 1978, p. 386.

[9] C. J. Tucker, "A comparison of satellite sensor bands for vegetation monitoring," *Photogrammetr. Eng.*, vol. 44, no. 11, pp. 1369–1380, 1978.

M. Kristine Butera (M'84) received the B.A. and M.A. degrees in plant physiology from the University of Missouri at Columbia in 1969 and 1970, respectively.

She is Deputy Program Manager at Science Applications International Corporation in Washington, DC, engaged in contract research for NASA Headquarters. She was principally responsible for the drafting of the revision of the agency-level basic agreement between NASA and NOAA on space-related programs and is currently leading a task to evaluate the status of access and capability for distributed data systems supporting NASA-sponsored Earth Science research. Formerly, she was an employee and principal investigator of NASA from 1974 to 1984 and conducted research and applications in remote sensing of coastal and forested areas from aircraft and satellite platforms. During her employment with NASA, she served as Headquarters Program Manager for fundamental remote-sensing science in the Land Processes Branch of the Office of Space Science and Applications and was involved with the selection of proposals related to the Thematic Mapper Announcement of Opportunity. She also worked at NASA/GSFC in the planning of the Pilot Land Data System and at NASA/NSTL where she conducted AgRISTARS-related studies and coastal remote-sensing investigations. She is a technical reviewer for two remote sensing journals and has published numerous invited papers.

Use of Remotely Sensed Data for Assessing Forest Stand Conditions in the Eastern United States

DARREL L. WILLIAMS AND ROSS F. NELSON

Abstract—**The results of three interrelated research activities conducted by Goddard scientists in support of the AgRISTARS Renewable Resources Inventory (RRI) project are summarized. The central theme of the research conducted at Goddard was the development of techniques for the detection, classification, and measurement of forest disturbances using digital, remotely sensed data. Three study areas located in Pennsylvania, North Carolina, and Maine were investigated with respect to: a) the delineation and assessment of forest damage associated with two different forest insect defoliators, and b) an assessment of the improved capabilities to be expected from Landsat Thematic Mapper (TM) data relative to Multispectral Scanner (MSS) data for delineating forest stand characteristics. Key results include the development of a statewide MSS digital data base and associated image processing techniques for accurately delineating (approximately 90 percent correct classification accuracy) insect damaged and healthy forest. Comparison of analyses using MSS and TM Simulator (TMS) data indicated that for broad land cover classes which are spectrally homogeneous, the accuracy of the classification results are similar. However, TMS data provided superior results (20 percent overall accuracy increase relative to MSS results) when detailed (Level III) forest classes were mapped. These studies also illustrated the utility of having at least one band in the visible, near infrared, and middle infrared portion of the electromagnetic spectrum for assessing specific (Level III) forest cover types.**

I. Introduction

THE RENEWABLE Resources Inventory Project was one of eight research and development projects within the joint program for Agricultural and Resources Inventory Surveys Through Aerospace Remote Sensing (AgRISTARS). The goal of the RRI project was "to develop, test, and evaluate methods for applying new remote sensing technology to the inventory, monitoring, and management of forest land and range land renewable resources" [1]. The RRI project, implemented and managed by the U.S. Forest Service, was conducted as a team effort involving researchers from four NASA Centers and the U.S. Forest Service.

Researchers in the Earth Resources Branch at the NASA Goddard Space Flight Center in Greenbelt, MD, conducted research in support of the RRI project during fiscal years 1980–1982. Goddard had lead role responsibilities in support of RRI Problem Area 4—Detection, Classification, and Measurement of Forest Disturbances. The RRI-related research effort at Goddard was partitioned into the following three tasks.

1) *Sensor comparison study*—The potential utility of Landsat Thematic Mapper data for forest resource mapping was examined relative to capabilities afforded by Multispectral Scanner data.[1]
2) *Forest disturbance assessment*—Techniques were developed and tested to facilitate the use of remotely sensed data to detect, classify, and assess the areal extent and severity of natural or man-induced disturbances of forest land, such as insect damage and clearcutting.
3) *Landsat forest change detection technique development*—Methods for the detection, classification, and measurement of forest change phenomena 5 acres or larger in size were refined using Landsat MSS data. (Note: The Forest Service was conducting a parallel effort to identify changes one to five acres in size using aerial photography.)

Goddard's activities were centered on three sites located in the eastern U.S.: North Carolina, Pennsylvania, and Maine. These sites covered four different major forest cover types found in the U.S., namely, southern pine, Appalachian and northern mixed hardwood, and northeastern spruce-fir (boreal) forests.

The analyses conducted on each study site had different objectives and utilized data from different instruments. In order of presentation, the studies involved: a) the use of MSS data to assess forest disturbances associated with gypsy moth (*Lymantria dispar*) defoliation in Pennsylvania, b) the analysis of TMS data, followed by comparisons to MSS capabilities for forest cover type mapping in North Carolina, and c) an assessment of the utility of simulated TM data for forest cover type mapping, as well as an assessment of the ability to delineate forest damage associated with another defoliator, the spruce budworm (*Choristoneura fumiferana*, Clem.) in Maine. Summaries of each of these research activities are provided in the remainder of the text. The summaries are relatively brief and oriented toward reporting results. A list of references which provide more detailed descriptions of the study areas, data collection activities, and analysis techniques are included at the end of each summary section.

Manuscript received February 15, 1985.

The authors are with Earth Resources Branch, NASA Goddard Space Flight Center, Greenbelt, MD 20771.

IEEE Log Number 8406228.

[1]At the time this research was being conducted, the TM was a "planned" sensor, and was not in orbit. Therefore, there was considerable interest in obtaining advance knowledge of what to expect from data provided by this new instrument.

II. An MSS Digital Data Base to Detect Forest Disturbance (Pennsylvania)

A. Background

In the mid to late 1970's, procedures were developed at Goddard which proved useful for delineating gypsy moth defoliation damage over relatively small areas (i.e., less than one Landsat scene) using Landsat MSS data. These procedures involved: a) the use of multitemporal Landsat data acquired "before" and "after" peak defoliation to facilitate the detection of change associated with the defoliation, b) the use of a simple band ratioing technique to assess the severity of defoliation, and c) the use of a digitally derived forest/nonforest mask to eliminate errors of commission with nonforest cover types when applying forest change detection techniques. The applicability of these procedures to large areas encompassing the equivalent of several Landsat scenes needed to be tested. Under RRI, these procedures were integrated to form an automated system for making annual assessments of the areal extent and severity of gypsy moth defoliation for the entire state of Pennsylvania using Landsat MSS data.

B. Data Base Characteristics

The assessment of insect defoliation damage over an area as extensive as Pennsylvania using Landsat MSS data required the processing and storage of tremendous quantities of data. The state is covered by portions of 10 Landsat scenes, with each scene containing approximately 7.5 million picture elements (pixels). Therefore, a system which could accommodate efficient digital processing as well as storage and retrieval of these data had to be developed.

A data base was created which incorporated Landsat data, thematic information, and digital data products. The data base was registered to the Universal Transverse Mercator (UTM) map projection and output in a grid format consisting of 57-m^2 cells.[2] The data base, which resides on an IBM 370/3081 computer at the Pennsylvania State University Computation Center, includes a number of "layers" of thematic information as depicted in Fig. 1.

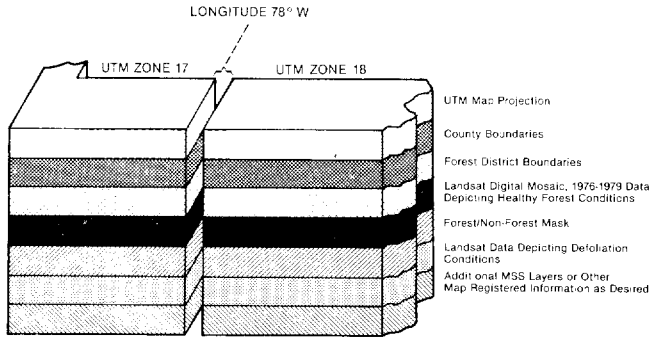

Fig. 1. Characteristics of the Pennsylvania Statewide Digital Data Base.

C. Analysis Procedures

Personnel of the Office for Remote Sensing of Earth Resources (ORSER) at the Pennsylvania State University developed a series of computer programs to facilitate the storage, retrieval, and analysis of data within the data base. With these programs, the user can step through a series of procedures to produce a defoliation assessment image over any portion of the state. The steps involved in a typical analysis scenerio follows.

1) Acquire the most recent MSS data and register it to the data base. This step requires a remote-sensing analyst familiar with image processing software. Steps 2 through 6, however, may be performed by nonremote-sensing personnel.
2) Select the area of interest. County and forest district boundaries are available in the data base. In addition, the user may specify any arbitrary subsection of the state.
3) Apply the forest/nonforest mask. Previous work at Goddard had shown that some agricultural areas are spectrally similar to defoliated forests. To overcome the associated errors of commission, nonforest areas are digitally masked and dropped from consideration. The forest/nonforest mask is an integral part of the digital data base and was developed from Landsat data depicting healthy forest conditions in Pennsylvania between 1976 and 1979. This mask would have to be updated periodically to reflect changes due to forest harvesting activities, regrowth, etc.
4) Calculate the MSS Band 7/Band 5 ratio. This ratio, comprising the near infrared spectral response in the numerator and the red response in the denominator, has been shown to be proportional to the amount of green biomass in the sensor field-of-view [23]. As the amount of green vegetation increases, the 7/5 ratio increases. Defoliated forests thus have low ratios relative to healthy forest.
5) Classify the 7/5 ratio image into defoliated and nondefoliated forest stands. This step entails image thresholding. Work done during this project established an approximate threshold for distinguishing between healthy forest and heavily defoliated forest. Subsequent work has shown that this threshold can vary between Landsat scenes and between years. Hence, a number of classification trials may be necessary to produce an acceptable classification.
6) Produce appropriate output products such as tabular statistics, classification images, or line printer maps.

D. Results

The utility of Landsat MSS data for assessing forest disturbances depends on the success of a preprocessing step—the delineation of forest and nonforest. Studies at Goddard have shown that MSS data can be used to reliably distinguish forested areas from nonforested areas using growing season data. Classification accuracies consistently fall within the 85–95 percent range. The accuracy of the forest/nonforest mask for the entire state of Pennsylvania was

[2]Fifty-seven meters is the nominal pixel size of processed MSS data. The instantaneous field-of-view of the MSS is approximately 80 m.

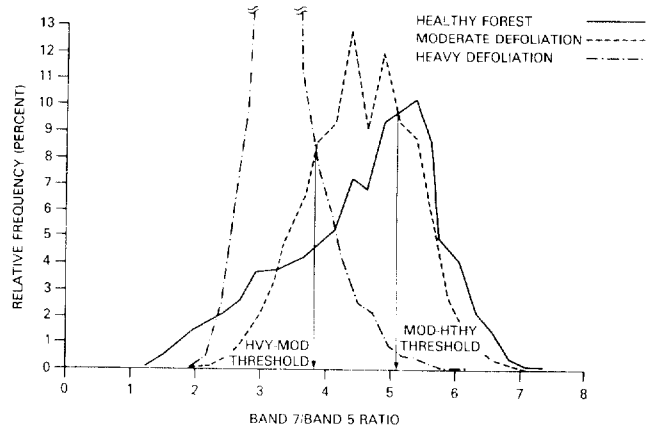

Fig. 2. The near infrared/red (band 7/band 5) ratio response of healthy forest, moderate defoliation, and heavy defoliation.

90 percent. A concise review of the production and assessment of the statewide forest/nonforest mask for Pennsylvania is provided by Russo and Stauffer [21].

The use of Landsat MSS data for delineating gypsy moth defoliation is limited by the spectral characteristics of different levels of canopy damage. MSS data may be used to differentiate heavy defoliation (60–100 percent of the canopy removed) from healthy vegetation. Attempts to differentiate three forest classes—heavy defoliation, moderate defoliation (30–60-percent canopy removed), and healthy forest (0–30-percent canopy removed)—have shown that moderate defoliation and healthy forest are spectrally inseparable (Fig. 2). Hence, only relatively gross canopy differences can be distinguished using Landsat MSS data. MSS defoliation classification results agreed with photo-interpreted results 77 percent of the time when two forest classes were considered (i.e., defoliated and healthy). It should be noted that the MSS-derived classification results were much more detailed at the local level than were the photointerpreted results. With MSS data, a decision is made on a pixel-by-pixel basis, where each pixel represents approximately three to four tenths of a hectare. On the other hand, a photointerpreter tends to assess general conditions over areas within the photo which may comprise several hectares.

The use of MSS data is somewhat limited by the temporal frequency of coverage (16 days), because the temporal window within which defoliation occurs at detectable levels is relatively short. Studies by Nelson [16] indicated that there was, at best, a two-month window from late June to mid-August for assessing gypsy moth defoliation damage. Given the 16-day repeat cycle of the current Landsat 4 and 5 satellites, one has at best three to four chances to acquire useful (i.e., relatively cloud-free) data over any given portion of the state during the window defined by Nelson.[3] Since the eastern states are often obscured by clouds more than 50 percent of the time during the summer months [6], a real problem exists in that one cannot count on MSS data as the only source of information for assessment purposes. Thus, the potential for significant cost savings is negated by the need to have a fallback source of data (i.e., to be safe, one must continue the currently used approach of aerial sketch mapping and/or acquisition of aerial photography).

[3]Actually the number of chances is increased by a factor of two when two satellites are in phased orbit at the same time, which is currently the case for MSS data acquisition by Landsat's 4 and 5.

TABLE I
COMPARISON OF TM/TMS[1] AND MSS SENSOR CHARACTERISTICS

	TM/TMS	MSS
SPECTRAL BAND 1	0.45 - 0.52 μm	0.5 - 0.6 μm
SPECTRAL BAND 2	0.52 - 0.60 μm	0.6 - 0.7 μm
SPECTRAL BAND 3	0.63 - 0.69 μm	0.7 - 0.8 μm
SPECTRAL BAND 4	0.76 - 0.90 μm	0.8 - 1.1 μm
SPECTRAL BAND 5	1.55 - 1.75 μm	
SPECTRAL BAND 7	2.08 - 2.35 μm	
SPECTRAL BAND 6	10.40 - 12.50 μm	
RFOV	30M (BANDS 1-5,7)[2] 120M (BAND 6)	82M
QUANTIZATION LEVELS	256	64

[1] For all practical purposes, TM and TMS waveband configurations are identical. The numbering convention used here is consistent with that used for the TM (see footnote 4).

[2] The RFOV specifications listed here are for the TM. For TMS data, the acquisition altitude above the ground determines the spatial resolution. In this paper, all TMS data were resampled to 30 meter cells.

For more information relative to the development of the Pennsylvania data base and the data analysis software, the following may be consulted: [5], [6], [24], [28], [30]. Works by Nelson [16], [18], [19] provide in-depth discussions of forest change detection using Landsat data and the temporal aspects of gypsy moth damage assessment.

III. MSS and Simulated TM Data for Forest Cover Type Mapping (North Carolina)

A. Background

Two airborne multispectral scanners capable of collecting data with spectral, spatial, and radiometric properties similar to those of the TM (Table I) were developed and flown by NASA Centers to provide simulated TM data to researchers prior to the launch of Landsat-D.[4] The rationale for these data collection/analysis efforts was: a) to allow researchers to become familiar with the improved spatial, spectral, and radiometric characteristics of TM data; b) to permit advance development of new software to take better advantage of the information contained in this data; and c) to quantify the improvements to be expected from TM data relative to MSS data for specific applications [26].

An investigation was undertaken to examine the utility of TM data for forest resource mapping. The study was divided into two segments. The first segment involved a comparison of simulated TM and actual MSS data to determine which sensor was more suitable for forest resources inventory and assessment. The second segment was directed toward developing methods of reducing the large volume of data inherent to the TM sensor by determining the optimum subset of spectral bands for identifying forest cover types.

[4]For all practical purposes, the spectral bands provided by the TM simulator devices were identical to those provided by the TM. However, for both TMS devices, the numbering of the bands differed slightly from the TM due to the inclusion of additional bands, etc. To reduce confusion in this paper, all TMS bands will be identified by their TM equivalent band number.

B. Study Area and Data Collection

The study area encompassed an intensively managed forest plantation located in eastern North Carolina. A full range of forest cover conditions such as recent clearcuts, various stages of growth following artificial regeneration of pine, and natural stands of both pine and hardwood were represented in the study area. An intricate system of logging access roads dissected the area and proved to be useful for accurately identifying any given forest compartment. A detailed analysis and evaluation of the separability of the forest cover types in the area had been previously conducted using multitemporal Landsat MSS data [25].

TMS data were collected over the area on June 14, 1979 with the NASA NS-001/MS instrument. The data acquisition occurred at approximately 9:35 A.M. local time from an altitude above the ground of 6 km. Five of the eight TMS channels were operational at the time of the overflight (TM1, 0.45–0.52 μm; TM2, 0.52–0.60 μm; TM3, 0.63–0.69 μm; TM4, 0.76–0.90 μm; and TM5, 1.55–1.75 μm). Color IR photographs at a scale of 1:40 000 were simultaneously collected with the TMS data, and additional color IR photography at a scale of 1:65 000 had been collected on April 18, 1979. Landsat MSS data were acquired over the site on July 3, 1979 for comparison with the TMS data. A forest type map generated in 1974 and updated from the more recent aerial photos was also available.

C. Comparison of Landsat MSS and Simulated TM Data

After the TMS data had been preprocessed (i.e., radiometric and geometric adjustments to correct for look angle effects, spatial degradation to approximate a sensor having 30-m resolution, etc.), an equivalent area was extracted from the Landsat MSS data, and a set of training statistics was developed for each data set using an ISOCLS [7] clustering function. Using the TMS data set, spectral classes representing the following seven forest types were identified from this training routine: 1) clearcut, 2) regeneration/pine 1–5 years old, 3) pine 6–10 years old, 4) pine 11–25 years old, 5) mature pine greater than 25 years old, 6) mixed pine/hardwoods, and 7) hardwoods. Using the MSS data, spectral classes representing all but the mixed pine/hardwood class could be identified.

The corresponding data sets were then classified using these training statistics and a maximum likelihood classifier. Classification performance was evaluated by extracting a stratified random sample of pixels from the classified images and comparing them to the ground reference data. The classification results are graphically summarized in Fig. 3. The TMS data yielded consistently higher classification performance levels for all cover types, and the overall performance was 60 percent for TMS, as compared to 39 percent for MSS. The markedly higher overall performance derived from the TMS data indicated that TM data would be superior to MSS data for these specific forest mapping purposes.

To compare the performance of the data from the two sensors for mapping general forest cover types, the seven

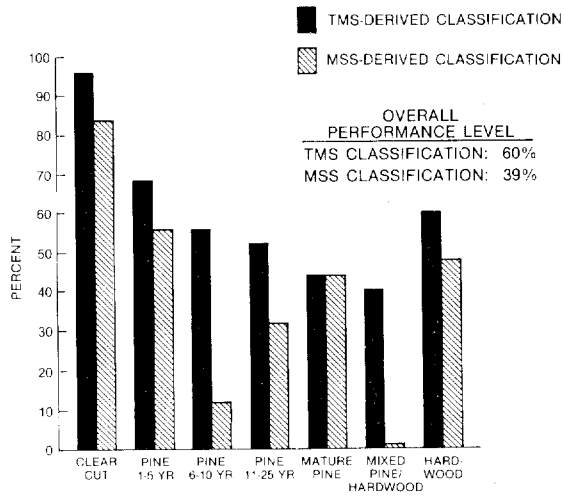

Fig. 3. Comparison of TM simulator and Landsat MSS classification performance levels for detailed forest type mapping.

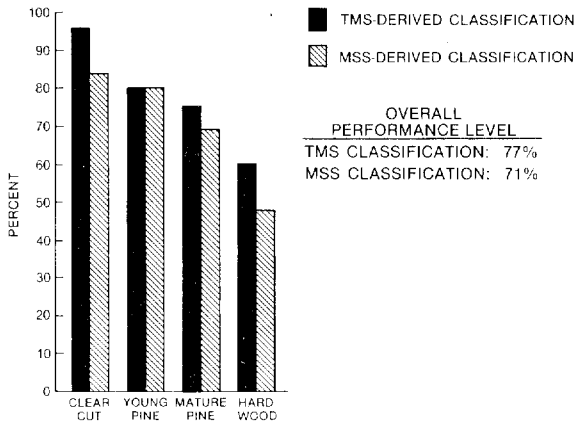

Fig. 4. Comparison of TM simulator and Landsat MSS classification performance levels for general forest cover mapping.

detailed, Level III cover type classes were regrouped into four general, Level II forest cover type classes (i.e., young pine, mature pine, hardwood, and clearcut) and the data were reclassified. In this case, the overall performance was comparable for both data sets (77 percent for TMS and 71 percent for MSS; see Fig. 4).

D. Selection of Appropriate TM Bands

A spectral band selection analysis was initiated to determine if acceptable levels of classification performance could be obtained using only a subset of spectral bands from the TM. If this were possible, data quantity and processing costs could be reduced. A stepwise discriminant analysis was performed on the sample statistics derived from the randomly selected pixels used during the classification performance evaluation conducted in the first phase of this study. Of the five TM bands evaluated for discrimination among forest cover types, the combination that permitted maximum separation of the land cover classes was TM2, TM4, and TM5. The near infrared band (TM4) provided the greatest discriminatory power for forest classes. The middle infrared (TM5) and green (TM2) bands were the second and third bands entered, respec-

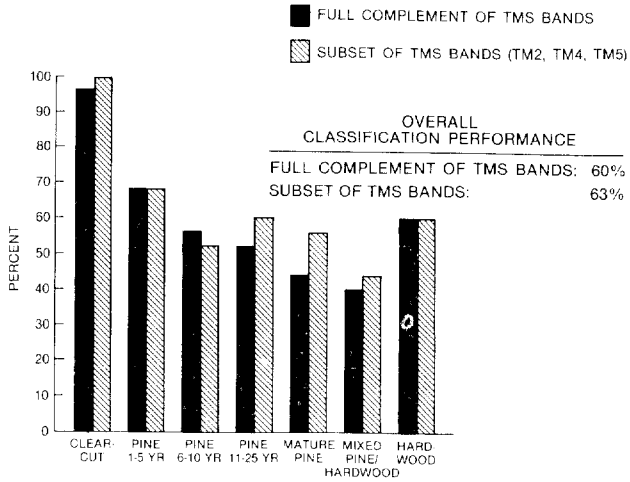

Fig. 5. Comparison of TM simulator classification performance using full complement of spectral bands available and a subset of those bands.

tively. The other wavelength bands did not significantly increase forest class separability and were, therefore, eliminated from consideration.

Following the statistical analyses to determine the optimum combination of TM spectral bands, a third classification was completed for the study area using only data from TM bands 2, 4, and 5. The results of this classification are summarized in Fig. 5, along with a comparison to the results obtained previously using all bands. Classification performance actually increased slightly (63 percent versus 60 percent) when the reduced number of bands were used. Thus, these results indicated that the amount of TM data to be analyzed could be reduced without sacrificing accuracy by selecting the appropriate subset of spectral bands for the specific application of interest.

E. Summary

The following conclusions were drawn based upon this study:

1) For broad forest cover-type classifications, Landsat MSS and simulated TM data provided similar results when the land cover categories were fairly homogeneous.
2) For detailed forest cover-type classifications, TM data provided superior results due to some combination of the spatial, spectral, and radiometric characteristics of the new sensor.
3) Significant challenges will arise in processing the approximate order of magnitude increase in data volume associated with the TM's improved sensor resolution. Reducing the data volume by quantitatively selecting a subset of spectral bands for analysis yielded results comparable to those derived from the full complement of spectral bands. This indicates that spectral band selection provided a suitable alternative for reducing data volume without significantly reducing class separability.

A more complete discussion of the research summarized here may be found in [4].

IV. Simulated TM Data Analyses for Forest Cover and Disturbance Mapping (Maine)

A. Background

Simulated TM data were acquired in order to make prelaunch determinations of the potential utility of TM data for assessing chronic forest disturbances (such as spruce budworm damage) and northern forest stand characteristics. It was felt that the characteristics of the TM data might permit the detection and classification of less obvious, long-term damage such as that caused by the spruce budworm. The research objectives of the study were to a) determine the TM wavebands most useful for differentiating boreal forest cover types and conditions, b) obtain a baseline assessment of classification accuracy as a function of waveband combination, and c) to identify those land cover types subject to confusion (misclassification) and suggest ways to alleviate the confusion.

B. Procedure

On October 12, 1981, TMS data (Texas Instruments RS-18 MS) and coincident aerial photography were acquired over a 23 200-ha study area located approximately 50 km northwest of Millinocket, ME. The study area included a portion of Baxter State Park and territory owned by the Great Northern Paper Company. Two sets of color IR aerial photography were available for the study area; 1:80 000 scale color IR photography was acquired coincidently with the TMS digital data, and 1:7200 scale color IR photography was acquired by the U.S. Forest Service on July 24, 1981. These two photo sets were used to create a digital ground reference data set. Thirteen land cover classes were identified, including three different classes of spruce budworm damage (Table II).

This ground reference data set was registered to the TMS data. Random pixels were chosen from each of the 13 land cover classes in order to spectrally characterize these classes. Stepwise linear discriminant analyses were run on the sampled spectral data in order to identify those spectral bands most useful for differentiating between cover types. Two analyses were run to determine those bands which best discriminated between 1) defoliated and healthy conifer cover types, and 2) all cover types.[5] Land cover classifications were performed using band combinations suggested by the discriminant analyses. The results of these classifications were evaluated using independent, randomly sampled pixels.

C. Results

The results of the discriminant analyses are given in Table III. Note that the band rankings at step 0 indicate band order (most useful to least useful) when the bands are considered individually. The forward stepping band selection identifies the order of band utility in the context of the bands previously entered. The band order suggested by

[5]Those cover types found to be significantly nonnormal in one or more bands (i.e., mixedwood, mixedwood defoliation, strip cut, and water) were not included in the discriminant analyses.

TABLE II
LISTING AND DESCRIPTION OF LAND COVER CLASSES FOUND IN GROUND REFERENCE DATA SET FOR MAINE STUDY AREA

Class	Number of Ground Reference Pixels	Description
1. Clearcut	3349	Predominantly slash on ground
2. Old Clearcut	10447	Some shrub-hardwood regeneration
3. Conifer*	19832	>70% of tree crown area is coniferous
4. Hardwood*	7336	>70% of tree crown area is hardwood
5. Mixed wood*	13228	<70% hardwood and <70% softwood
6. Bog	6102	Alder and spruce bogs
7. Blowdown	6176	<80% of trees standing, remainder blown down
8. Water	17806	
9. Strip cut	11050	
10. Meadow	301	Short shrub or grassland
11. Severe Conifer Defoliation	2691	80–100% of canopy removed
12. Heavy conifer Defoliation	2664	60–80% of canopy removed
13. Mixed wood Defoliation	2298	60–100% of conifer canopy removed

* A area is considered forested if >80% of area is covered by tree crown.

TABLE III
RESULTS OF DISCRIMINANT ANALYSES FOR MAINE DATA SET

a. Defoliated and Healthy Conifer Cover Types:

Cover types considered:
healthy conifer
heavy conifer defoliation
severe conifer defoliation

Alpha level <0.05 (4.0 F-to-enter)

Band Ranking at Step 0, most informative to least informative (F-to-enter in parentheses):

1. band 1 (57.3)	5. band 5 (22.0)
2. band 7 (45.2)	6. band 3 (8.6)
3. band 4 (27.7)	7. band 2 (6.5)
4. band 6 (23.9)	

Forward Stepping Band Selection:

Step 1 -- band 1	Step 3 -- band 5
Step 2 -- band 7	Step 4 -- band 3

Bands 2, 4, and 6 were not entered.

b. All Cover Types:

Cover types considered: All cover types listed in Table 2 except mixedwood, mixedwood defoliation, stripcut, and water.

Alpha level <0.01 (4.0 F-to-enter)

Band Ranking at Step 0, most informative to least informative (F-to-enter in parentheses):

1. band 4 (178.0)	5. band 3 (89.8)
2. band 7 (176.8)	6. band 5 (66.6)
3. band 1 (175.1)	7. band 2 (50.4)
4. band 6 (146.7)	

Forward Stepping Band Selection:

Step 1 -- band 4	Step 4 -- band 7
Step 2 -- band 1	Step 5 -- band 3
Step 3 -- band 5	Step 6 -- band 6

Band 2 was not entered.

the results of the forward stepping discriminant analyses (all cover types) was used to determine the effects of additional spectral bands on classification accuracy. An analysis of the best single band, the best two bands, best three, four, · · · , seven bands showed that test pixel classification accuracy did not increase with the inclusion of the sixth and seventh bands. When the best five TMS bands were used to classify the scene and test pixel accuracies were calculated, the overall classification accuracy was 57.7 percent (TMS classification results compared with photointerpreted ground reference data). The five TMS bands which were used were the blue (TM1), red (TM3), near infrared (TM4), and two middle infrared bands (TM5 and TM7). Table IV reports the individual land cover classification accuracies using these bands.

The land cover classification results in Table IV exhibit a wide range of accuracies. Severe (80–100 percent canopy removed) and heavy (60–80 percent canopy removed) coniferous defoliation were confused with each other and to a limited extent with blowdown. Evidently the TMS data could not be used to distinguish detailed canopy closure classes. However, TMS data did permit the delineation of mixedwood defoliation from the pure conifer damage. Meadows (grassland) were classified very poorly, in part due to the small areal extent of the grassy areas, coupled with minor misregistration problems between the TMS data and the digitized photointerpretation results. Hardwoods, which are often spectrally similar to grasslands, were confused with meadow; however, the greatest source of hardwood misclassification error was the mixedwood defoliation category. This situation may be an artifact of the October 12 data collection date. Hardwood leaves had begun to drop, and the hardwood cover type exhibited a great deal of spectral variability due to fall leaf coloration. On the basis of these results, the following observations were made:

1) The discriminant analyses suggested that useful waveband combinations include at least one band from the visible (0.4–0.7 μm), near infrared (0.7–1.3 μm), and middle infrared (1.3–3.0 μm) spectral regions.
2) The blue band (TM1) proved to be the most useful for discriminating coniferous defoliation categories. The forward stepping selection process ranked the blue band second in overall utility for assessing all cover types.
3) The two middle infrared bands (TM5 and TM7) provided significant spectral information for differentiating all cover type groups considered. TM7 proved most useful for coniferous defoliation assessment, while TM5 proved most useful for differentiating all cover types. The two middle infrared bands do not appear to contain redundant information. The discriminant analyses indicate that TM4 and TM7 contain redundant information since the inclusion of one in the discriminant function precludes or delays the inclusion of the second (compare Step 0 results to the forward stepping results (Table III).

TABLE IV
TEST PIXEL CLASSIFICATION MATRIX USING FIVE TMS BANDS TO DISCRIMINATE 13 LAND COVER CLASSES FOR MAINE STUDY AREA
(Table accuracies are in percent.)

	Ground Reference Data (Air photointerpretation)												
Landsat Classification	Clearcut	Old Clearcut	Conifer	Hard	Mixed	Bog	Blowdown	Water	Strip Cut	Meadow	Severe Con. Def.	Heavy Con. Def.	Mixed, Sev. Def
Clearcut	65.6	12.8	1.6	12.8	0.8	0.8	7.2				2.4	4.0	0.8
Old Clearcut	12.0	71.2	3.2	2.4		3.2	2.4		4.8	1.6			
Conifer	0.8	0.8	50.4		25.6	10.4		0.8	11.2		1.6	3.2	
Hardwood	2.4	0.8		36.0	3.2	2.4	3.2	1.6	1.6	9.6	1.6	2.4	9.6
Mixed Wood		0.8	19.2	0.8	51.2	9.6		2.4	12.8	2.4			0.8
Bog		4.0	9.6	1.6	4.8	57.6	0.8	0.8	11.2	4.0	1.6	1.6	
Blowdown	6.4	3.2	0.8	0.8	1.6	1.6	61.6		5.6	8.0	6.4	15.2	3.2
Water			0.8		1.6			93.6	0.8	0.8			
Strip Cut		4.0	1.6	2.4	7.2	10.4	8.8	0.8	42.4	33.6	1.6	0.8	
Meadow	5.6	2.4	3.2	4.0	0.8		7.2		6.4	25.6	1.6	0.8	0.8
Severe Con. Def.	4.0		1.6	9.6	1.6		6.4		0.8	2.4	64.8	20.0	6.4
Heavy Can. Def.	2.4		7.2		1.6	2.4	2.4		2.4	8.0	13.6	52.0	0.8
Mixed Wd, Sev. Def	0.8		0.8	29.6		1.6				4.0	4.8		77.6
Total	100.0	100.0	100.0	100.0	100.0	100.0	100.0	100.0	100.0	100.0	100.0	100.0	100.0
Number of Test Pixels	125	125	125	125	125	125	125	125	125	125	125	125	125

Total Number of Test Pixels 1625 Overall Accuracy 57.7%

4) Three of the four most useful bands for discriminating northern forest cover types (bands 1, 5, and 7) are not available on the Landsat MSS sensor. Therefore, significant improvements may be expected in the ability to spectrally differentiate these Level II and III land cover categories using TM data.
5) The use of data acquired on October 12 presented problems in terms of adequately describing hardwood spectral variability. The New England fall coloration and subsequent leaf drop should be avoided, especially when dealing with multi-colored cover types such as bogs and coniferous stands which include tamarack (*Larix laricina*, (Du Roi) K. Koch), a deciduous conifer. Data should be obtained during the growing season (June, July, or August). To assess budworm damage, investigators have suggested that mid-July data would be optimal for current year budworm activity, whereas August data should be best for assessing overall tree condition [2].

The reader should realize that the classification accuracies which were obtained were relatively low due to the constraints of the statistical design of the research project. In this study it was important for the classification results to be comparable when different waveband combinations were employed. Therefore, analysts were not permitted to interact or "groom" the class statistics to increase spectral class separability. The lack of analyst interaction in the classification process removes any human bias from the results; unfortunately, it also reduces the accuracies of the resultant products. Therefore, one could expect significant increases in classification accuracy if skilled analysts were allowed to interact in the classification process.[6]

A more complete description of the research conducted on this site may be found in [20].

[6]Williams *et al.* [29] documented a 25-percent increase in percent correct classification accuracy when analysts were allowed to interact in the classification process.

V. DISCUSSION

Based on the results of Goddard's RRI-related research, as well as past and present results published in the remote-sensing literature, one can make generalizations concerning the utility of satellite remote sensing data for forest resource assessment. MSS data are most useful for reconnaissance level forest surveys. MSS data were found to be useful for accurately delineating a) forest from nonforest at accuracies on the order of 90 percent, and b) heavily damaged forest stands (i.e., 60–100 percent canopy removed) from relatively healthy forest stands. However, MSS data could not be used to reliably distinguish between three forest canopy closure conditions (i.e., 0–30 percent, 30–60 percent, and 60–100 percent canopy removed) in the relatively uniform hardwood forests of Pennsylvania.

Previous work by numerous authors (Kalensky and Scherk [12], Williams [25], Fleming and Hoffer [8], Schubert [22], Nelson [17]) has shown that MSS data may be used to discriminate hardwoods, conifers, and other Level II cover types (e.g., grassland/pasture, water, urban, bare soil) at accuracies generally between 70 and 80 percent. Conifers are (in general) classified more accurately than hardwoods; hardwoods generally tend to have spectral responses similar to some grasslands and agricultural crops at certain times of the year. Studies have also shown conclusively that MSS data cannot be used to consistently identify tree species or forest cover types at detailed levels (i.e., Level III) even when topographic data is utilized (Hoffer *et al.* [9], Williams and Ingram [27]). Hence MSS data may best serve as a primary stratification tool in a multistage forest inventory at the regional level.

Work with simulated and actual TM data has shown that the improved spectral and radiometric characteristics afforded by the TM should improve classification performance significantly, especially for delineating detailed Level III categories [3], [15], [20]. Conversely, improvements in spatial resolution from 80 to 30 m can cause classification problems which may merit a change in the

"standard" approaches to classifying a scene. Studies which have used TM or TMS data on forested study sites have produced classification accuracies higher than, equal to, or below equivalent MSS data products [4], [10], [13], [29]. The effects of changing spatial resolution on classification accuracy are discussed and quantified by Markham and Townshend [14] and Irons *et al.* [11]. Evidently digital image processing techniques must be revised in order to handle the spatial and spectral information available in TM data. The information content of the TM data far exceeds that of MSS data, as evident in a visual comparison of MSS and TM imagery.

The remote sensing research community is now faced with the problem of devising algorithms to efficiently extract information from TM data. Until such techniques are developed, photointerpretation of TM image products may be of most immediate benefit to foresters. The imagery has many of the qualities of high-altitude small-scale (1:100 000+) aerial photography. TM photo products, which are available in black and white, true color, and false color infrared, may be used to identify clearcuts, strip cut areas (with strips being only one chain wide, $\simeq$ 20 m), water, bare soil, roads, and, most likely, hardwood and softwood stands. The quality of the small-scale imagery, the synoptic coverage, and the cost of the product behooves potential users to investigate the use of TM imagery if plans are being made to fly a high-altitude reconnaissance mission.

In summary, it is apparent that we now have the capability to assess forest resources on local, regional, and continental scales using data from sensors currently in Earth orbit. There are distinct trade-offs associated with data acquired by different sensors, and the research conducted in support of the Renewable Resources Inventory project helped to develop a better understanding of the applicability of satellite data for forest resource assessment.

References

[1] AgRISTARS, Renewable Resources Inventory Implementation Plan, NASA/Lyndon B. Johnson Space Center, Houston, TX, 1979.

[2] M. D. Ashley, J. Rea, and L Wright, "Spruce budworm damage evaluations using aerial photography," *Photogrammetr. Eng.*, vol. 42, no. 10, pp. 1265–1272, 1976.

[3] M. K. Butera "A correlation and regression analysis of percent canopy closure vs. TMS spectral response for selected forest sites in the San Juan National Forest, Colorado," in Proc. AgRISTARS Symp. NASA/Johnson Space Center, Houston, TX, 1982.

[4] C. L. Dottavio and D. L. Williams, "Mapping a southern pine plantation with satellite and aircraft scanner data: a comparison of present and future Landsat sensors," *J. Appl. Photographic Eng.*, vol. 8, no. 1, pp. 58–62, 1982.

[5] C. L. Dottavio and D. L. Williams, "Satellite technology: An improved means for monitoring forest insect defoliation," *J. Forestry*, vol. 81, no. 1, pp. 30–34, 1983.

[6] C. L. Dottavio, R. F. Nelson, and D. L. Williams, "Final Report: Monitoring the defoliation of hardwood forests in Pennsylvania using Landsat," NASA/Goddard Space Flight Center, Greenbelt, MD, 1983.

[7] *IDIMS Functional Guide*, vol. 1, Electromagnetic Systems Lab. Sunnyvale, CA, 1982.

[8] M. D. Fleming and R. M. Hoffer, "Computer-aided analysis techniques for an operational system to map forest lands utilizing Landsat MSS data," Lab. Applications of Remote Sensing, Purdue Univ., West Lafayette, IN, Tech. Rep. 112277, 1977.

[9] R. M. Hoffer, M. D. Fleming, L. A. Bartolucci, S. M. Davis, and R. F. Nelson, "Digital processing of Landsat MSS and topographic data to improve capabilities for computerized mapping of forest cover types," Lab. Applications of Remote Sensing, Purdue Univ., West Lafayette, IN, Tech. Rep. 011579, 1979.

[10] R. M. Hoffer, M. E. Dean, D. J. Knowlton, and R. S. Latty, "Evaluation of SLAR and simulated Thematic Mapper data for forest cover mapping using computer-aided analysis techniques," Lab. Applications of Remote Sensing, Purdue Univ., West Lafayette, IN, Tech. Rep. 083182, 1982.

[11] J. R. Irons, B. L. Markham, R. F. Nelson, D. L. Toll, D. L. Williams, R. S. Latty, R. L. Kennard, and M. L. Stauffer, "The effects of sensor advancements on Thematic Mapper data classification," in *Proc. 18th Int. Symp. Remote Sensing Environment* (Paris, France), pp. 1759–1773, 1984.

[12] Z. Kalensky and L. R. Scherk, "Accuracy of forest mapping from Landsat computer compatible tapes," in *Proc. 10th Int. Symp. Remote Sensing of Environment*, vol. II, ERIM (Ann Arbor, MI), pp. 1159–1167, 1975.

[13] R. S. Latty and R. M. Hoffer, "Computer-based classification accuracy due to the spatial resolution using per-point and per-field classification techniques," in *Proc. Machine Processing of Remotely Sensed Data Symp.* (West Lafayette, IN), pp. 384–392, 1981.

[14] B. L. Markham and J. R. G. Townshend, "Land cover classification accuracy as a function of sensor spatial resolution," in *Proc. 15th Int. Symp. Remote Sensing Environment* (ERIM, Ann Arbor, MI), pp. 1075–1090, 1981.

[15] "A prospectus for Thematic Mapper research in the earth sciences," NASA/Goddard Space Flight Center, Greenbelt, MD, NASA Tech. Memo 86149, 1984.

[16] R. F. Nelson, "Defining the temporal window for monitoring forest canopy defoliation using Landsat," in *Proc. ASP-ACSM Meet., Tech. Pap.* (Washington, DC), pp. 367–382, 1981.

[17] R. F. Nelson, "A comparison of two methods for classifying forestland," *Int. J. Remote Sensing*, vol. 2, no. 1, pp. 49–60, 1981.

[18] R. F. Nelson, "Detecting forest canopy change using Landsat," NASA/Goddard Space Flight Center, Greenbelt, MD., AgRISTARS Final Rep. RR-62-04258, 1982.

[19] R. F. Nelson, "Detecting forest canopy change due to insect activity using Landsat MSS," *Photogrammetr. Eng.*, vol. 49, no. 9, pp. 1303–1314, 1983.

[20] R. F. Nelson, R. S. Latty, and G. Mott, "Classifying northern forests using Thematic Mapper simulator data," *Photogrammetr. Eng.*, vol. 50, no. 5, pp. 607–617, 1984.

[21] S. A. Russo and M. L. Stauffer, "The statewide forest/non-forest classification of Pennsylvania using Landsat MSS data," NASA/Goddard Space Flight Center, Greenbelt, MD, CSC/TM-83/6073, Contr. Rep., NAS5-24350, 1983.

[22] J. S. Schubert "The Canada land inventory—Computer processing of Landsat data for Canada land inventory land use mapping," Gregory Geosciences Ltd., Ottawa, Ontario, Rep. 13, 1978.

[23] C. J. Tucker "A comparison of satellite sensor bands for vegetation monitoring," *Photogrammetr. Eng.*, vol. 44, no. 11, pp. 1369–1380, 1978.

[24] B. J. Turner and D. L. Williams, "The ORSER Landsat data base of Pennsylvania," in *Proc. Nat. Conf. Energy Res. Management*, vol. 1 (Baltimore, MD), pp. 149–160, 1982.

[25] D. L. Williams, "A canopy-related stratification of a southern pine forest using Landsat digital data," in *Proc. ASP Fall Conv.* (Seattle, WA), pp. 231–239, 1976.

[26] D. L. Williams and M. L. Stauffer, "What can the forestry community expect from Landsat-D Thematic Mapper data?" in *Proc. Symp. Remote Sensing of Nat. Res.* (Univ. of Idaho, Moscow, ID), pp. 475–492, 1979.

[27] D. L. Williams and K. J. Ingram, "Integration of digital elevation model data and Landsat MSS data to quantify the effects of slope orientation on the classification of forest canopy condition," in *Proc. 7th Int. Symp. Machine Proc. Remotely Sensed Data* (Purdue Univ., West Lafayette, IN), pp. 352–362, 1981.

[28] D. L. Williams, C. L. Dottavio, and R. F. Nelson, "Development of a statewide Landsat digital data base for forest insect damage assessment," in *Proc. Auto-Carto 5/ISPRS IV Symp.* (Crystal City, VA), pp. 191–203, 1982.

[29] D. L. Williams, J. R. Irons, B. L. Markham, R. F. Nelson, D. L. Toll, R. S. Latty, and M. L. Stauffer, "A statistical evaluation of the advantages of Landsat Thematic Mapper data in comparison to Mul-

tispectral Scanner data," *IEEE Trans. Geosci. Remote Sensing*, vol. GE-22, no. 3, pp. 294–302, 1984.

[30] D. L. Williams, R. F. Nelson, and C. L. Dottavio, "A georeferenced Landsat digital database for forest insect-damage assessment," *Int. J. of Remote Sensing*, vol. 6, no. 5, pp. 643–656, 1985.

*

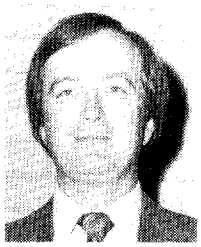

Darrel L. Williams received the B.S. and M.S. degrees in forest science from the Pennsylvania State University in 1973 and 1974, respectively. He is currently working toward the Ph.D. degree in biogeography and remote sensing at the University of Maryland.

He has been employed as a Physical Scientist in the Earth Resources Branch, Laboratory for Terrestrial Physics, NASA Goddard Space Flight Center, since 1975. His research at Goddard has involved the development of techniques to enhance the utility of digital remotely sensed data for assessing the forest canopy. He served as Landsat-4 Assistant Project Scientist from 1979 through 1983.

*

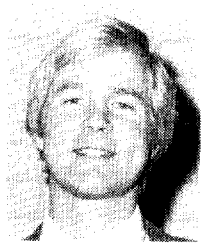

Ross F. Nelson received the B.S. degree in forest management in 1974 from the University of Maine, Orono, and the M.S. degree in forestry/remote sensing in 1979 from Purdue University.

As a Physical Scientist in the Earth Resources Branch at the NASA Goddard Space Flight Center since 1979, he has been involved with the use of digital remotely sensed data for assessing the forest canopy. He has worked with Landsat MSS data to evaluate gypsy moth damage, Thematic Mapper Simulator data to evaluate spruce budworm damage, and AVHRR and MSS data to assess deforestation in South America. He has worked with geobotanical scientists to determine the effects of mineralization on forest canopy condition, and is investigating the utility of laser-induced fluorescence for tree species identification.

Coniferous Forest Classification and Inventory Using Landsat and Digital Terrain Data

JANET FRANKLIN, THOMAS L. LOGAN, CURTIS E. WOODCOCK, AND ALAN H. STRAHLER

Abstract—**Accurate cost-effective stratification of forest vegetation and timber inventory is the primary goal of a Forest Classification and Inventory System (FOCIS) developed at the University of California, Santa Barbara, and the Jet Propulsion Laboratory, Pasadena. Conventional timber stratification using photointerpretation can be time-consuming, costly, and inconsistent from analyst to analyst. FOCIS was designed to overcome these problems by using machine-processing techniques to extract and process tonal, textural, and terrain information from registered Landsat multispectral and digital terrain data. FOCIS was developed in northern California's Klamath National Forest (KNF), where the rugged terrain and diverse ecological conditions provided an excellent area for testing Landsat-based inventory techniques. The FOCIS procedure was further refined in the Eldorado National Forest (ENF), where the portability and flexibility of FOCIS was verified.**

Using FOCIS as a basis for stratified sampling, the softwood timber volume of the western portion of the Klamath (944 833 acres; 422 340 ha) was estimated at 3.83×10^9 ft^3 (1.08×10^8 m^3), with a standard error of 4.8 percent based on 89 sample plots. For the Eldorado, the softwood timber volume was estimated at 1.88×10^9 ft^3 (0.53×10^8 m^3) for an area of 342 818 acres (138 738 ha) with a standard error of 4.0 percent, based on 56 sample plots. These results illustrate the power of FOCIS methods to produce timely accurate large-area inventories with comparable accuracies and reduced costs when compared to conventional timber inventory methods.

Key Words—**Classification, timber inventory, digital terrain data, forest vegetation, Landsat.**

I. Introduction

IN FORESTRY and range science, the need often arises to sample and inventory natural vegetation. Conventional methods use manual interpretation of aerial photography to delineate areas of homogeneous vegetation (termed stands) using attributes of image tone, texture, and topography. Stands with like attributes are then grouped into strata from which samples are drawn to yield inventory data that describe attributes of interest of the natural vegetation. Because this process is based on manual photointerpretation, it can be time-consuming and costly, as well as inconsistent from analyst to analyst. In this paper we describe an automated system for natural-vegetation inventory which utilizes digital image processing of multispectral Landsat data and registered digital terrain information. This technology, referred to as the Forest Classification and Inventory System (FOCIS), has shown the capability to classify and stratify forest vegetation for timber-volume inventory as precisely and more cost-effectively than conventional methods of manual photointerpretation.

An earlier article discussed the general nature of the problem of stratifying registered digital terrain and Landsat data for timber and rangeland inventory, and included a brief review of FOCIS procedures as they existed at that time [1]. This article focuses on some of the more important procedural steps in FOCIS, and describes the accuracy of timber inventories of the Klamath and Eldorado National Forests using FOCIS procedures. Technical details concerning the information-extraction process can be found in our technical reports [2], [3].

Thus far, FOCIS presents the only example of a fully integrated methodology for conducting large-area timber inventory using satellite and DTM data, although a number of studies have employed Landsat data (and, for some, digital terrain data as well) in forest cover type mapping [4]–[7]. Unfortunately, an extensive review of the various approaches that have been utilized is beyond the scope of this paper.

II. Background

A. Conventional Methodology for Timber-Volume Inventory

To provide a background for the description of FOCIS, we will summarize the conventional methodology used to produce timber volume estimates by Region 5 (California) of the U.S. Forest Service. Timber inventory is executed in three steps: stand mapping, stratification, and sample collection and data processing.

Foresters skilled in air photo interpretation use conventional resource photography to delineate timber stands by drawing boundaries around areas of uniform vegetation of at least 10 acres (4 ha) in size.[1] These stand boundaries are transferred from the air photos to $7\frac{1}{2}$-min topographic quadrangles, and labels are affixed to each stand indicat-

Manuscript received May 8, 1985; revised July 18, 1985. This work was supported by NASA under Contract NAS-9-15509, by the USFS-UCSB under Joint Agreement 37, by the USFS under Contract 53-91S8-0-6362, and by the California Institute of Technology's President's Fund, Award PF-123, under NASA Contract NAS-7-100.

J. Franklin is with the Department of Geography, University of California, Santa Barbara, CA 93106.

T. L. Logan is with the Jet Propulsion Laboratory, California Institute of Technology, Pasadena, CA 91103.

C. E. Woodcock is with the Department of Geography, Boston University, Boston, MA 02215.

A. H. Strahler is with the Department of Geology and Geography, Hunter College of the City University of New York, New York, NY 10021.

IEEE Log Number 8406237.

[1]Since American forestry still uses English units, this research was planned and carried out in the English system. Accordingly, English units are shown first with metric equivalents in parentheses.

ing the species composition, height, crown density, and other features of interest for forest-management purposes.

The next step is to scan photomechanically a photographic transparency of the stand boundaries as scribed on each quadrangle. The output of the scanner, stored on computer-compatible tape, is read by the RID*POLY software system, a polygon-based digital cartographic information system developed by the Forest Service [8]. Stratification of the stand maps for inventory then follows. All unique stand labels are aggregated to form a dozen or so strata that are differentiated with respect to per-acre timber volume by attributes of crown density, height, and species composition. The area of each stratum within each quadrangle can be obtained by interrogating the RID*POLY database.

Sample locations for the collection of timber-inventory data are chosen from a subset of all $7\frac{1}{2}$-min quadrangles in the Forest using a random method that weights the probability of selection of a quadrangle by Forest-owned area and within-stratum area. The number of samples allocated to each stratum is determined by the variability in per-acre timber volume anticipated within the stratum. Assuming a typical coefficient of variation of 0.5, six samples per stratum will yield an areal inventory estimate with a standard error of 6–7 percent of the mean.

The last phase of timber inventory is the collection and processing of plot data from the designated locations, yielding mean per-acre timber volumes for strata and total timber volume by species. The means are then weighted by the areas of their respective strata, and the total timber volume by species, as well as other inventory statistics, is calculated.

The methodology described above has two disadvantages. First, conventional photointerpretation is time consuming, costly, and can be inconsistent when more than one photoanalyst is involved. Second, the digitizing and labeling of stand maps required to enter them into the RID*POLY database is costly, time consuming, and prone to error. The Forest Classification and Inventory System described in this article bypasses manual photointerpretation by using automatic classification of Landsat and registered digital terrain data. Labeling of the automatically defined classes is still required, but this labeling can be done much more rapidly and cost-effectively than in the conventional procedure. And, because FOCIS utilizes the raster-based VICAR/IBIS software system [9], [10], the classified images of stands that serve as maps can be directly interfaced through software to the polygon-format files of the RID*POLY system [3].

B. Test Areas

The Klamath National Forest (KNF), located in northern California, is the study area where FOCIS was developed and initially tested (Fig. 1). The Forest includes approximately 2500 mi^2 (6700 km^2) of rugged terrain in the Siskiyou, Scott Bar, and Salmon Mountains. It provides approximately 260×10^9 board-feet (61 000 m^3) of timber per year, ranking sixth nationally in timber production.

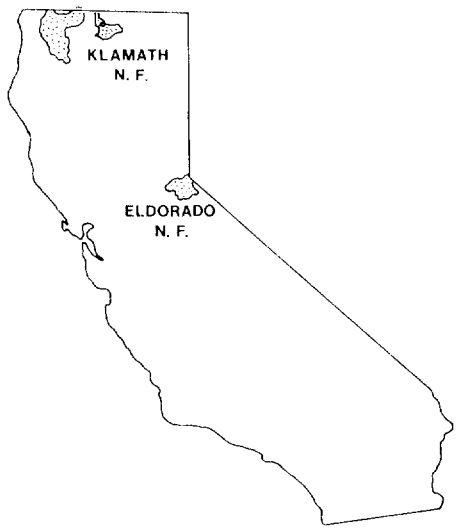

Fig. 1. Index map showing locations of Klamath and Eldorado National Forests within California.

Past research conducted in the KNF includes species-specific forest cover classification [11], [12], and modeling timber-volume proportions of species and ecological relationships of species to terrain [13]. Its high relief and diverse ecological conditions throughout made this Forest an excellent location to develop and test Landsat-based forest classification and stratification techniques.

The results of the Klamath inventory were sufficiently encouraging that the Forest Service contracted with us for an inventory of the Eldorado National Forest (ENF), located in the central Sierra Nevada of California. The ENF includes about 900 mi^2 (2400 km^2) on the west slope and crest of the Sierra Nevada, with similar species composition to the KNF, but variations in species-terrain relationships, and different physiography. This work provided an opportunity to test the flexibility of FOCIS methods and illuminate new problems not encountered in the development of FOCIS in the Klamath.

III. FOCIS Procedure

A. Introduction

To introduce our discussion of the FOCIS procedures, it will be helpful to 1) discuss the concept of regional types; 2) briefly describe our treatment of image texture; and 3) present an outline of the stratification steps.

In conventional stratification of forest vegetation for large-area inventory, three attributes characterize each stand: tree height, crown density, and regional type. Regional type refers to species composition and is often defined by the dominant species on the stand (e.g., red fir, Douglas fir, ponderosa pine, or mixed conifer). It is important to distinguish between regional types because, for a given size and density, the timber volume will differ with regional type. This difference is related to the growth form of the species and the productivity of the site.

Because forest composition varies systematically with terrain in many western conifer forests, regional type can be modeled using elevation and slope orientation (aspect) data. The simplest method of expressing the relationship

between elevation, aspect, and regional type involves systematically observing regional type at all aspects and elevations, and plotting regional type on a graph with elevation and the cosine of aspect as axes. The regional type of any point on the ground can thus be predicted by determining the elevation and aspect of the point and then consulting the graph. This procedure is discussed in more detail in a following section.

The FOCIS automated stratification procedure uses the same three characteristics of tone, texture, and terrain that the photointerpreter uses in delineating timber stands. Landsat multispectral reflectance data provide tonal and textural information and digital elevation models provide the required terrain information.

Classification of the Landsat and texture data into size-and-density-based strata using FOCIS is accomplished in the following steps[2]:

1) unsupervised clustering;
2) statistical editing;
3) classification using a hybrid parallelepiped/maximum-likelihood classifier;
4) differential illumination compensation; and
5) spatial-spectral editing and labeling of strata.

This basic procedure was refined in the ENF to include:

6) iterative clustering, classification, and editing; and
7) spatial simplification to provide a stand map with stands of a minimum areal extent.

B. Digital Terrain Processing

Digital terrain data for the Klamath and Eldorado National Forests were obtained from the National Cartographic Information Center. For the Klamath, data were of the DMA series, produced by scanning of 1:250 000 contour maps. For the Eldorado, Digital Land Mass Simulator data were used. In this type of digital terrain model, an elevation is provided for each 3-s interval on a geographic grid. In the Klamath, terrain data were registered to the Landsat image using a geometric resampling algorithm that employs a two-dimensional correction grid derived from control points. In the Eldorado, Landsat and terrain data were each registered to Universal Transverse Mercator projection using a similar procedure.

After registration of the Landsat and terrain data, separate images of slope angle and aspect were generated from elevation by the least squares fitting of a plane through each pixel and its four nearest neighbors. The aspect image was then transformed using a cosine transformation with a shifted axis, following the suggestion of Hartung and Lloyd [14]. The transformation was: cos (aspect–45°). This function is based on the ecological observation that sites on northeast-facing slopes are most productive, those on southwest-facing slopes are least productive, and those on southeast and northwest slopes are intermediate. This phenomenon has been observed in other areas [15]–[17], and is documented in the Klamath and Eldorado by our regional type graphs (discussed in a following section).

[2]Except as noted, the procedures discussed below are the same for the Klamath and Eldorado National Forests.

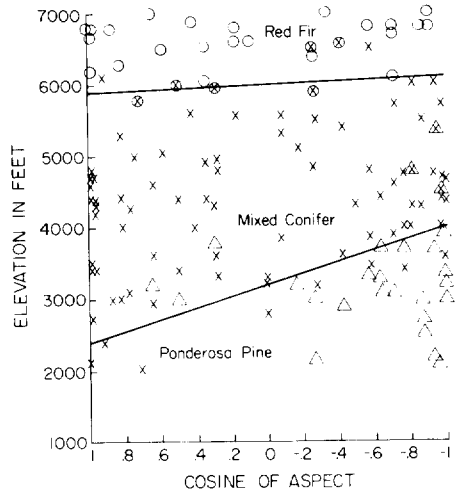

Fig. 2. Regional-type field graph for Doggett Natural Region, Klamath National Forest. Points plot regional type as observed in the field: red fir (circles), mixed conifer (×'s), and ponderosa/Jeffrey pine. Lines divide elevation/aspect space into areas associated with the three regional types. (Note: triangles on lower right above lower line denote pine sites on serpentine, which are atypical of the region as a whole and were ignored when fitting the line.)

C. Modeling Regional Type Using Digital Terrain Data

Observations in the Klamath, Eldorado, and other western coniferous forest areas have shown that forest composition typically varies systematically with topography, responding regularly to changes in elevation and slope aspect. Aspect tends to influence elevational relationships; north to northeast exposures are typically more favorable for tree growth than drier southwestern exposures, so that species exhibiting elevational zonation tend to occur at lower elevations on northeast-facing slopes.

Regional type is a level of classification used by the U.S. Forest Service to divide forests into broad categories based on species composition. In the Klamath, four regional types were recognized: red fir (*R*), mixed conifer (*M*), Douglas fir (*D*), and ponderosa/Jeffrey pine (*P*); In the Eldorado, only three were present: red fir, mixed conifer, and subalpine conifer (*SA*). The subalpine type was found in the Eldorado only within the Desolation Wilderness area. Although this type was mapped, no samples were allocated to it since harvesting is not possible within the wilderness area. Consequently, timber volume calculations omitted this type.

Field graphs were used to model regional type from the digital terrain data (Fig. 2). To construct the field graphs, elevation, aspect, and regional type were observed at locations chosen to represent the full range of the elevation-aspect combinations. Types were then plotted by elevation and by cos (aspect–45°). Lines fitted by eye partitioned the elevation-aspect measurement space into areas representing each regional type.

Functions defining those lines were input to a VICAR image-processing program to determine the most likely

Fig. 3. Regional-type map for Doggett Natural Region, Klamath National Forest. Lightest tone is ponderosa/Jeffrey pine; medium tone is mixed conifer; dark tone is red fir. Black areas are outside region. White lines show road net, digitally scribed on image from regional maps.

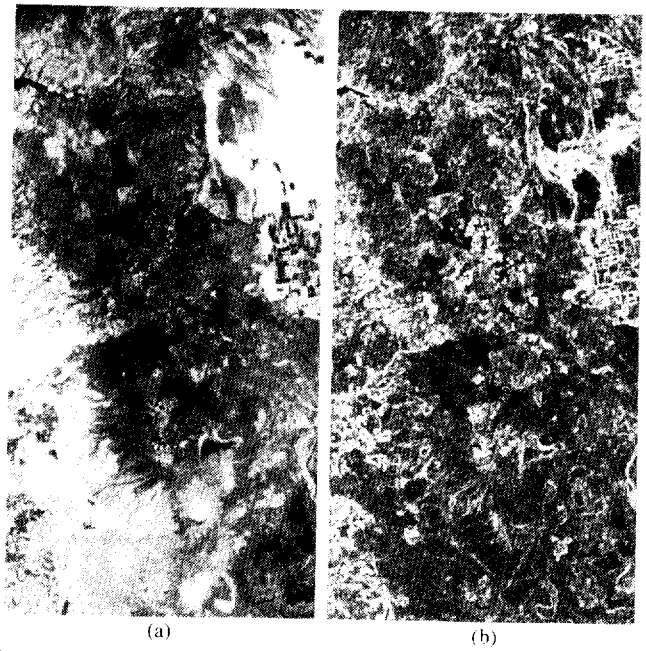

(a) (b)

Fig. 4. (a) Landsat MSS Band 5 image of portion of Goosenest Ranger District of Klamath National Forest. (b) Standard deviation texture image of same area.

regional type for each pixel in the terrain image based on the elevation and aspect of the pixel. In this way, a new registered image was created in which the value of each pixel specified a regional type (Fig. 3).

D. Natural Region Concept

The FOCIS stratification procedure was not applied to an entire Forest at once, but rather to a group of smaller geographical areas called natural regions. Because a large forest may exhibit extensive climatic, geologic, and ecological diversity, species-terrain relationships and the spectral signatures that characterize particular timber types are not likely to be the same in all portions. Therefore, the forests were divided into natural regions in which ecological relationships remain fairly constant and signature extension should be valid.

Natural regions were designated primarily on the basis of the field graphs described above. Elevation-aspect ranges of the various regional types must remain constant within a region. A natural region boundary has therefore been crossed when the elevation-aspect range of a regional type shifts significantly or a new regional type appears. In the KNF, which is particularly large and diverse, eight natural regions were defined for this study: two in the eastern Goosenest Ranger District and six in the larger western portion of the Forest. Three natural regions were identified in the ENF: the Northern and Southern natural regions in the western portion of the forest at lower and middle elevations, and a higher elevation Alpine region in the eastern portion.

E. Landsat- and Texture-Based Classification

The second stage of the stratification process used Landsat and texture data to assign a label indicating tree height and density to each pixel within a natural region. Landsat imagery was acquired from EROS Data Center. The Klamath scene was imaged on July 15, 1976, by Landsat-2. The Eldorado scene, from Landsat-3, was imaged on August 15, 1980.

The use of texture derived from Landsat multispectral data greatly increased the ability to discriminate timber-volume strata in the FOCIS procedure. The use of texture by photointerpreters for forest-stand discrimination is well established, but digital texture information has not been widely incorporated into Landsat-based classifications. A simple texture measure was derived from Landsat Band 5 by calculating the standard deviation of reflectance numbers within a 3×3 moving window. This standard deviation value was scaled, assigned to the center pixel of the 3×3 window, and output as a new data plane. In forested areas, low standard-deviation-texture values indicate continuous canopy cover and higher values are associated with areas of discontinuous canopy. The largest texture values occur at abrupt vegetation boundaries, thus enhancing edges (Fig. 4).

F. Clustering and Classifying the Landsat Image

The classification of an area into height- and density-homogeneous classes was based on five information channels: four Landsat MSS bands and the synthesized texture channel. Unsupervised clustering was performed using a modified version of an algorithm obtained from Pennsylvania State University, and implemented as the VICAR program USTATS. The algorithm is based on a method suggested by Tryon and Bailey [18] for clustering large numbers of observations. When the process is completed, clusters found are ranked from largest to smallest, and a user-specified number of clusters is retained to define

classes for input to classification programs. Through classification trials, the 200 largest cluster classes were found to contain all the significant variation in the forested portion of the image. This number was thus retained for future processing.

Because the clustering process produces an unwieldy number of tightly defined classes, the classes are edited and assigned stratum labels in two steps. The first step is interactive spectral editing, based on the spectral similarity of classes. Second is a spatial-spectral editing and labeling, in which classes are combined into strata depending on their spatial contiguity as well as spectral similarity.

For spectral editing, a VICAR program was written to calculate a symmetric matrix of standardized Euclidean distances between all class centroids, and construct a dendrogram and list of class means using a complete linkage algorithm [19]. In the editing process, classes are either merged, pooled, or deleted. Because the editing is not automated, the analyst can compensate easily for variations in scaling and relative importance of the various layers of the database, drawing on knowledge of the forest characteristics. Usually, 70 to 100 spectral classes will remain after the spectral-editing phase. A hybrid parallelepiped/maximum-likelihood classifier is then used to assign each pixel in the image to one of these spectral classes.

G. Differential-Illumination Compensation

Although a large number of tightly defined spectral classes are retained, some are found to contain more than one height-density class when they are inspected on a display monitor. This variation is not the result of loose spectral definition, but is produced by differential illumination of slopes caused by the combination of high topographic variation and an oblique sun angle at the time of the Landsat overpass. More densely stocked areas with "normal" illumination can have the same spectral reflectance as more sparsely stocked areas in poorly illuminated or shaded areas. This problem, also noted by Sadowski and Malila [20], ruled out the separation of forest strata based solely on spectral reflectances.

To account for this differential-illumination effect, the registered terrain data were used to model illumination conditions on a pixel-by-pixel basis. For each pixel z, the angle between a normal to the land surface and the sun at the time of the Landsat overpass, was calculated. For a diffuse (Lambertian) reflector, the apparent brightness of a surface under constant illumination at an angle z will be proportional to cos (z). Thus, the cos (z) image displays the brightest values for pixels directly facing the sun and the darkest values for pixels in shade (Fig. 5). From the cos (z) image, a mask was created to divide the image into two categories based on illumination: well illuminated and poorly illuminated (shaded). The cutoff between these two categories was an angle of $z = 60°$. Using this cutoff, approximately 10 percent of the image was considered shaded in the KNF. Another, related problem is shadowing due to adjacent terrain features. In processing, we did not specifically check for this effect. With a sun elevation angle of about 53° at the time of the Landsat overpass, steep northeast-facing cliffs would be required to produce such shadowing, and in any event the areas in shadow would comprise only a very small portion of the image.

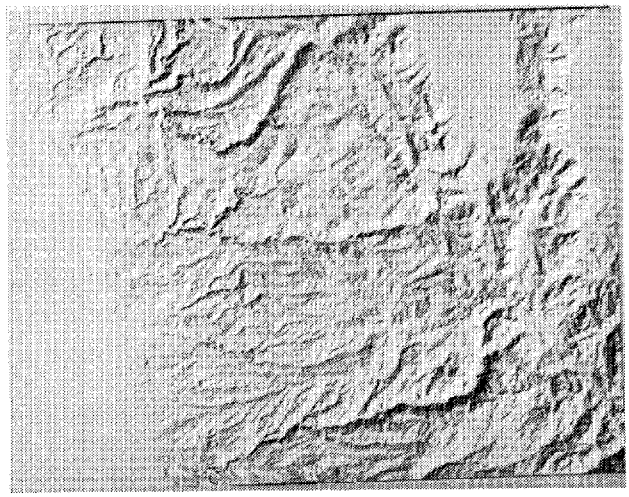

Fig. 5. Cos (z) image for area containing Eldorado National Forest. Light areas directly face the sun; dark areas are illuminated at oblique angles. Derived from slope and aspect images obtained by processing the digital terrain model. Lake Tahoe is the flat surface at the upper right.

The mask of shaded and well-illuminated pixels was then digitally added to the classified image, serving to divide each spectral class into shaded and unshaded components. This effectively reduced the within-class variation and removed a potentially adverse effect on the stratification process. Since only 10 percent of the image was shaded, however, many classes remained undivided.

In the Eldorado, the terrain is less rugged and illumination masking was only required in the northern natural region, where the Rubicon River canyon produced deeply shaded slopes. Using a similar illumination cutoff, only 1.5 percent of the natural region was shaded, and only a few shaded classes needed to be labeled separately from their unshaded components.

H. Spatial-Spectral Editing

The spatial-spectral editing phase is the most analyst-intensive of the stratification process and involves the aggregation of classes that are spatially continuous as well as spectrally similar. This phase constitutes the final editing in the classification process and serves to reduce the number of classes to approximately the same number of height and density strata differentiated by the Forest Service. Spatial contiguity of classes is established by interactive viewing of the classified image on a color video display that allows the viewing of up to six color-differentiated classes overlaid on a Landsat background image. While the classes are displayed, aerial photographs of selected test areas are inspected to verify that classes to be aggregated contain trees of similar size and spacing.

As they are created, height-density labels are attached to the new classes. The labels follow U.S. Forest Service notation [21]. For height, labels 2, 3, and 4 were used to indicate crown diameters of 12 ft (3.6 m), >12–24 ft

(>3.6–7.3 m), and >24–40 ft (>7.3–12.2 m), respectively; stand densities were noted as *S* (sparse), *P* (poor), *N* (adequate), and *G* (good), indicating crown closures of 10–19, 20–39, 40–69, and 70–100 percent, respectively. In the western portion of the Klamath National Forest, 10 height-density types remained after the spatial-spectral editing phase for all natural regions. In the Eldorado, 5 height-density types remained, corresponding to new Forest Service policy to merge *N* with *G* and *S* with *P* density classes.

I. Natural Regions and the Landsat Classification

Because the spectral signatures that characterize particular timber types are not constant over large areas, each natural region should be classified and stratified separately. However, to reduce time and cost, we carried out unsupervised clustering, spectral editing, classification, and differential-illumination compensation for four of the six natural regions in the western KNF pooled together; the remaining two regions were also pooled to reduce processing time. Although this procedure may possibly have restricted the number and composition of spatial-spectral classes extracted from the image base, the final editing and labeling of classes were carried out independently for each region.

An important modification to the stratification procedure was made for the Eldorado. After the image was edited to 70 to 100 classes for labeling, the largest classes were too heterogeneous with respect to tree height and stocking to be assigned accurate labels. This was due to the small dynamic range of the Landsat spectral values observed in the forested areas. To solve this problem, an iterative procedure that repeated the clustering, classifying and labeling sequence was used. Classes that appeared heterogeneous or hard to label were pooled, reclustered using a smaller cluster size parameter, and reclassified. Up to three such iterations were performed. Thirteen to 16 percent of the area in each natural region remained after well-defined classes were labeled, and these remaining pixels produced another 50 to 100 classes for labeling. This change illustrates the ease of modification to the FOCIS procedures and the importance of analyst interaction in applying the technology to the stratification of diverse and heterogeneous natural vegetation.

J. Merging Regional Type and Height-Density Classes

To derive the final strata, the regional type map and the Landsat- and texture-based height-density classification were merged, thus providing each pixel with a combined height-density regional-type label. This merging was accomplished by scaling the regional type image in multiples of the number of height-density classes and adding the height-density image. In the KNF, there were four regional types and 10 height-density classes. In the ENF, there were three regional types and four height-density classes. With these values, 40 and 12 strata, respectively, could have resulted from this addition, but all possible combinations did not occur. Further, some strata contained very few pixels and were merged with similar types. The selection of those strata to be retained for final output was based primarily on areal extent, with large strata always preserved. The final strata retained for sampling are listed in Table I.

TABLE I
WEST KLAMATH TIMBER INVENTORY

Stratum	Mean Volume	Standard Error	Number Of Plots	Area	Stratum Volume	Standard Error
D3G	56.88[1]	25.778[1]	4	25,771[2]	1,465,855[3]	332,162[3]
D3N	38.74	22.758	4	25,127	973,420	285,920
D3P	20.95	11.023	4	26,663	558,590	146,953
D4N	40.42	18.044	11	81,797	3,306,235	445,015
D4P	33.37	27.894	3	48,451	1,616,810	780,284
MS	27.75	21.904	4	127,403	3,535,433	1,395,317
M2P	19.81	10.833	4	22,679	449,271	122,841
M3G	40.25	25.635	4	87,005	3,501,951	1,115,187
M3N	41.90	26.525	4	100,800	4,223,520	1,366,360
M4G	89.09	21.858	4	121,220	10,799,430	1,324,813
M4P	62.58	0.569	2	174,685	10,931,787	70,283
PS	21.97	18.396	4	14,862	326,518	136,701
P2G	44.11	9.329	3	5,629	248,295	30,318
P2N	18.82	8.858	4	10,768	202,654	47,691
P3G	54.14	13.789	4	4,068	220,242	28,047
P3N	35.21	11.763	4	8,548	300,975	50,275
P3P	15.15	3.745	4	20,277	307,197	37,969
R3G	47.75	15.900	7	18,060	862,365	108,534
R3P	24.93	25.650	4	14,155	352,844	181,538
R4G	54.52	25.740	7	6,915	377,006	67,275
TOTALS			89	944,883	44,561,143	2,801,326

[1] Units are hundreds of cubic feet per acre.

[2] Units are acres.

[3] Units are hundreds of cubic feet.

K. Spatial Filtering

Conventional timber inventories are obtained by sampling from stand maps produced from photointerpretation. These typically contain stands of some minimum size. However, because there are no spatial contraints on the FOCIS classification, the final classification maps produced have a minimum resolution of 1 acre (0.4 ha) (the area corresponding to a pixel after resampling), and therefore these maps often exhibit a complex spatial pattern. While a classification this detailed can serve as a sampling base for inventory, the units in the classified image are too small for management purposes. Thus, in the Eldorado the FOCIS procedure was modified at the request of the Forest Service to produce regions (groups of connected pixels) no smaller than 6 acres (2.4 ha). Note that if the original classification is accurate, the spatial filtering will degrade accuracy by adding pixels to classes they do not represent. This added variance is an unavoidable by-product of providing a stand map with improved spatial coherence, and, presumably, it is worth the trade-off.

A spatial filtering program was written to simplify the classified image. The algorithm used was modified from one developed by Davis and Peet [21], which removes all groups of pixels below a user-specified minimum size for each class in the image. The first step is to remove all single pixel regions. When all eight neighbors in a 3×3 window are of a different class than the center pixel, the class of the center pixel is changed. In the algorithm implemented in FOCIS, the classes are assumed to be weakly ordinal, and *a priori* class conversion weights are used. The number of neighboring pixels in each class is scaled

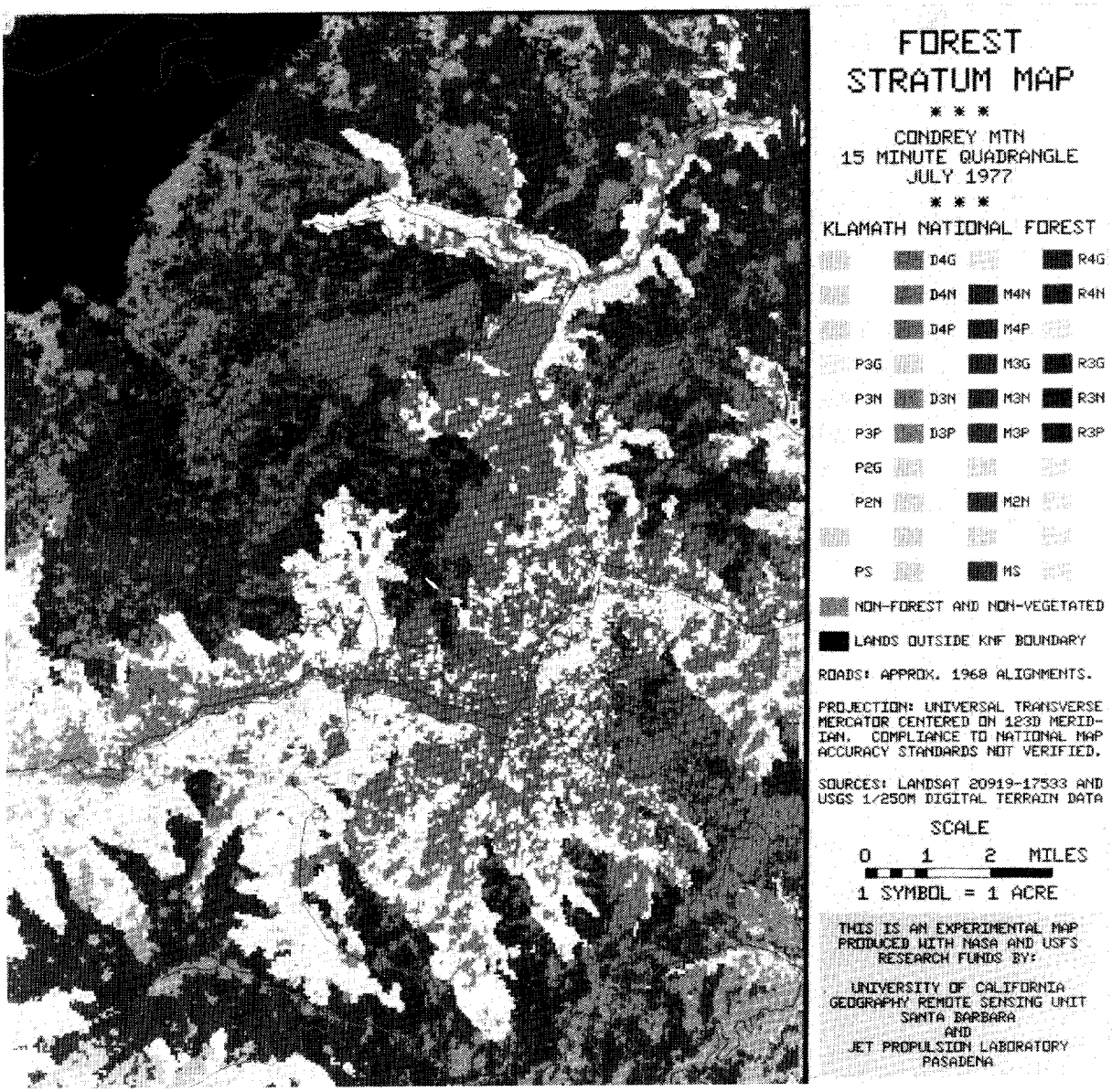

Fig. 6. Final stratified image of the Condrey Mountain 15-min quadrangle. Although not visible here, gray tones are composed of fine symbols that allow identification of the timber type associated with each pixel when the photo is enlarged to proper map scale.

by the conversion weighting for that class, and the class with the largest resulting product "wins" the center pixel. Conversion weighting is effected to reduce the relabeling of timber types into nontimber types; we preferred to expand timber types by including pixels from edges and holes, thus increasing the variance of the timber types, rather than "lose" timber altogether to nontimber classes. The conversion weights also reduce the tendency of large classes to grow larger simply because they have a large perimeter.

The resulting image, which has all isolated single pixels removed, is sorted into "regions"—contiguous areas of the same class. The second step is region conversion. If a region is larger than the specified minimum size for that class, it is not changed. If it is smaller, the entire region is changed to another class, again using the composition of the perimeter pixels and the class conversion weights to determine the new class.

L. *Final Products*

Besides inventory statistics, UTM-projection quadrangle maps were produced for both forests (Fig. 6). For the Eldorado, these were converted to a vector format compatible with direct entry to RID*POLY. For the Klamath, tabulations of timber strata by slope and elevation class within quadrangles were also prepared and delivered to the Forest Service.

IV. Results

A. *Assessing the Quality of the Stratification*

For a large-area inventory based on stratification and sampling, accuracy is normally measured by the coeffi-

cient of variation of the estimated quantity—the lower the standard error of the estimate with regard to the mean, the more accurate is the inventory. Since the Klamath and Eldorado inventories included ground samples of timber volume, it was possible to estimate this standard error in both cases. For the Klamath, however, a concurrent timber inventory carried out by the Forest Service using conventional techniques was also available. In the case of the Eldorado, a full and complete Landsat-based inventory was the objective. Thus, no concurrent alternative inventory was available for comparison there. The remaining sections in this portion of the paper document sample allocation, data collection, and calculation of totals and standard errors.

B. Field Data Collection

Following definition of the final strata, the actual per-acre timber volume associated with each stratum must be estimated. These estimates are obtained from ground samples, or "cluster plots," collected according to standardized procedures specified by Region 5 of the USFS [21]. These ground samples are termed cluster plots because each consists of five subplots clustered in the shape of an "L," with one subplot at the vertex and two along each arm. The arms of the cluster plot are oriented due north and due east with the subplots located two chains (132 ft, 40.2 m) apart. The use of such spatially clustered samples is a classic sampling technique that is invoked when local variance is high and the travel cost to reach randomly located points is excessive [23]. In the case of the Eldorado, the distance between subplots was adjusted to 100 ft (30.5 m), or about half the interpixel ground distance, to avoid interaction between the cluster plot layout and the pixel grid.

The cluster plot data collected at the individual points included height, diameter at breast height (DBH), and growth increment for a systematically selected subsample of trees; and height and DBH class, damage and defect codes, and other information for all remaining trees falling within variable-radius plots defined using standard wedge prism methods [21]. In the processing of the plots by the Forest Service, variables are averaged over all the subplots and weighted by the number of subplots within the plot for which it was actually possible to collect data. Degrees of freedom in inventory calculations, however, are determined by the number of plots, not subplots. This procedure results in a conservative estimate of within-stratum variance.

C. Sample Allocation

Estimating the average timber volume for each Landsat-derived stratum requires allocating cluster-plot samples to each stratum. A random stratified sample design with equal numbers of samples for each stratum is considered appropriate by the Forest Service for this purpose. A minimum of four cluster plots per stratum is the rule of thumb used for Region 5 forests; this criterion implies 68 cluster plot samples for the Landsat-based strata in the KNF. Unfortunately, funds were not available to collect this large number of cluster plots independently, and it became necessary to rely in part on the cluster plots collected by the Forest Service for their forest-wide inventory. This plot-sharing procedure added an unknown bias to the FOCIS timber-volume total, but it was unlikely to affect the standard error of the estimate [2].

Another problem in sample allocation in the Klamath inventory arose because of a Forest Service decision to merge strata with similar stocking densities, thus creating a smaller number of strata than originally planned. In addition, since the new strata were expected to be somewhat more variable than the older ones, the intensity of Forest Service sampling by the Forest Service was increased, with at least six cluster samples obtained for each stratum. Thus, the final strata used by the USFS and produced by FOCIS did not correspond exactly for the KNF.

Neither of these problems arose in the Eldorado inventory, since all samples were allocated according to the FOCIS stratification. Fifty-six plots were allocated in the eight FOCIS timber strata, and after collection, the data were processed by Forest Service software to derive timber volume estimates.

D. Landsat-Based Timber Volume Inventory

In order to assess the accuracy of the inventories, we focused on one inventory statistic—total softwood timber volume for the forest—obtained by areal weighting of within-stratum volume averages. Areas of strata were easily obtained from tabulations of pixels; mean and variance of softwood volume were derived from the processing of the cluster plots.

Table I presents the inventory total and its standard error for the western region of the KNF. For the mapped areas of 944 833 acres (422 340 ha), the value is 3.83×10^9 ft^3 (1.08×10^8 m^3), with a standard error of 0.187×10^9 ft^3 (0.053×10^8 m^3). This standard error represents 4.88 percent of the total timber volume. In comparison, the Forest Service inventory yielded a timber total of 2.69×10^9 ft^3 (0.76×10^8 m^3), with a standard error of 0.067×10^9 ft^3 (0.019×10^8 m^3) for an area of 1 082 000 acres (438 000 ha) [2]. This error is about 2.5 percent of the total.

A comparison of the two inventories shows that each yielded significantly different timber-volume totals—the FOCIS volume was about 40 percent larger than that estimated by the Forest Service. However, the higher value for the FOCIS inventory results largely from high mean values for the two M4 strata. Although four Forest Service plots were allocated to M4P, data for only two of the plots were received. Also note that the standard error of the M4P FOCIS stratum is very low—0.569×10^2 ft^3 (1.61 m^3)—compared to the rest of the values, which range roughly from 5 to 25. This value is probably accidental, resulting because the two plots were, by chance, very close in timber volume. This low standard error, multiplied by the large area of the stratum, reduces the standard error of the total significantly, making it look better than it really

TABLE II
ELDORADO TIMBER INVENTORY

Stratum	Mean Volume	Standard Error	Number Of Plots	Area	Stratum Volume	Standard Error
M3G	56.851[1]	8.300[1]	8	78,532[2]	4,464,623[3]	230,486[3]
M3P	42.759	15.148	8	122,400	5,233,702	655,628
M4G	74.015	10.255	8	51,469	3,809,478	186,639
M4P	54.071	10.364	8	43,579	2,356,360	159,707
R3G	86.634	23.310	6	10,701	927,070	101,854
R3P	30.936	6.722	6	12,288	380,142	33,728
R4G	91.536	24.427	6	10,493	960,487	104,660
R4P	51.419	11.205	6	13,356	686,752	61,108
Totals			56	342,818	18,818,614	754,545

[1]Units are hundreds of cubic feet per acre.

[2]Units are acres.

[3]Units are hundreds of cubic feet.

is. If the means and variances for M4P and M4G obtained in the Forest Service inventory are substituted for those obtained by the FOCIS procedure, the FOCIS total drops to 2.87×10^9 ft^3 (0.81×10^8 m^3), with a standard error of 0.161×10^9 ft^3 (0.046×10^8 m^3). This adjustment brings the two timber volume totals to within approximately one and one-quarter standard errors of each other.

Note also that these modifications raise the FOCIS standard error to 5.61 percent of the total timber volume. This accuracy value, approximately 6 percent, probably better represents the true value achieved using the Landsat-based methodology of FOCIS. Compared to the value of 2.51 percent of the Forest Service inventory, it is more than twice as large. However, that the standard errors are not directly comparable, since the total areas of the two inventories are different and each is based on a different number of samples chosen from a different number of strata. By expressing the timber volume on a per-acre basis, and by correcting for degrees of freedom in sampling, the per-acre per-sample standard errors are 0.573 and 0.332 ft^3 (0.0162 and 0.0094 m^3), respectively, for FOCIS and Forest Service inventories. In this comparison, the FOCIS value is higher than that of the Forest Service, but is still well within the 7.5-percent USFS guideline.

Table II presents inventory statistics for the Eldorado National Forest. The inventory showed a total softwood volume of 1.88×10^9 ft^3 (0.53×10^8 m^3) for an area of 342 818 acres (138 738 ha). The standard error of the timber volume estimate was 0.075×10^9 ft^3 (0.021×10^8 m^3), representing almost exactly 4.0 percent of the mean. This value compares favorably with that obtained in the Klamath, and is also well within Forest Service guidelines.

In the Eldorado, the accuracy of the stratification labeling for all strata, including nonforest types, was also assessed. Table III presents a crosstabulation of predicted and actual labels for a set of points randomly selected to verify accuracy. Of the 128 points, 108 were correctly labeled, yielding an overall accuracy of 84.4 percent. The table does not reveal that any strata were consistently mislabeled; at least five of the eight points were correct for all strata, and 10 of the 16 strata showed seven or eight correct points. The overall accuracy compares favorably with the highest values heretofore reported [11] and is close to the 90-percent level, which is occasionally achieved in Level I classification of Landsat MSS imagery [24]. Because many of our classes correspond to Level III classes, our accuracy probably represents the maximum attainable in a realistic situation. Using the binomial distribution, it is possible to place confidence intervals on the accuracy; a 5-percent confidence interval ranges from 76.6 to 89.8 percent [25].

An alternative method for evaluating a confusion table was suggested by Card [26] in which the marginal totals of the table and the area of each stratum are used to provide an overall accuracy and confidence interval, as well as estimates of the true area for each stratum and associated confidence intervals. The overall accuracy calculated by this method improved to 87.0 percent, but the confidence interval widened to 79.5 to 94.4 percent, indicating that there is no significant difference between the two accuracy estimates. Using the new estimate of the area for each stratum, the timber inventory statistics can be recalculated. The total timber volume estimate increased by 3.7 percent and the standard error of this new estimate was reduced to 3.5 percent.

V. CONCLUSION

The FOCIS procedure for timber volume inventory using Landsat MSS, texture and digital terrain information was developed, tested and refined over a 6-year period in two large forests in California. By incorporating the same elements of tone, texture, and terrain used in manual delineation of forest stands, FOCIS can produce a softwood timber volume estimate for very large areas with a standard error comparable to estimates produced by conventional means. Because part of the FOCIS procedure is automated and based on Landsat technology, the per-acre cost of timber inventory should be significantly lower than that of conventional methodologies. Further, FOCIS meth-

TABLE III
CONFUSION TABLE FOR ELDORADO STRATIFICATION

Actual Class Label	FOCIS Label																
	Water	Barren	Sparce Vegetation	Brush	Hardwood	M4G	M4P	M3G	M3P	Plantation	R4G	R4P	R3G	R3P	SA3G	SA3P	Total
Water	8																8
Barren		8															8
Sparce Vegetation			7													2	9
Brush				7	1					2							10
Hardwood				1	7												8
M4G						8	1		1								10
M4P							7				1			1			9
M3G								8	1				2	1			12
M3P									6								6
Plantation										6							6
R4G											7		1				8
R4P												6		1			7
R3G													5				5
R3P														5			7
SA3G															7		7
SA3P															1	6	7
Total	8	8	8	8	8	8	8	8	8	8	8	8	8	8	8	8	128

ods can produce an inventory within 9 to 12 months at a reasonable level of effort, as compared to 2 to 3 years for conventional manual photointerpretation, map compilation and drafting, field sampling, and data processing.

ACKNOWLEDGMENT

The authors would like to acknowledge the assistance of many people who provided help throughout the course of the project. Most important were J. Levitan and H. Bowlin, U.S. Forest Service Region 5, who provided field support, wise counsel, and collaboration. D. L. Amsbury, Johnson Space Center, and F. P. Weber, National Forestry Applications Program, USFS, provided valuable coordination and support. M. Cosentino, J. Scepan, J. Soto, J. Dozier, A. Means, J. Minsk, J. Lange, F. Furlong, C. Wu, and others helped in field data collection, data analysis, and manuscript preparation.

REFERENCES

[1] A. H. Strahler, "Stratification of natural vegetation for forest and rangeland inventory using Landsat digital imagery and collateral data," *Int. J. Remote Sensing*, vol. 2, pp. 15–41, 1981.

[2] A. H. Strahler, J. Franklin, C. E. Woodcock, and T. L. Logan, "FOCIS: A forest classification and inventory system using Landsat and digital terrain data," Final Rep., NASA Contract NAS-9-15509, Geography Remote Sensing Unit, Univ. of California, Santa Barbara, 1981.

[3] A. H. Strahler, T. L. Logan, J. Franklin, and H. Bowlin, "Automated forest classification and inventory in the Eldorado National Forest," Final Rep., U.S.F.S. Contract 53-91S8-1-6504, U.S.D.A. Forest Service, Region 5, 630 Sansome St., San Francisco, CA 94111, 1983.

[4] R. M. Hoffer and Staff, "Natural resource mapping in mountainous terrain by computer-analysis of ERTS-1 satellite data," Research Bull. 919, Agricultural Experiment Station and Lab. for Applications of Remote Sensing, Purdue Univ., West Lafayette, IN, 1975.

[5] R. M. Hoffer and Staff, "Computer-aided analysis of Skylab multispectral scanner data in mountainous terrain for land use, forestry, water resource, and geologic applications," LARS Tech. Rep. 121275, Lab. for Applications of Remote Sensing, Purdue Univ., West Lafayette, IN, 1975.

[6] S. Khorram and E. F. Katibah, "Vegetation/land cover mapping of the Middle Fork of the Feather River watershed using Landsat digital data," *Forest Sci.*, vol. 30, pp. 248–258, 1984.

[7] R. M. Hoffer, M. D. Fleming, L. A. Bartolucci, S. M. Davis, and R. F. Nelson, "Digital processing of Landsat MSS and topographic data to improve capabilities for computerized mapping of forest cover types," LARS Tech. Rep. 011579, Lab. for Applications of Remote Sensing, Purdue Univ., West Lafayette, IN, 1979.

[8] D. Blakeman, Pacific Southwest Forest and Range Experiment Station, Berkeley, CA, personal communication.

[9] K. R. Castleman, *Digital Image Processing*. Englewood Cliffs, NJ: Prentice-Hall, 1982.

[10] N. A. Bryant and A. L. Zobrist, "IBIS: A geographic information system based on digital image processing and image raster data type," in *Proc. 2nd Purdue Symp. Machine Processing Remotely Sensed Data* (West Lafayette, IN), 1976.

[11] A. H. Strahler, T. L. Logan, and N. A. Bryant, "Improving forest cover classification accuracy from Landsat by incorporating topographic information," in *Proc. 12th Int. Symp. Remote Sensing Environ.* (Ann Arbor, MI), pp. 927–942, 1978.

[12] A. H. Strahler, T. L. Logan, and C. E. Woodcock, "Forest classification and inventory system using Landsat, digital terrain, and ground sample data," in *Proc. 13th Int. Symp. Remote Sensing Environ.* (Ann Arbor, MI), pp. 1541–1557, 1979.

[13] A. H. Strahler and P. F. Maynard, "A logit classifier for multiimage data," in *Proc. Workshop Picture Data Description and Management* (Asilomar, CA), IEEE Computer Society Pub. 80 CH1530-5, pp. 5–11, 1980.

[14] R. E. Hartung and W. J. Lloyd, "Influence of aspect on forests of the Clarksville soils in Dent county, Missouri," *J. Forestry*, vol. 26, pp. 178–182, 1969.

[15] T. W. Bowersox and W. W. Ward, "Prediction of oak site index in the Ridge and Valley region of Pennsylvania," *Forest Sci.*, vol. 18, pp. 192–195, 1972.

[16] D. L. Graney and E. R. Ferguson, "Shortleaf pine site-index relationships in the Ozark Highlands," *Proc. Soil Sci. Soc. America*, vol. 36, pp. 495–500, 1972.

[17] A. H. Strahler, "Response of woody species to site factors in Maryland, U.S.A.: Evaluation of sampling plans and of continuous and binary measurement techniques," *Vegetatio*, vol. 35, pp. 1–19, 1977.

[18] R. Tryon and D. Bailey, *Cluster Analysis*. New York: McGraw-Hill, 1970, pp. 147–150.
[19] F. J. Rohlf, J. Kishpaugh, and D. Kirk, "NT-SYS: Numerical taxonomy system of multivariate statistical programs," documentation and programs available from F. J. Rohlf, State University of New York, Stony Brook, NY, 1974.
[20] F. G. Sadowski and W. A. Malila, "Reflectance modeling and empirical multispectral analysis of forest canopy components," Final Rep., Investigations of Techniques for Inventorying Forest Regions, vol. I, Environmental Research Institute of Michigan Tech. Rep. 122700-35-F1, Ann Arbor, MI, 1977.
[21] U.S. Forest Service, "Compartment Inventory Analysis: Region 5 C.I.A. Handbook, Mar. 19, 1979," Timber Management Staff, U.S. Forest Service, San Francisco, CA, 1979.
[22] W. A. Davis and F. G. Peet, "The identification and reclassification of small regions in digital thematic maps," Forest Management Institute, Ottawa, Ont., Canada, Information Rep. FMR-X-90, 1976.
[23] W. G. Cochran, *Sampling Techniques*, 3rd ed. New York: Wiley, 1977.
[24] J. R. Anderson, "A land use and land cover classification system for use with remotely sensed data," *U.S. Geo. Surv. Prof. Paper 964*, 1976.
[25] F. J. Rohlf and R. R. Sokal, *Statistical Tables*, 2nd ed. San Francisco: W.H. Freeman, 1981.
[26] D. H. Card, "Using known map category marginal frequencies to improve estimates of thematic map accuracy," *Photogrammetr. Eng.*, vol. 48, pp. 431–439, 1982.

*

Janet Franklin received the B.A. degree in environmental biology in 1979 and the M.A. degree in geography in 1983, both from the University of California at Santa Barbara. She is working toward the Ph.D. degree in geography under a Graduate Research Fellowship from NASA at the University of California at Santa Barbara in conjunction with ongoing research at the NASA Goddard Space Flight Center.

She has been involved in vegetation/remote-sensing research since 1978, and her current research interests include forest canopy reflectance modeling, and spatial pattern analysis in natural vegetation.

Thomas L. Logan received the B.A. degree from the California State University, Northridge, in 1976 and the M.A. and Ph.D. degrees from the University of California at Santa Barbara in 1978 and 1983, respectively.

He is a geographer with 10 years of experience in the Cartographic Applications Group of the Image Processing Applications and Development Section at the Jet Propulsion Laboratory, California Institute of Technology. His emphasis has been on the remote sensing and image processing of forest and range applications, as well as general geographical information systems technology, classification techniques, database development, and cartographic applications.

*

Curtis E. Woodcock received the B.A., M.A., and Ph.D. degrees from the Department of Geography, University of California, Santa Barbara.

He is currently an Assistant Professor in the Department of Geography and Acting Director of the Center for Remote Sensing at Boston University. Applications of remote sensing to forest inventory and other problems in natural environments have been a primary research interest. He has conducted both empirical and theoretical studies on the spatial properties of images, assessing the influence of both spatial resolution and the nature of environments on observed spatial patterns. The ability to incorporate other types of data in remote sensing analyses, such as digital elevation models, has resulted in an interest in geographic information systems.

Dr. Woodcock is a member of the American Society of Photogrammetry and Remote Sensing.

*

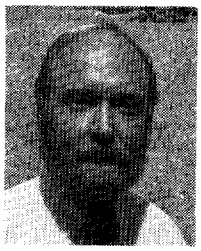

Alan H. Strahler was born in New York City, NY, on April 27, 1943. He received the B.A. and Ph.D. degrees from the Johns Hopkins University in 1964 and 1969, respectively.

He is currently Professor and Chair of the Department of Geology and Geography at Hunter College of the City University of New York. He has held prior academic positions at the University of California, Santa Barbara, and at the University of Virginia. Originally trained as a biogeographer, he has been actively involved in remote-sensing research since 1978. He has been a Principal Investigator on numerous NASA contracts and grants. His primary research interests are in spatial modeling and spatial statistics as they apply to remote sensing, and in geometric-optical modeling of remotely sensed scenes.

On the Design of Classifiers for Crop Inventories

RICHARD P. HEYDORN AND HELEN C. TAKACS

Abstract—**Crop proportion estimators that use classifications of satellite data to correct, in an additive way, a given estimate acquired from ground observations are discussed. A linear version of these estimators is optimal, in terms of minimum variance, when the regression of the ground observations onto the satellite observations is linear. When this regression is not linear, but the reverse regression (satellite observations onto ground observations) is linear, the estimator is suboptimal but still has certain appealing variance properties. In this paper we derive expressions for those regressions which relate the intercepts and slopes to conditional classification probabilities. These expressions are then used to discuss the question of classifier designs that can lead to low-variance crop proportion estimates. Variance expressions for these estimates in terms of classifier omission and commission errors are also derived.**

Keywords—**Regression, Bayes, and Maximum Likelihood Classifiers, Sampling Efficiency, and Landsat Satellite Data.**

I. Introduction

CROP INVENTORY approaches that make use of remotely sensed observations of the crop from satellites have been discussed by MacDonald *et al.* [1] and Hanuschak *et al.* [2]. These approaches are based on a sampling design in which areal segments are randomly selected from strata within an agricultural sampling frame. In the design discussed by Hanuschak *et al.*, each segment is approximately one square mile in size and contains about 664 Landsat pixels. (A pixel is 1.1 acres in size.) The segments considered by MacDonald *et al.* are 30 square miles in size and contain 22 932 Landsat pixels. Spectral observations from each segment pixel are acquired from the satellite. These observations are classified into two categories; one is the crop of interest and the other is the category of all other material on the ground. By counting the number of pixels classified as the crop of interest, and dividing by the total number of pixels classified, an estimate of the proportion of the segment that is the crop of interest is acquired. However, since these classifications are error prone, each segment estimate can be biased. (See Tenebein [3] or Heydorn [4] for a discussion of this problem.)

In domestic surveys, the USDA conducts a crop and livestock survey by visiting randomly selected farms. This survey is a source of ground truth observations which can be used along with the satellite observations. The use of the ground truth data makes it possible to obtain (at least theoretically) unbiased estimates, while the satellite data can be used to increase the precision of the ground-acquired survey. The increase in precision implies that it is possible to reduce the number of ground observations while still keeping the sampling error within a prescribed interval. Given that the satellite is in place, the data and data-processing costs related to the satellite generally render a satellite observation cheaper than a ground-acquired observation, so that this combined approach can reduce the cost of a crop survey.

In this paper we consider a crop proportion estimator that is discussed by Cochran [5] and is used by USDA in their domestic satellite crop survey studies (cf. Hanuschak *et al.* [2]). This estimator is optimal (minimum variance), among a class of estimators in which an additive correction is made to the ground survey estimate using the satellite data, when the regression of the ground observations onto the satellite observations is linear. When the observations regressed in the reverse way give a linear regression, the estimator can be suboptimal, but it still has certain appealing properties. We establish sufficient conditions that the classifier must satisfy to have a linear regression and under these sufficient conditions examine the variance properties of the estimator.

II. The Crop Proportion Estimator

Given a segment, let y denote the true proportion of the crop of interest in the segment, obtained from the ground truth sample, and let x denote the corresponding proportion derived from the classifier. Let X, Y denote the random variables corresponding respectively to the x, y observations from randomly drawn segments. Finally let $E(X) = \nu$ and $E(Y) = \mu$.

Given an (independent and identically distributed) (iid) sample (X_i, Y_i), $i = 1, 2, \cdots, n$, consider an estimator for μ of the form

$$\hat{\mu}_g = \bar{Y} + E(g(\underline{X})) - g(\underline{X})$$

where $\bar{Y} = (1/n)\,\Sigma Y_i$, $\underline{X}' = (X_1, X_2, \cdots, X_n)$ and g is some integrable (i.e., L_1) function of $\underline{X}$. Let $\mathcal{G}$ be the class $\{\hat{\mu}_g\colon g \in L_1\}$.

Cochran [5] discusses estimators of this kind when g is a linear function. That is

$$\hat{\mu} = \bar{Y} + b(\nu - \bar{X}) \tag{1}$$

where $\bar{X} = (1/n)\,\Sigma X_i$. This estimator (see (1)) is also used in the USDA studies mentioned in the Introduction (cf. Hanuschak *et al.* (2)).

Manuscript received June 12, 1985; revised September 10, 1985.

R. P. Heydorn is with the NASA Johnson Space Center, Houston, TX 77058.

H. C. Takacs is with the Department of Computer Science, Mississippi State University, Mississippi State, MS 39762.

IEEE Log Number 8406226.

Both $\hat{\mu}_g$ and $\hat{\mu}$ are clearly unbiased and since

$$\begin{aligned}\text{Var}(\hat{\mu}_g) &= E(\text{Var}(\hat{\mu}_g|\underline{X})) + \text{Var}(E(\hat{\mu}_g|\underline{X})) \\ &= E(\text{Var}(\overline{Y}|X)) + \text{Var}(E(\overline{Y}|X) - g(\underline{X})). \quad (2)\end{aligned}$$

$\hat{\mu}_g$ will have minimum variance (and therefore minimum mean square error since $E(\hat{\mu}_g) = \mu$) among the members of class $\mathcal{G}$ if $g(\underline{X}) = E(\overline{Y}|\underline{X}) + c$ where c is any constant.

The last term in (2) measures the increase in variance when failing to match (within a constant) the true regression function when selecting g. In particular the linear version in (1) may be suboptimal, but since b is the only parameter that needs to be estimated, it is an appealing choice. We are assuming that the satellite provides us with a large number of observations, and therefore, ν can be computed (i.e., estimated with virtually zero variance). This is the case in the above-mentioned USDA studies.

For the estimator of (1)

$$\text{Var}(\hat{\mu}) = (1 - R^2)\frac{\text{Var}(Y)}{n} + \left(b - \frac{\text{cov}(X, Y)}{\text{Var}(X)}\right)^2 \frac{\text{Var}(X)}{n} \quad (3)$$

where $R = \text{cov}(X, Y)/\sqrt{\text{Var}(X)\,\text{Var}(Y)}$. The best choice for b is cov (X, Y)/Var (X) regardless of the form of the regression function. The term $1 - R^2$ is the variance reduction afforded by using $\hat{\mu}$ in place of $\overline{Y}$ as an estimator for μ.

If $E(\overline{X}|\underline{Y})$ were linear (where $\underline{Y}' = (Y_1, Y_2, \cdots, Y_n)$), then the minimum mean square error (MSE) estimator for ν among estimators of the form $\hat{\nu}_f = \overline{X} + E(f(\underline{Y})) - f(\underline{Y})$, $f \in L_1$, would have a variance reduction that is again $1 - R^2$. Hence, $\hat{\mu}$ will estimate μ at least as well (in terms of R^2) as $\hat{\nu}_f$ can estimate ν when $E(\overline{X}|\underline{Y})$ is linear.

Based on these considerations related to the estimator of (1), we next consider some possible properties of the classifier that can lead to linear regression models.

III. The Classifier and Regressions

To introduce some of the ideas in this section, we will need the following notation.

Let Z be the random variable of satellite pixel observations z. Since the satellite is capable of acquiring data within several spectral wavelengths (Landsats 1 through 3 acquire data within four wavelength ranges and Landsat 4 within up to seven) and views the same spot on the Earth multiple times during a year, Z is generally a vector rather than a scalor. Let θ be the random variable that denotes the label of an observed pixel. When θ assumes a value of 1, the pixel being observed is the crop of interest, and when θ assumes the value of 0, the pixel is some other material. The satellite provides us only with values of Z. Values of θ must be obtained by other means, such as from ground observations. The purpose of the classifier will be to use Z to estimate θ. We denote the classifier by the function ϕ where $\phi(z) \in \{0, 1\}$. We classify z as an observation on the crop of interest when we write $\phi(z) = 1$ and on some other material when we write $\phi(z) = 0$. Finally we let Δ be a random variable that indexes the segments in the sample.

In the development to follow we will allow for the option to alter the classifier depending upon some property of the segment being classified, i.e., the classifier can be a functional of Δ. We denote this fact by writing ϕ_Δ.

Given the early definition of X and Y along with the above definitions, we see that

$$X = E(\phi_\Delta(Z)|\Delta)$$

and

$$Y = E(\theta|\Delta).$$

We will be interested in the regression functions $E(Y|X)$ and $E(X|Y)$ and to study these functions we will start with simple "two-point-models"

$$\theta = \alpha_{1\Delta} + \alpha_{2\Delta}\phi_\Delta(Z) + \epsilon_\theta, \qquad E(\epsilon_\theta|\phi_\Delta(Z), \Delta) = 0 \quad (4)$$

$$\phi_\Delta(Z) = \beta_{1\Delta} + \beta_{2\Delta}\theta + \epsilon_\phi, \qquad E(\epsilon_\phi|\theta, \Delta) = 0 \quad (5)$$

which, as we will show in the next theorem, have the capability of generating our regression functions. Notice that since θ and $\phi_\Delta(Z)$ can only assume two values, the conditional expectations of the errors are zero when we make proper choices for the α's and the β's. Clearly, these choices should be

$$\alpha_{1\Delta} = E(\theta|\phi_\Delta(Z) = 0, \Delta),$$

$$\alpha_{2\Delta} = E(\theta|\phi_\Delta(Z) = 1, \Delta) - \alpha_{1\Delta}$$

$$\beta_{1\Delta} = E(\phi_\Delta(Z)|\theta = 0, \Delta),$$

$$\beta_{2\Delta} = E(\phi_\Delta(Z)|\,\theta = 1, \Delta) - \beta_{1\Delta}.$$

Theorem

(i) $E(Y|X) = \alpha_{1X} + \alpha_{2X}X$

(ii) $E(X|Y) = \beta_{1Y} + \beta_{2Y}Y$

where

$$\alpha_{1X} = E(\theta|\phi_\Delta(Z) = 0, X)$$
$$\alpha_{2X} = E(\theta|\phi_\Delta(Z) = 1, X) - \alpha_{1X}$$
$$\beta_{1Y} = E(\phi_\Delta(Z)|\theta = 0, Y)$$
$$\beta_{2Y} = E(\phi_\Delta(Z)|\theta = 1, Y) - \beta_{1Y}.$$

A proof of this theorem is given in the Appendix.

We saw in the previous section that $\hat{\mu}$ of (1) is optimal among members of class $\mathcal{G}$ when $E(Y|X)$ is linear. The theorem shows that this regression function will be linear if (but not only if) α_{1X} and α_{2X} are constants. The functions α_{1X} and α_{2X} are made up of conditional expectations (or conditional probabilities since θ assumes only 0 or 1) where the conditioning depends on the classifier ϕ_Δ. If we fix X, at say $X = x$, then x could be treated as a parameter; and further, if ϕ_Δ were a function of θ, rather than z, the

requirement that α_{1X} and α_{2X} be constants would imply that ϕ_Δ would be a sufficient transformation. Since ϕ_Δ is a transformation on Z rather than θ, this interpretation of ϕ_Δ's role is not strictly correct. Nevertheless, since Z is a predictor of θ, it is reasonable to suspect that ϕ_Δ needs to be some sort of information-preserving transformation, relative to the family of probability distributions $\{P_x\}$ defined on θ if α_{1X} and α_{2X} are to be constant.

To gain some insight on the possible effect of classifier design on the regression function $E(Y|X)$, we offer the following numerical example.

In this example the population of z-values from the crop of interest in a segment was simulated as being normally distributed with mean m_1 and variance σ^2. The z-values from the class of all other material was also normally distributed with mean m_0 and variance σ^2. These two means we allowed to vary according to a uniform distribution (on [0, 1]) from segment to segment. The true proportions of the crop of interest, i.e., the y-values, were also drawn from a uniform distribution on [0, 1]. Each segment was classified, and from the classification results the x-value for that segment was determined.

In the first set of experiments, a maximum likelihood classifier was used. Here $\phi_\Delta(z) = 1$ if $N(z; m_1, \sigma) > N(z; m_0, \sigma)$ and $\phi_\Delta(z) = 0$ if the reverse inequality holds, where $N(\cdot; m_1, \sigma)$ is the likelihood (normal density) of the crop of interest and $N(\cdot; m_0, \sigma)$ is the likelihood for the class of all other material. The results are shown in Fig. 1(b), (d), and (f).

With this classifier, the commission errors (calling a pixel the class of interest when it is not) dominate the segment estimates when y is small. This means that for small y, x is too large. Where y is large, on the other hand, the omission errors (calling a pixel the class of all other material when it is not) forces the x-values to be too small. This distortion at the two extremes of the y-values gives the regression function $E(Y|X)$ in Fig. 1(b) a sigmoidal functional form.

A classifier that cannot compensate for these commission and omission errors at the extreme values of y is likely to give rise to a sigmoidal regression function. Since the Bayes classifier does compensate in this way, one might suspect that the Bayes classifier would give rise to a regression function that is more linear than the one resulting from the maximum likelihood classifier. This conjecture was examined by weighing the densities $N(\cdot; m_1, \sigma)$ and $N(\cdot; m_0, \sigma)$ with y and $1 - y$, respectively, in the above-mentioned classifications rule. The results are shown in Fig. 1(a), (c), and (e). For this case the regression is reasonably linear. While α_{2X} appears to be constant, α_{1X} shows a slight linear trend with x; and hence the information preserving analogy discussed above does not quite hold.

To construct the Bayes classifier, however, we would have to know the true proportions in each segment. If these proportions were known, there would, of course, be no need to consider our estimator that uses the satellite data, since we could compute the desired answer directly. We propose that a more workable solution would be to consider classifier designs that can force β_{1Y} and β_{2Y} to be constant. This can sometimes be done without having a knowledge of the y-value for each segment. We now discuss some examples of this approach.

For the remainder of the discussion we will consider only classifiers that represent a fixed transformation on Z. Accordingly, we will drop the Δ subscript and write ϕ in place of ϕ_Δ. From Theorem 1 we therefore have that

$$\beta_{1Y} = E(\phi(Z)|\theta = 0, Y)$$

$$\beta_{2Y} = E(\phi(Z)|\theta = 1, Y) - \beta_{1Y}.$$

The conditional expectations in these expressions depend only upon distributions of Z that are conditional on Y rather than on Δ. In other words, we are not concerned with the behavior of the classification results for individual segments but rather with the classification of observations pooled from any group of segments which have the same y-value.

A particular class of problems come from the case where the regression of Z on Y, when sampling from the class of interest ($\theta = 1$), follows the model

$$Z = h_1(Y) + \epsilon_1, \qquad \epsilon_1 \sim N(\cdot; 0, \Sigma_1) \tag{6}$$

and when sampling from the class of other material ($\theta = 0$) follows the model

$$Z = h_0(Y) + \epsilon_0, \qquad \epsilon_0 \sim N(\cdot; 0, \Sigma_0) \tag{7}$$

where h_1, h_0 are distinct vector valued functions of y and ϵ_1 and ϵ_0 are independent errors. If we can find a transformation T such that

$$T(Z) = c_1 + \tilde{\epsilon}_1, \qquad \tilde{\epsilon}_1 \sim N(\cdot; 0, \tilde{\Sigma}_1)$$

$$T(Z) = c_0 + \tilde{\epsilon}_0, \qquad \tilde{\epsilon}_0 \sim N(\cdot; 0, \tilde{\Sigma}_0).$$

$c_1 \neq c_0$ where c_1, c_0 are constant vectors and $\tilde{\epsilon}_1$ and $\tilde{\epsilon}_0$ are again independent, then $E(\phi(T(Z))|\theta = 0, Y)$ and $E(\phi(T(Z))|\theta = 1, Y)$ would both be constant. Treating observations on Y as parameter values, $\phi o T$ would then be an ancillary transformation (see Rao [6] for a definition of an ancillary transformation) for the families $\{F_y(\cdot|\theta = 0)\}$ and $\{F_y(\cdot|\theta = 1)\}$ of distributions of Z conditioned on $Y = y$.

Rao [6] considers a version of the models in (6) and (7) in which for $\theta = 1$

$$Z = c_1 + Bb_1(Y) + \epsilon_1, \qquad \epsilon_1 \sim N(\cdot; 0, \Sigma_1) \tag{8}$$

and for $\theta = 0$

$$Z = c_0 + Bb_0(Y) + \epsilon_0, \qquad \epsilon_0 \sim N(\cdot; 0, \Sigma_0) \tag{9}$$

where $c_0 \neq c_1$ are constant vectors, b_1, b_0 are some vector valued functions of y, and B is a $p \times k$ matrix, $k < p$. Here p is the dimension of the observations on Z. These models simply restrict the functions h_0 and h_1 of (6) and (7) to assume values only in a k dimensional subspace of R^p. For these models, T is a matrix that annihilates B (i.e., $TB = 0$) but $Tc_1 \neq Tc_0$.

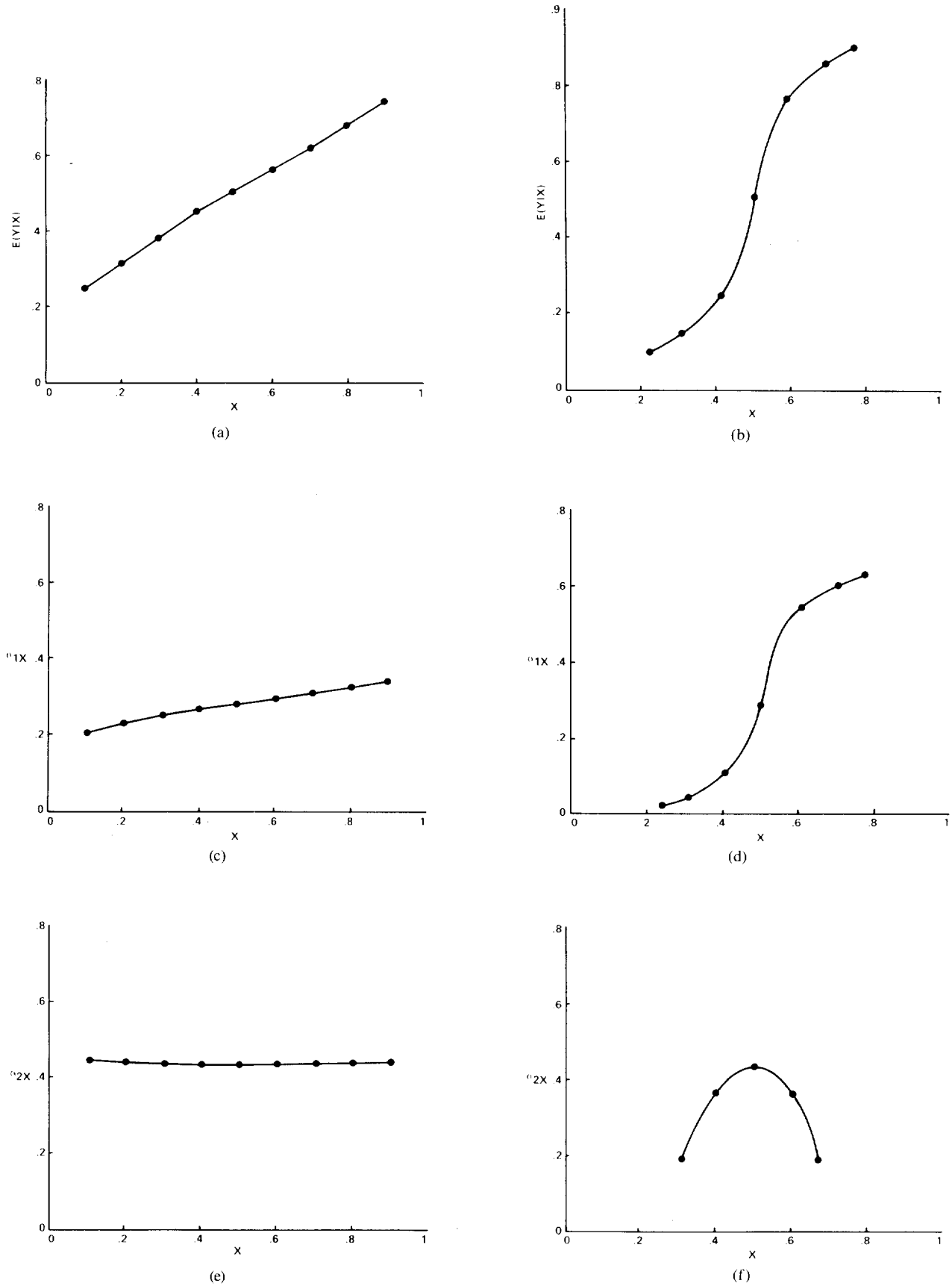

Fig. 1. (a) $E(YIX)$ for the Bayes Classifier. (b) $E(YIX)$ for the Maximum Likelihood Classifier. (c) α_{1X} for the Bayes Classifier. (d) α_{1X} for the Maximum Likelihood Classifier. (e) α_{2X} for the Bayes Classifier. (f) α_{2X} for the Maximum Likelihood Classifier.

The models in (8) and (9) may be a plausible representation for Z. The physical explanation is as follows:

As a crop grows, it develops a green vegetative canopy that covers the soil. In the early stages of growth, a large part of the z-measurements represent soil color, while in later stages, as the canopy thickens, the soil contribution decreases. Kauth and Thomas [7] found that the four Landsat observations on any given pass can be represented by a special orthogonal coordinate system. In this system one axis (called soil color) accounts for most of the z-variation due to soil color, while an orthogonal axis (called greenness) accounts for the variation due to the amount of green vegetative matter. Since the amount of green matter at a given point in time is a distinguishing feature of that crop, the coordinate along the greenness axis is generally a good crop discriminating variable. Also, since it is often more economical to grow a crop on certain kinds of soils, the proportion of a crop in a segment is likely to be soil dependent. Since the z-measurements are also soil dependent, a transformation which annihilates variations along the soil color axis, but preserves variation along the greenness axis, may be a suitable transformation T.

IV. Efficiency of the Estimator

From (3) we see that the efficiency of the estimator $\hat{\mu}$ is determined by $1 - R^2$ where $R = \text{cov}\,(X,Y)/\sqrt{\text{Var}\,(X)\ \text{Var}\,(Y)}$. If β_{1Y} and β_{2Y} are constant then

$$R = \beta_2 \sqrt{\frac{\text{Var}\,(Y)}{\text{Var}\,(X)}} = (Pr(\phi_\Delta(Z) = 1|\theta = 1) - Pr(\phi_\Delta(Z) = 1|\theta = 0)) \sqrt{\frac{\text{Var}\,(Y)}{\text{Var}\,(X)}}$$

$$= (1 - \Psi_o - \Psi_c) \sqrt{\frac{\text{Var}\,(Y)}{\text{Var}\,(X)}}$$

where Ψ_o, Ψ_c are the omission and commission error probabilities of the classifier and defined, respectively, as $Pr(\phi_\Delta(Z) = 0|\theta = 1)$ and $Pr(\phi_\Delta(Z) = 1|\theta = 0)$. Letting $\rho_1 = \text{Var}\,(X)/\lambda(1 - \lambda)$ and $\rho_2 = \text{Var}\,(Y)/\pi(1 - \pi)$, where $\lambda = Pr(\phi(Z) = 1)$ and $\pi = Pr(\theta = 1)$, the correlation can be rewritten as

$$R = (1 - \Psi_o - \Psi_c) \sqrt{\frac{\pi(1 - \pi)}{\lambda(1 - \lambda)} \frac{\rho_2}{\rho_1}}. \tag{10}$$

Here ρ_1 and ρ_2 measure the effect on the variance from packing the pixel observations in segments rather than randomly dispersing them throughout the entire sampling frame. For example, since $1 - \rho_2 = E(\text{Var}\,(\theta|\Delta))/\Pi(1 - \Pi)$, $1 - \rho_2$ is the expected ratio of the within segment variance of θ to the total variance.

It is interesting to compare the efficiency of the estimator $\hat{\mu}$ with that of a stratified estimator. To create the stratified estimate, we allocate in a simple random way N pixels rather than N segments. We then classify each pixel into class "1" or class "0" as we did to obtain $\hat{\mu}$, and thereby stratify our sample in two strata whose approximate sizes are $N\lambda$ and $N(1 - \lambda)$, respectively. If we pick a random subsample of size n from this allocation of N pixels (where n is much smaller than N) and obtain a ground truth label for each of the n pixels (i.e., determine if $\theta = 0$ or 1 for each of the n pixels), then we could form the estimator

$$\hat{\hat{\mu}} = \frac{n_{11}}{n_1}\lambda + \frac{n_{10}}{n_0}(1 - \lambda)$$

provided neither n_1 or n_0 are 0. Here n_1 is the number of pixels in the sample of size n that fell into the stratum classified as class 1 and n_0 is the number that fell into the stratum called class "0." Also, n_{11} is the subset of the n_1 pixels that received the label $\theta = 1$ and n_{10} is the subset of the n_0 pixels that received the label $\theta = 1$. It can happen that in the sample of size n one of the strata will not get sampled (i.e., n_1 or n_0 could be 0), and so our formulation is somewhat incomplete. As n gets large, however, this empty strata event becomes highly unlikely. Heydorn [4] offers a more precise formulation of this estimator. Here we wish to keep our description as simple as possible.

Tenebein [3] shows that

$$\text{Var}\,(\hat{\hat{\mu}}) = \left(1 - (1 - \Psi_o - \Psi_c)^2 \frac{\Pi(1 - \Pi)}{\lambda(1 - \lambda)}\right) \cdot \frac{\Pi(1 - \Pi)}{n}. \tag{11}$$

Using (10) (and hence assuming that β_{1Y} and β_{2Y} are constant) the variance of $\hat{\mu}$ can be written as

$$\text{Var}\,(\hat{\mu}) = \left(1 - (1 - \Psi_o - \Psi_c)^2 \frac{\Pi(1 - \Pi)}{\lambda(1 - \lambda)} \frac{\rho_2}{\rho_1}\right) \cdot \rho_2 \frac{\Pi(1 - \Pi)}{n}. \tag{12}$$

For both estimators the variance is a function of the omission and commission errors of the classifier as well as the variances $\pi(1 - \pi)$ and $\lambda(1 - \lambda)$. In addition, Var $(\hat{\mu})$ is also a function of the coefficients ρ_1 and ρ_2 which account for the additional observations used by $\hat{\mu}$ and that are packed in segments. The comparison of the variances of the two estimators depends upon the behavior of ρ_1 and ρ_2. We now discuss some extreme situations in an attempt to understand the variance properties of the two estimators.

From (5), $E(\phi(Z)|\Delta) = \beta_{1\Delta} + \beta_{2\Delta}E(\theta|\Delta)$ or $X = \Psi_o(\Delta) + (1 - \Psi_o(\Delta) - \Psi_c(\Delta))\ Y$ where we have written the omission and commission errors, $\Psi_o(\Delta)$ and $\Psi_c(\Delta)$, as functions of Δ, since these classification errors can vary across segments even though β_{1Y}, β_{2Y} are constant. If classification is consistently poor so that $\Psi_o(\Delta)$ and $\Psi_c(\Delta)$ remain near $\frac{1}{2}$, then Var (X) is much smaller than Var (Y). Moreover, λ will be close to $\frac{1}{2}$, and thus ρ_1 will be small. In view of (11) and (12), we would therefore expect that Var $(\hat{\mu})$ < Var $(\hat{\hat{\mu}})$. Since the term $1 - \Psi_o - \Psi_c$ will also

be near zero in this case, the magnitude of Var $(\hat{\hat{\mu}})$ − Var $(\hat{\mu})$ may depend largely on ρ_2. This is, of course, consistent with the general theory of cluster sampling in which one tries, if possible, to make each segment as heterogenous as possible (ρ_2 small), i.e., so that the segment populations look like the total population.

When the classifier performs extremely well so that $\Psi_o(\Delta)$ and $\Psi_c(\Delta)$ remain near zero, then both estimators do well. In this case both $\Pi(1-\Pi)/\lambda(1-\lambda)$ and $\Pi(1-\Pi)\,\rho_2/\lambda(1-\lambda)\,\rho_1$ are near unity and so again Var $(\hat{\mu})$ can be smaller than Var $(\hat{\hat{\mu}})$ if ρ_2 is small.

If it were possible to hold the omission and commission errors constant on every segment, then Var $(\hat{\mu}) = 0$, since we would have an exact linear relationship between X and Y. That is, $X = \Psi_o + (1 - \Psi_o - \Psi_c)\,Y$, which implies $1 - (1 - \Psi_o - \Psi_c)^2\,(\Pi(1-\Pi)\,\rho_2/\lambda(1-\lambda)\,\rho_1) = 0$. In practice, however, this may be an impossible task since local disturbances (such as, for example, from varying optical depth properties of the atmosphere) can cause variations in the omission and commission errors across segments.

V. Concluding Remarks

From (4) we have $Y = \alpha_{1\Delta} + \alpha_{2\Delta}X$ and from (5) $X = \beta_{1\Delta} + \beta_{2\Delta}Y$. If either the α's or the β's are constant across segments, we therefore have an exact linear relationship between X and Y. For these cases Var $(\hat{\mu}) = 0$. The loss in efficiency of $\hat{\mu}$ therefore occurs when variances are introduced into the α's or β's. It appears to us that controlling the α's through classifier design is a difficult problem. We choose therefore to concentrate on controlling the β's, or as we saw, controlling the omission and commission errors of the classifier. It seems plausible to us that this can be done to some extent through suitable transforms which make the classifier behave like an ancillary statistic.

We compared $\hat{\mu}$ to a poststratified estimator, which we denoted by $\hat{\hat{\mu}}$, in order to examine the possible benefits of replacing a simple random sample with a cluster sample where the clusters are the segments. Our comparison was not complete, but our observations suggest that the additional observations may lead to a significant reduction in variance at least in some extreme cases. In all cases the general notion that one should, if possible, design the cluster sample so that the segments are as heterogenous as possible, which means that ρ_2 should be small, follows also for this estimator.

Finally, notice that we did not discuss cases where the coefficient b was estimated. When b is estimated, it is useful to notice that (1) can be written as

$$\hat{\mu} = \frac{1}{n}\sum_{i=1}^{n}(Y_i + b(\nu - X_i)).$$

If the estimator for b has a variance that is inversely proportional to n, then n Var $(\hat{\mu})$ will be close to $(1 - R^2)$ Var (Y), and hence our conclusions approximately hold for large n.

Appendix

Proof of the theorem:

We will prove i). The assertion in ii) can be proved by similar means.

From (4)

$$E(\theta|\phi_\Delta(Z), \Delta) = \alpha_{1\Delta} + \alpha_{2\Delta}\phi_\Delta(Z).$$

Since $X = E(\phi_\Delta(Z)|\Delta)$ then $\mathcal{B}(X) \subset \mathcal{B}(\Delta)$ and hence[1]

$$\begin{aligned} E(\theta|\phi_\Delta(Z), X) &= E(E(\theta|\phi_\Delta(Z), \Delta)|\phi_\Delta(Z), X) \\ &= E(\alpha_{1\Delta}|\phi_\Delta(Z), X) \\ &\quad + E(\alpha_{2\Delta}|\phi_\Delta(Z), X)\,\phi_\Delta(Z). \end{aligned}$$

Therefore

$$E(\theta|\phi_\Delta(Z) = 0, X) = E(\alpha_{1\Delta}|\phi_\Delta(Z) = 0, X) \triangleq \alpha_{1X}$$

$$\begin{aligned} E(\theta|\phi_\Delta(Z) = 1, X) &= E(\alpha_{1\Delta} + \alpha_{2\Delta}|\phi_\Delta(Z) = 1, X) \\ &\triangleq \alpha_{1X} + \alpha_{2X} \end{aligned}$$

which implies

$$\alpha_{2X} = E(\theta|\phi_\Delta(Z) = 1, X) - \alpha_{1X}.$$

Thus

$$E(\theta|\phi_\Delta(Z), X) = \alpha_{1X} + \alpha_{2X}\phi_\Delta(Z)$$

or

$$E(\theta|X) = \alpha_{1X} + \alpha_{2X}E(\phi_\Delta(Z)|X).$$

But since $\mathcal{B}(X) \subset \mathcal{B}(\Delta)$, this is the same as

$$E(E(\theta|\Delta)|X) = \alpha_{1X} + \alpha_{2X}E(E(\phi_\Delta(Z)|\Delta)|X)$$

or

$$E(Y|X) = \alpha_{1X} + \alpha_{2X}X$$

which completes the proof.

References

[1] R. B. MacDonald and F. G. Hall, "Global crop forecasting," *Science*, vol. 208, no. 16, pp. 670–679, May 1980.

[2] G. Hanuschak, R. Sigman, M. Craig, M. Ozga, R. Luebbe, P. Cook, D. Klewno, and C. Miller, "Obtaining time of crop area estimates using ground gathered and Landsat data," USDA/ESCS Tech. Bull. 1609, Aug. 1979.

[3] A. Tenebein, "A double sampling scheme for estimating from binomial data with misclassifications," *JASA*, vol. 65, no. 331, pp. 1350–1361, Sept. 1970.

[4] R. P. Heydorn, "Using satellite remotely sensed data to estimate crop proportions," *Comm. Stat.*, vol. 13, no. 23, pp. 2281–2903, 1984.

[5] W. G. Cochran, *Sampling Techniques*, 3rd ed. New York: Wiley.

[6] C. R. Rao, "Discriminant function between composite hypotheses and related problems," *Biometrika*, vol. 53, nos. 3 and 4, pp. 339–345, 1966.

[7] R. J. Kauth and G. S. Thomas, "The tasselled cap—A graphic description of the spectral-temporal development of agricultural crops as seen by Landsat," in *Proc. 2nd Int. Sym. Machine Processing of Remotely Sensed Data* (Purdue Univ.), 1976.

[1] $\mathcal{B}(\bullet)$ means the "Borel field generated by."

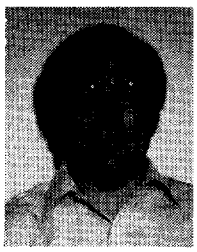

Richard P. Heydorn received the B.E.E. degree in electrical engineering and the M.A. degree in mathematics from the University of Akron and the Ph.D. degree in statistics from Ohio State University.

He joined the NASA Johnson Space Center in 1974 and worked in a research capacity on LACIE and AgRISTARS. He also served as the science manager of the NASA program in Mathematical Pattern Recognition and Image Analysis.

Helen C. Takacs received the Ph.D. degree in applied statistics from the University of Alabama.

She is an Associate Professor of Computer Science at Mississippi State University, where she also serves as Coordinator of Graduate Programs in Computer Science. She has worked as a NASA-ASEE Fellow at the Johnson Space Center, Houston, TX.

Dr. Takacs chairs the Professional Development Committee and Tutorial Weeks for the Education Board of the Association for Computing Machinery.

Crop Acreage Estimation Using a Landsat-Based Estimator as an Auxiliary Variable

RAJ S. CHHIKARA, JAMES C. LUNDGREN, AND A. GLEN HOUSTON

Abstract—**The problem of improving upon the ground survey estimates of crop acreages by utilizing Landsat data is addressed. Three estimators, called regression, ratio, and stratified ratio, are studied for bias and variance, and their relative efficiencies are compared. The approach is to formulate analytically the estimation problem that utilizes ground survey data, as collected by the U.S. Department of Agriculture, and Landsat data, which provide complete coverage for an area of interest, and then to conduct simulation studies. It is shown over a wide range of parametric conditions that the regression estimator is the most efficient unless there is a low correlation between the actual and estimated crop acreages in the sampled area segments, in which case the ratio and stratified ratio estimators are better. Furthermore, it is seen that the regression estimator is potentially biased due to estimating the regression coefficient from the training sample segments. Estimation of the variance of the regression estimator is also investigated. Two variance estimators are considered, the large sample variance estimator and an alternative estimator suggested by Cochran. The large sample estimate of variance is found to be biased and inferior to the Cochran estimate for small sample sizes.**

I. INTRODUCTION

THE STATISTICAL Reporting Service (SRS) of the U.S. Department of Agriculture (USDA) collects crop data each year during its annual June Enumerative Survey (JES) by interviewing farm operators located in randomly selected area segments. Each sample segment is completely enumerated for its land use and cover types, and their crop acreages determined. With the launch of Landsat-1 in the early seventies, SRS proposed to utilize Landsat data as auxiliary information for improving its regular crop acreage estimates made from JES data. The USDA-SRS started a remote sensing program and participated in the Large Area Crop Inventory Experiment (LACIE) and Agricultural Resources Inventory Surveys Through Aerospace Remote Sensing (AgRISTARS), joint programs with other U.S. Government agencies. The proposed approach was to acquire Landsat data for an area of interest and use it in conjunction with the JES data to reduce the sampling error for the regular crop acreage estimates at the state and lower levels [1].

Manuscript received February 4, 1985; revised June 26, 1985. The portions of this work completed by R. S. Chhikara and J. C. Lundgren were supported by the Statistical Reporting Service of the U.S. Department of Agriculture, under NASA Contract 9-15800.

R. S. Chhikara is with the University of Houston—Clear Lake, Houston, TX 77058.

A. G. Houston was with the NASA Johnson Space Center, Houston, TX 77058. He is now with the University of Houston-Clear Lake, Houston, TX 77058.

J. C. Lundgren was with Lockheed Engineering and Management Services, Houston, TX 77058. He is now with Texas Instruments, Dallas, TX.

IEEE Log Number 8406238.

Basically, the approach is to acquire Landsat data over a stratum, called an analysis district, containing a number of JES sample segments. The Landsat data are classified, using data from the sample segments for training, and crop acreage or proportion estimates are obtained for each sample segment in the stratum as well as for the entire stratum for the crop of interest. The crop acreages for the sample segments observed in the JES are regressed onto the corresponding estimates obtained from the classification of the Landsat data and the resulting relationship is used to obtain a crop acreage estimate for the stratum based on the classifier estimate for the stratum [2].

Suppose x denotes the Landsat-estimated and y the ground-observed acreage for a crop in a segment. Suppose segments in a stratum are of the same size and $\bar{X}$ is the average Landsat estimated crop acreage from all segments in the stratum. Let $\bar{Y}$ denote the corresponding actual stratum average crop acreage. For the n sample segments in the stratum, suppose $y_1, y_2, \cdots, y_n$ are the actual crop acreages and $x_1, x_2, \cdots, x_n$ are their corresponding Landsat estimated crop acreages. Then a regression estimator of $\bar{Y}$ is given by

$$\hat{\bar{Y}} = \bar{y} + b(\bar{X} - \bar{x}) \tag{1}$$

where

$$\bar{y} = \sum_{1}^{n} y_i/n$$

$$\bar{x} = \sum_{1}^{n} x_i/n \tag{2}$$

are the sample means of actual and Landsat estimated crop acreages, respectively, and

$$b = \sum_{1}^{n} (x_i - \bar{x})(y_i - \bar{y}) \Big/ \sum_{1}^{n} (x_i - \bar{x})^2 \tag{3}$$

is the sample-based regression coefficient [3]. An estimate may be obtained for the stratum total crop acreage by multiplying the estimate $\hat{\bar{Y}}$ in (1) by the total number of segments covering the stratum. On the other hand, the standard USDA estimator of the stratum crop acreage is obtained by multiplying the sample mean $\bar{y}$ by the number of segments in the stratum. The latter is called a direct expansion estimator and is based solely on the ground survey data from the JES segments.

In the past, SRS/USDA conducted extensive empirical

0196-2892/86/0100-0157$01.00

studies to evaluate the relative efficiency of this regression estimator over their direct expansion estimator. The relative efficiency (RE) is defined by the variance ratio for the two estimators and is a measure of the relative sample size required to achieve the same precision for the two estimators. For example, if the ratio of the variance of the regression estimator to that of the direct expansion estimator is 0.5, then the regression estimator has an RE of 2.0, and it would take twice the number of sample segments for the direct expansion estimator to obtain the same precision as the regression estimator. These studies showed that the RE of regression estimators were sometimes substantial; for example, 2.43 and 2.38 for corn and soybeans, respectively, in Iowa for crop year 1978, and at the analysis district level, it ranged from .93 to 5.98 for corn and from 2.73 to 7.59 for soybeans [1]. This indicates that the use of the regression estimator may lead to a substantial savings in sampling of ground survey data. Since this assertion is based on purely empirical studies, it is important to investigate the properties of the regression estimator analytically, if possible, and compare it with other alternative estimators before it should be recommended for operational purposes. A basis for the regression estimator is that the two variables x and y can be modeled as

$$y = \alpha + \beta x + \epsilon. \tag{4}$$

If the error term ϵ is expected to be zero for any given value of x, the model in (4) is linear, otherwise it is not a linear model. When the Landsat data are classified using a maximum likelihood decision rule (as described in Section II) to obtain x, the model in (4) is not linear [4]. Because of the potential nonlinearity in the model, the least squares estimates of the regression coefficients α and β may be biased [5]. On the other hand, the model relating x in terms of y

$$x = \gamma + \delta y + e \tag{5}$$

is linear, i.e., the conditional mean of e given y, is zero. This suggests that if x is regressed on y, the least squares estimates of γ and δ are unbiased and the resulting calibration equation can be used to obtain another estimate of Y. This estimator, however, has been shown to be less efficient than the regression estimator [4].

Besides the regression estimator, the sample mean estimator can be improved upon by considering the use of a ratio estimator [3]. Furthermore, another estimator of $\bar{Y}$ can be obtained if the individual pixels in sample segments are stratified as to how they were classified, correctly or incorrectly, and this additional information is utilized [6]. A stratified ratio estimator thus constructed is also studied.

An analytical formulation of the estimation problem, the estimators, and the bias and variance of these estimators are discussed in Section II. A sampling study was conducted to compare the relative efficiencies of the estimators. The results of this study are presented in Section III. In this sampling study, the number of pixels per segment was assumed to be infinite and parametric values were generated at the segment level. Another more comprehensive simulation study was conducted in which Landsat data were simulated at the pixel level and then classified to determine x at the segment level. The simulation study is described in Section IV. This study was limited to investigation of the regression and ratio estimators.

II. Classification and Estimators

The present estimation problem, in its general form, can be formulated as follows: consider a large population consisting of N segments. Each segment is a cluster of measurement units (presently, pixels). Let $C_1, C_2, \cdots, C_m$ be m distinct classes of units in the population. Suppose the measurement vector z is q-dimensional and has the multivariate normal distribution with mean vector μ_i and covariance matrix Σ_i for class C_i, $i = 1, 2, \cdots, m$. Suppose a set of training samples are obtained from each class and the unknown parameters μ_i and Σ_i are estimated from the sampled data. Let $\hat{\mu}_i$ and $\hat{\Sigma}_i$ denote their estimators. If $\hat{f}_i(z) = f(z, \hat{\mu}_i, \hat{\Sigma}_i)$ denotes the estimated density function for class C_i, obtained by replacing the unknown parameters by their estimates, and the classes are assumed to have equal *a priori* probabilities, a measurement unit u with observation z can be classified on the basis of the *maximum likelihood decision rule* as follows [7]:

Assign u to C_k if z belongs to region R_k, where

$$R_k = \{z: \ln \hat{f}_k(z) = \max_i \ln \hat{f}_i(z)\},$$

$$k = 1, 2, \cdots, m \tag{6}$$

with

$$\ln \hat{f}_i(z) = K_i - (\tfrac{1}{2})(z - \hat{\mu}_i)' \hat{\Sigma}_i^{-1} (z - \hat{\mu}_i)$$

and

$$K_i = -(p/2) \ln 2\pi - (\tfrac{1}{2}) \ln |\hat{\Sigma}_i|.$$

(Here, ln stands for the natural logarithm.) Define the random variables

$$\psi_k(z) = \begin{cases} 1, & \text{if } z \in R_k \\ 0, & \text{otherwise} \end{cases} \tag{7}$$

and

$$\eta_k(z) = \begin{cases} 1, & \text{if } u \in C_k \\ 0, & \text{otherwise} \end{cases}. \tag{8}$$

Then the set of pairs $(\eta_k(z), \psi_k(z))$, $k = 1, 2, \cdots, m$, characterizes the m-way classification of measurement units as actual versus classifier assigned. If $\psi_k(z) = \eta_k(z)$ for all units, $k = 1, 2, \cdots, m$, then the classification is perfect; otherwise it is fallible. The maximum likelihood decision rule is optimum in terms of minimizing the classification errors, provided the underlying assumptions hold true [8].

A. Estimation of a Single Class in a Cluster

Suppose C_1 is the class of interest and C_0 is the set of remaining classes in the population. Let y be the proportion of measurement units actually in C_1 for a cluster and let x be its estimate obtained from the classification of units in the cluster. Assume that the number of measurement units in a cluster is infinitely large. Then y and x can be approximated by the probabilities

$$x = P[\psi_1(z) = 1],\ y = P[\eta_1(z) = 1]. \tag{9}$$

Similarly, the two classification error rates are approximated by the conditional probabilities

$$\theta_0 = P[\psi_1(z) = 0 | \eta_1(z) = 1]$$

and

$$\theta_1 = P[\psi_1(z) = 1 | \eta_1(z) = 0]. \tag{10}$$

Here θ_0 will be known as the omission error rate and θ_1 as the commission error rate. From (9) and (10), one gets

$$\begin{aligned} x &= P[\psi_1(z) = 1] \\ &= P[\psi_1(z) = 1 | \eta_1(z) = 0]\ P[\eta_1(z) = 0] \\ &\quad + P[\psi_1(z) = 1 | \eta_1(z) = 1]\ P[\eta_1(z) = 1] \\ &= \theta_1 (1 - y) + (1 - \theta_0)\, y \\ &= \theta_1 + (1 - \theta_0 - \theta_1)\, y. \end{aligned} \tag{11}$$

Thus, for a cluster, x is a linear function of y.

One may similarly express y as a function of x by interchanging the role of the two variables $\psi_1(z)$ and $\eta_1(z)$ in (10). Define the conditional probabilities

$$\begin{aligned} \phi_0 &= P[\eta_1(z) = 1 | \psi_1(z) = 0] \\ \phi_1 &= P[\eta_1(z) = 0 | \psi_1(z) = 1]. \end{aligned} \tag{12}$$

Here, ϕ_0 is a measure of the relative frequency that a unit actually belongs to C_1 when it has been classified as being in C_0. The conditional probability ϕ_1 is for the reverse situation. From (9) and (12), taking a similar approach as in (11), one obtains

$$\begin{aligned} y &= \phi_0(1 - x) + (1 - \phi_1)\, x \\ &= \phi_0 + (1 - \phi_1 - \phi_0)\, x. \end{aligned} \tag{13}$$

Consider the joint probability of the two random variables given by

$$\lambda = P[\eta_1(z) = 1,\ \psi_1(z) = 0]. \tag{14}$$

Then it follows from (9) and (12) that

$$\phi_0(1 - x) = \lambda \tag{15}$$

and, hence, from (13)

$$(1 - \phi_1)\, x = y - \lambda. \tag{16}$$

Equations (15) and (16) relate x and y through the joint probability λ for the two random variables $\eta_1(z)$ and $\psi_1(z)$.

In the case of a finite size cluster containing M measurement units, the probabilities in (9) are replaced by relative frequencies as follows:

$$x = \frac{1}{M} \sum_{i=1}^{M} \psi_1(z_i)$$

and

$$y = \frac{1}{M} \sum_{i=1}^{M} \eta_1(z_i). \tag{17}$$

It may be observed that x and the error rates θ_0, θ_1, ϕ_0, and ϕ_1 are random quantities because the classification rule in (6) is based on randomly selected training samples. Thus, one may want to evaluate their distributional properties. The present study is restricted to the case of a large training sample size and hence, the variability in these quantities will be ignored.

B. Estimators of the Population Mean

Suppose n clusters are randomly selected from the population consisting of N clusters and (x_i, y_i), $i = 1, 2, \cdots, n$ are the pairs of observations for x and y in the sampled clusters. If $\bar{X}$ is the mean of the estimated proportions of units in C_1 for all N clusters in the population and $\bar{Y}$ is the actual mean value, then the following estimators of $\bar{Y}$ are considered.

a) Sample Mean:

$$\hat{\bar{Y}}_M = \bar{y} \tag{18}$$

where

$$\bar{y} = \sum_{1}^{n} y_i/n$$

b) Regression Estimator:

$$\hat{\bar{Y}}_R = \bar{y} + b(\bar{X} - \bar{x}) \tag{19}$$

where $\bar{x}$ and $\bar{y}$ are the means for the observed sample data and b is the estimated regression coefficient as defined in (3) in Section I.

c) Ratio Estimator:

$$\hat{\bar{Y}}_r = (\bar{y}/\bar{x})\, \bar{X} \tag{20}$$

d) Stratified Ratio Estimator:

$$\hat{\bar{Y}}_s = (\bar{y}_1/\bar{x}_1)\, \bar{X}_1 + (\bar{y}_0/\bar{x}_0)\, \bar{X}_0 \tag{21}$$

where $\bar{X}_1$ and $\bar{X}_0$ are the proportions of units in the population classified as C_1 and C_0, respectively, whereas $\bar{x}_1$ and $\bar{x}_0$ are the corresponding proportions of units in the sampled clusters. $\bar{y}_1$ and $\bar{y}_0$ are the proportions of units in the sampled clusters assigned to C_1 and C_0, respectively, that actually belong to C_1. The rationale for the stratified ratio estimator is to treat the two strata of units classified as C_1 and C_0 separately by constructing their ratio estimators individually, and then adding these two together. This estimator utilizes the additional information as to how accurate the units in the sample clusters were classified. This type of estimation approach was used in LACIE at a cluster level and led to better estimates than those based solely on the nonstratified approach [6].

In the Appendix, it is shown that the stratified ratio estimator can be expressed as

$$\hat{\bar{Y}}_s = \hat{\bar{Y}}_r + [\bar{\lambda}/(\bar{x}(1 - \bar{x}))] (\bar{x} - \bar{X}) \tag{22}$$

where $\bar{\lambda}$ is the average of the λ_i for the sampled clusters, λ_i is the joint probability of (14) for cluster i, and $\hat{\bar{Y}}_r$ is the ratio estimator given in (20). Note that the second term on the right side in (22) is analogous to that in (19) for the regression estimator. The coefficient $\bar{\lambda}/(\bar{x}(1 - \bar{x}))$ is a relative measure of the discrepancy between the actual and classifier assigned labels for units. If there is complete agreement, that is every sample unit is correctly classified, then $\bar{\lambda} = 0$ and $\hat{\bar{Y}}_s = \hat{\bar{Y}}_r$; otherwise the second term accounts for the fallibility of the classification rule.

C. Sampling Properties of the Estimators

For the standard survey estimation case, the bias and variance for estimators *a*)–*c*) are well known [3]. Thus, we will state here the main results, skipping details unless warranted.

a) The estimator $\hat{\bar{Y}}_M$ is simply the sample mean and hence it is unbiased and has variance

$$V(\hat{\bar{Y}}_M) = (1 - n/N)\, S^2/n \tag{23}$$

where S^2 is the population variance and n is the sample size. An estimate of the variance in (23) is given by

$$v(\hat{\bar{Y}}_M) = (1 - n/N)\, s^2/n \tag{24}$$

where N is the population size and

$$s^2 = \sum_1^n (y_i - \bar{y})^2/(n - 1). \tag{25}$$

b) The regression estimator $\hat{\bar{Y}}_R$ can be used even when the underlying regression function is not strictly linear, provided a sample plot of the y_i against x_i appears approximately linear [3, p. 193]. Presently, the regressor values x_i are estimated and therefore, the previously known results for bias and variance of $\hat{\bar{Y}}_R$ as given in [3] hold true only if the x_i are assumed known. Recently, Hung [9] investigated the case where the x_i are estimates and showed that under certain conditions, the estimator $\hat{\bar{Y}}_R$ with the x_i estimated has the same limiting distribution as when the x_i are known.

The bias of $\hat{\bar{Y}}_R$ is of order $1/n$, and its variance for large n is given by

$$v(\hat{\bar{Y}}_R) = (1 - n/N)\, S^2\, (1 - R^2)/n \tag{26}$$

where R is the population correlation coefficient between the y_i and x_i. An estimate of this variance using the large sample variance formula given in [3, p. 194] is given by

$$v(\hat{\bar{Y}}_R) = (1 - n/N)\, s_e^2/n \tag{27}$$

where

$$s_e^2 = \sum_1^n (y_i - \hat{y}_i)^2/(n - 1)$$

$$\hat{y}_i = \bar{y} + b(x_i - \bar{x}).$$

The variance estimator in (27) generally underestimates the true variance for small sample sizes [10]. Another variance estimator based on a formula on p. 197 in [3], given next, is considered to be superior for small sample sizes.

$$v(\hat{\bar{Y}}_R) = [(1 - n/N)\, s_e^2/n]\, [1 + 1/(n - 3) + 2g_1^2/n^2] \tag{28}$$

where

$$g_1 = \frac{1}{N - 1} \sum_1^N (x_i - \bar{x})^3 \Big/ \left| \frac{1}{N - 1} \sum_1^N (x_i - \bar{x})^2 \right|^{3/2} \tag{29}$$

is the relative skewness of the distribution of x_i in the population.

c) In general, the ratio estimator is biased and is no more efficient than the regression estimator. The bias and variance of $\hat{\bar{Y}}_r$ with x_i assumed known are discussed in [3, p. 160]. When the x_i are estimated, the properties of $\hat{\bar{Y}}_r$ have not been investigated; however, in the limiting case these are expected to be the same as in [3].

d) The estimator $\hat{\bar{Y}}_s$ is new and its properties need to be established. In the appendix, we derive expressions of the bias and the mean squared error of $\hat{\bar{Y}}_s$ to terms of order n^{-1}. It is shown that in the limit, as the sample size n increases without bound, $\hat{\bar{Y}}_s$ has the same bias and mean squared error as the ratio estimator $\hat{\bar{Y}}_r$.

III. An Evaluation of Estimators

In this section we discuss a certain sampling study conducted to evaluate the above estimators. For simplicity, we restrict attention to a two-class case in which the measurement vector z is distributed normally with mean vectors μ_1 and μ_0 for C_1 and C_0, respectively, and common covariance matrix Σ. By a set of linear transformations, the class structure can be obtained in the canonical form so that the vector z can be assumed to have class mean vectors $(-\Delta/2, 0, 0, \cdots, 0)$ and $(\Delta/2, 0, \cdots, 0)$ for C_1 and C_0, respectively, and common covariance matrix I, where

$$\Delta = [(\mu_1 - \mu_0)'\, \Sigma^{-1}\, (\mu_1 - \mu_0)]^{1/2} \tag{30}$$

is the Mahalanobis distance between the two classes and is a measure of class separability. When Δ is known, the maximum likelihood classification rule is to classify a measurement unit in C_1 if $z_1 < 0$, and in C_0 otherwise, where z_1 is the first component of measurement vector z. Observe that z_1 has a univariate normal distribution and the omission and commission error rates for the population are each equal to $\Phi(-\Delta/2)$, where Φ denotes the cumulative distribution function for the standard normal [11].

For the stratified ratio estimator, the classification error rates must be evaluated for individual clusters. Since the cluster size is assumed infinitely large, the class distributions for each cluster can be approximated by the normal distribution. For cluster i, let $\xi_i e$ and $(\xi_i + \Delta_i) e$ be the mean vectors of the measurement vector z for C_1 and C_0, respectively, where $e = (1, 0, 0, \cdots, 0)$ is a $q \times 1$ vector and I is the common covariance matrix. This dis-

tributional assumption allows variation in class distributions across clusters in the population. To have the class means as in the first paragraph, we assume that the average value of ξ_i across clusters is $-\Delta/2$ and that of $(\xi_i + \Delta_i)$ is $\Delta/2$.

In practice, the parametes ξ_i, Δ_i, and y_i are unknown except for the sampled clusters, and hence the error rates cannot be obtained for all clusters. However, once the classification of data is completed the x_i can be computed directly for each cluster as the proportion of units from cluster i that are assigned to C_1 by the classifier. Accordingly, the estimators of $\bar{Y}$ described in Section II can be easily computed.

To investigate the bias and variance of the estimators and to compare their relative performances, the following simulation study was conducted: A hypothetical population consisting of 500 clusters was considered. The number of units per cluster is assumed infinite. For a given population mean $\bar{Y}$, the beta distribution (IMSL subroutine GGBTR [12]) was used to generate the actual proportions y_i of the class of interest for each of the 500 clusters. For each cluster, the distribution of the measurement variable z_1 for the class of interest was assumed normal with mean $\xi_i = \nu_i - \Delta_i/2$ and variance 1. For the other class, the distribution was assumed normal with mean $\xi_i + \Delta_i = \nu_i + \Delta_i/2$ and variance 1. The ν_i allow the mean of the distribution of the measurement variable for the class of interest to vary from cluster to cluster. The ν_i were generated from a normal distribution with mean 0 and variance σ^2 (IMSC subroutine GGNML [12]), with σ^2 specified. The Δ_i allow the distance between the means for the two classes to vary from cluster to cluster. The triangular distribution (IMSL subroutine GGTRA [12]) over the interval $(\Delta - p, \Delta + p)$, which has mean Δ, variance $p^2/6$ and range $2p$, was used to generate the Δ_i, given Δ and p. To ensure $\Delta_i > 0$, it was assumed that $\Delta > p$.

The indices of each of the variables for the 500 clusters were randomly permuted (IMSL subroutine GGPER [12]) and the first n indices were selected as the sample for which the actual proportions were assumed known. For the maximum likelihood classification rule, the discriminant boundary point was estimated from the parametric values of the sampled clusters by

$$\tau = \sum_1^n y_i(\nu_i - \Delta_i/2) \Big/ \sum_1^n y_i + \sum_1^n (1 - y_i)(\nu_i + \Delta_i/2) \Big/ \sum_1^n (1 - y_i) \quad (31)$$

and the classification rule for all measurement units in the population was to assign a unit to C_1 if $z_1 < \tau/2$, and to C_0, otherwise. Note that τ estimates the distance between the means of the measurement variable for the class of interest C_1, and the other class C_0. The individual means are estimated by a weighted average of the sampled cluster means, the weights being the proportion of the cluster belonging to the class. In terms of the random variable ψ defined in (7), we have

$$\psi(z) = \begin{cases} 1, & \text{if } z_1 < \tau/2 \\ 0, & \text{otherwise.} \end{cases} \quad (32)$$

Note that we did not actually generate the measurement vector z. These results correspond to having an infinite number of measurement units for training, since we assumed the number of units per cluster to be infinite. The errors of misclassification were computed for each of the 500 clusters.

It follows from (10) and (32) that for cluster i, the omission and commission error rates are

$$\theta_{0i} = \Phi(-(\tau + \Delta_i)/2 + \nu_i)$$

and

$$\theta_{1i} = \Phi((\tau - \Delta_i)/2 - \nu_i). \quad (33)$$

Thus, the estimated proportion of units in C_1 for cluster i is obtained from (11) and (33) as

$$x_i = \Phi((\tau - \Delta_i)/2 - \nu_i) + [\Phi((\tau + \Delta_i)/2 - \nu_i) - \Phi((\tau - \Delta_i)/2 - \nu_i)]\, y_i \quad (34)$$

noting that $1 - \Phi(x) = \Phi(-x)$.

This process was replicated 500 times for each combination of parameters considered in order to compute the bias, variance, and mean squared error for each of the estimators of $\bar{Y}$. Fig. 1(a) shows a histogram of the 500 actual proportions generated from a beta distribution with mean 0.25. The actual mean and variance of these 500 proportions are 0.2575 and 0.02366, respectively.

Fig. 1(b) shows a corresponding histogram of one realization of the classified proportions determined from (34) with input generated using $n = 10$, $\sigma = 0.1$, $\Delta = 1.5$, and $p = 1$. A scatter plot of the actual versus the classified proportions is given in Fig. 1(c). In this case, the relationship is approximately linear (but not through the origin) and a linear regression model should hold reasonably well. The summary results for the estimators for 500 replications (one of which is plotted in Fig. 1(c)) from this combination of parameter values are presented in Table I. All estimators are truncated at 0 and 1 before computing the summary statistics. The MSE ratio is the ratio of the mean squared error (MSE) for an estimator to the MSE of the sample mean estimator $\hat{Y}_M$. This, of course, is an estimate of the relative efficiency of the sample mean relative to the estimator.

The bias is negligible for each estimator, though it is statistically significant in the case of the regression estimator. The MSE ratio of 0.342 for the regression estimator is the smallest.

Simulations were conducted for many other parametric values to evaluate the performance of estimators across a wide range of situations. Table II shows the values of the parameters used in the simulation. It encompasses cases of low and high class separability, small and large sample size, and equal and unequal class proportions. Increasing

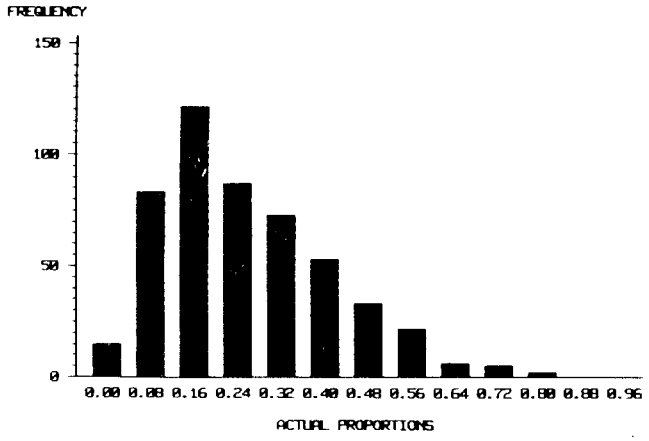

(a)

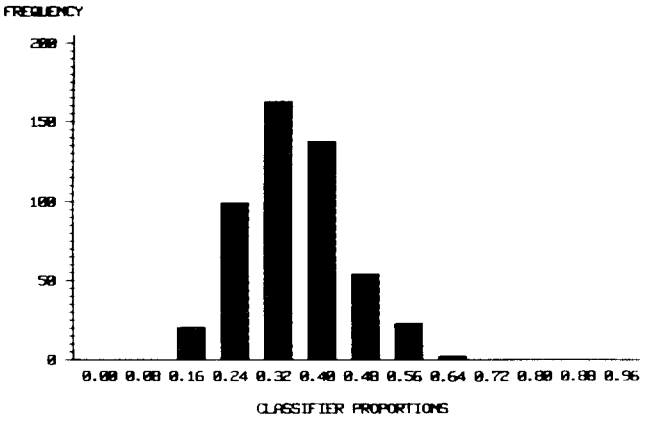

(b)

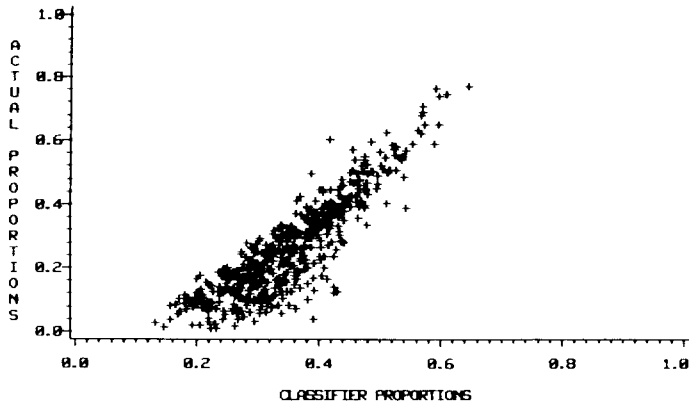

(c)

Fig. 1. Histograms and scatter plot of class proportions when $\bar{Y} = 0.25$, $\sigma = 0.1$, $\Delta = 1.5$, $p = 1$, and $n = 10$.

TABLE I
SUMMARY STATISTICS FOR 500 REPLICATIONS WITH $\bar{Y} = 0.25$, $n = 10$, $\sigma = 0.1$, $\Delta = 1.5$, AND $p = 1.0$

Estimator	Bias	Variance	MSE	MSE Ratio	t-Statistic
Sample Mean	.0020	.0021	.0021	1.000	.97
Regression	-.0033	.0007	.0007	.342	-2.77
Ratio	-.0003	.0009	.0009	.425	- .19
Stratified Ratio	.0011	.0012	.0012	.595	.72

values of p or σ give rise to larger variability in separability, resulting in lower correlation between the x_i and y_i.

In each simulation run, the square of the correlation coefficient between the x_i and y_i, R^2, was computed for both the population and the sample. Variation in the population correlation coefficient arises due to the decision rule for the maximum likelihood classifier varying from sample to sample for the 500 replications. Figs. 2 and 3 summarize the MSE ratios of the estimators as a function

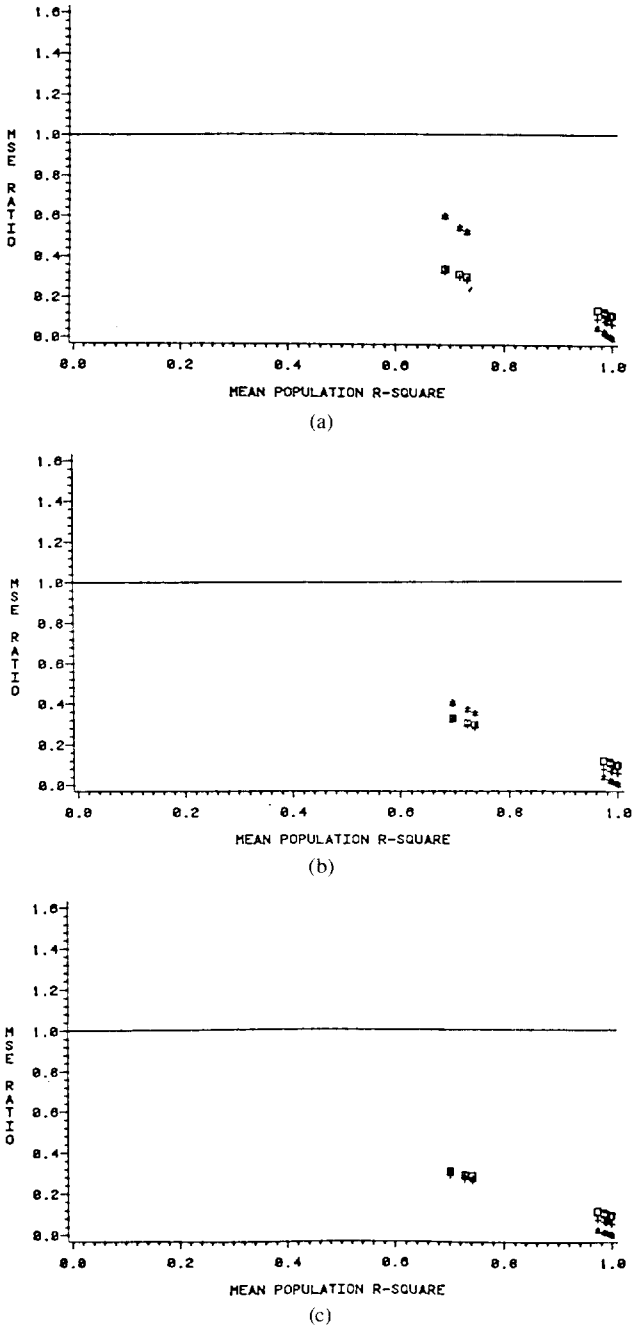

Fig. 2. The MSE ratios of the three estimators for sample sizes (a) 4, (b) 10, and (c) 30 when $\bar{Y} = 0.25$ and $\Delta = 3$. (Legend: Regression = *, Ratio = +, and Stratified Ratio = □).

TABLE II
INPUT PARAMETRIC VALUES

n = 4, 10, 30
$\bar{Y}$ = .25, .5
σ = .01, .10, .50
Δ = 1.5, 3.0
p = 0, .5, 1

of the mean population R^2 for the 500 replications. These two figures are based on $\bar{Y} = 0.25$ and all combinations of the other parameter values in Table II. Fig. 2 shows the results for a Δ value of 3, corresponding to high separability between C_1 and C_0. Fig. 3 is for a Δ value of 1.5, corresponding to low separability between C_1 and C_0. The different symbols in each scatterplot represent the three different estimators. The three lowest values of mean population R^2 in each plot correspond to $\sigma = 0.50$. The three largest values correspond to $\sigma = 0.01$; the middle three to $\sigma = 0.10$. Within each of these three sets, the largest R^2 corresponds to $p = 0$ and the smallest to $p = 1$.

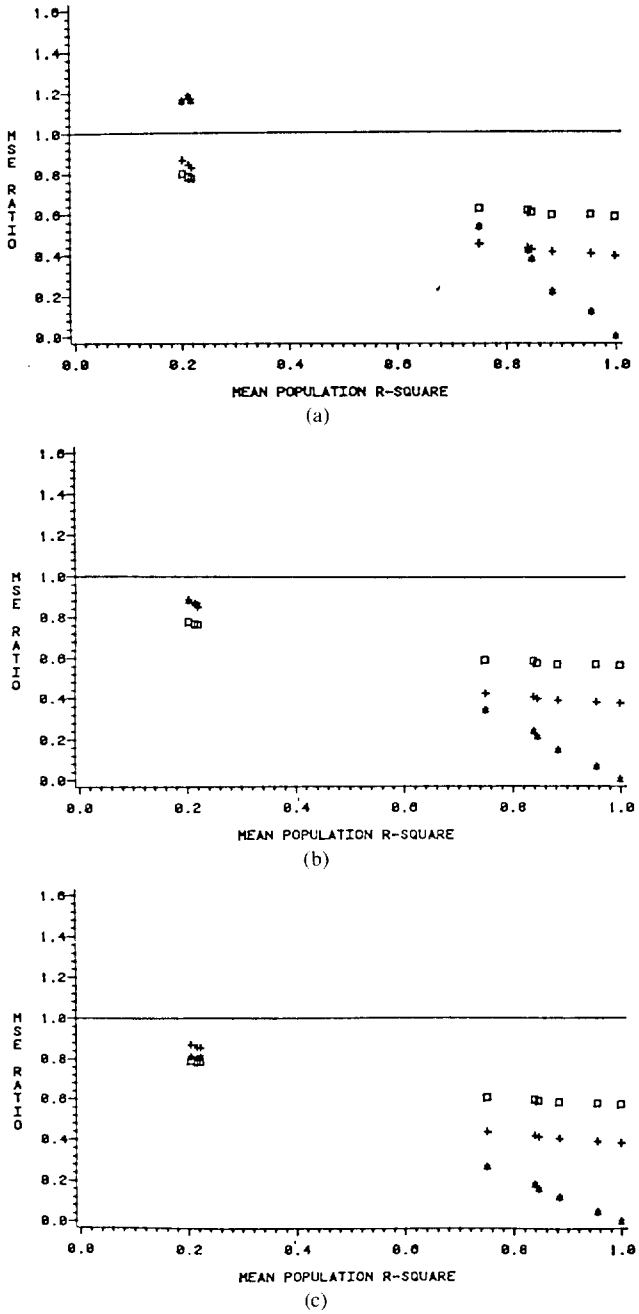

Fig. 3. The MSE ratios of the three estimators for sample sizes (a) 4, (b) 10, and (c) 30 when $\bar{Y} = 0.25$ and $\Delta = 1.5$. (Legend: Regression = *, Ratio = +, Stratified Ratio = □).

Fig. 2 indicates that when the class separability is quite good across clusters and the sample size is large, all three estimators are similar in performance and significantly improve the efficiency relative to the sample mean. When the sample size is reduced, the ratio and stratified ratio

TABLE III
MEANS AND STANDARD DEVIATIONS OF THE VARIANCE RATIOS

Sample Size	Statistics	Variance Estimator	
		Large Sample	Cochran
4	Mean	.602	1.227
	Standard Deviation	.108	.215
10	Mean	.884	1.015
	Standard Deviation	.074	.083
30	Mean	.972	1.000
	Standard Deviation	.096	.094

estimators are hardly affected. The regression estimator performs well overall with some decrease in efficiency when the sample size is small.

When the separability between classes is reduced (Fig. 3), the stratified ratio estimator appears to be the most robust. It is the only estimator that provided improvement over the sample mean for all cases considered (for $\bar{Y} = 0.5$, not shown, the ratio estimator had MSE ratios greater than 1 for $\Delta = 1.5$ and low mean population R^2 values). For moderate to large values of R^2, however, the regression estimator is superior. Similar results were obtained in the case of $\bar{Y} = 0.5$.

Because of a greater interest in the regression estimator, its variance estimation was also investigated in this sampling study. The large sample variance estimator given in (27) and the alternative estimator due to Cochran given in (28) were computed for all 108 combinations of parameter values in Table II. The sampling results showed that the Cochran estimator tends to reduce the bias for the lower sample sizes, while retaining the large sample property. In fact, it tended to be conservative for the lower sample sizes as compared to the large sample estimator which significantly underestimated the variance of $\hat{\bar{Y}}_R$. Presented in Table III are the means and standard deviations of the ratios of estimated to actual variance in each case for different sample sizes. It is seen that in the case of $n = 4$, the underestimation of the variance using the large sample variance estimator could be substantial. The Cochran estimator is seen to be almost unbiased except when $n = 4$.

IV. A Simulation Study

The evaluation study in Section III is fairly general and applies not only to the present problem addressed in Section I, but it is also applicable to any other sample survey problem in which the auxiliary variable is obtained using a classifier. In order to investigate the crop acreage estimation using a Landsat-based estimator as auxiliary variable, we conducted another simulation study where the Landsat data were simulated at the pixel level with input derived from a real situation and these were classified using the classification rule discussed in Section II to obtain the estimated crop acreages for the segments. This study and its results are described in this section.

A. Simulation of Landsat Data

A simulation program was developed to create segments and their simulated multispectral scanner (MSS) data similar to the real MSS data for the 33 JES segments in northern Missouri acquired by Landsat in May and August 1979. The simulated segments were designed to be similar to the actual data in the expected crop acreage proportions, field size distributions, segment size, and MSS data. To achieve this, fields were selected randomly according to the empirical distribution of crop fields observed for the 33 JES segments. These fields were joined together by arranging them in horizontal and vertical arrays and then segments were randomly located on the generated field patterns. A pixel grid was overlaid on each simulated segment such that the angle between the pixel and field edges was similar to that of actual data. Segments with an expected area of 1 mi^2 rather than 0.5 mi^2, as was the case for the 33 Missouri segments, were simulated. This was done to conform with a more standard size for JES segments.

MSS data were simulated for the segments in each of the four channels for each of the two Landsat acquisitions, and for both pure and mixed pixels. The first step in the spectral data simulation was to find the principal components of the observed eight spectral values for pure pixels in each crop or cover type. The component values were generated corresponding to each of these principal components. By definition, the principal components are uncorrelated, therefore, these were independently simulated. This simulation was done so as to have the same variance for within fields, between fields (within segment), and between segments as observed for the real data for each cover type. A nested analysis of variance model with these three variance components was used for each of the four principal components for each cover type. Each of the random components (effects) due to pixel, field, and segment was assumed to have the normal distribution with mean 0 and variance equal to the computed variance component using the real data. These simulated principal component values were then transformed into spectral values for the pure pixels through the use of inverse eigen-vector matrices and applicable mean values. A mixed pixel was simulated by linearly combining spectral values of pure pixels with weights equal to the proportions of pure areas in the mixed pixel. The statistical distributions of the simulated spectral values were found to closely approximate their corresponding distributions of Landsat observed MSS data.

B. Classification and Estimation

There were 12 cover types of which four cover types accounted for less than one percent of pixels in the 33 JES segments, and hence these were eliminated from the study. Spectral data were simulated for each of the remaining cover types consisting of pasture, soybeans, corn, waste, wood, hay, winter wheat, and alfalfa. These data were classified using the maximum likelihood decision rule de-

TABLE IV
THE OVERALL PERCENT OF CORRECTLY CLASSIFIED PURE PIXELS OF EIGHT COVER TYPES

No. of Channels	Actual Data	Simulated Data
2	41	37
4	44	42
8	50	65

TABLE V
NUMBER OF EVALUATIONS AND POPULATION—SAMPLE SIZE COMBINATIONS

		Sample Size (n)			
		4	6	10	15
Population Size (N)	25	6	6		
	50	6	6	6	
	100	2	2	2	2

scribed in Section II. The classification accuracies for the first i) two channels, ii) four channels, and iii) all eight channels are compared to that obtained using the actual Landsat data as shown in Table IV.

The best agreement is in the case of four channels. Because of this and because computations are reduced considerably with the use of four channels versus eight channels, the first four channels were used in our study.

For each simulated segment, the actual crop acreage proportions were determined by tabulating the number of pixels assigned to each crop or cover type. The estimated proportions are the relative frequencies of pixels that were classified into these crop or cover types by the maximum likelihood rule. Both ratio and regression estimates were obtained following the estimation procedures described in Section II.

Table V shows the various combinations of population size and sample size for which evaluations of estimators were made. However, due to extensive and very time consuming computations involved in simulation and classification of MSS data, the evaluation for each of these combinations was split into several sets, each based on 20 replications. The numbers of evaluation sets for different population and sample size combinations are also listed in Table V.

C. Numerical Results

Table VI lists the estimated bias, variance, and relative efficiency for each estimator of the mean number of pixels per segment in a cover type for each combination of population and sample sizes. Alfalfa was frequently found to have too few pixels to compute estimates so it was not included in the evaluations. (The figures in the table are the mean values obtained from the number of simulation sets shown in Table V.) The bias for each individual case of population and sample size combination is insignificant using a t-test at the 5-percent level. Since the estimates are based upon a small number of replications, this test has a low power. Hence, a nonparametric sign test was

TABLE VI
MEAN DIFFERENCE BETWEEN AN ESTIMATE AND POPULATION MEAN (ESTIMATED BIAS), VARIANCE, AND RELATIVE EFFICIENCY

			BIAS		VARIANCE		RELATIVE EFFICIENCY	
COVER TYPE	N	n	Regression Estimator	Ratio Estimator	Regression Estimator	Ratio Estimator	Regression Estimator	Ratio Estimator
Pasture	25	4	-9.6	-12.1	2972	2284	1.2	1.5
		6	-6.8	-6.5	1470	984	1.2	1.7
	50	4	-2.7	-6.8	5011	2431	.9	1.6
		6	-8.8	-10.1	2609	1832	1.0	1.4
		10	-5.0	-5.6	1103	1056	1.3	1.4
	100	4	-25.1	-16.7	3661	2736	1.3	1.4
		6	-16.8	-18.1	1240	993	1.9	2.2
		10	-2.4	-2.1	1256	892	1.1	1.7
		15	2.0	-0.5	1021	851	1.1	1.3
Soybeans	25	4	1.5	-1.2	1158	909	2.2	2.8
		6	-1.2	-2.2	685	496	1.7	2.1
	50	4	5.6	-1.7	1679	1126	1.4	3.0
		6	1.7	-1.2	609	525	2.6	2.9
		10	2.0	0.7	319	307	2.6	2.8
	100	4	-8.8	-2.6	844	905	2.7	2.9
		6	1.9	2.2	544	462	3.1	3.7
		10	-1.8	-2.6	400	345	2.2	2.5
		15	-2.5	-3.6	354	310	1.9	2.0
Corn	25	4	-9.4	-4.5	746	508	1.7	2.4
		6	-5.1	-3.4	293	335	2.8	2.2
	50	4	-9.0	-6.0	664	501	1.6	2.2
		6	-9.1	-7.2	453	393	1.7	2.0
		10	-5.6	-5.3	216	242	1.9	1.7
	100	4	-14.1	-7.9	248	257	3.0	4.1
		6	-5.3	-3.3	376	321	2.2	2.6
		10	-4.5	-3.5	241	191	2.1	2.3
		15	-4.3	-1.7	187	167	1.7	2.1
Waste	25	4	22.6	14.5	3310	1692	0.5	0.9
		6	9.2	8.2	1035	813	1.0	1.2
	50	4	16.3	12.0	3725	2102	0.4	0.9
		6	14.5	12.8	1401	1132	0.7	0.9
		10	6.5	3.8	557	434	1.1	1.5
	100	4	30.4	22.1	3581	2586	0.4	0.6
		6	18.9	14.2	1853	1372	0.5	0.7
		10	8.1	7.8	804	633	0.8	1.0
		15	2.2	-1.0	235	225	2.2	2.8
Woods	25	4	-1.8	0.1	1288	521	1.0	1.6
		6	-1.4	-1.3	423	362	1.4	1.6
	50	4	-0.4	0.4	1180	786	0.8	1.3
		6	0.0	0.7	551	494	1.2	1.4
		10	-0.4	-1.2	314	266	1.2	1.3
	100	4	4.8	5.1	1483	660	0.7	1.5
		6	0.4	1.0	460	309	1.9	2.4
		10	-0.4	1.3	434	416	0.8	1.1
		15	0.8	0.3	159	160	1.3	1.3
Hay	25	4	5.6	2.9	1118	511	0.7	1.1
		6	-1.6	-2.4	381	321	1.1	1.2
	50	4	3.6	1.4	1248	672	0.6	1.0
		6	2.0	0.2	678	457	0.6	0.9
		10	3.3	2.3	266	240	0.8	1.0
	100	4	2.3	-1.0	1241	711	0.5	0.8
		6	6.4	5.3	416	296	0.9	1.3
		10	0.2	-3.0	246	158	1.0	1.4
		15	1.5	1.5	259	249	0.6	0.6
Wheat	25	4	2.0	0.2	171	115	0.9	1.3
		6	-0.3	-0.3	77	65	0.9	1.2
	50	4	0.2	0.5	231	162	0.8	1.2
		6	-0.4	-0.9	124	103	0.8	1.0
		10	0.1	-0.1	44	42	1.3	1.4
	100	4	-3.9	-4.2	264	163	0.8	1.3
		6	-1.1	-1.1	107	109	1.1	1.1
		10	0.7	0.1	44	35	1.2	1.6
		15	1.5	0.9	49	41	1.0	1.2

used to test for significant bias for each cover type across all population and sample size combinations. For this test, the null hypothesis is that the median bias is zero. Hence, one would expect an equal number of negative and positive estimates of bias under the null hypothesis. The hypothesis is rejected at the 5-percent significance level if there are either less than two or more than seven negative estimates out of nine independent estimates considered here [13].

Using the sign test, it can be determined from Table VI that the bias is significant for pasture, corn, and waste for both estimators and for hay only for the regression estimator. The mean percent of actual pixels simulated for the cover types are as follows: pasture—30 percent, soybeans—25 percent, corn—12 percent, waste—13 percent, woods—9 percent, hay—7 percent, wheat—3 percent, and alfalfa—1 percent.

Thus, there was no apparent pattern to significant bias in terms of the relative size of a cover type. The relative efficiencies of the ratio estimator are consistently higher

TABLE VII
MEAN POPULATION REGRESSION SLOPE AND MEAN DIFFERENCE BETWEEN THE SAMPLE AND POPULATION REGRESSION SLOPES

PARAMETER	N	n	COVER TYPES						
			Pasture	Soybeans	Corn	Waste	Woods	Hay	Wheat
Population Slope	25	4	1.54	.97	1.00	1.56	.89	.29	.32
		6	1.49	.84	1.06	2.04	1.01	.32	.29
	50	4	1.49	1.04	.95	1.33	.73	.26	.37
		6	1.79	1.01	.96	1.71	.72	.21	.37
		10	1.67	.98	.99	1.84	.74	.21	.38
	100	4	1.81	.97	.97	1.15	.64	.19	.28
		6	1.87	.96	.91	1.31	.69	.22	.35
		10	1.45	.93	.91	2.16	.77	.23	.29
		15	2.10	1.03	1.02	2.04	.62	.16	.36
Mean Difference In Slopes	25	4	.67	.08	.09	1.13	.23	.33	.12
		6	.46	.06	.07	.24	-.01	.14	.04
	50	4	.64	-.04	-.04	1.11	.26	.33	.15
		6	.11	-.01	.00	.67	.18	.19	.08
		10	.22	.07	.05	.89	.17	.16	.07
	100	4	-.11	-.05	.02	1.27	.67	.11	.08
		6	.23	.04	.03	1.28	.29	.31	.13
		10	.34	-.03	.06	.76	.20	.19	.01
		15	.27	-.02	-.05	.50	.08	.14	.10
Mean Population R^2			.37	.52	.36	.14	.28	.05	.09

than those of the regression estimator. The maximum gain in efficiency due to the use of either estimator is in soybeans, showing a substantial savings (more than half over the direct expansion estimator) in sampling of JES segments for ground enumeration. For corn, the range in RE is from 1.6 to 3.0 for the regression estimator and from 1.7 to 4.1 for the ratio estimator. For other cover types, the relative efficiencies are not substantially different from 1.0.

To investigate the cause of bias in the regression estimator, the regression coefficient (slope) was computed using the data on (x, y) from segments in the sample as well as those in the population. Table VII lists the mean slopes obtained for the population case and the mean difference between the sample and population slopes. Overall, the slopes are nearly one for soybeans and corn, but differ substantially from one for other cover types. The two slopes are significantly different for all cover types except soybeans and corn at the 5-percent significance level of the sign test and the slope from the sample tends to be larger than that of the population. This is an expected result since the MSS data from the sample segments are used in training the classifier and thereby, will have better classification accuracy than the remaining MSS data. Hence, it may lead to a significantly different relationship between x and y in the sample relative to the population. Overall, there is a tendency for differences to exist in both the slopes and means as can be seen in [14, Tables III and V].

Also included in Table VII are the mean population R^2 values for each cover type. Better correlations are seen for the prevalent cover types.

In general, the regression estimator is biased [3] and the bias due to the use of training sample segments to estimate the regression line may confound with the inherent bias of the regression estimator. To investigate this problem, a small study was conducted. A test set of six segments was repeatedly selected at random from a population of 25, after an independent set of six sample segments had been used to train the classifier. A regression estimate was computed from each test set for all seven crops in each of

TABLE VIII
MEAN BIAS OF REGRESSION ESTIMATES FOR NUMBER OF PIXELS PER SEGMENT USING INDEPENDENT SETS OF SAMPLES FOR CLASSIFICATION AND REGRESSION ($N = 25$, $n = 6$)

	Pasture	Soybeans	Corn	Waste	Woods	Hay	Wheat
Bias	-0.91	-4.68	-1.46	3.84	2.83	5.07	-0.50
t-statistic	-0.79	-5.22*	-1.38	2.20*	2.57*	4.80*	-1.64
Relative Bias @	-0.50	-2.20	-1.32	2.90	4.44	8.77	-2.07

* Significant at the 5% level of significance.
@ Percent bias relative to the crop area.

20 replications for each of 20 different classifications of the single population (2800 regression estimates). Table VIII contains the results obtained for the bias per crop in this analysis. It shows signifiant biases for soybeans, waste, woods, and hay, indicating a confounding effect since the bias was not significant earlier for this set of cover types. Only one population was used in this analysis (thus the bias may be population specific) and a further study is necessary to make a conclusive inference.

The two variance estimators, the large sample and Cochran, given in (27) and (28), were evaluated for underestimation of the variance of the regression estimator as in the earlier sampling study. The results were similar. The large sample variance estimate underestimated the actual variance and the Cochran estimator was essentially unbiased.

V. SUMMARY AND CONCLUSIONS

The USDA-proposed method of improving the probability survey crop acreage estimates using Landsat derived estimates as auxiliary information was analytically formulated. The bias and variance of the regression, ratio and stratified ratio estimators were outlined for the large sample case. Simulation studies were conducted to investigate the small sample properties of the estimators, as this is a typical situation in the described USDA problem.

In the sampling study segment-level data were simulated for a wide variety of situations corresponding to low and high separability, small to large sample sizes, and equal and unequal class proportions. It was found that no estimator was uniformly superior. Variation of class separability across clusters and the sample size influenced the performance of an estimator most. The regression estimator was most efficient unless the sample size was very small or R^2 was low due to the class separability varying considerably across clusters, in which case the stratified ratio estimator was preferable. The ratio estimator showed significant bias in the case of $\bar{Y} = 0.25$ whereas the regression estimator had significant yet negligible bias when sample size was moderate to large. The stratified ratio estimator was robust.

For the regression estimator, the large sample variance estimator underestimated the variance considerably in small to moderate sample size cases. On the other hand, the Cochran variance estimator overestimates the variance when the sample size is small.

A Review of Three Discrete Multivariate Analysis Techniques Used in Assessing the Accuracy of Remotely Sensed Data from Error Matrices

RUSSELL G. CONGALTON AND ROY A. MEAD

Abstract—**Three discrete multivariate analysis techniques were used to assess the accuracy of land use/land cover classifications generated from remotely sensed data. Error matrices or contingency tables were analyzed using these techniques and the results reported. The first technique is a normalization procedure using an "iterative proportional fitting" algorithm that allows for direct comparison of corresponding cell values in different matrices irregardless of sample size. The second technique provides a method of testing for significant differences between error matrices that vary by only a single variable or factor. The third technique allows for multivariable comparisons to be made between matrices. Each technique is implemented through the use of a computer program.**

I. INTRODUCTION

THE NEED FOR procedures to assess the accuracy of remotely sensed data has been adequately documented in the literature (e.g., [14]–[16], [5]). With the arrival of Landsat Thematic Mapper imagery and SPOT imagery, the need for such techniques becomes even more important. The objective of this paper is to review three discrete multivariate analysis techniques used in assessing the accuracy of remotely sensed data from error matrices. Following the description of the techniques, some example analyses will be presented. It is not within the scope of this paper to review other methods of accuracy assessment, nor is it possible to present all the theoretical details of the three techniques described here. Those researchers interested in pursuing this topic further should see [4].

The method of accuracy assessment described in this paper employs discrete multivariate analysis techniques. Other names for this type of analysis include contingency table analysis and the analysis of cross-classified categorical data. These techniques are appropriate for remotely sensed data because they are designed for the analysis of discrete data. Remotely sensed data are discrete (noncontinuous) and multinomially distributed. Most previous work in accuracy assessment involves the use of parametric statistical techniques which assume that the data is continuous and normally distributed.

The most common way to represent the accuracy of a classification derived from remotely sensed data is in the form of an error matrix [2], [8], [10]. An error matrix is a square array of numbers set out in rows and columns which express the number of pixels assigned a particular land cover type relative to the actual ground-verified land cover type. The columns of the matrix represent the reference data (assumed correct) while the rows indicate the classification of the remotely sensed data (satellite data or aerial photography). This form of expressing accuracy as an error matrix is an effective way to evaluate both errors of inclusion (commission errors) and errors of exclusion (omission errors) present in the classification of the remotely sensed data. In addition, the error matrix allows for the analyst to determine the performance of individual categories as well as for the overall classification [9]. In a 100-percent correct classification, all the nondiagonal elements of the error matrix would be zero, indicating no misclassifications. An error matrix is typically generated using only a sample of the data within the area of interest. An important assumption made here is that this sample be representative of the entire area.

Given an error matrix, a simple procedure can be used to determine the overall performance accuracy of the classification. The values on the major diagonal (i.e., correctly classified pixels) are summed up and divided by the total number of pixels classified. This number is then a measure of overall performance accuracy and is the most common use of the error matrix in accuracy assessment. However, two more sophisticated statistical techniques are now being used to further assess the accuracy of remotely sensed data. These two techniques are analysis of variance and discrete multivariate analysis.

The analysis of the variance technique uses only the diagonal elements in the error matrix. Also, the technique requires that the diagonal element values (data) be continuous and normally distributed. As previously mentioned, error matrix values are discrete and multinomially distributed. The diagonal elements of the error matrix can be converted to a normal distribution using various transformations [13]. However, another assumption of analysis of

Manuscript received April 1, 1985; revised July 17, 1985. This work was supported by the Nationwide Forestry Applications Program, Renewable Resources Inventory Project, Cooperative Agreement 13-1134, under the AgRISTARS program. This paper is intended as a review of techniques published in a previous paper. These materials are reproduced, with permission, from *Photogrammetric Engineering and Remote Sensing*, vol. 49, no. 12, pp. 1671-1678, 1983.

R. G. Congalton is with the Department of Forestry and Resource Management, University of California, Berkeley, CA 94720.

R. A. Mead is with the USDA Forest Service, Atlanta, GA 30309.

IEEE Log Number 8406240.

variance is that the values along the diagonal (i.e., the categories) in the error matrix are independent. This assumption does not hold for remotely sensed data. Additional details and examples of this technique can be found in [12].

The discrete multivariate analysis techniques do not assume that the categories are independent nor do they require any transformation of the data. Instead, these techniques were designed to deal specifically with categorical data. Discrete multivariate analysis also uses the entire error matrix and not just the diagonal elements. As suggested by [2], "contingency table analysis is the most natural framework for accuracy assessment, both for the convenient display of empirical results and for the ease of statistical analysis."

II. Discrete Multivariate Analysis Techniques

Three different methods of comparing error matrices using discrete multivariate analysis techniques are reviewed here. The first method allows for the direct comparison of values within the error matrices through a process called normalization. The second method computes a measure of agreement between error matrices, which can be used to test if the matrices are statistically significantly different. The third method provides for the simultaneous examination of all factors affecting the classification accuracy.

The first comparison procedure allows for corresponding cell values in different error matrices to be directly compared. This comparison is made possible by a standardizing process called normalization [1]. Normalization of an error matrix is performed by a procedure called "iterative proportional fitting." The rows and columns of a matrix are successively balanced until each row and each column adds up to a given value called a marginal. In the examples in this paper, the row and column marginals will be set to 1.0. This process forces each cell value to be influenced by all the other cell values in its corresponding row and column. Each cell value is then representative of both the omission and commission errors for that land cover category. In this way, all the information in the entire error matrix is forced to be a part of each cell value.

Prior to the normalization procedure, comparisons of corresponding cell values in different matrices was only possible if the matrices had the same sample size. Even then, the cell value may have been misleading as a measure of accuracy since the errors of omission and commission were ignored. However, due to the normalization procedure, corresponding cell values of two or more error matrices can now be directly compared without regard for differences in sample size and including omission and commission errors. As yet, there is no test for significance between corresponding cell values. However, since all rows and columns in the matrix are forced to add to a given marginal, direct comparison of individual cell values can provide a relative measure of which is better.

The second method of comparison reviewed here is a procedure that allows one to test if the overall agreement (i.e., accuracy) in two error matrices is significantly different. A measure of overall agreement is computed for each matrix based on the difference between the actual agreement of the classification as indicated by the major diagonal and the change agreement as indicated by the product of the row and column marginals. This measure of agreement, called KHAT (i.e., $\hat{K}$), is computed by the following equation:

$$\hat{K} = \frac{N \sum_{i=1}^{r} x_{ii} - \sum_{i=1}^{r} (x_{i+} * x_{+i})}{N^2 - \sum_{i=1}^{r} (x_{i+} * x_{+i})}$$

where r is the number of rows in the matrix, x_{ii} is the number of observations in row i and column i (i.e., the ith diagonal element, x_{i+} and x_{+i} are the marginal totals of row i and column i, respectively, and N is the total number of observations [1].

A KHAT value is computed for each matrix and is a measure of how well the classification agrees with the reference data (i.e., a measure of overall accuracy). Confidence intervals and statistical tests are performed using the approximate large sample variance given in [1, p. 396]. A test for significance of KHAT can be performed for each matrix separately to determine if the agreement between the remotely sensed data and the reference data is significantly greater than zero. In other words, this test is performed to see if the classification is significantly better than a random assignment of land cover types to pixels. More importantly, a pairwise test of significance can be performed between two independent KHAT's (a value of KHAT computed from an independent sample for each matrix) using the normal curve deviate to determine if the two error matrices are significantly different [3]. The test statistic for significant difference in large samples is given by

$$Z \sim \frac{\hat{K}_1 - \hat{K}_2}{\sqrt{\hat{\sigma}_1^2 + \hat{\sigma}_2^2}}. \tag{1}$$

The confidence intervals and significance tests are based on the asymptotic normality of the KHAT statistic.

The above test between two independent KHAT's allows any two error matrices to be compared in order to determine if they are significantly different. In other words, error matrices generated from several classification algorithms can now be compared, two at a time, to determine which classifications are significantly better than the rest. Researchers can also use this procedure to test the effects of individual factors such as time of the year or analyst on the accuracy of the classification. However, this procedure is limited to varying only one factor at a time. For example, in order to determine which date of imagery yields the best results, all other factors (i.e., algorithm, analyst, Landsat scene, etc.) must be held constant. Actually, since this condition is common in accuracy assessments, this method is very useful.

The third method of comparison reviewed here allows

one to simultaneously analyze more than a single factor affecting the classification accuracy. This procedure is the most complicated of the three and is based on the log-linear model approach as described by [1], [6]. In this method, many variables (factors) affecting the accuracy and their interactions can be tested together to determine which are necessary (i.e., significant) in fully explaining the classification accuracy.

In this method, the simplest model (combination of variables and their interactions) that provides a good fit to the data (error matrices) is chosen using a model selection procedure. This procedure, which is similar to model selection procedures used in regression (i.e., forward selection, etc.), allows the user to systematically search all possible combinations of variables and their interactions and choose the simplest combination that provides a good fit to the data. First, all uniform order log-linear models (i.e., models with all possible n-way interactions, where $n = 1$ to the number of variables) are examined and the simplest good fit model is chosen. Each interaction of the chosen uniform order log-linear model is then tested for significance. If the interaction is not significant, it is dropped from the model. The process continues for each interaction until a model is found in which all the variables and their interactions are significant. For more details on this model selection procedure, see [6, Section 5.3]. The criteria used for determining the significance of the variables and interactions in a model is based on the likelihood ratio G^2 and the corresponding degrees of freedom for that model.

This procedure uses a method of successive approximations (i.e., "iterative proportional fitting") which converges to the maximum likelihood estimates of the minimum sufficient statistics as defined by the model. In other words, the "iterative proportional fitting" procedure attempts to fit the model of interest to the data. This procedure is tedious and complicated and is almost always done on the computer. The likelihood ration G^2 is then used as a measure of "goodness of fit" of the model to the data. The likelihood ratio statistic is used in place of the Pearson chi-square statistic because G^2 can be partitioned, as is necessary in the model selection procedure, and still retain an approximate chi-square distribution while Pearson's statistic cannot. Therefore, the critical value for testing if the model of interest is a good fit can be obtained from a chi-square table with the appropriate degrees of freedom [1], [6].

The log-linear model approach, unlike the KHAT statistic, allows for the analysis of multi-way error matrices with many factors. For example, error matrices generated using different dates, different algorithms, and different analysts all of the same scene of imagery, can be put together and the factors significant in explaining the classification accuracy identified. A possible practical result of such an analysis could be that the image date is insignificant, and therefore the imagery with the highest quality, irregardless of the date obtained, could be used in the study.

It should be realized here that performing any of these three comparison methods by hand is a very tedious process. Computer programs have been written to implement all three techniques and are available from the author. The first and second procedures are very easy to use while the third is somewhat more complicated.

III. Example Analyses

Data used to demonstrate the normalization procedure and the test of agreement procedure were part of a study done on various image processing software packages by the U.S. Army Engineer Waterways Experiment Station Environmental Laboratory [11]. Each software package was used to produce the best possible classification o the Simeon Southeast USGS $7\frac{1}{2}$-min quadrangle into three general land cover categories: water (WA), wetlands (WE), and nonwetlands (NW). The three software packages evaluated were: the EDITOR software developed at NASA Ames Research Center, the GISS software developed at the Goddard Institute for Space Sciences, and the VICAR software developed at Washington State University. The original and normalized error matrices for each of the three software packages are given in Tables I–III. Table IV presents a comparison between the overall performance accuracy, the measure of agreement (KHAT), and the normalized performance accuracy for the three software packages. Normalized performance accuracy is computed in the same way as overall performance accuracy except on the normalized matrix. This measure of accuracy differs from the overall performance accuracy in that the cell values along the major diagonal in the normalized matrix now incorporate the omission and commission error in the matrix as a result of the "iterative proportional fitting" procedure. Note that in this case all three measures of accuracy yield the same ranking (best to worst). However, because these are three different measures of accuracy and contain different levels of information, they do not always have to yield the same ranking.

As previously mentioned, normalization allows for the direct comparison of corresponding cell values in each of the three matrices. For example, Table V contains the percent correct and normalized values for the water category in each matrix. In the percent correct calculation only errors of omission are accounted for. However, the normalized value considers both errors of omission and commission as well as negating the effect of sample size. The result of considering both omission and commission errors in the accuracy measure is clearly demonstrated by comparing the values in the water category for the EDITOR software and the VICAR software (Table V). Notice that the EDITOR software has a percent correct for the water category of 71 percent and a normalized value of 0.8729 while the VICAR software has a much higher percent correct of 81 percent and yet a normalized value of 0.8630. This apparent discrepancy in results is mostly due to the large commission error (placing 4184 wetland pixels in the water category) in the VICAR error matrix (see Table III). The

TABLE I
THE ORIGINAL AND NORMALIZED ERROR MATRICES FOR THE EDITOR SOFTWARE CLASSIFICATION OF THE SIMEON SOUTHEAST QUADRANGLE

Landsat Data \ Reference Data	WA	WE	NW
WA	9681	2205	249
WE	3270	35254	10408
NW	724	14377	82225

Landsat Data \ Reference Data	WA	WE	NW
WA	.8729	.1168	.0110
WE	.1125	.7123	.1751
NW	.0147	.1709	.8139

TABLE II
THE ORIGINAL AND NORMALIZED ERROR MATRICES FOR THE GISS SOFTWARE CLASSIFICATION OF THE SIMEON SOUTHEAST QUADRANGLE

Landsat Data \ Reference Data	WA	WE	NW
WA	11084	2167	164
WE	1994	39786	11436
NW	663	10227	82095

Landsat Data \ Reference Data	WA	WE	NW
WA	.9060	.0930	.0049
WE	.0755	.7655	.1587
NW	.0184	.1445	.8364

TABLE III
THE ORIGINAL AND NORMALIZED ERROR MATRICES FOR THE VICAR SOFTWARE CLASSIFICATION OF THE SIMEON SOUTHEAST QUADRANGLE

Landsat Data \ Reference Data	WA	WE	NW
WA	11075	4184	335
WE	2216	31233	8980
NW	450	16762	84380

Landsat Data \ Reference Data	WA	WE	NW
WA	.8630	.1285	.0093
WE	.1249	.6940	.1809
NW	.0121	.1775	.8098

TABLE IV
A COMPARISON OF THE OVERALL PERFORMANCE ACCURACY, THE MEASURE OF AGREEMENT (KHAT), AND THE NORMALIZED PERFORMANCE ACCURACY

Software Package	Overall Performance Accuracy	KHAT	Normalized Performance Accuracy
EDITOR	.803	.629	.800
GISS	.833	.692	.836
VICAR	.794	.612	.789

practical application of this result is that perhaps the EDITOR software is not as bad at distinguishing water as it would at first appear.

The data supplied by Rekas *et al.* [11] were also used to test for significant differences between error matrices. The error matrices generated from the three software packages can be tested to see which are significantly different. The KHAT statistic can be used as an accuracy measurement as shown in Table IV. In addition, it can be used to test which matrices are significantly different and therefore which software package is best. Table VI shows the results of the pairwise significance tests for the three software packages. These results indicate that the three software packages are significantly different from each other with the GISS package being the best and the VICAR package the worst for this particular data set. Without this statistical test, it would have been impossible to distinguish between the overall performance accuracy of the EDITOR software (0.803) and the VICAR software (0.794). A more practical application of such an analysis would be to test if a very expensive software package produces results that are not significantly different from a less expensive package. If this were the case, then the less expensive package should be used. Table VII contains the KHAT statistic and the variance for each of the three error matrices. In addition, this table contains the Z statistic used to test if the agreement between the reference data and the remotely sensed data was significantly greater than zero for each matrix separately.

Data used to demonstrate the multifactor comparison

TABLE V
A COMPARISON OF THE WATER CLASSIFICATION FOR THE THREE SOFTWARE PACKAGES

Software Package	Number of Correctly Classified Pixels	Number of Pixels in the water Category	% Correct	Normalized Value
EDITOR	9681	13675	.7079	.8729
GISS	11084	13741	.8066	.9060
VICAR	11075	13741	.8059	.8630

TABLE VI
THE RESULTS FOR THE TEST OF AGREEMENT BETWEEN ERROR MATRICES FOR THE THREE SOFTWARE PACKAGES

Pairwise Comparison	Z Statistic [1]	Result 95% [2]	Result 90%
EDITOR vs. GISS	-24.6372	S	S
EDITOR vs. VICAR	6.7160	S	S
GISS vs. VICAR	31.4763	S	S

[1] Use equation (1) to calculate the Z statistic

[2] S = significant result

TABLE VII
KHAT STATISTIC AND VARIANCE FOR EACH ERROR MATRIX USED TO COMPUTE CONFIDENCE INTERVALS AND PERFORM SIGNIFICANCE TESTS

Error Matrix	KHAT Statistic	Variance
EDITOR	.62932	.00000347
GISS	.69183	.00000297
VICAR	.61155	.00000354

TABLE VIII
THE UNIFORM ORDER MODELS FOR THE FOUR-WAY TABLE COMPARING ENHANCEMENT TECHNIQUES AND CLASSIFICATION ALGORITHMS

MODEL	G^2	df	RESULT
[1][2][3][4]	10888.87281	352	poor fit
A [12][13][14][23][24][34]	145.86428	294	good fit
[123][124][134][234]	20.90917	54	good fit

procedure were supplied by Gregg *et al.* [7]. These data were collected as part of an operational study of Landsat imagery for inventory purposes in the State of Washington. In this example, two classification algorithms, two enhancement techniques, 10 reference data categories, and 10 Landsat data categories were studied resulting in a four-way table of dimensions 2 by 2 by 10 by 10. Unfortunately, due to the size of this four-way table, it cannot be printed here. However, the original data can be found in the paper cited above.

As previously described, a model selection procedure was used to determine the simplest good fit model to the data. Table VIII contains the uniform order log-linear models for these data. Notice that, because this is a four-way table, the uniform order models consist of the models with all three-way, all two-way, and all one-way interactions. The uniform order model of all four-way interactions (written as [*1 2 3 4*]) is the complete or saturated model and will always fit the data because it contains all the factors and their interactions. However, the object here is to eliminate the nonsignificant factors or interactions and find the simplest good fit model.

In this example, classification algorithm (denoted variable [*1*]), enhancement technique (denoted variable [*2*]), and the reference data (denoted variable [*3*]) are called explanatory variables while the Landsat data (denoted variable [*4*]) is called the response variable. This terminology is derived from the idea that the first three variables are being used to try to explain the response (i.e., the Landsat classification). The interaction terms in the model are represented as combinations of these variables enclosed in brackets (e.g., [*12*] is the interaction between algorithm and enhancement).

Table VIII shows that the two-way interaction uniform order log-linear model is the simplest good fit model as determined by the likelihood ratio G^2. The one-way uniform order model is a poor fit while the three-way uniform order model is a good fit, but is more complicated than the two-way model. Notice that the two-way uniform order model consists of six two-way interaction terms. The object then is to systematically eliminate all the nonsignificant factors or their interactions leaving just the simplest good fit model to the data. Table IX shows the steps of this process. The next step in the model selection process then is to eliminate a two-way interaction term from the two-way uniform order model. By eliminating one two-way term, six new models result, each with a different combination of the five remaining two-way interaction terms. These six new models are tested for "goodness of fit" based on the G^2 and the appropriate degrees of freedom (df), and model B is chosen to be the simplest good fit model. The eliminated two-way interaction term is tested for significance by comparing the fit of the two-way uniform order model, labeled A in Table VIII, with model B. This test is possible because partitioning G^2 still results

TABLE IX
THE MODEL SELECTION PROCESS FOR THE FOUR-WAY TABLE COMPARING ENHANCEMENT TECHNIQUES AND CLASSIFICATION ALGORITHMS

MODEL	G^2	df	RESULT
[12][13][14][23][24]	10732.65712	315	poor fit
[12][13][14][23][34]	230.22104	243	good fit
[12][13][14][24][34] B	147.83246	243	good fit
[12][13][23][24][34]	227.51772	243	good fit
[12][14][23][24][34]	156.53131	243	good fit
[13][14][23][24][34]	146.04061	235	good fit

model B best and good fit
$G^2(B) - G^2(A) = 2.06819 \sim \chi^2_{9df}$ not significant so drop [23]

[12][13][14][24]	10733.8278	324	poor fit
[12][13][14][34]	231.3918	252	good fit
[12][13][24][34]	229.4802	252	good fit
[12][14][24][34]	158.4941	252	good fit
[13][14][24][34] C	148.0034	252	good fit

model C best and good fit
$G^2(C) - G^2(B) = 0.1709195 \sim \chi^2_{1df}$ not significant so drop [12]

[13][14][24]	10733.99876	325	poor fit
[13][14][34][2]	231.43485	253	good fit
[13][24][34]	229.52108	253	good fit
[14][24][34] D	158.66500	253	good fit

model D best and good fit
$G^2(D) - G^2(C) = 10.66162 \sim \chi^2_{1df}$ not significant so drop [13].

[14][24][3]	10734.29202	334	poor fit
[14][34][2]	242.09646	262	good fit
[24][34][1] E	229.81433	262	good fit

model E best and good fit
$G^2(E) - G^2(D) = 71.14933 \sim \chi^2_{9df}$ significant so choose D can't drop [14]

in a chi-square distribution. Because this test is not significant, the [23] interaction term can be dropped from the model (see Table IX).

This same process is then repeated on model B by eliminating another two-way interaction term and testing the resulting five models. The results of the test yield model C as the simplest good fit model. Also, the test shows the [12] interaction term to be not significant; therefore, it is dropped from the model. The process is repeated again, leading to model D and the elimination of the [13] interaction. Note that one of the possible models tested here contained a one-way interaction term. The process is repeated one last time, resulting in model E as the simplest good fit model. However, the test between models D and E was significant; therefore the [14] interaction cannot be eliminated from the model without losing some of the critical information about the data. Therefore, model D [14] [24] [34]) is selected as the simplest good fit model to the data.

Model D indicates that there are no three-way interactions necessary to explain the data. Instead, there is a combined effect due to each explanatory variable (i.e., algorithm, enhancement, and reference data) separately with the response. In other words, for this example each factor contributes significantly to the performance of classifying the image and, therefore, none can be eliminated.

IV. Summary and Conclusions

The three discrete multivariate analysis techniques reviewed here are very helpful in assessing the accuracy of classifications derived from remotely sensed data. These techniques have the advantage of allowing the user to quantitatively compare the different aspects of the classification process and assess the results. In addition, each technique is easily implemented by a computer program. However, the results of these quantitative techniques are only as good as the error matrices used in the computations. A great deal more research is needed in the sampling aspects of accuracy assessment to insure that the error matrices are indeed representative of the entire area classified using the remotely sensed data.

References

[1] Y. Bishop, S. Fienberg, and P. Holland, *Discrete Multivariate Analysis—Theory and Practice*. Cambridge, MA: MIT Press, 1975.

[2] D. Card, "Using known map category marginal frequencies to improve estimates of thematic map accuracy," *Photogrammetr. Eng.*, vol. 48, no. 3, pp. 431–439, 1982.

[3] J. Cohen, "A coefficient of agreement for nominal scales," *Education. Psych. Measurement*, vol. XX, no. 1, pp. 37–40, 1960.

[4] R. Congalton, "The use of discrete multivariate analysis techniques for the assessment of Landsat classification accuracy," M.S. thesis, Virginia Polytech. Inst. and State Univ., 1981.

[5] R. Congalton, R. Oderwald, and R. Mead, "Assessing Landsat classification accuracy using discrete multivariate analysis statistical techniques," *Photogrammetr. Eng.*, vol. 49, no. 12, pp. 1671–1678, 1983.

[6] S. Fienberg, *The Analysis of Cross-Classified Categorical Data*. Cambridge, MA: MIT Press, 1980.

[7] T. Gregg, E. Barthmaier, R. Aulds, and R. Scott, "Landsat operational inventory study," Div. Tech. Serv., State of Washington, Dep. Nat. Res., Olympia, WA, 1979.

[8] R. Hoffer, "Natural resource mapping in mountainous terrain by computer analysis of ERTS-1 satellite data," *LARS Res. Bull.* 919, Purdue Univ., 1975.

[9] R. Hoffer and M. Fleming, "Mapping vegetative cover by computer aided analysis of satellite data," *LARS Tech. Rep.* 011178, Purdue Univ., 1978.

[10] R. Mead and M. Meyer, "Landsat digital data application to forest vegetation and land use classification in Minnesota," in *Proc. Mach. Process. Remotely Sensed Data* (Purdue Univ.), pp. 270–280, 1977.

[11] A. Rekas, J. Stoll, and H. Struve, "An evaluation of Landsat classification procedures for wetlands mapping," Tech. Rep. EL-84-(in press), U.S. Army Waterways Experiment Station, Vicksburg, MS, 1984.

[12] G. Rosenfield, "Analyzing thematic maps and mapping for accuracy,"U.S. Geo. Survey Open File Rep. 82–239, 1982.

[13] G. Snedecor and W. Cochran, *Statistical Methods*, 6th ed. Ames, IA: Iowa State Press, 1976.

[14] M. Hord and W. Brooner, "Land-use map accuracy criteria," *Photogrammetr. Eng.*, vol. 42, no. 5, pp. 671–677, 1976.

[15] J. van Genderen and B. Lock, "Testing land use map accuracy," *Photogrammetr. Eng.*, vol. 43, no. 9, pp. 1135–1137, 1977.

[16] S. Aronoff, "Classification accuracy: A user approach," *Photogrammetr. Eng.*, vol. 48, no. 8, pp. 1299–1307, 1982.

*

Russell C. Congalton received the B.S. degree in forestry from Rutgers University in 1979 and the M.S. and Ph.D. degrees in forest biometrics and remote sensing from Virginia Polytechnic Institute and State University in 1981 and 1984, respectively.

He spent 1985 as a post-doctorate researcher for the Remote Sensing Group of the Environmental Laboratory at the U.S. Army Corps of Engineers Waterways Experiment Station. Presently, he is employed as an Assistant Professor of Remote Sensing in the Department of Forestry and Resource Management at the University of California, Berkeley.

*

Roy A. Mead received the B.S. degree in botany from Northern Arizona State University, the M.S. degree in remote sensing from Colorado State University, and the Ph.D. degree in remote sensing from the University of Minnesota.

He has considerable experience in remote sensing and geographic information systems with government agencies, private industry, and academia. He is currently employed as a Geographic Information Systems Specialist for the U.S. Forest Service.

Landsat Large-Area Estimates for Land Cover

GEORGE A. MAY, MARTIN L. HOLKO, AND NED JONES, JR.

Abstract—**A methodology for using ground-gathered and Landsat MSS data to obtain natural resources information over large areas was developed by the USDA, Statistical Reporting Service (SRS) and NASA/NSTL, Earth Resources Laboratory. The SRS's remote-sensing techniques for improving crop area estimates were expanded and modified to obtain land-cover data. These techniques employ statistical relationships between field-level ground data and corresponding Landsat pixels to determine classification accuracy and variances for acreage estimates. State-level and land-cover surveys were conducted in Kansas, Missouri, and Arkansas. During the Missouri project, all costs for person-hours, materials, and computer time were tracked for the various analysis steps. Classified Landsat data stored on computer tapes and area estimates with known precision are two products obtained from these surveys.**

I. Introduction

THE U.S. Department of Agriculture's (USDA) Statistical Reporting Service (SRS) uses digital data from the Landsat satellite to improve crop-area statistics based on ground-gathered survey data. This is accomplished by using Landsat digital data as an auxiliary variable in a regression estimator. Several reports ([5], [7], [9], [11], [14]) discuss results from this procedure which has been applied to major crops in the midwest. Briefly, the SRS Landsat procedure for major crops consists of the following steps:

Ground truth collected during an operational survey, plus corresponding Landsat MSS digital data, are used to develop discriminant functions which in turn are used to classify Landsat pixels which represent specific ground covers.

Areas sampled by the ground survey are classified and regression relationships developed between classified results and ground truth.

All of the pixels contained in the Landsat scene(s) within the area of interest are classified.

Crop-area estimates are calculated by applying the regression relationship to the full scene classification results.

In 1979, the land-cover classification and measurement program within AgRISTARS gave the SRS a research charter to develop and evaluate techniques for obtaining land resources information. The overall objective was to determine if land-cover data obtained using the above methodology could be useful to other USDA agencies, or state and county level agencies, concerned with natural resources management. The National Areonautics Space Administration's Earth Resources Laboratory (ERL) at the National Space Technology Laboratory (NSTL) had prior experience in examining land cover and geographic information needs. Thus, NSTL and SRS personnel began joint remote-sensing research efforts to address land-cover information needs with major emphasis placed on SRS's methology for obtaining crop area estimates.

The following is a brief overview of land-cover research that was conducted during AgRISTARS:

1979 The SRS has a lead role along with NASA/ERL in land-cover research.
1980 Pilot study conducted in Kansas.
1981 Seventeen land covers classified and estimated at the state level in Kansas using unitemporal Landsat data.
1982 Results from 1981 analyzed and preparations made for 1983 test.
1983 Twenty-three land covers and five major crops classified and state-level estimates produced in Missouri using multitemporal Landsat data.
1984 The Soil Conservation Service (SCS), the Forest Service (FS), and the SRS jointly fund a state-level crop and land-cover survey in Arkansas using the SRS's June Enumerative Survey and multitemporal Landsat data.

This report will discuss, starting in Section III, each of the above studies in chronological order and will show how the results and experiences gained in one year helped to improve the survey for subsequent years. Section II presents the basic techniques and methodologies used to combine ground-gathered and Landsat MSS data to obtain crop classification and acreage estimates. Cited references which give additional details on these techniques are readily obtainable from the SRS. Modifications were made to these procedures to allow the classification and estimation of noncrop cover types. These changes are discussed within the appropriate land-cover study presentation.

II. Methodology

A. June Enumerative Survey

Every year during the last week in May and first week in June the SRS conducts a June Enumerative Survey (JES) in 48 conterminous states [3]. The JES is a probability survey based on a stratified area-frame sampling technique [6]. In this technique the area of a State is divided into homogeneous subdivisions called strata (Table I). Each stratum is further subdivided into smaller areas

Manuscript received March 20, 1985; revised July 2, 1985.

The authors are with the U.S. Department of Agriculture, Statistical Research Section, Washington, DC 20250.

IEEE Log Number 8406239.

TABLE I
KANSAS AREA SAMPLING FRAME STRATA

Stratum	Description	Population Size	Sample Size	Average Segment Size (mi^2)
11	> 80% cultivated	25,028	170	1.00
12	50 to 80% cultivated	21,704	120	1.00
20	15 to 49% cultivated	21,286	100	1.00
31	Agri-urban	2,774	12	0.25
32	City	2,941	12	0.10
33	Resort area	247	2	0.25
40	Rangeland	3,147	15	4.00
50	Nonagricultural	294	2	1.00
61	Potential water	29	2	0.50
62	Water	231	0	1.00
	TOTAL	77,681	435	

called primary sampling units (PSU's). Out of each stratum a suitable number of PSU's are randomly chosen with probability of selection proportional to the area of the PSU. Each of the sampled PSU's is divided into sampling units called segments (a segment is a well-defined area of land that can be delineated on photographs and readily identified by data collection personnel in the field). In strata that are predominantly cultivated land, the average segment size is about 1 mi^2. After each sampled PSU is subdivided, one segment is randomly selected from each PSU.

The JES procedure requires that information be obtained for all the land within each of the sampled segments. To ensure that all the land is accounted for, aerial photographs are used as an enumeration aid. The boundaries for each segment are drawn on individual noncurrent photographic prints. These segment photographs and corresponding questionnaires are sent to field enumerators for data collection. As part of the data collection procedure, each enumerator is instructed to draw the boundaries of all fields, within each segment, on the segment photography (a field is defined as a continuous block of land containing the same crop or land cover). On the corresponding questionnaire the enumerator records the cover and size of each field, as well as livestock numbers and other agricultural information obtained from the operator.

The information collected during the JES is aggregated to the segment level and direct expansion estimates are then calculated to obtain state level estimates for crop acres [12]. The formulas for the direct-expansion estimator and its variance are as follows:

Let $\hat{Y}_c$ be the unbiased direct expansion estimate for the acres of crop c

$$\hat{Y}_c = \sum_{s=1}^{S} \frac{N_s}{n_s} \sum_{j=1}^{n_s} y_{jsc}$$

where

- y_{jsc} is the acres reported to crop c, in segment j, for stratum s,
- n_s is the number of segments sampled in stratum s,
- N_s is the total number of potential segments in stratum s, and
- S is the total number of strata.

The estimated variance is:

$$V(\hat{Y}) = \sum_{s=1}^{S} \frac{(N_s - n_s)N_s}{n_s(n_s - 1)} \sum_{j=1}^{n_s} (y_{jsc} - \bar{y}_{.sc})^2$$

where

$$\bar{y}_{.sc} = \sum_{j=1}^{n_s} \frac{y_{jsc}}{n_s}.$$

In 1972, SRS personnel started to investigate the potential of using *digital* Landsat data to improve the precision of the estimates obtained from the JES. The procedure developed consists of the following steps:

1) Analysis District Selection: Landsat data are selected and boundaries of Landsat analysis districts defined.

2) Signature Development: Data collected during the JES and corresponding Landsat data are used to develop a maximum likelihood classifier for each analysis district.

3) Small-Scale Processing: The Landsat pixels representing the area within each segment contained in an analysis district are classified. A regression relationship is developed between the number of pixels classified to a crop and the acres recorded for that crop on the JES.

4) Full-Frame Processing: All of the Landsat pixels within the analysis district are classified. Estimates are calculated at the analysis district level by applying each crop regression relationship to the all-pixel classification results.

5) State-Level Accumulation: The estimates for all analysis districts are combined to create a state level estimate for each crop of interest.

B. Analysis District Selection

An analysis district is an area of land covered by Landsat imagery of the same overpass date. Depending on the location and availability of Landsat data, each state is divided into a number of districts with each being analyzed separately. The Landsat analysis district location is treated as a geographical post-stratification imposed on the original strata. As a result of this post-stratification, SRS personnel must determine the number of PSU's and the sampled segments which fall into each post-stratum. This results in two strata categories:

1) The first stratum category corresponds to the area of the state for which there is no Landsat coverage. This area may be noncontiguous. The portion of each land-use stratum within these geographical areas makes up the post-strata. We let M_s be the total number of segments in the nonLandsat area in land use stratum s, and m_s be the number of sampled segments in the non-Landsat area in land use stratum s.

2) The second stratum category corresponds to the areas of the state where the analysis districts are defined. In these areas each stratum consists of the area of intersection between the land use strata and a Landsat analysis district. Here, we let M_{as} be the number of PSU's in analysis district a, land use stratum s, and m_{as} be the number of sampled segments in analysis district a, land use stratum s.

C. Signature Development

Signature development is done independently for each analysis district and consists of four phases. The first phase is segment calibration and digitization. Segment calibration is a first-order linear transformation that maps points on the segment photograph to a USGS map base. Segment digitization is the process by which field boundaries drawn on the segment photograph are recorded in computer-compatible form. The combined process of calibration and digitization gives us the capability of digitally locating every JES field relative to a map base.

The next phase in signature development is the registration of each Landsat scene. The SRS's Landsat registration process is a third-order linear transformation that maps each Landsat pixel within a scene to a map base [4]. Corresponding points selected on a 2° map and a 1:250 000 Landsat image are used to generate this mathematical transformation. The combination of segment calibration, digitization, and Landsat registration provides the capability to locate each JES segment in its corresponding Landsat scene (to within about 5 pixels of the correct location). Since this registration is not accurate enough for selecting training data, line plots of segment field boundaries and corresponding greyscale prints are overlaid and each segment is manually located to within $\frac{1}{2}$ pixel of the correct location. This procedure allows accurate identification of all the pixels associated with any JES field. The result of this is a set of pixels labeled by JES cover.

The third phase of signature development is supervised clustering. In supervised clustering all of the pixels for each cover are processed through one of two available clustering algorithms: classy or ordinary clustering. Classy is a maximum likelihood clustering algorithm developed at Johnson Space Center in Houston, TX [8]. Ordinary clustering is an algorithm derived from the ISODATA algorithm of Ball and Hall [2]. Each clustering algorithm generates several spectral signatures (categories) for each cover. Each spectral signature consists of a mean vector and the covariance matrix for the reflectance values for that category.

In the fourth phase, the statistics for all categories from all covers are reviewed and combined to form the discriminant functions of the maximum likelihood classifier.

D. Small-Scale Processing

In small-scale processing, each pixel associated with a JES segment is classified to a category. The category totals corresponding to crops of interest are summed to segment crop totals. These crop totals are used as the independent variable in a regression estimator. Correspondingly, the acres reported on the JES for each crop are summed to segment totals and used as the dependent variable. The segment totals are used to calculate least squares estimates for the parameters of a linear regression.

The linear regression equations for analysis district a, stratum s, and crop c are of the form

$$y_{jasc} = b_{0asc} + b_{1asc}x_{jasc}$$

where

y_{jasc} is the reported acres of crop c, from segment j, analysis disctrict a, land use stratum s;

x_{jasc} is the crop total classification for segment j, analysis district a, land use stratum s, and

b_{0asc}, b_{1asc} are the least squared estimates of the regression intercept and slope parameters for crop c, analysis district a, land use stratum s.

E. Full-Frame Processing

The classifier used in small-scale processing is used to classify every pixel in the analysis district. The classified results are tabulated by category and land-use stratum. For each crop of interest, the category totals are summed to stratum crop totals. From these totals the population averages per segment are calculated. Using the population average, a stratum-level regression estimate is made for that analysis district for each crop.

Let $\hat{Y}_{\grave{a}sc}$ be the analysis district level regression estimator for crop c and stratum s. Then

$$\hat{Y}_{\grave{a}sc} = M_{\grave{a}s}[\bar{y}_{.asc} + b_{1asc}(\bar{X}_{.asc} - \bar{x}_{.asc})]$$

where

$$\bar{y}_{.asc} = \sum_{j=1}^{m_{\grave{a}s}} \frac{y_{jasc}}{m_{\grave{a}s}}$$

$$\bar{x}_{.asc} = \sum_{j=1}^{m_{\grave{a}s}} \frac{x_{jasc}}{m_{\grave{a}s}}.$$

$M_{\grave{a}s}$, $m_{\grave{a}s}$, x_{jasc}, and y_{jasc} are as defined above, and $\bar{X}_{.asc}$ is the population average number of pixels per segment classified to crop c, analysis district a, and land use stratum s.

The estimated variance is

$$V(\hat{Y}_{\grave{a}sc}) = \frac{(m_{\grave{a}s} - 1)}{(m_{\grave{a}s} - 2)}(1 - r_{asc}^2)\frac{(M_{\grave{a}s} - m_{\grave{a}s})M_{\grave{a}s}}{m_{\grave{a}s}(m_{\grave{a}s} - 1)} \cdot \sum_{j=1}^{m_{\grave{a}s}} (y_{jasc} - \bar{y}_{.asc})^2$$

where r_{asc} is the sample correlation between y_{jasc} and x_{jasc}.

F. State-Level Accumulation

The final step of Landsat analysis is the combining of all of the estimates (one for each post stratum) into a state-level estimate of the area of the desired crop.

Let $\hat{Y}_{\hat{c}}$ be the final state level estimate for the acres of crop c.

Then

$$\hat{Y}_{\hat{c}} = \sum_{a=1}^{A} \sum_{s=1}^{S_{\grave{a}}} \hat{Y}_{\grave{a}sc} + \sum_{f=1}^{L} M_f \bar{y}_{.fc}$$

where

$$\bar{y}.fc = \sum_{j=1}^{m_f} \frac{y_{jfc}}{m_f}.$$

M_f, m_f are as previously defined with subscript f used to distinguish from strata with Landsat coverage,
$\hat{Y}_{asc}$ is as defined earlier,
y_{jfc} is the acres reported to crop c for segment j in the non-Landsat post stratum f,
S_a is the number of land use strata in analysis district a,
A is the number of analysis districts, and
L is the number of land use strata in the area where there is no Landsat coverage.

The estimated variance is

$$V(\hat{Y}_c) = \sum_{a=1}^{A} \sum_{s=1}^{S_a} V(\hat{Y}_{asc}) + \sum_{f=1}^{L} \frac{(M_f - m_f)M_f}{m_f(m_f - 1)} \cdot \sum_{j=1}^{m_f} (y_{jfc} - \bar{y}_{.fc})^2.$$

G. Evaluation of the Landsat Estimate

Landsat data are used as supplemental information to improve the precision of the area estimates obtained from the JES. Unlike area frame construction, the effectiveness of this use of Landsat data can be measured. The measure used is the efficiency of the Landsat estimator relative to the JES direct expansion estimator. This relative efficiency (RE) is defined as the ratio of the variance of the direct expansion to the variance of the Landsat estimate. Equivalently, this is the factor by which the sample size would have to be increased to produce a direct expansion estimate with the same precision as the Landsat estimate.

$$RE = \frac{V(\hat{Y}_c)}{V(\hat{Y}_c)}.$$

Recent studies have suggested possible bias in the Landsat regression estimates. During 1985 SRS is conducting research in two mid-western states to examine this problem.

III. 1980 Kansas Pilot Study

A. Objectives

The first step in implementing and expanding the above procedures for land-cover research was to determine if land-cover information could be obtained using JES techniques and methodology. A pilot study was conducted in Kansas using 86 SRS segments from nonagricultural strata. The objectives were 1) test the feasibility of having regular enumerators use land cover definitions to classify parcels of land, and 2) obtain preliminary variance information for direct expansions of cover types in the nonagriculture strata.

B. Selection of Land Cover Definitions

The short-time period between the initiation of the AgRISTARS program and this study required that land-cover definitions be used that were readily available and accepted by other land classification systems. Because of these restrictions, the land-cover classification system set forth in USGS Professional Paper 964 [1] was used as a basis for defining the land-cover codes. This resulted in a scheme which combines the Level I and Level II classification system in the above paper.

Using these definitions, the enumerators went to each of the 86 segments during August and observed the land covers present. Everything inside a segment was placed into one of the defined land covers. The minimum mapping size was 1 acre.

C. Results

Enumerators did an excellent job in conducting the survey and in many instances extracted more information than necessary. Analysis of the land-cover data indicated that some land-cover terms were too broadly defined. This indicated a need for increasing the number of land-cover types for enumeration and a better definition of these terms. Direct expansion estimates were obtained using the 86 segments and the variances examined. Specific conclusions were difficult to make due to the small sample sizes. The results did indicate that the JES may have the potential for providing state-level acreage estimates for several noncrop cover types.

IV. 1981 Kansas Study

A. Objectives

The objectives for the 1981 study were to 1) produce land cover classifications and acreage estimates for the entire state using ground-gathered and Landsat MSS data; 2) incorporate the land-cover survey into the SRS's regular June Enumerative Survey; 3) produce statistically based regional land-cover estimates and maps, and 4) determine if land-cover information obtained from this study could be useful to federal and state agencies.

B. Land Cover Definitions

The approach taken in developing terms and definitions for the 1981 survey was to solicit inputs from federal and state agencies that gather, analyze, and/or disseminate land-cover information within Kansas. Definitions used for surveys conducted by the Soil Conservation Service and Forest Service were added to this study. Seventeen land covers pertinent to the landscape of Kansas were defined and are presented in the left-hand column of Table II.

C. Ground Data Collection

The land-cover ground data were collected during the JES and were considered a part of the regular crop survey. Ground data for crop and noncrop cover types were collected in 435 sample segments. The addition of land covers required some modification to JES forms. A training school was held prior to the survey to familiarize enumerators with the land-cover terms and to discuss enumeration techniques. After collection, the ground data went

TABLE II
DIRECT EXPANSION AND REGRESSION ESTIMATES FOR LAND COVERS WITHIN KANSAS

Land Cover Categories	DIRECT EXPANSION Estimate (Acres)	DIRECT EXPANSION Standard Error	REGRESSION Estimate (Acres)	REGRESSION Standard Error	Relative Efficiency
Cropland	28,349,166	487,446	28,008,390	363,571	1.8
Permanent Pasture	3,145,220	525,561	2,970,378	486,070	1.2
Rangeland	16,452,963	752,294	15,828,804	466,533	2.6
Farmstead	404,467	22,710	416,270	19,521	1.4
Forest (Not Grazed)	935,398	151,104	1,009,638	70,832	4.6
Forest (Grazed)	693,086	194,579	744,089	98,132	4.0
Wooded Strips	481,442	52,665	480,958	48,840	1.2
Residential	461,235	69,559	450,713	33,838	4.2
Commercial/Industrial	116,629	28,391	89,438	18,139	2.4
Transp. Commun., & Util.	503,095	132,872	506,319	123,320	1.2
Other Urban	143,434	29,072	145,683	27,288	1.1
Stripmines, Quarries, G. Pits	137,775	56,683	109,434	29,026	3.8
Sand Dunes	4,818	1,833	-	-	-
Ponds (<40 AC)	199,557	28,074	182,520	18,715	2.3
Lakes (>40 AC)	183,447	17,983	-	-	-
Rivers	138,298	72,672	131,717	65,913	1.2
Transitional	78,742	41,249	-	-	-

through a quality-control process and were digitized into computer readable format.

D. Landsat Data

The 1981 Landsat data obtained for this study are shown in Fig. 1. The earliest date was April 25 and the latest August 31. These data were registered and classified according to the procedures described in Section II.

E. Results

The direct expansion (ground data only) and regression (ground and Landsat data) acreage estimates, for the seventeen land covers within Kansas are given in Table II. The relative efficiency of the regression estimates are also listed.

The direct expansion standard error is high for several noncrop cover types. One reason for this is because the JES sample is designed for an agricultural survey. As indicated in Table I, most of the 435 sample segments fall in agricultural strata 11, 12, and 20, while very few fall in the remaining nonagricultural strata. One method for lowering the standard error of noncrop covers is to select more segments from nonagricultural strata. For example, precision of the estimates for commercial/industrial and other urban categories can be improved by selecting additional samples in strata 31, 32, and 33 and enumerating these segments during the JES. This can be accomplished with minimal effort because, as shown in Table I, the population for each stratum has been defined.

The standard errors for the regression estimates were lower than the direct expansion for all cover types. For example, the regression standard error for grazed forest, not grazed forest, and residential was less than one-half the direct expansion standard errors. The regression standard errors were lowered for commercial/industrial and other urban, but additional improvement in these estimates will have to come from increasing the sample size or from the use of multitemporal Landsat data.

A state-level land-cover classification must be produced in order to derive these regression estimates. Therefore, this classification can be used to obtain land cover map-type products and associated acreage counts for any land area within the state whose boundaries are recorded in a computer-readable format. Map-type products of several counties were obtained from an electrostatic plotter and a cathode ray tube display using NASA/NSTL's software [10].

In summary, the feasibility of using USDA SRS crop area estimation methodology to obtain land-cover classification products and area estimates was demonstrated in Kansas. The 1981 Kansas study indicated that some noncrop cover types were poorly estimated using the current JES sample allocation. Incorporating the collection of land-cover ground data with the JES eliminates the need for two separate ground data activities.

V. 1982 Study

Based on analysis of the Kansas results, another state-level land-cover study needed to be conducted in a more diversified geographic location. Missouri was selected for the next study, and changes were made to the JES sample allocation and enumeration procedures. Ground data were collected, but the study was cancelled due to inadequate Landsat data. Only 25 percent of the state had adequate Landsat coverage due to cloud problems throughout the summer and fall months.

VI. 1983 Missouri Study

A. Objectives

During 1983 the SRS wanted to estimate several crops within Missouri using JES and Landsat data. Other federal and state agencies expressed interest in classifying and estimating several noncrop covers, especially forest categories. To meet these various requirements, the following objectives were established.

1) Provide SRS with area estimates for winter wheat, rice, cotton, corn, and soybeans from a combined crop and land-cover Landsat analysis.

2) Provide classified data tapes and area estimates of defined Missouri land covers.

3) Determine the additional cost of doing land cover analysis with crop analysis.

B. Land-Cover Definitions

Potential users of SRS-generated land-cover data were contacted and asked to determine what land-cover types should be included in this study. The final list of land covers are presented in the left-hand column of Table IV (given later).

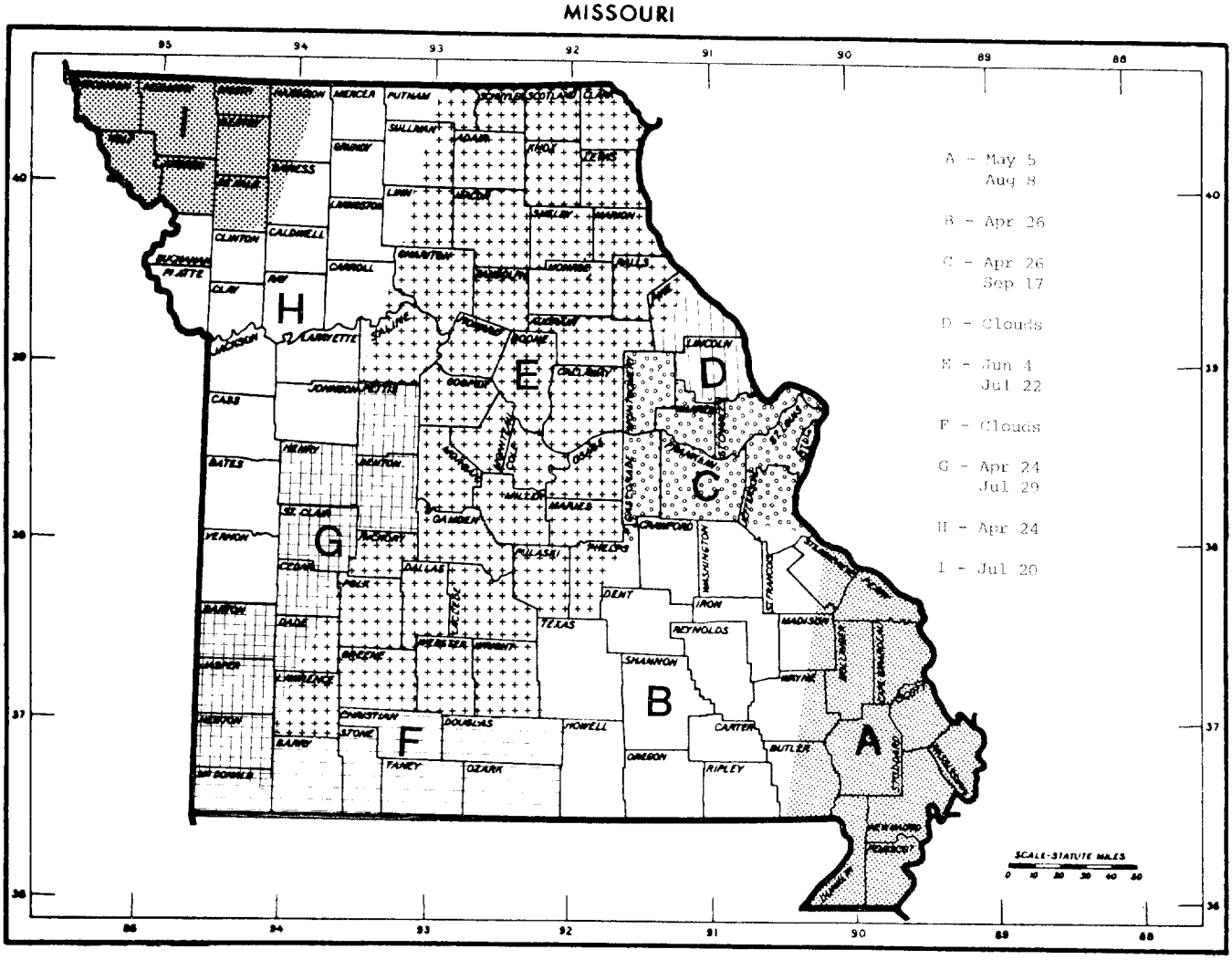

Fig. 1. 1981 dates of Landsat MSS digital dates analyzed for the Kansas land cover study.

C. JES Sample Size

Forest is an important and extensive land cover in Missouri and several agencies expressed interest in this cover. The results from previous years indicated that the sample allocation of 450 operational JES segments did not adequately sample forest land, especially coniferous forests. To provide better ground data, 67 segments from the nonagriculture strata were added.

D. Landsat Data

Two dates of Landsat data were used to enable the estimation of crop acreages for a spring crop (winter wheat) and fall crops (corn, soybeans, rice, cotton) and improve land cover classification results. Fig. 2 shows the analysis districts and Landsat dates which comprised the multitemporal data set. These data sets were created by overlaying the fall imagery onto the spring imagery. Only spring data were used to produce regression estimates for winter wheat.

E. Crop Acreage Results

During the first two weeks in December, the SRS's Crop Reporting Board was provided direct expansion and regression estimates for all five crops. These estimates were timely input data for the SRS's year-end crop acreage reports. Table III lists these estimates and associated statistics.

Several points should be made concerning these regression estimates. The relative efficiencies for the estimates of winter wheat, corn, and soybeans was less than anticipated. In 1983, USDA implemented the "Payment in Kind" (PIK) program, which enabled farmers to enroll acreage normally planted in wheat in a program that would guarantee the farmer a specified price for wheat for not planting the acreage. This program was implemented after the winter wheat was planted, which caused some confusion between the ground and Landsat data.

The improvement in the precision for corn and soybeans are poor considering the use of multitemporal data. Part of the loss in efficiency was due to the lack of fall Landsat data in a large corn and soybean producing area (area *H*

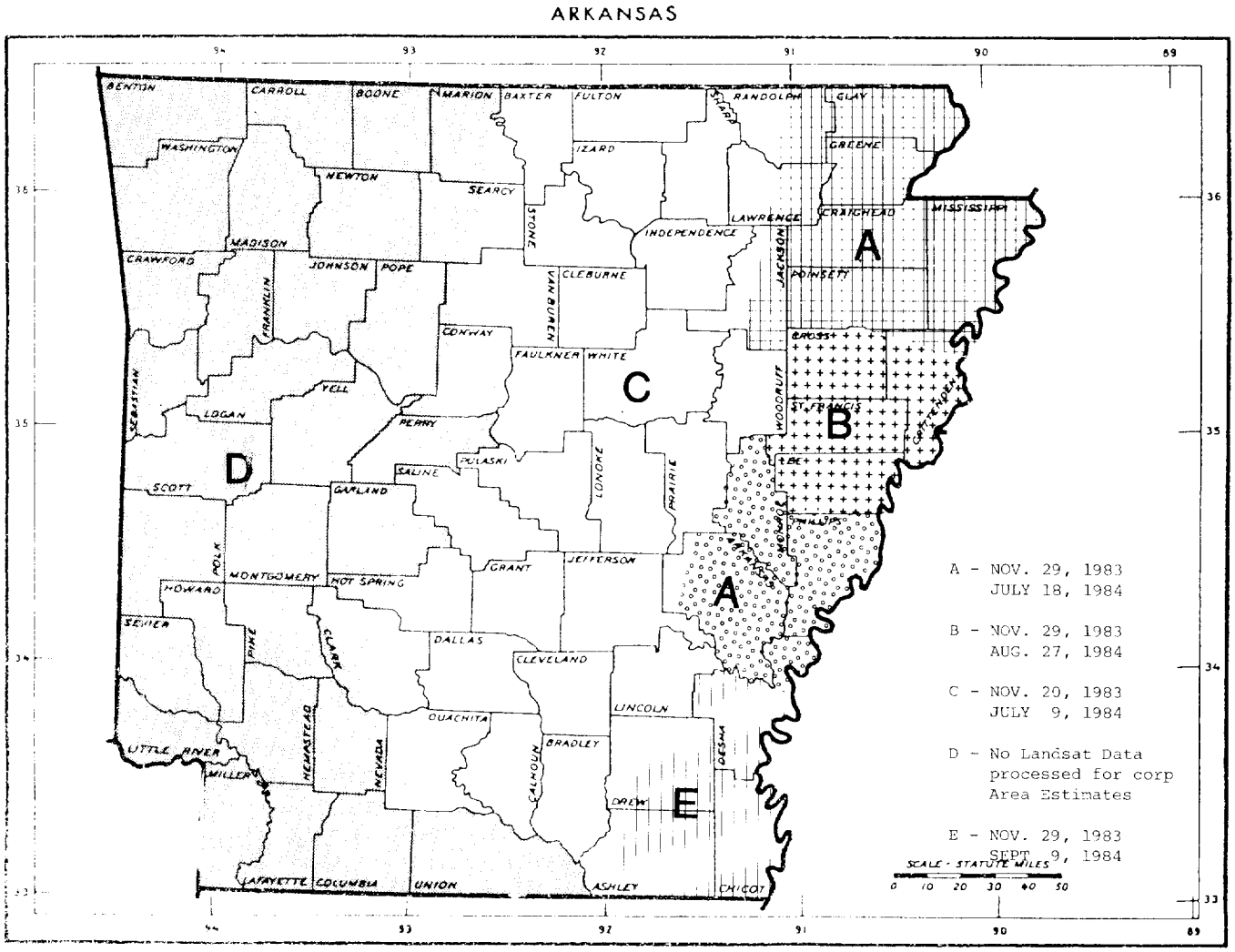

Fig. 2. Multitemporal Landsat digital data analyzed in Missouri.

TABLE III
PLANTED ACREAGE ESTIMATES FOR MAJOR CROPS IN MISSOURI

	DIRECT EXPANSION		LANDSAT REGRESSION		
Crops	Estimate	Standard Error	Estimate	Standard Error	Relative Efficiency
Winter Wheat	2,229,000	174,000	2,314,000	131,000	1.8
Cotton	62,000	35,000	75,000	11,000	10.1
Rice	128,000	54,000	149,000	27,000	3.9
Corn	1,762,000	140,000	1,555,000	110,000	1.6
Soybeans	5,556,000	303,000	4,961,000	239,000	1.6

in Fig. 2). The regression precisions for cotton and rice estimates improved dramatically. These are specialized crops grown only in the Missouri "Boot Heel" region. The JES is not designed to estimate crops concentrated in a small area of a state and this is shown by the high standard error of the direct expansion estimates for these two crops.

F. Land-Cover Results

The direct expansion and regression estimates for land covers are listed in Table IV. Potential users of the land-cover data who participated in defining terms for this project were interested in the outcome of the forestland estimates. The latest state survey conducted by the Forest Service was in 1972 [13]. Table V is a comparison of SRS and FS estimates for these various categories. The "unproductive" and "reserved" categories are special breakdowns by the FS for hardwoods and conifers. This study was not able to provide estimates for these specialty categories, but the acreages associated with these categories are contained in the estimates for hardwood, conifer, or conifer-hardwood.

G. Project Costs

A specific objective of the 1983 study was to determine costs for the various crop and land-cover estimates. The 1983 cost for conducting the JES in the 450 operational segments for crops and land covers was $43 788. This was an 11.5-percent increase when compared to the average JES costs of 1980 and 1981 when no additional land covers were enumerated. Some of this increase is due to an increase in salaries. Total cost for Landsat tapes, prints, and transparencies was $21 240.

Person hours, CPU (in minutes), and computer costs

TABLE IV
LAND COVER DIRECT EXPANSION AND REGRESSION ESTIMATES FOR MISSOURI

	DIRECT EXPANSION		REGRESSION		
Cover	Estimate	Standard Error	Estimate	Standard Error	Relative Efficiency
Hardwood	10,499,754	529,061	11,139,532	443,461	1.4
Conifer	181,568	43,325	187,650	21,782	4.0
Conifer-Hardwood	1,149,738	247,934	1,148,447	245,461	1.0
Grazed Forest	2,884,732	297,743	2,705,512	299,958	1.0
Brushland	1,286,435	143,382	1,318,875	138,723	1.1
Row Crops	8,539,851	361,734	7,742,383	246,344	2.2
Sown Crops	2,391,119	175,337	2,547,815	127,349	1.9
Idle/cropland	2,100,277	163,574	2,015,582	139,389	1.4
Hay	3,110,286	197,393	2,980,606	171,303	1.3
Cropland/Pasture	1,434,850	234,325	1,245,797	149,895	2.4
Other Pasture	7,698,684	423,699	7,624,049	380,381	1.2
Idle Grassland	1,403,300	140,411	1,331,205	133,127	1.1
Farmsteads	385,091	23,474	387,434	23,515	1.0
Residential	962,910	105,045	823,018	95,629	1.2
Commercial	328,253	81,590	305,556	41,463	3.9
Other Urban	140,229	39,114	122,873	30,365	1.7
Transportation	296,577	53,422	288,724	53,398	1.0
Lakes	307,755	118,936	265,246	108,556	1.2
Ponds	84,270	17,563	84,438	13,130	1.8
Rivers	129,922	43,887	103,729	23,368	3.5
Disturbed Land	44,223	17,741	42,455	16,020	1.2
Transitional	183,379	137,668	-	-	-
Wetlands	106,830	87,386	-	-	-

*Fields that are double cropped are included in the estimates for each crop.

TABLE V
COMPARISON OF 1983 FORESTLAND ESTIMATES FROM SRS LANDSAT STUDY WITH 1972 FOREST SERVICE ESTIMATES

Category	SRS	FS
Hardwood	11,139,532	11,619,900
Conifer	187,650	204,300
Conifer-Hardwood	1,148,447	540,500
(Unproductive)	(included above)	298,300
(Reserved)	(included above)	256,100
TOTAL	12,475,629	12,919,100
Grazed Forest	2,705,512	2,803,100

were recorded for various steps required to process the Landsat data and to generate regression estimates. These steps and associated costs were tracked separately for winter wheat, summer crops, and land covers.

In this study, winter wheat was analyzed using unitemporal spring Landsat data. A second analysis using multitemporal spring and fall data was done for summer crops and land covers. Table VI presents the total resource requirements for Landsat analysis. Analyzing and estimating the 23 land covers with summer crops required 51 percent more person hours and a 62-percent increase in computer cost. A majority of these costs were incurred during the acreage estimation processes. Since this study these estimation programs have been rewritten which should reduce future costs of producing land-cover estimates.

In summary, 23 land covers and five major crops were classified and estimated. The classifications were saved on

TABLE VI
TOTAL RESOURCE REQUIREMENTS FOR DIFFERENT LANDSAT ANALYSES USING A COMMON TEST AREA

Category	Person-hours	CPU (min.)	Computer Cost
Unitemporal Winter Wheat	237	773	$ 5,262
Multitemporal Summer Crops	467	1,294	12,634
Multitemporal Summer Crops and Land Covers	707	2,380	20,481

TABLE VII
COST FOR 1984 ARKANSAS CROP AND LAND COVER PROJECT

MATERIALS		
Landsat Data	-	$17,000 ($730x20 scenes + B/W Prints)
Blank Tapes	-	$ 2,000 ($25 x 80)
DATA PROCESSING		
Martin Marietta	-	$2,000 (ground data)
ARPANET	-	$4,000 (Electronic data transmissions)
IBM 33-30	-	$2,000 (tape reformat & data editing)
DEC-10	-	$36,000 (multitemporal overlay, digitizing, registration, signature development)
CRAY-1S	-	$8,000 (full scene classification)
PERSONNEL		
Data Analyst	-	$25,000 (1/2 MYE at GS13)
Support Staff	-	$10,000
TOTAL		$106,000

tape and the utility of the classified data are being assessed by potential users of the land-cover data. Increasing the sample allocation of the regular JES provided improved estimates of forest categories due to more samples in the forest strata. Cost figures were kept for all analysis steps and the additional cost of doing land cover was determined. The increase in precision of crop and land-cover estimates, when using multitemporal Landsat data, was not as high as originally anticipated. Research is needed to determine if the addition of land covers had an adverse affect on the classification results of summer crops.

VII. 1984 ARKANSAS STUDY

A. Objectives

Land-cover results obtained from the Kansas and Missouri studies generated interest within the Soil Conservation Service and Forest Service. These two agencies along with the SRS jointly defined and funded a crop and land-cover study in Arkansas. The overall objectives of this study were to 1) utilize SRS's ground data collection and Landsat analysis techniques to produce a crop and land-cover classification for the entire state and 2) provide this classification on tapes so that each agency could independently utilize the land-cover data in their respective programs.

The SRS used the classified data to obtain 1984 planted acreage estimates for cotton, rice, soybeans, and sorghum. SCS will use the classified data in their next national resources inventory and FS will utilize the data in their forest land inventory.

B. Project Costs

The additional costs over normal JES costs for conducting this project are given in Table VII. These costs were evenly divided between the three agencies.

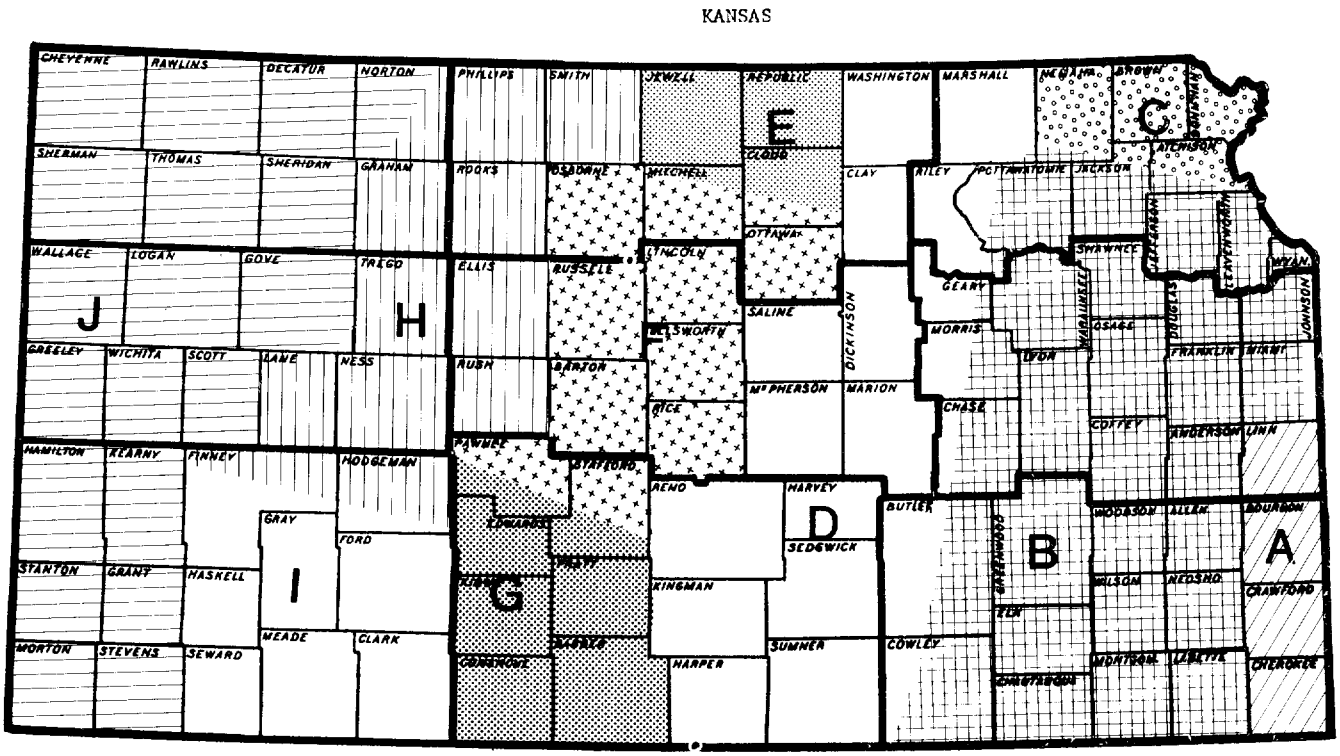

A - June 17 D - May 14 G - August 31 J - July 10

B - April 25 E - May 24 H - July 9

C - August 11 F - April 27 I - June 21

Fig. 3.

TABLE VIII
DIRECT EXPANSION AND REGRESSION ESTIMATES FOR MAJOR CROPS IN ARKANSAS

	DIRECT EXPANSION		LANDSAT REGRESSION		
Cover	Estimate	Standard Error	Estimate	Standard Error	Relative Efficiency
Cotton	442,000	94,000	458,000	61,000	2.4
Rice	1,161,000	118,000	1,133,000	69,000	2.9
Soybeans	4,124,000	204,000	3,989,000	136,000	2.3
Sorghum	671,000	85,000	559,000	60,000	2.0

C. Land Cover Definitions

Representatives from the three agencies met and established the terms and definitions for the survey. A listing of the land cover classification categories are shown below:

Hardwood Forest	Native Pasture
Mixed Forest	Improved Pasture
Conifer Forest	Row Crops
Clearcut Forest	Sown Crops
Barren Land	Hay
Urban	Other Land Use
Water	

D. Landsat Data

Multitemporal Landsat data were obtained for most of the state. Conifers are an important land cover; therefore, late fall 1983 and winter 1984 were obtained for the first date of the multitemporal data set. The second date of Landsat data were obtained from summer and fall 1984. Most of the crop land is located in the eastern half of Arkansas. To meet the SRS due dates for crop estimates, eastern Arkansas was analyzed first. Fig. 3 delineates the analysis districts and Landsat dates.

E. Results

The direct expansion and regression estimates for the crops generated for the SRS are given in Table VIII. These estimates were produced and delivered on December 1 in time for the year-end crop acreage report. The land-cover estimates and classified tapes for the SCS and FS will be generated during the first quarter of 1985. Therefore, these results were not available for inclusion in this paper.

VIII. Conclusions

Five years of research were conducted in developing and evaluating techniques for obtaining large-area land-cover classifications and area estimates. The remote-sensing techniques developed by the USDA's SRS for improving crop area estimates formed the basis for this research. The overall objective of applying this technology for the purpose of obtaining land-cover information was met. The following are specific conclusions from the land-cover research.

1) SRS's JES provides a vehicle, on an annual basis, for

obtaining ground truth data for land cover surveys that utilize Landsat data.

2) For classification and estimation purposes the operational JES segment allocation does not adequately sample many noncrop cover types. This can be corrected by increasing the sample size in strata for which the land cover(s) are located.

3) The SRS's deadline for timely crop area estimates can still be met when noncrop covers are included in the survey and Landsat analyses.

4) Two products can be obtained from the techniques discussed in this report: a) acreage estimates with measures of precision and b) classified Landsat data contained on tapes.

5) The utility of classified Landsat data for land-cover studies by other federal and state agencies is still being assessed.

6) Large increases in computer time and person hours were incurred when analyzing noncrop covers with crops. This can be offset by multiple agencies sharing the cost of a crop and land-cover survey.

REFERENCES

[1] J. R. Anderson, E. E. Hardy, J. T. Roach, and R. E. Witmer, "A land use and land cover classification system for use with remote sensor data," Geological Survey Professional Paper 964, U.S. Dept. of Interior, 1976.

[2] G. H. Ball and D. J. Hall, "A clustering technique for summarizing multivariate data," *Behavioral Sci.*, vol. 12, pp. 153–155, 1967.

[3] C. E. Caudill, "Current methods and policies of the statistical reporting service," in *Proc. Symp. Machine Processing of Remotely Sensed Data* (West Lafayette, IN), pp. 1–5, 1976.

[4] P. W. Cook, "Landsat registration methodology used by U.S. Department of Agriculture's Statistical Reporting Service 1972–1982," U.S. Department of Agriculture, Statistical Reporting Service Tech. Rep., presented at the American Statistical Association Meetings, Cincinnati, OH, 1982.

[5] M. L. Holko, "1982 results for the California cooperative remote sensing project," Statistical Reporting Service, U.S. Dep. of Agriculture. Washington, DC, 1984.

[6] E. E. Houseman, "Area sampling in agriculture," U.S. Dep. of Agriculture, Statistical Reporting Service, SRS-20, 1975.

[7] D. D. Kleweno and C. E. Miller, "1980 AgRISTARS DC/LC Project Summary: Crop area estimates for Kansas and Iowa," U.S. Dep. of Agriculture, Statistical Reporting Service, AGESS-810414, 1981.

[8] R. K. Lennington and M. E. Rassback, "Classy—An adaptive maximum likelihood clustering algorithm," in *Proc. LACIE Symp.* (Houston, TX), pp. 671–690, 1978.

[9] J. Mergerson, C. Miller, M. Ozga, M. Holko, S. Winings, P. Cook, and G. Hanuschak, "1981 AgRISTARS DCLC four state project," in *Proc. Symp. Machine Processing of Remotely Sensed Data* (West Lafayette, IN), pp. 34–44, 1982.

[10] NASA, "Earth resources laboratory applications software," Earth Resources Lab. Rep. 183, National Space Technology Lab., MS, 1980.

[11] M. Ozga and W. E. Donovan, "An interactive system for agricultural acreage estimates using Landsat data," in *Proc. Symp. Machine Processing of Remotely Sensed Data* (West Lafayette, IN), pp. 113–123, 1977.

[12] R. S. Sigman, G. A. Hanuschak, M. E. Graig, P. W. Cook, and M. Cardenas, "The use of regression estimation with Landsat and probability ground sample data," U.S. Dep. of Agriculture, Statistical Reporting Service Tech. Rep., presented at the Amer. Statistical Asso. Meetings, San Diego, CA, 1978.

[13] J. S. Spencer and B. L. Essex, "Timber in Missouri," USDA Forest Service Res. Bull. NC-20, North Central Forest Experiment Station, St. Paul, MN, 1976.

[14] S. B. Winings, P. W. Cook, and G. A. Hanuschak, "1982 corn and soybean area estimates for Iowa and Illinois," U.S. Dep. of Agriculture, Statistical Reporting Service Tech. Rep., presented at the 17th Int. Symp. on Remote Sensing of Environment, Ann Arbor, MI, 1983.

*

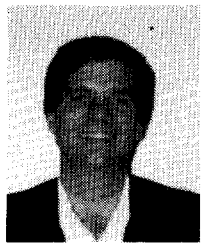

George A. May received the B.S., M.S., and PhD. degrees in agronomy from The Pennsylvania State University, University Park, PA, in 1971, 1973, and 1976, respectively.

From 1976 to 1980, he was a remote sensing specialist assigned to the Large Area Crop Inventory Experiment (LACIE), in Houston, TX, and was involved in AgRISTARS from 1981 to 1984. Currently, he is an Agricultural Statistician with the U.S. Department of Agriculture involved in remote-sensing-data application in California.

*

Martin L. Holko received the B.S. degree in forest science from The Pennsylvania State University, University Park, in 1973, and the M.S. degree in mathematical statistics from Michigan State University, East Lansing, in 1980.

He was an Agricultural Statistician with the U.S. Department of Agriculture, Statistical Reporting Service, assigned to the New York State Statistical Office (SSO) from 1973 to 1976, the New England SSO from 1976 to 1978, and the Michigan SSO from 1978 to 1980. He has been a Mathematical Statistician with the U.S. Department of Agriculture: SRS:SRD:RSB since 1980. He is currently involved in the application of remotely sensed data and microprocessor technology to area frame development.

*

Ned Jones, Jr., received the B.S. and M.S. degrees from the Virginia Polytechnic Institute and State University, Blacksburg, in 1971 and 1977, respectively. From 1982 to 1983 he did graduate work in statistics at North Carolina State University, Raleigh.

He was a Commodity Statistician with the U.S. Department of Agriculture, Statistical Reporting Service, assigned to the Kentucky State Statistical Office (SSO) from 1977 to 1981, and the North Carolina SSO from 1981 to 1983. Since 1983, he has been a Mathematical Statistician with the USDA:SRS:SRD:RSB.

Authors must enclose a signed copy of this form when submitting manuscripts to the Editor of this journal.

IEEE COPYRIGHT FORM

Signed form, appropriately completed, MUST ACCOMPANY any paper to be published by IEEE.
PLEASE READ REVERSE OF THIS FORM FOR FURTHER DETAILS.

TITLE OF PAPER:

RETURN FORM TO:

AUTHOR(S):

PUBLICATION TITLE: **IEEE Transactions on Geoscience and Remote Sensing**
MONTH AND YEAR:

PART A — COPYRIGHT TRANSFER FORM

(NOTE: Company or other forms may not be substituted for this form. U.S. Government employees whose work is not subject to copyright may so certify by signing Part B below.)

The undersigned, desiring to publish the above paper in a publication of the IEEE or cosponsored by the IEEE, hereby transfer their copyrights in the above paper to The Institute of Electrical and Electronics Engineers, Inc., known as the IEEE.

Returned Rights: In return for these rights, the IEEE hereby grants to the above authors, and the employers for whom the work was performed, royalty-free permission to:

1. Retain all proprietary rights other than copyright, such as patent rights.
2. Reuse all or portions of the above paper in other works.
3. Reproduce, or have reproduced, the above paper for the author's personal use or for company use provided that (a) the source and IEEE copyright are indicated, (b) the copies are not used in a way that implies IEEE endorsement of a product or service of an employer, and (c) the copies per se are not offered for sale.
4. Make limited distribution of all or portions of the above paper prior to publication.
5. In the case of work performed under U.S. Government contract, the IEEE grants the U.S. Government royalty-free permission to reproduce all or portions of the above paper, and to authorize others to do so, for U.S. Government purposes.

IEEE Obligations: In exercising its rights under copyright, the IEEE will make all reasonable efforts to act in the interests of the authors and employers as well as in its own interest. In particular, the IEEE requires that:

1. The consent of the first-named author be sought as a condition in granting republication permission to others.
2. The consent of the undersigned employer be obtained as a condition in granting permission to others to reuse all or portions of the paper for promotion or marketing purposes.

In the event the above paper is not accepted and published by the IEEE or is withdrawn by the author(s) before acceptance by the IEEE, this agreement becomes null and void.

AUTHORIZED SIGNATURE | TITLE IF NOT AUTHOR

EMPLOYER FOR WHOM WORK WAS PERFORMED | DATE FORM SIGNED

PART B — U.S. GOVERNMENT EMPLOYEE CERTIFICATION

(NOTE: If your work was performed under Government contract but you are not a Government employee, sign transfer form above and see item 5 under Returned Rights.)

This will certify that all authors of the above paper are employees of the U.S. Government and performed this work as part of their employment and that the paper is therefore not subject to U.S. copyright protection.

AUTHORIZED SIGNATURE | TITLE IF NOT AUTHOR

NAME OF GOVERNMENT ORGANIZATION | DATE FORM SIGNED

IEEE COPYRIGHT FORM
(continued)

Information to Authors

IEEE POLICY

Thank you for your interest in the IEEE. As you know, the IEEE distributes its technical publications throughout the world, and it is necessary to translate and abstract its publications, and articles contained therein, for inclusion in various compendiums and similar publications, etc. When an article is submitted for publication by the IEEE, the IEEE understands that its acceptance of the article implies that the IEEE has the rights to do all of the things it normally does with such an article.

In connection with its publishing activities, it is the policy of the IEEE to own the copyrights in its technical publications, and to the contributions contained therein, in order to protect the interests of the IEEE, its authors and their employers, and at the same time to facilitate the appropriate re-use of this material by others.

The new United States copyright law requires that the transfer of copyrights in each contribution from the author to the IEEE be confirmed in writing. It is therefore necessary that you execute either Part A-Copyright Transfer Form or Part B-U.S. Government Employee Certification on the reverse side of this sheet and return it to the Editor (or person who supplied this sheet) as promptly as possible.

AUTHOR/COMPANY RIGHTS

If you are employed and you prepared your paper as a part of your job, the rights to your paper initially rest with your employer. In that case, when you sign the copyright transfer form, we assume you are authorized to do so by your employer and that your employer has consented to all of the terms and conditions of this form. If not, it should be signed by someone so authorized.

> NOTE RE RETURNED RIGHTS: Just as the IEEE now requires a signed copyright transfer form in order to do "business as usual," it is the intent of this form to return rights to the author and employer so that they, too, may do "business as usual." If further clarification is required, please contact: Ms. Patricia Penick, Manager, Publication Administrative Services, IEEE, 345 E. 47th St., New York, NY 10017 (212) 705-7550.

JOINT AUTHORSHIP

For jointly authored papers, only one signature is required, but we assume all authors have been advised and have consented to the terms of this form.

U.S. GOVERNMENT EMPLOYEES

Authors who are U.S. Government employees are not required to sign the Copyright Transfer form (Part A), but any co-authors outside the Government are.

Part B of the form is to be used instead of Part A only if all authors are U.S. Government employees and prepared the paper as part of their job.

> NOTE RE GOVERNMENT CONTRACT WORK: Authors whose work was performed under a U.S. Government contract but who are not Government employees are required to sign Part A-Copyright Transfer Form. However, item 5 of the form returns reproduction rights to the U.S. Government when required even though the IEEE copyright policy is in effect with respect to the reuse of material by the general public.

Thank you for your prompt cooperation.

Now is the best time to join our society.

It's always time to upgrade your career. Membership gives you ready access to state-of-the-art meetings and conferences in your areas of interest, and to their published proceedings. You get to meet experts from other organizations and to participate in technical activities with the prime movers in engineering, science and business. Our membership is worldwide.

At least one periodical is included in your Society fee, keeping you abreast of the latest developments in your field. And, as an IEEE member, you may choose from a wide range of books, Standards, conference records, employment surveys, short courses and other career-building aids—all at discounted member prices.

Please take this opportunity, now, to broaden your outlook, open your mind to new concepts, new techniques, new fields of interest. There will be no better time. Return the Membership Application form below. *(Students should contact their IEEE counselor or write for a Student Membership brochure.)*

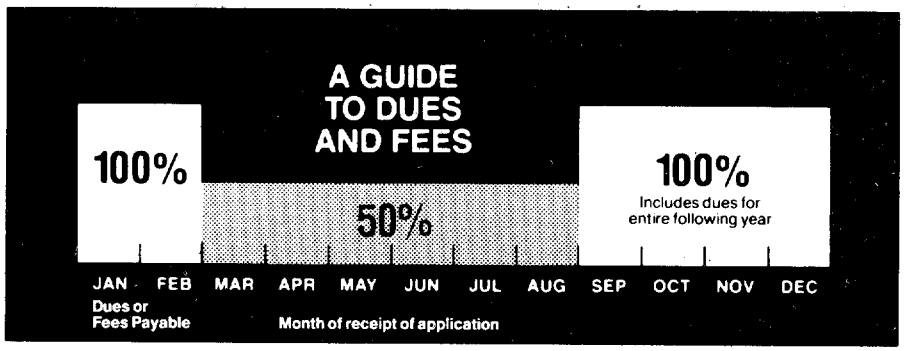

MEMBERSHIP APPLICATION

Please check appropriate box(es) below:

All dues and fees below (except for the IEEE entrance fee) are annual rates. Indicate here whether you are remitting either 100% or 50% of these rates. (See chart above.)

☐ 100% ☐ 50%

Society fee: $7.00 (Includes *Transactions on Geoscience and Remote Sensing*) ☐ $ _____

IEEE entrance fee (for non-IEEE members only): Remit $15.00 regardless of month of application. ☐ $ _____

IEEE membership annual dues and (if applicable) Regional assessment payments

U.S. (Region 1-6) $67.00 ☐ $ _____

Canada (Region 7) $62.00 ☐ $ _____

Europe, Africa & Mid. East (Region 8) $59.00 ☐ $ _____

Latin America (Region 9) $52.00 ☐ $ _____

Asia & Pacific (Region 10) $53.00 ☐ $ _____

PAYMENT ENCLOSED ☐ $ _____

Remit in U.S. dollars drawn on a U.S. bank. Make check payable to IEEE.

Please mail to:
IEEE Service Center
445 Hoes Lane
Piscataway, NJ 08854-4150 U.S.A.
(201) 981-1393

IEEE

GEOSCIENCE AND REMOTE SENSING SOCIETY

I am applying for the following as indicated:

☐ I am an IEEE member. Please enroll me in the above Society.
IEEE member No. ☐☐☐☐☐☐☐

☐ IEEE membership plus Society membership.
☐ IEEE membership only.

Full signature _____ Date _____

First name (print) _____ Middle initial(s) _____ Last name _____

Street address _____

City _____ State/Country _____ Postal Code _____

APPLICANTS FOR IEEE MEMBERSHIP PLEASE COMPLETE THE FOLLOWING INFORMATION:

Date of birth _____ (Month / Day / Year) ☐ Male ☐ Female

Were you ever a member of IEEE? ☐ Yes ☐ No If Yes, please furnish (if known): _____ Grade _____ Membership No.

EDUCATION (Highest level completed):

Name of educational institution _____

Course _____ Degree received _____ Date _____

ENDORSEMENT (Signature of one IEEE member, who knows you professionally.) _____

← TRACKING CODE →			
EVENT CODE	EVENT DATE	BROCHURE CODE	BROCH. DATE
P 2 9 0 8 8 6		2 9 0 8 8 6	
56 57 58 59 60 61 62 63 64 65 66 67		68 69 70 71 72 73 74 75 76 77 78	

Presenting
the first title in the new

SPECTRUM
SERIES

NEXT-GENERATION COMPUTERS

It's possibly the most important book you could own.

A concise and comprehensive examination of next-generation computer technologies, the worldwide effort to advance them, the likely technical and sociotechnical fallout.

The technology is not yet in place for the so-called "fifth" generation of user-friendly, superfast and supersmart computers. But it will soon come to pass.

Multiprocessors . . . artificial intelligence . . . networking—fundamental breakthroughs in every sector of computer science will be needed to achieve this new class of computers capable of processing

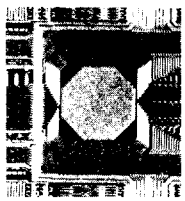

AT&T Technologies, Inc. manufactures a memory chip that can store a quarter of a million bits of information.

symbolic information a thousand times faster than anything we have today.

In the U.S., in Europe and Japan, governments and R & D centers have budgeted billions in a determined effort to dominate the impending information revolution.

At stake: World supremacy of the advanced-computer and high-technology markets of the 1990s and beyond.

Are you—is your company—prepared to compete in the upcoming technological revolution?

NEXT-GENERATION COMPUTERS reveals how the new computer capabilities are likely to change the way you perform your job, the new products you are likely to take part in designing, the various ways your job life could be affected.

The impending revolution has a greater potential to alter your career path, to reposition your company in the marketplace, than *any* technological advance in our lifetime.

This book will increase your awareness of the opportunities and pitfalls that could lie ahead, will help you and your company's management to make informed, intelligent decisions about the parts *you* will be playing in the scenario of things to come.

Don't pass up this opportunity. Send for your copy today.

About this book

Based in part on articles in the *Spectrum* special issue "Tomorrow's Computers," NEXT-GENERATION COMPUTERS includes contributions by 40 recognized leaders in artificial intelligence, hardware and software, architecture, and technology assessment. Major features include.

- A review of current developments in the key, emerging technologies of artificial intelligence, computer vision, expert systems, and many more.
- A special tutorial review section that provides a solid foundation in each of the major technologies.
- A look at the competing teams and players worldwide who are intent on being first with tomorrow's machines, including time-lines showing the probable development of constituent technologies.
- An in-depth analysis by leading engineers, scientists and technology-watchers on what the future is likely to hold.

A choice to delay or not to adopt these technologies is equivalent to accepting a significantly lower standard of living.
M. Granger Morgan, Carnegie-Mellon U.

Spectrum Series

This is the first title in the new Spectrum Series of books to be published by the IEEE PRESS. Upcoming volumes will be single-topic books devoted to such areas as design case histories, innovation, engineering management and retrospective themes. Each volume will be produced by the expert editors who have earned for *Spectrum* two National Magazine Awards for excellence.

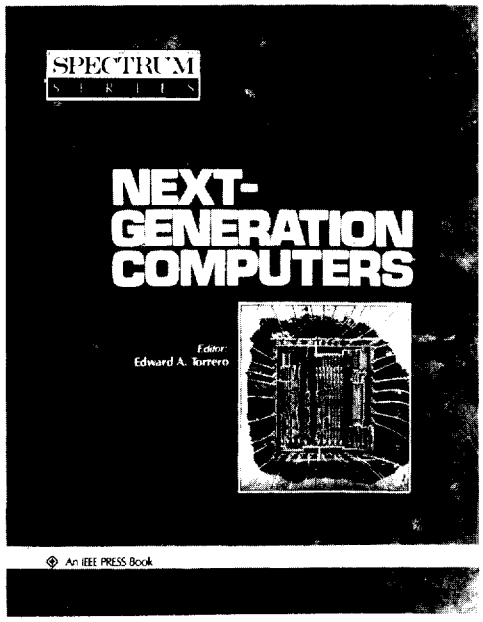

NEXT-GENERATION COMPUTERS
An IEEE PRESS Spectrum Series Book. 1985. 360 pp. 125 illustrations. ISBN—0-87942-194-0
List: $39.95; IEEE Member: $35.95. *First copy only for personal use. Additional copies at list.*

Meet the Next Generation *NOW.* Use this coupon.

Yes, please send me _____ copy (ies) of NEXT-GENERATION COMPUTERS (PCO1883) right away. List: $39.95; IEEE Member $35.95 *(first copy only.)*

Purchase amount: $_____.
New Jersey residents add sales tax.

☐ Payment enclosed. (Make check payable to IEEE in U.S. dollars drawn on a U.S. bank.)

☐ Charge the credit card indicated:
☐ MasterCard/Eurocard ☐ Visa
☐ American Express

Card No. _____

Exp. Date _____

Signature _____

NG-C

☐ Bill me. (A $2.00 billing charge is added to all non-cash and non-credit card orders under $100.00.)

Name (print) _____

IEEE No. _____

Address _____

City _____

State/Country _____ Postal Code _____

IEEE

Mail to:
IEEE Service Center
445 Hoes Lane
Piscataway, NJ 08854-4150. U.S.A.

INFORMATION FOR AUTHORS

Subject Matter: The IEEE TRANSACTIONS ON GEOSCIENCE AND REMOTE SENSING is concerned with the publication of both theoretical and applied papers on geoscience and remote sensing. Papers should relate to the field of interest of the IEEE Geoscience and Remote Sensing Society, which is "the theory, concepts, and techniques of science and engineering as applied to sensing the earth, oceans, atmosphere, and space, and the processing, interpretation, and dissemination of this information."

Membership in IEEE or associated technical organizations is not required of authors.

Papers: Except in the case of review or tutorial papers, the technical content of papers should be both new and significant. Experimental data should be complete and should include sufficient description of experimental apparatus, methods, and relevant experimental conditions.

Process for Submitting Papers: Five copies (original plus four copies) of the manuscript should be submitted to the appropriate Executive Editor or Associate Executive Editor. In addition, five copies of the illustrations should be provided and an abstract of not more than 200 words.

Style for Manuscript: This TRANSACTIONS is addressed to readers with a wide variety of interests. Few will be expert in the author's field. Consequently, authors should refrain from using or should take care to explain any terminology which may not be familiar to such readers and should provide brief introductory remarks and references which will permit the reader to relate the paper to other work in the author's field of specialty. Clarity of both writing and illustrations is required of all authors.

Manuscripts should be limited to twenty-five double-spaced typewritten pages, on one side of the sheet only, with a maximum of fifteen figures. Specific references should be numbered footnotes, appearing on the page where cited; general references should be numbered and should appear in order of reference at the end of the paper. A separate bibliography, listed alphabetically, may be added. References should be complete and in the IEEE style. (See "Information for IEEE Authors," available from the IEEE Publications Department, 345 East 47th Street, New York, NY 10017.)

Illustrations should be provided in quintuplicate with titles and numbers typed on a separate sheet. If the paper is accepted, original illustrations will be required. (See *Review Process*, below.)

Review Process: Papers are reviewed by qualified referees. Decisions on disposition of the manuscript are made in six weeks. The author is then notified of the decision. If the paper has been accepted, originals of the illustrations, a photograph of the author, and a short biography of the author are requested at this time.

Voluntary Page Charges: After a paper has been accepted, the author's organization will be requested to pay a voluntary charge of $110 per printed page to cover part of the cost of the publication. The author will receive 100 reprints of his paper or communication if the page charge is honored.

Excessive Paper Length Charges: A mandatory *Excessive Paper Length* charge of $125.00 per page is required for papers longer than six (6) printed pages. The author will be notified of the estimated paper length upon *Receipt* of the original manuscript. The author will be requested, conditional upon favorable technical review, to pay *Voluntary Page Charges* for all pages and *Mandatory Excessive Paper Length Charges*. If the author will not agree to pay mandatory charges, the author will be required to reduce the manuscript to six printed pages or less prior to final acceptance and scheduling for publication. This reduction will occur after technical review of the manuscript. The above policy has no relationship to requests by the Editor to reduce very long manuscripts prior to technical review.

Brief Papers and Letters to the Editor: These items should be prepared and submitted according to the instructions given above for regular papers, but for these changes: they should not exceed five pages; they should not contain more than three illustrations; abstracts should be limited to 50 words.

Copyright: It is the policy of the IEEE to own the copyright to the technical contributions it publishes on behalf of the interests of the IEEE, its authors, and their employers, and to facilitate the appropriate reuse of this material by others. To comply with the U.S. Copyright Law, authors are required to sign an IEEE copyright transfer form before publication. This form, a copy of which appears in the January 1985 issue of this Transactions, returns to authors and their employers full rights to reuse their material for their own purposes. Authors must submit a signed copy of this form with their manuscripts.

Submit Correspondence for Manuscripts, Brief Papers, Letters to the Editor to:

Prof. Fawwaz T. Ulaby
Editor
The University of Michigan Radiation Laboratory
Department of Electrical and Computer Engineering
4072 East Engineering Building
Ann Arbor, MI 48109

INSTITUTIONAL LISTINGS

The IEEE Geoscience and Remote Sensing Society invites application for Institutional Listings from firms interested in geoscience and remote sensing.

An Institutional Listing recognizes contributions to support the publication of the IEEE TRANSACTIONS ON GEOSCIENCE AND REMOTE SENSING. Minimum rates are $50.00 for listing in one issue; $200.00 for six consecutive issues. Larger contributions will be most welcome. No agency fee is granted for soliciting such contributions. Inquiries, or contributions made payable to the IEEE, plus instructions on how you wish your Institutional Listing to appear, should be sent to TAB Finance Office, The Institute of Electrical and Electronics Engineers, 345 East 47 Street, New York, NY 10017.